STRAIN RATE AND DENSITY DEPENDENT BEHAVIOUR OF BOVINE CANCELLOUS BONE IN COMPRESSION

by

SUZANNE HIGGINS

A dissertation submitted in part fulfillment of the requirements for the Degree MSc (Engineering)

Department of Mechanical Engineering
University of Cape Town
February 2008

DECLARATION

I, Suzanne Lydia Higgins, declare that this dissertation contains my own work, except where reference and acknowledgement is made to contribution by others. I declare that this material has not been submitted for any purpose or examination to any other Department or University.

Signed this …….. day of ……..…

……..

ABSTRACT

The mechanical properties of bone are determined by means of low strain rate testing performed quasi-statically on the Zwick Universal Testing Machine and high strain rate testing performed on the Split Hopkinson Pressure Bar. Cancellous bone is sourced from the vertebrae of five bovine of slaughtering age. Two sizes of specimens are machined. For quasi-static testing an aspect ratio of 2:1 is used (10 mm high and 5 mm in diameter). A ratio of 1:1 is utilised for the dynamic testing (5 mm in both length and diameter). Tests are conducted at four different strain rates of 10^{-4}, 10^{-3}, 10^{-2} and 10^{-1} /s for quasi-static tests and a range of approximately 800 to 1300 /s for the high impact tests. A total of 68 specimens are tested quasi-statically, with 17 specimens assigned to each strain rate. The dynamic data is gathered from tests on 18 specimens. Therefore, a total of 86 specimens are used for the combined data.

The trends in yield stress, yield strain and Young's modulus as a function of both strain rate and density were investigated. Results show that, as expected, density has a far greater effect on the mechanical properties of cancellous bone than strain rate. Due to the high scatter in results, the exact relationships are difficult to determine, although results of this work generally fall within the findings of the literature reviewed.

Using the determined strain rate and density dependent relationships, a one-dimensional viscoelastic equation, based on the work by Shim [1], was determined to describe the dynamic behaviour of bone:

$$\sigma = (1814\rho - 1198)\varepsilon + \int_0^t -3.47x10^4\,\dot{\varepsilon}(\tau)\exp\left(-\frac{t-\tau}{5.37x10^7}\right)d\tau + 0.142\dot{\varepsilon}^{1/2}$$

The yield stresses were determined to be:

$$\sigma_y^d = 11.4\rho^{2.86} + 4\times10^6\dot{\varepsilon}^{-1.823}$$

Results between the fitted and experimental trends show a large variation due to the high scatter in the quasi-static test data used to determine the equation constants.

ACKNOWLEDGEMENTS

I would like to express my deepest thanks to Annie van der Westhuizen for her continual support, advice and guidance during every stage of this project. Her enthusiasm, words of encouragement and friendship are much appreciated.

In addition, I would like to extend my sincere appreciation to the following people for their help, advice and guidance, without which this thesis would not have been possible.

Professor Gerald Nurick for his supervision of the work and guidance throughout the project.

Rueben Govender for his knowledge and assistance with the Hopkinson bar and his general willingness to help.

Trevor Cloete for his enthusiasm and advice concerning the Hopkinson bar testing.

Dr Steeeve Chung for the operation of the high-speed camera.

Dr Dean Bonorchis for his help and advice at various stages throughout the project.

Charles Harris in the workshop of the Department of Human Biology for the machining of the specimens. His willingness to work overtime and the delivery of the specimens is much appreciated.

Penny Park-Ross for her assistance with the laboratory equipment in the Materials Department.

Professor Annasuya Chinsamy-Turan for her expert advice, assistance and the use of her facilities for the microstructural work.

Dundee Butchery for the provision of bones and their friendly service.

The NRF (National Research Foundation) and ARMSCOR (Armaments Corporation of South Africa) for the financial support.

TABLE OF CONTENTS

LIST OF FIGURES

LIST OF SYMBOLS

A	Cross-sectional area
c	Sonic velocity
c_1	Stiffness modulus
E	Young's modulus
E_b	Specimen bulk modulus
F	Force
L_s	Instantaneous length
t	time
T	Ratio of contacting surface layer to specimen height
u	Displacement
Y	Ratio of surface to bulk specimen modulus
ρ	Fresh bone density
ρ_a	Apparent density
σ_y	Yield stress
σ_u	Ultimate compressive stress
ε_y	Yield strain
ε_u	Strain corresponding to ultimate compressive stress
θ	Relaxation time of the Maxwell model
η	Viscosity
τ	Dummy variable of integration
$\dot{\varepsilon}$	Strain rate

Sub/superscripts

d	Determined dynamically
qs	Determined quasi-statically
e	Derived from linear elasticity
v	Derived from non-linear viscoelasticity
i	Incident wave
r	Reflected wave
t	Transmitted wave
b	Bar
s	Specimen

1 INTRODUCTION

This study investigates the strain rate and density dependency of cancellous bone by testing bovine vertebral specimens in compression over a range of strain rates. Based on these results, the viscoelastic behaviour of bone is explored and used to predict the behaviour of cancellous bone under dynamic loading.

This work forms part of the research conducted by the Blast Impact and Survivability Research Unit (BISRU) in the Department of Mechanical Engineering at the University of Cape Town. At present, a number of students are conducting research focusing on the lower extremities of the human body. Understanding of the biomechanics of bone is necessary in determining the human response to blast and impact. Through this understanding, dynamic injury criteria can be developed.

Therefore the main objectives of this work are to:

1. Characterise the mechanical behaviour of cancellous bone with regard to strain rate and density.
2. Use these relationships to determine a one-dimensional viscoelastic equation (based on the equation derived by Shim [1]) to describe dynamic behaviour.

This research thesis is composed of the following ten sections:

- An overview of the types and the structure of bone.
- Review of the existing literature pertaining to mechanical testing of bone. The trends of strength, modulus and strain with density and strain rate are discussed. The viscoelastic behaviour of bone is examined.
- An overview of the split Hopkinson pressure bar and derivation of the governing equations.
- Details of the quasi-static and dynamic test procedures.
- Results and analysis of the quasi-static tests.

- Results and analysis of the dynamic tests.
- Analysis of the combined set of data, including derivation of the constants for the viscoelastic equation and comparison of the fitted and experimental dynamic results.
- An investigation into the microstructure of the specimens in order to provide a visual description of failure.
- Conclusions based on the work done.
- Recommendations for future work.

2 THE MATERIAL BONE

Bone is a non-homogenous composite material. Its main constituents are mineral content (mainly calcium phosphate) which can account for over half the wet weight, collagen and water, which comprises approximately 10% to 20% of the wet weight [2, 3, 4, 5]. The collagen and mineral crystals are oriented longitudinally, giving bone much higher strength and stiffness properties in this direction. As a result, bone is highly anisotropic. The calcium phosphate is responsible for stiffness and strength, while collagen plays a role in the post-yield behaviour and fracture properties. Bone is hard and lightweight with a relatively high compressive strength and low tensile strength [2, 6]. Typical strength values for cortical bone are 135 MPa under tensile loading and 205 MPa under compressive loading [7].

2.1 Types of bone

Bone is generally classified into two main architecture-based types, namely cortical and cancellous bone. The difference is shown for a single vertebra in Figure 2.1.

Figure 2.1: Vertebra composed of cortical and cancellous bone [8]

Cortical or compact bone accounts for a substantial portion (80%) of skeletal mass in the human body and has a high density in the region of 1.8 g/cm^3, with a porosity generally below 15%. Cortical bone is a rigid and dense composite material found mainly in the shafts of long bones. The hard outer layer of the skeleton is also composed of cortical bone, which forms a compact

shell around the softer cancellous bone in order to protect it. This compact layer is responsible for bearing most of the body's weight [2, 6].

Cancellous or trabecular bone accounts for 20% of skeletal mass, however due to its low density it has a relatively large surface area. The porosity is approximately 75% to 95% and dimensions of the pores vary substantially within the bone, which causes highly variable densities between specimens. Apparent densities typically range from 0.14 to 1.10 g/cm^3. The bone has a spongy or honeycomb-like structure, consisting of a number of bony composite rods and/or plates called trabeculae. The pores are filled with bone marrow, which has the function of supplying the bone tissue with nutrients. Cancellous bone is found in the end of long bones, in the vertebrae and in flat bones such as the pelvis [2, 6]. This is indicated in Figure 2.2, which shows some of the trabecular bone sites in the human skeleton.

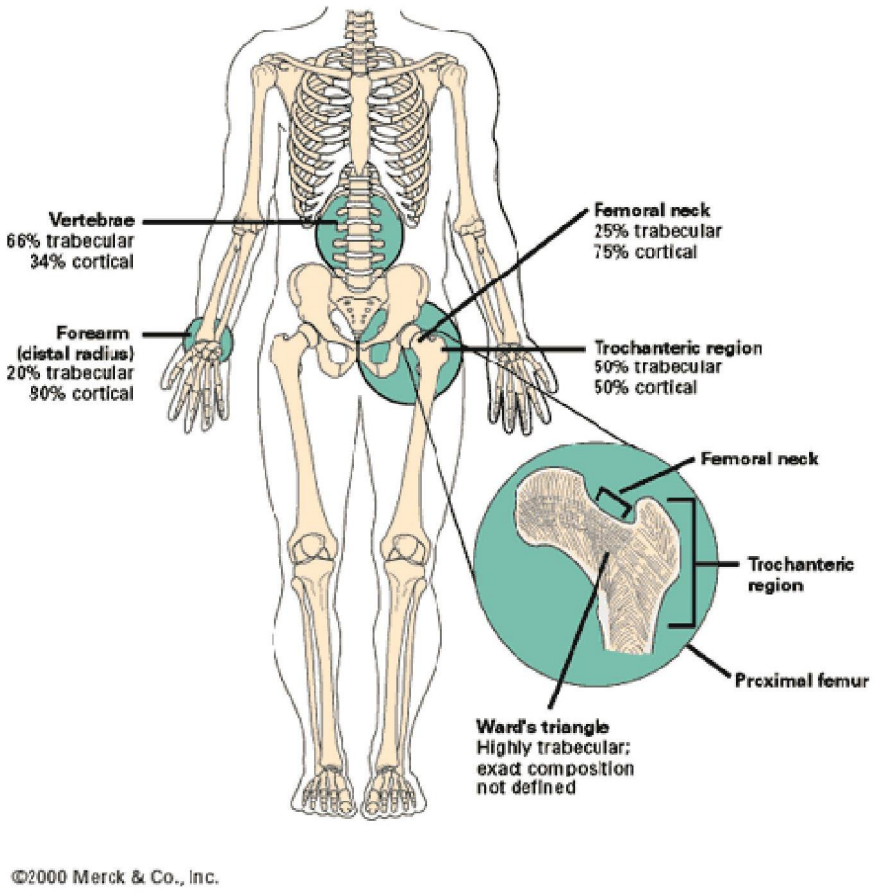

Figure 2.2: Typical locations of cancellous bone in the human skeleton [9]

In 1978, Singh [10] classified cancellous bone into three distinct types, shown in Figure 2.3:

- Type I consists of a fine mesh of straight or curved rods, 0.08 to 0.14 mm in diameter. These rods are randomly orientated and extend for approximately 1 mm before connecting with each other. This form of cancellous bone is typically found deep inside the ends of long bones, e.g. the femur.
- Type II is composed of both rods and plates, of which the ratio of rod to plate is highly variable. At the lower end of the human femur, this trabecular bone consists of roughly parallel plates 0.16 to 0.3 mm thick connected by a number of rods, 0.4 to 0.8 mm in length.
- Type III is wholly made up of irregularly sized plates. One sub-type of this bone architecture is generally found in the vertebrae. The plates are 0.12 to 0.24 mm thick and contain holes 0.7 to 2 mm in diameter, which give the bone a preferred orientation.

The high bone porosity of 75% to 95% results in more free surfaces, and therefore more exposed bone cells. This leads to the cancellous bone being more metabolically active and responsive to mechanical changes than cortical bone [11].

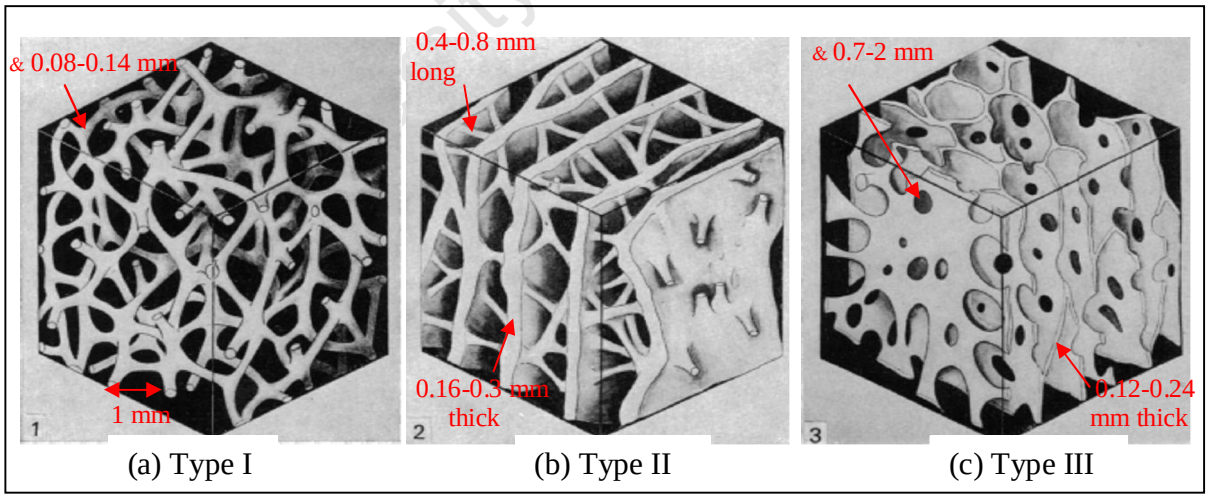

Figure 2.3: Morphology of cancellous bone [10].

2.2 Bone structure

On a microstructural level, bone (cortical or cancellous) can be classified as either having a woven or lamellar structure. Woven bone is formed rapidly during bone growth or repair at a rate of 4 μm a day. This "rapid" formation leads to a disorganised structure of random fibres, which has a low strength. Lamellar bone is formed more slowly, less than 1 μm a day, and consists of organised parallel fibres, which give the bone strength [12].

There are two methods by which new bone can be laid down, namely modelling and remodelling. Modelling is the process by which bone is either added or taken away from the surface of the bone. Remodelling of bone is the replacement of old bone by new by the formation of Haversian systems (secondary osteons), and can occur throughout the bone [6, 12].

2.3 Comparison of bovine to human bone

Bone size and structure vary according to species. In times of rapid growth, woven bone is laid down initially. In humans, continued bone growth leads to replacement of the woven bone by the stronger lamellar bone. Therefore, human bone that has been remodelled will usually consist of circumferential lamellar bone. In the case of bovines, remodelling does not generally occur and the bone will keep its original structure, known as plexiform or fibrolamellar bone, which consists of alternating layers of woven and lamellar bone (Figure 2.4). Plexiform bone is found mainly in large mammals, such as cattle or sheep, whose bones need to grow quickly in diameter.

Investigations have shown that the composition of bovine cortical bone closely approximates human cortical bone. However, bovine bone is stronger and stiffer than human bone [6, 12]. This is illustrated in Figure 2.5, which compares the strength and stiffness of various animal bone to a number of biomaterials. Both rabbit and rat bone are slightly stronger than human bone, but not as strong as bovine bone. However, the stiffness values of rabbit and rat bone are lower than the values for human and bovine bone. In particular, rat bone has a low stiffness compared to other

animal bone. The strength and stiffness of human cartilage is shown to be negligible compared to human and animal bone.

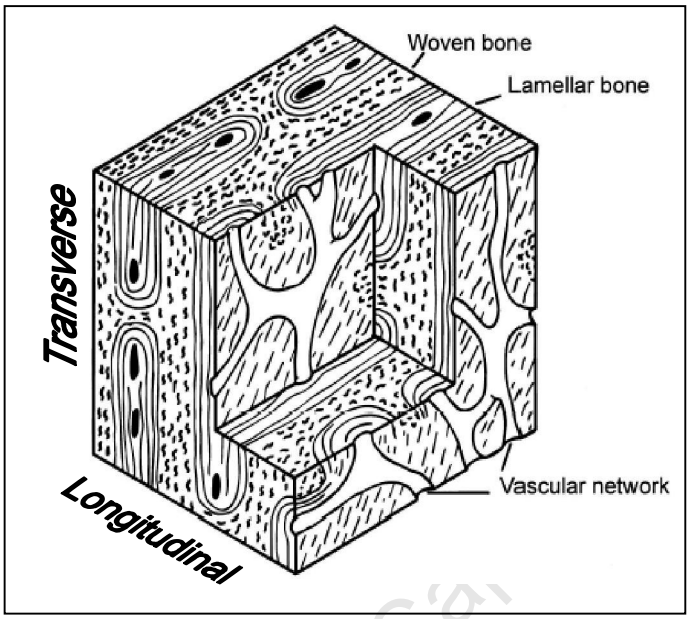

Figure 2.4: Block diagram of plexiform bone [12].

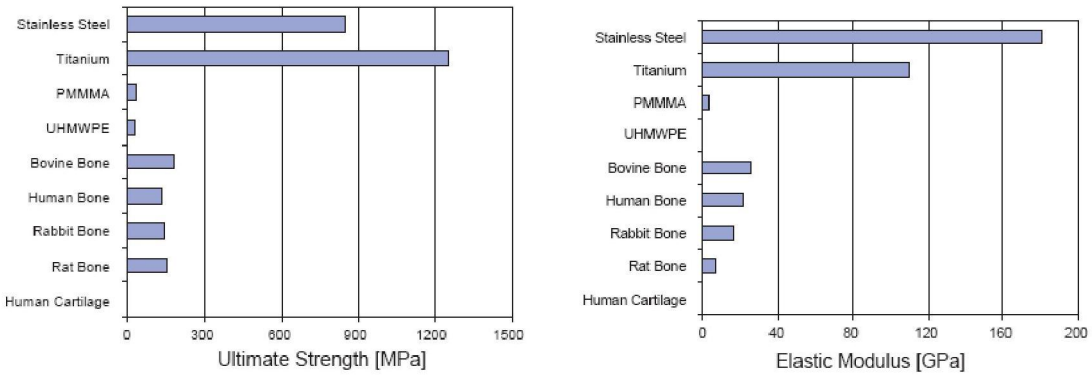

Figure 2.5: Comparison of mechanical properties of cortical bone from various animals to common biomaterials [6]

3 LITERATURE REVIEW

3.1 Mechanical behaviour of bone

Bone is able to adapt its mass, shape and properties to changes in its mechanical environment. It exhibits viscoelastic behaviour, i.e. it is characterised by properties of both a linear elastic solid and a viscous fluid. This results in non-linear load-deformation and stress-strain characteristics. In addition, bone is highly anisotropic in its behaviour.

The complex structure of cancellous bone makes it difficult to describe its behaviour from a biomechanics perspective. Turner [7] characterises cancellous bone by two definitions of "stiffness". The material stiffness is that of the individual trabeculae, while the structural stiffness incorporates the entire trabecular structure. It is this structural stiffness that is generally used as a means of comparison in biomechanical studies. This is due to the difficulty associated with measuring the individual trabeculae.

A number of studies have been conducted to illustrate the viscoelastic nature of bone. These studies involve the characterisation of the mechanical properties, such as strength and stiffness, of bone in compression at low and high strain rates. In these studies, compressive strength and modulus have often been shown to be dependent on the apparent density of bone. In addition, some of these studies investigated the strain rate dependence of bone. Carter and Hayes [13] hypothesised that the structure of trabecular bone is similar to that of cellular solids and consequently, the material properties would be highly dependent on density. The mechanical behaviour of bone was therefore described by means of a power law function of the form:

$$y = a\rho_a^b \dot{\varepsilon}^c \tag{3.1}$$

where y is the dependent variable (strength or modulus), ρ_a is the apparent density, $\dot{\varepsilon}$ is the strain rate and a, b and c are all arbitrary constants. Since its development, this power law relationship has been used in further investigations of trabecular bone e.g. Ouyang [14] and Shim [1].

It has been shown that the compressive modulus can vary 100 fold within a single tibia and strength can vary 5 fold within a single femur. These values were determined by Brown [15] and Ferguson [16] respectively.

Although compact and trabecular bone have different morphologies and mechanical behaviour, all bone can be viewed as a single material of variable density, as stated by Carter and Hayes [17].

3.2 Factors affecting test results

The response of bone during mechanical testing depends on a number of factors, including bone age, type and composition, specimen preparation, geometry and preservation, previous specimen stress history and testing conditions.

3.2.1 Bone age

McCaldon [18] studied the effects of age on human femoral trabecular bone in compression. It was found that the mechanical properties deteriorated significantly with age, with compressive strength decreasing by 8.5 % per decade.

A study by Ding [19] conducted on young, medium and old-aged human trabecular bone specimens also shows a decrease in mechanical properties with age. However, it is suggested that this is as a result of a decrease in the quantity and not quality of trabecular bone with age i.e. the trabecular bone structure becomes thinner, but the properties of the remaining bone are unchanged.

3.2.2 Specimen Geometry

In order to assume that trabecular bone behaves as a continuum, specimen dimensions must be considerably larger, at least an order of magnitude, than that of the individual trabeculae [20].

In addition, each test type has its own conditions regarding optimal specimen geometry.

3.2.2.1 Quasi-static testing

Zhu et al. [21] performed compression tests on cellular materials, including cancellous bone specimens, in order to examine the effect of the load-bearing surface on Young's modulus values. Specimens with a cross-sectional area of 81 mm^2 and heights of 5, 9 and 16 mm were compared. The elastic modulus of the 5 mm specimen was found to be approximately 42 % lower than that of the 16 mm specimen. An equation was derived to relate the ratio (Y) of surface to bulk specimen modulus, to the ratio (T) of the contacting surface layer height to sample height:

$$\frac{E}{E_b} = \frac{Y}{Y(1-T)+T}$$

This formula was verified experimentally and it was recommended that the minimum specimen height for cellular material, and therefore cancellous bone, compression tests should be 10 mm.

Keaveny et al. [22] investigated the effects of specimen geometry on the modulus and strength of bone. Compression tests were performed on trabecular bovine bone cylindrical specimens with an aspect ratio (length/diameter) of 2:1 (10 mm high with a diameter of 5 mm) and on 5 mm bone cubes. Standard errors in the estimated values for both modulus and strength were considerably higher in the cubic specimens. These results indicate that specimen geometry plays a part in determining the modulus and strength. Therefore errors may be introduced in comparisons between studies using different specimen geometries. These authors recommended that a standard cylindrical bone specimen with an aspect ratio of 2:1 be used in future studies.

A similar study was conducted by Linde et al. [23], in which cubic and cylindrical specimens were compressed non-destructively. It was recommended that cubic specimens of side length 6.5 mm or cylindrical specimens of 7.5 mm diameter and 6.5 mm length be used for compression testing of trabecular bone. This corresponds to an aspect ratio of 1:1 and 1:1.15 for the cubic and cylindrical specimens respectively.

3.2.2.2 Dynamic testing

The equations governing the split Hopkinson pressure bar theory are based on the assumption that the stress within the specimen is uniform. A further assumption is that the radial inertia and friction do not affect test results.

The assumption of stress uniformity is only valid after an initial period during which the stress pulse must reverberate between the ends of the specimen approximately three times [24]. Soft materials, such as cancellous bone, have a low wave speed, which means that the transit time in the specimen is long and dynamic equilibrium cannot be reached quickly, relative to harder materials. Therefore, thin specimens should be utilised for the testing of soft materials.

Gray [25] proposed using an aspect ratio (L/d) of between 0.5 and 1 to combat the effects of radial inertia and friction. Davies and Hunter [26] found the optimal aspect ratio to be 0.5 for a material with a Poisson's ratio of 0.333.

The optimal specimen design will be such that equilibrium is achieved quickly and the radial inertia and friction effects will be minimal.

3.2.3 Preservation of specimens

Water is responsible for approximately 20% of the wet weight of cancellous bone and 10% of cortical bone [3, 4, 5]. The mechanical properties of bone therefore depend on the method of storage of specimens, since these methods determine the levels of hydration in bone.

Specimens can be preserved in a 50% saline and 50% ethanol solution at room temperature without significant changes to the mechanical properties of the bone. Ashman et al. [27] found a decrease in elastic modulus of less than 2% for specimens stored in this solution for a period of 90 days. Sedlin [28] examined bone specimens stored in 40% ethanol for 5 to 10 days and found a 2.5% to 4% decrease in modulus. In unpreserved specimens stored at room temperature for 24 hours, the Young's modulus

showed a 3% decrease [7]. However, these values are not significant for the scope of this project.

Dry bone is more brittle than wet bone and has a higher strength and stiffness, but lower toughness. Evans and Lebow [29] compared results of dry and wet whole human femur bones. Their results show an increase of 17% for Young's Modulus, 31% for ultimate tensile stress and a corresponding 55% decrease in toughness in the case of dry bone. Therefore testing bone in its hydrated state will yield the most accurate results.

Adharapurapu [30] soaked bone specimens (5 mm cubes of bovine bone) in Hanks balanced salt solution (HBSS) for at least 30 hours prior to testing. Passi and Gefen [31] soaked whole chicken femoral bones for 2 hours before testing. It is not made clear what solution was used. Other studies reviewed did not make mention of the details of the rehydration process.

An investigation by Currey [32] shows that the drying and rewetting of the bone specimens do not significantly affect the mechanical properties of cortical bone.

For long-term preservation of bone, the specimens should be soaked in saline, wrapped in gauze and frozen at –20 °C in airtight containers [7].

3.2.4 Testing conditions

In its natural environment, bone is subjected to forces while staying at an approximately constant body temperature of 37 ˚C. The mechanical properties of bone should therefore be tested at this temperature to ensure accuracy of measurements. However it is more practical to test at room temperature. Tests conducted at 23 ˚C have shown a 2% to 4% increase in Young's Modulus compared to tests at 37 ˚C [7]. However, this is not a significant increase and will not be considered in this study. Results from fatigue tests performed at room temperature show twice as many cycles to failure as test conducted at body temperature [33].

3.3 Mechanical testing of bone

3.3.1 Accuracy of quasi-static compression testing

Compression testing on bone is generally less accurate than tensile testing [7]. This is because the behaviour of the bone at its cut surface will directly affect results. The contact surfaces of the specimens have been machined or cut in preparation for testing. In trabecular bone, in particular, considerable material inhomogeneity exists due to the irregular network of trabeculae. Cutting of the individual trabeculae causes the specimen to be weaker at the surface, a phenomenon designated as the end artifact. Therefore measurements that take the specimen boundaries into account may be inaccurate.

In addition, the cut surfaces may not be completely aligned with the loading plates, resulting in portions of the surface not being supported and areas of stress concentrations being formed. This leads to further inaccuracies. During compression tests, the cut or machined contact surfaces of the specimen tend to experience higher strains than the midsection. This leads to the average strain being over predicted and modulus and compressive strength being under predicted in results obtained from the crosshead position measurements from the testing machine. In order to ensure a higher degree of accuracy, it is recommended that strain gauges or extensometers be attached to the specimens [7].

Odgaard and Linde [34] explored the underestimation of Young's modulus in non-destructive compressive testing of rectangular cancellous bone specimens. Strain was measured by means of an extensometer and by an optical method. The authors found that the strain has an uneven distribution across the specimen face due to the lack of structural support caused by cutting of the trabeculae. This is believed to be the reason for the underestimation of Young's modulus (approximately 20%) by compression testing.

Keaveny [22] recommends using specimens with a 2:1 aspect ratio as a means of minimising the experimental end-artifact.

In the body, cancellous bone is housed within a cortical bone shell. This is in contrast to biomechanical tests, where the sides of the specimen are not contained. A study by Un [35] using finite element methods to explore the effect of this side artifact found modulus values to be underestimated by approximately 50% for some of the specimens. Although none of the experimental studies reviewed took this side artifact into account, it is important to be aware of it.

3.4 Determining the mechanical properties of cancellous bone

3.4.1 Typical stress-strain behaviour

A typical stress-strain curve of bovine cancellous bone in compression is shown in Figure 3.1(a) to failure. It shows a non-destructive pre-conditioning cycle to 0.7% strain, performed in order to reduce the initial nonlinear region of the stress-strain curve. This is followed by destructive testing to 4.5% strain at a strain rate of 0.35×10^{-3} s^{-1}. The yield point has been determined by the 0.2% offset strain method. Figure 3.1(b) shows a stress-strain curve, to total failure, taken from a separate study.

In general, the cancellous bone stress-strain curve to failure exhibits two important characteristics:

- The initial elastic portion of the curve is non-linear, making the modulus difficult to determine.
- There is no well-defined yield point.

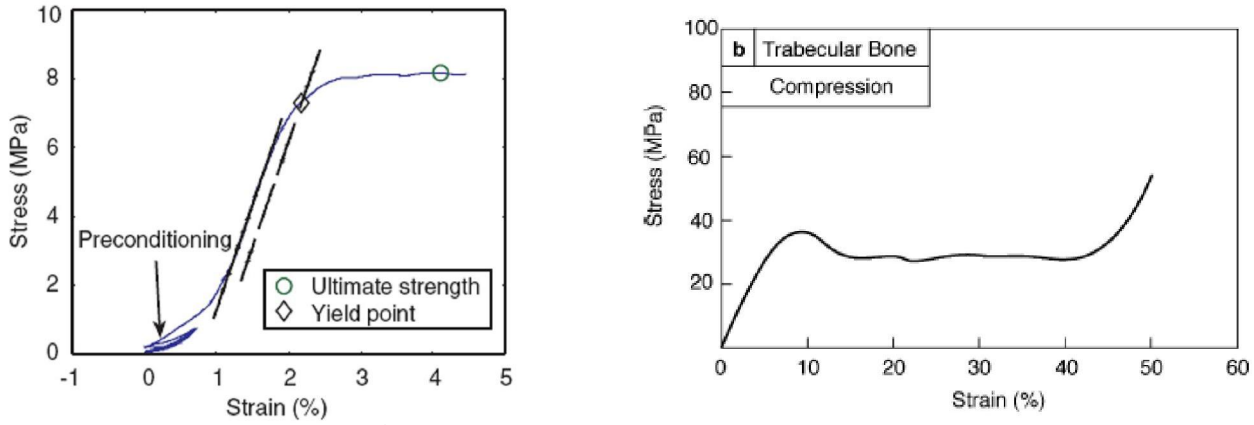

(a) Stress-strain curve to failure [36]. (b) Stress-strain curve to 50% strain [37].

Figure 3.1: Typical stress-strain curves of cancellous bone.

The smooth stress-strain curve characteristic of cancellous bone testing means that the yield point cannot be determined visually. Instead, it is usually defined by means of an offset method, whereby a line representing the slope or modulus of the linear portion of the curve is offset by a certain strain. The yield point is found at the intersection of the line and the curve. Therefore the definition of modulus is critical in determining the yield point.

A typical stress-strain curve showing extensive post-yield behaviour is shown in Figure 3.1(b). This behaviour shows vast inelastic deformation at a relatively constant stress until the individual trabeculae are all crushed, usually at approximately 50% strain. The stress and stiffness then increase sharply due to the contacting trabeculae and closed pores, in a process known as densification.

3.4.2 Determining the elastic modulus

A study by Morgan [38] was undertaken to investigate the non-linear behaviour and to gain understanding of the failure mechanisms of cancellous bone at small strains. Bone cores from human vertebrae, femora and tibia, as well as from bovine tibiae, were tested to yield at 0.5% s^{-1} in both compression and tension. Results from these quasi-static tests were verified using an extensometer, showing that the non-linear behaviour was not due to slipping of the specimens. Due to the non-linearity of the stress-strain curve, a single modulus cannot be defined in the elastic region. This affects the location of the yield point since an offset method is usually used to determine the yield stress and strain. Morgan defines the initial modulus to be the slope of the curve in the 0% to 0.1% strain range. The tangent modulus for the 0.2% and 0.4% strain graphs are taken from the 0.15% to 0.25% and 0.35% to 0.45% strain ranges respectively.

Therefore, over two different strain ranges, the elastic moduli (initial and tangent), yield stresses and yield strains were defined and results were compared. Results show that the degree of non-linearity depends on the type of loading, strain range, anatomic site and the density of the specimen. The reduction in the modulus ($\Delta E = (E_{initial} - E_{tangent})/E_{initial}$) is shown in Figure 3.2 for the 0.2% and 0.4% levels of strain.

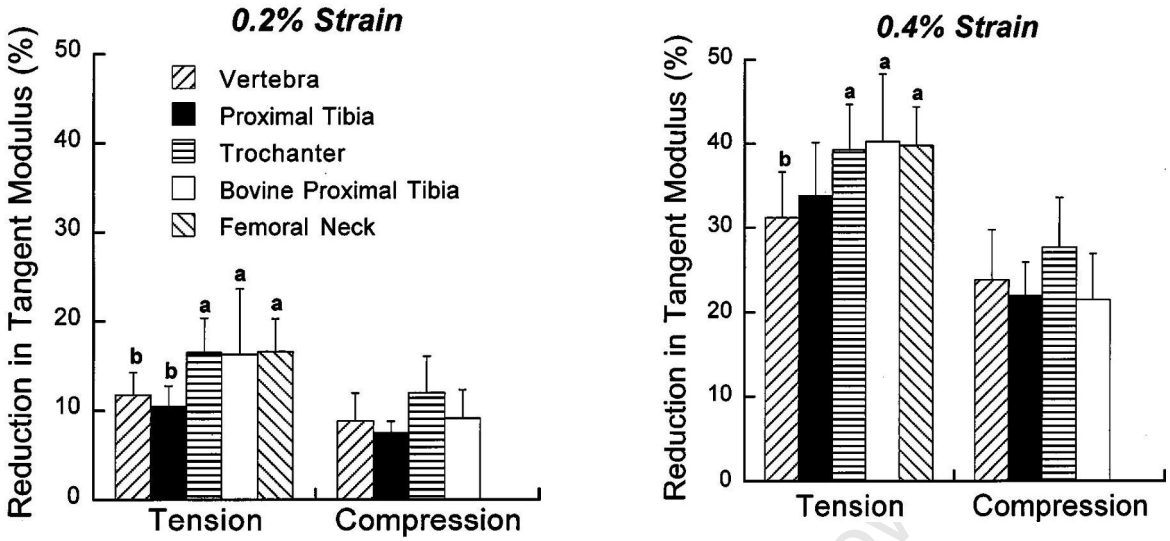

Within each graph, groups marked "a" are significantly different from groups marked "b".

Figure 3.2: Reduction in modulus [38]

The elastic modulus is generally defined as the maximum slope or the "most linear portion" of the curve prior to failure.

3.4.3 Determining the yield point

The yield stress of a material whose stress-strain curve shows no distinct yield point is usually found by using the 0.2% strain offset method. However, in the case of bone these offsets range from 0.03% to 0.2% across different studies [7]. In his study on compression testing of human cancellous bone, Shim [1] defined the yield stress as 95% of the ultimate compressive stress.

3.4.4 Yield strain as a failure parameter

Morgan and Keaveny [39] studied the dependence of yield strain of cancellous bone on anatomic site. Human specimens taken from the vertebra, tibia, femoral trochanter and femoral neck were tested in tension and compression. Results (see Table 3.2, p 31) show that the yield strain does indeed differ according to site. However, while the yield stress and the elastic modulus may vary considerably within a specific site, the yield strain can be assumed to be constant.

Keaveny et al. [40] explored the relationship between tensile and compressive strengths of cancellous bone, and modulus. Bovine tibial specimens were used to compare tensile and compressive yield stresses and strains. It was found that the difference between tensile and compressive strengths is dependent on the modulus and density of the specimens and increases linearly with both parameters. Yield strain for both loading modes was found to be independent of modulus and density. In a further study by Kopperdahl and Keaveny [41], human vertebral specimens were used to determine that, under tensile loading, yield strains are independent of density, but under compressive loading, there is a weak linear relationship between the two.

Chang [42] investigated the isotropy of bovine cancellous bone. Tibial specimens were tested along the direction of principal trabecular orientation and at 30° to 40° to this orientation. Results show that while modulus and strength were dependent on the direction of loading, yield strains were similar for both orientations in tension and compression. Therefore these results show cancellous bone to be isotropic in terms of yield strain.

Combining these four studies, yield strain is shown to be isotropic, uniform within a given site, and to have, at most, a weak dependence on density. This provides good motivation for using strain as a description of failure for trabecular bone and as a means of comparison between studies.

3.4.5 Results of other investigations into trabecular bone

Bayraktar [43] investigated the hypothesis that the elastic and yield properties of cancellous and cortical bone tissue in tension and compression are similar. Cancellous specimens were obtained from the neck and cortical specimens from the diaphysis of human femur bones. Two groups of cancellous specimens were tested at a strain rate of 0.5% s^{-1}, one group in tension and the other in compression, while cortical specimens were tested at a rate of 0.2% s^{-1} in tension only.

When compared to cortical bone, the elastic modulus and yield strain of cancellous bone tissue were found to be lower by 10% and 15% respectively. The combination of these

two effects leads to the cortical tissue being approximately 25% stronger than the trabecular tissue. The ratio of tensile to compressive stress was found to be 0.62 on average for trabecular bone.

Reilly [44] found there to be no significant difference in the elastic modulii of human and bovine bone tested in tension or compression.

3.5 Definition of density

It is important to note that the definition of density varies between studies. Cancellous bone consists of a network of rod or plate-like trabeculae, which house pores containing marrow. Fresh bone density (ρ) takes this marrow into account and is defined as the ratio of specimen mass to the bulk volume, both measured prior to testing. Apparent density (ρ_a) is the specimen mass, determined after testing in a sample that has been de-marrowed, divided by the bulk volume. Tissue density (ρ_t) is calculated by using both the mass and volume of the de-marrowed bone structure.

3.6 Mechanical property trends of bone with strain rate and density

A number of factors, mainly density, and, to a lesser extent, strain rate, influence the mechanical properties of bone.

3.6.1 McElhaney; Crowninshield and Pope

McElhaney [45] performed compression tests at strain rates varying from 10^{-3} to 1500 s^{-1} on various materials, including fresh bovine femoral cortical bone cubes. Crowninshield and Pope [46] investigated the strain rate dependence of compact bovine tibial bone loaded in tension. Specimens were tested either in the longitudinal or the transverse direction at strain rates ranging from 10^{-3} to 200 s^{-1}. Figure 3.3 shows the comparison of the stress, elastic modulus and strain curves to those derived by McElhaney [45].

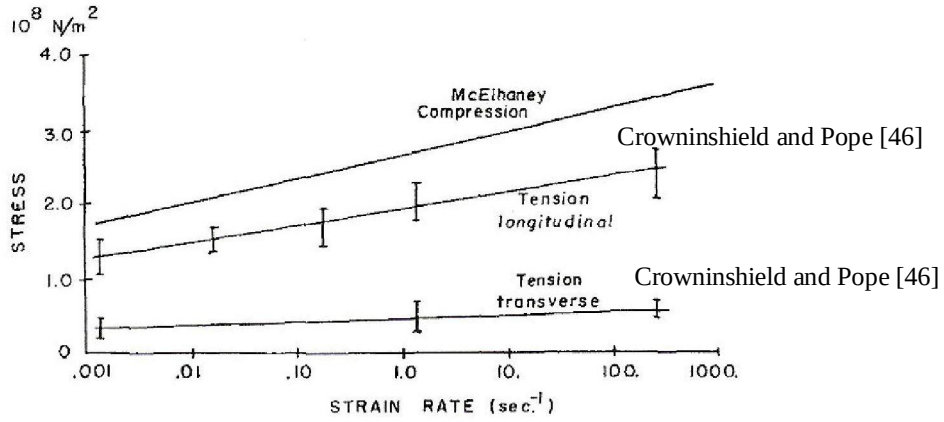

(a) Ultimate strength versus strain rate.

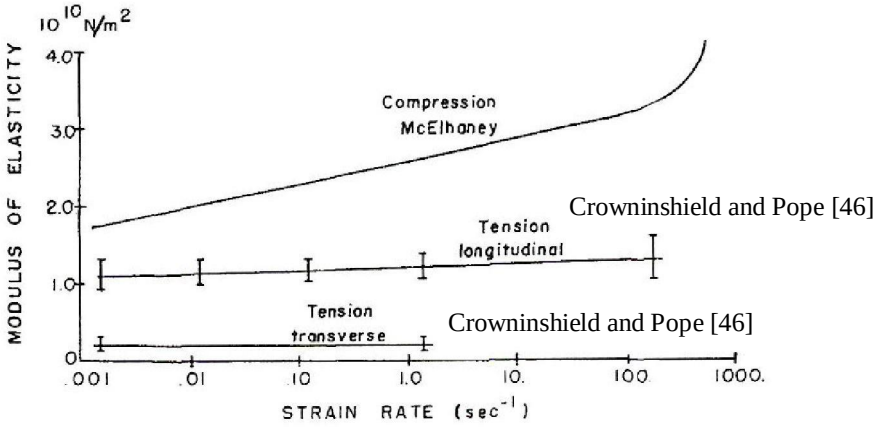

(b) Elastic modulus versus strain rate.

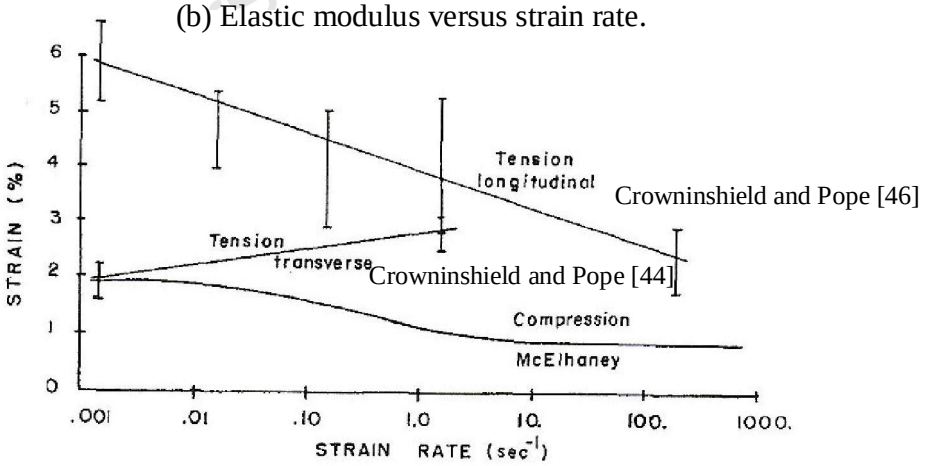

(c) Ultimate strain versus strain rate.

Figure 3.3: Comparison of results of influence of strain rate on mechanical properties: Crowninshield and Pope [46].

In both studies, the ultimate stress of bone was shown to have an exponential relationship to strain rate, with bone having a greater strength in compression and in the longitudinal direction. McElhaney found that the stress depends on strain rate according to the following equation:

$$\sigma_u = 29.7 ln\dot{\varepsilon} + 269 \quad (3.2)$$

Behaviour of Young's modulus with strain rate differs between studies. McElhaney found the modulus to increase with increasing strain rate, while results from Crowninshield and Pope show no significant correlation between the two parameters.

McElhaney also found that the strain to failure decreases with increasing strain rate i.e. the bone becomes more brittle. However, Crowninshield and Pope remarked that these results are generally viewed with skepticism since strain gauges were glued to the bone specimens, causing drying of the surfaces. Failure strain is greatly affected by the moisture content of the specimen [47]. Strain results for Crowninshield and Pope exhibited high scatter, believed to be due to imperfections on the specimen surface caused during machining.

3.6.2 Carter and Hayes

Carter and Hayes [13] used human tibial and bovine femoral cancellous bone specimens to investigate the effects of apparent density and strain rate on bone strength. Cancellous bone cylinders with an aspect ratio of 1:4 (5 mm thick with a diameter of 20 mm) were compressed to more than 50% of their original thickness at constant strain rates over the range of 10^{-3} to 10 s^{-1}. Half of the human, and all of the bovine, specimens were tested with the marrow removed. In order to compare the trends of cancellous and cortical bone, data for cortical bone was taken from existing literature (studies by McElhaney [45], Crowninshield and Pope [46], Wright and Hayes [48] and Galante [49]) and is shown on the graphs in Figures 3.4 and 3.5.

The density dependence results (illustrated in Figures 3.4(b) and 3.5(b)) show that strength is proportional to the square of the apparent density and modulus to the cube of apparent density.

Strength and modulus values as a function of density at each of the five strain rate groups are described by power fit curves. Utilising these curves, adjusted values for strength and modulus were determined for a mean density of 0.31 g/cm^3. As demonstrated in Figures 3.4(a) and 3.5(a), both strength and modulus are approximately proportional to the strain rate raised to the 0.06 power.

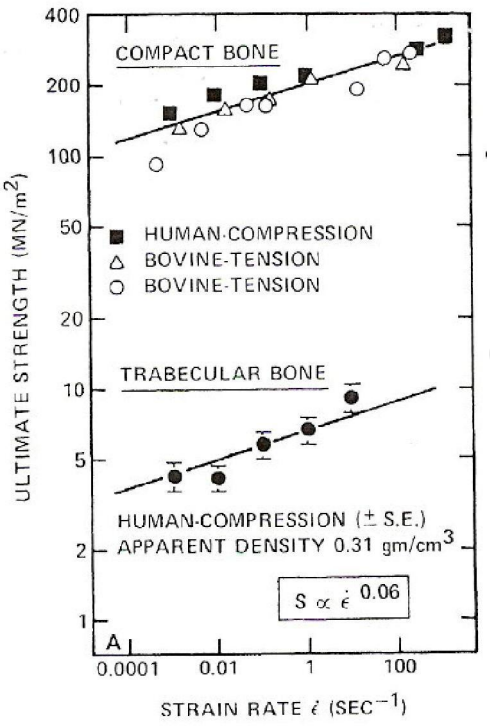

■ Embalmed human compact: McElhaney [45]
□ Bovine compact, tension: Crowninshield and Pope [46]
Δ Bovine compact, tension: Wright and Hayes [48]

(a) Influence of strain rate.

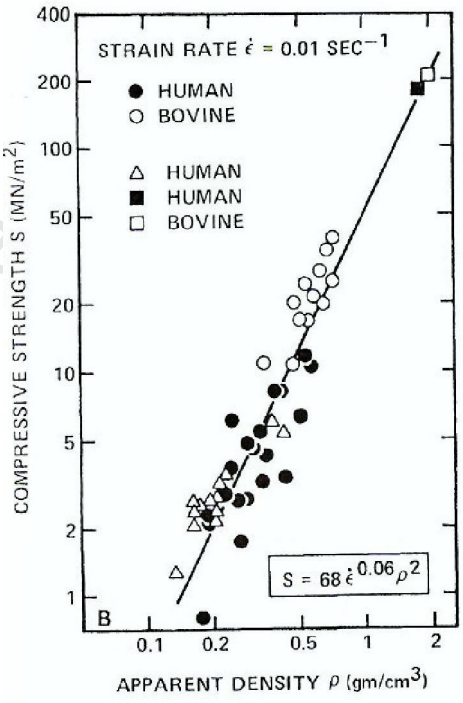

■ Embalmed human compact: McElhaney [45]
□ Bovine compact: McElhaney [45]
Δ Human compact: Galante [49]
● Human trabecular: Carter and Hayes [13]
○ Bovine trabecular: Carter and Hayes [13]

(b) Influence of density.

Figure 3.4: Factors affecting strength of bone: Carter and Hayes [17].

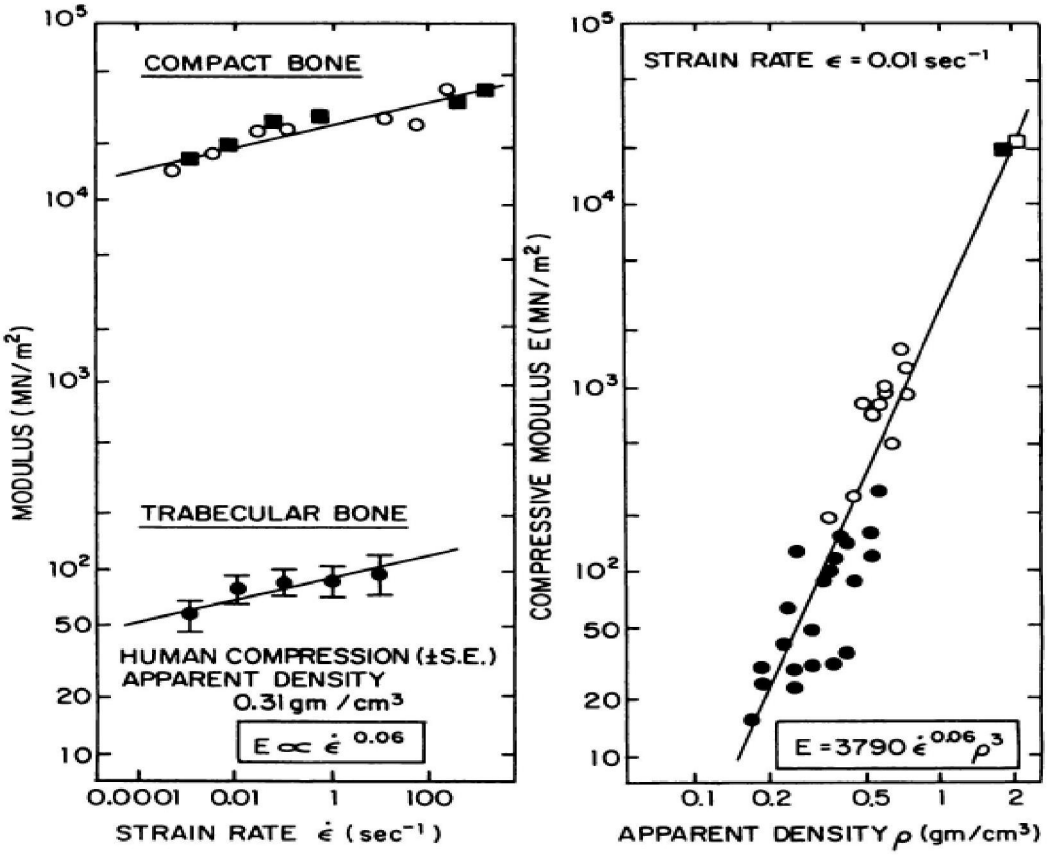

■ Embalmed human compact: McElhaney [45]
● Human trabecular: Carter and Hayes [13]
○ Bovine compact, tension: Wright and Hayes [48]

(a) Influence of strain rate.

■ Embalmed human compact: McElhaney [45]
□ Bovine compact: McElhaney [45]
● Human trabecular: Carter and Hayes [13]
○ Bovine trabecular: Carter and Hayes [13]

(b) Influence of density.

Figure 3.5: Factors affecting modulus of bone: Carter and Hayes [13].

These relationships suggest that strength and modulus vary greatly with apparent density and only slightly with strain rate in both cancellous and cortical bone, according to the following equations:

$$\sigma_u = 68\dot{\varepsilon}^{0.06}\rho_a^2 \quad (3.3)$$

$$E = 3790\dot{\varepsilon}^{0.06}\rho_a^3 \quad (3.4)$$

Results from tests conducted at strain rates below 1 s^{-1} show that the marrow does not significantly affect stiffness or strength results. The specimens tested with the marrow intact at a strain rate of 10 s^{-1} have considerably higher strength and stiffness properties compared to those without marrow.

3.6.3 Morgan and Keaveny

Morgan and Keaveny conducted a study [39] of yield strain dependence on anatomic site, mentioned in section 3.4.4. It shows the following relationship between stress and apparent density of trabecular bone (Figure 3.6):

Vertebra: $\sigma_y = 37.1\rho_a^{1.74}$ (3.5)

Proximal tibia: $\sigma_y = 90.2\rho_a^{2.17}$ (3.6)

Greater trochanter: $\sigma_y = 85.5\rho_a^{2.26}$ (3.7)

Femoral neck: $\sigma_y = 38.5\rho_a^{1.48}$ (3.8)

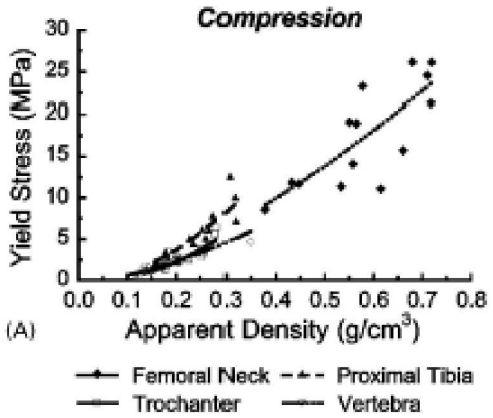

Figure 3.6: Effect of density on yield stress: Morgan and Keaveny [39].

3.6.4 Ouyang

In a study by Ouyang [14], compression tests were performed at different strain rates in order to determine the effects of strain rate, apparent density and tissue density on the elastic modulus, ultimate strength and ultimate strain of human cancellous vertebral bone specimens.

Analysis of results was based on the formula determined by Carter and Hayes (Equation 3.1). Using non-linear curve fit analysis, the results were found to be:

$$E = 2383\rho_a^{1.88}\dot{\varepsilon}^{0.07} \quad (3.9)$$

$$\sigma_u = 7.5\rho_a^{1.29} \quad (3.10)$$

The ultimate strain was found to be 2.55±1.53%. However, there was no significant correlation between ultimate strain and density or strain rate.

3.6.5 Kopperdahl

Kopperdahl [41] investigated the density dependence of the mechanical properties, in particular yield strain, on cancellous bone samples tested in compression and tension. Quasi-static uniaxial compression tests were performed on low apparent density specimens (0.18 g/cm^3) of human vertebral bone. Yield stress and elastic modulus both exhibited strong positive correlations with density (Figure 3.7):

$$\sigma_y = 32.6\rho_a^{1.6} \quad (3.11)$$

$$E = 2100\rho_a - 80 \quad (3.12)$$

The results for human vertebral specimens were compared to those of a previous study on high apparent density (0.51 g/cm^3) bovine tibial bone. The tensile tests showed that yield strain is independent of apparent density across the density range. Compression testing showed yield strain to have a strong positive linear correlation to density at low densities (human bone), shown by equation 3.13. The high-density data (bovine specimens) showed a far weaker correlation.

$$\varepsilon_y = 0.66\rho_a + 1.09 \quad (3.13)$$

Kopperdahl hypothesised that the weak density dependence of yield strain of cancellous bone in compression may not be detected statistically due to high scatter in the data. This theory is used as an explanation why studies based on small sample sizes report no significant relationship between strain and density, while those with more specimens do show a relationship.

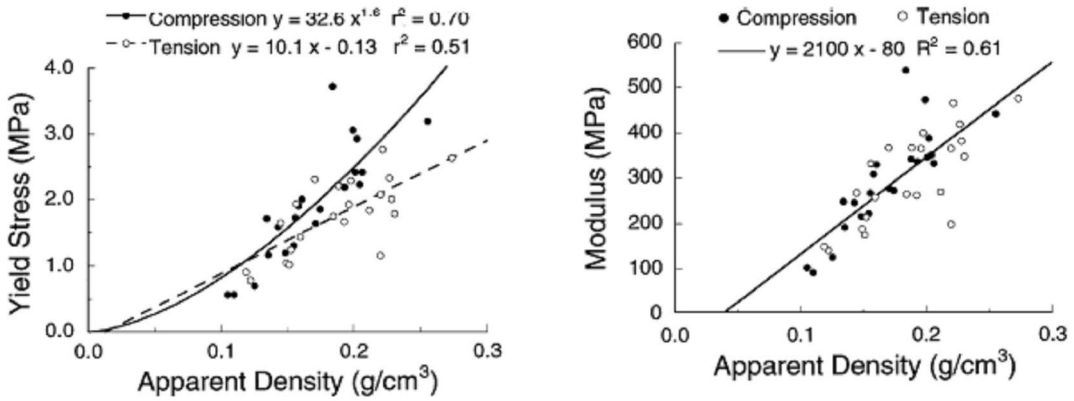

Figure 3.7: Influence of density on mechanical properties: Kopperdahl [41].

3.6.6 Shim

A study by Shim [1] investigated the mechanical properties of cancellous bone by subjecting 5x5x8 mm samples from the human cervical spine to either quasi-static or dynamic compression. Quasi-static compression testing was conducted at a strain rate of 10^{-3} s^{-1}, while strain rates for dynamic testing were in the range of 10^2 to 10^3 s^{-1}. These tests were performed on a split Hopkinson pressure bar equipped with magnesium bars.

The quasi-static compressive stress and elastic modulus are shown to increase with fresh bone density according to the following power law functions, illustrated in Figures 3.8 and 3.9:

$$\sigma_y = 5.09\ \rho^{2.35} \quad (3.14)$$

$$E = 242\rho^{1.95} \quad (3.15)$$

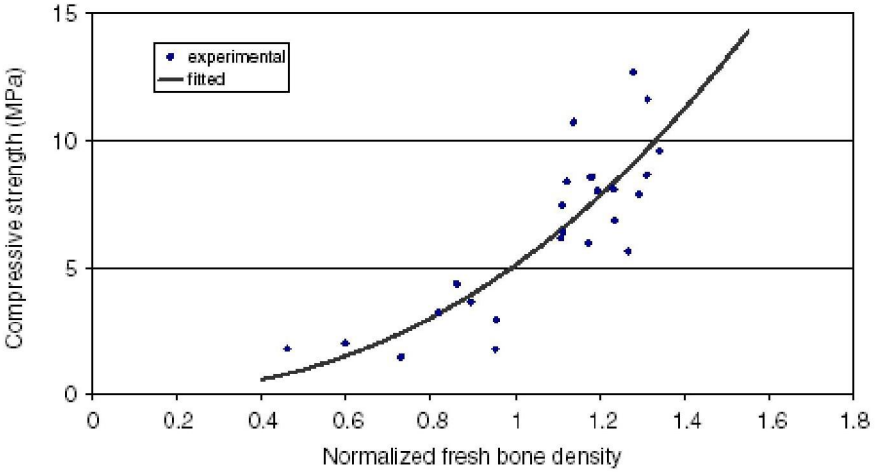

Figure 3.8: The effect of density on strength: Shim [1].

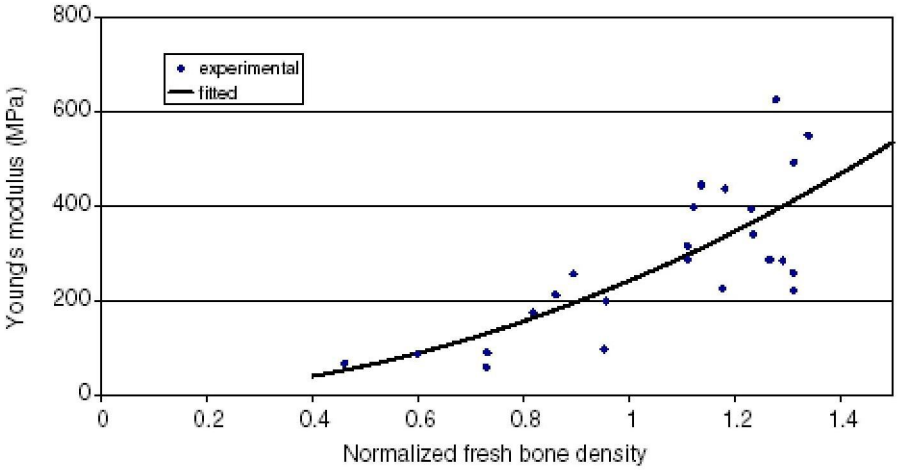

Figure 3.9: The effect of density on modulus: Shim [1].

It was found that, although the bone strength increases with both density and strain rate, the relationship between these parameters was not immediately apparent. The difference between the static and dynamic strengths was explored and plotted as a function of strain rate, yielding a power law function of the form:

$$(\sigma_y^d - \sigma_y^{qs}) = 0.545\dot{\varepsilon}^{0.45}$$

On substitution of equation 3.14, an expression for dynamic strength was determined as:

$$\sigma_y^d = 5.09\rho^{2.35} + 0.545\dot{\varepsilon}^{0.45} \quad (3.16)$$

The first term highlights the dependence of strength on density and the second shows the contribution of strain rate to compressive strength.

Table 3.1 summarises the trends of mechanical properties of bone as a function of density and strain rate discussed in this section. Included are studies by Linde [50, 55], Lotz [51], Hansson [52], Mosekilde [53], Dalstra [56] and Li and Aspden [57]. The units for stress and stiffness are MPa. Density is measured in g/cm^3 and strain rate in s^{-1}.

Table 3.1: Trends of mechanical properties of bone.

Bone type	y	$y = ax^b\dot{\varepsilon}^c$				y = ax + b			r^2	Ref.
		x	a	b	c	x	a	b		
Cortical, trabecular	σ_u	ρ_a	68	2	0.06				-	Carter, Hayes [13]
Cortical, trabecular	E	ρ_a	3790	3	0.06				-	Carter, Hayes [13]
Trabecular	σ_y	ρ_a	37.1	1.74	0				0.80	Morgan, Keaveny [39]
Trabecular	σ_y	ρ_a	90.2	2.17	0				0.90	Morgan, Keaveny [39]
Trabecular	σ_y	ρ_a	85.5	2.26	0				0.92	Morgan, Keaveny [39]
Trabecular	σ_y	ρ_a	38.5	1.48	0				0.62	Morgan, Keaveny [39]
Trabecular	σ_u	ρ_a	7.5	1.29	0				-	Ouyang [14]
Trabecular	E	ρ_a	2383	1.88	0.07				-	Ouyang [14]
Trabecular	σ_y	ρ_a	32.6	1.6	0				0.7	Kopperdahl [41]
Trabecular	E					ρ_a	2100	-80	0.61	Kopperdahl [41]
Trabecular	ε_y					ρ_a	0.66	1.09	0.49	Kopperdahl [41]
Trabecular	σ_y	ρ	5.09	2.35	0				-	Shim [1]
Trabecular	E	ρ	242	1.95	0				-	Shim [1]
Trabecular	σ_u	ρ_a	34.2	1.56	0				0.79	Linde [50]
Trabecular	σ_u	ρ_a	25.0	1.80	0				0.93	Lotz [51]
Trabecular	σ_u	ρ_a	50.3	2.24	0				0.76	Hansson [52]
Trabecular	σ_u	ρ_a	24.9	1.80	0				0.83	Mosekilde [53]
Trabecular	E	ρ_a	4.78	1.99	0				-	Linde [55]
Trabecular	E	ρ_a	2.02	2.46	0				0.58	Dalstra [56]
Trabecular	E					ρ_a	0.573	-0.009	0.59	Li, Aspden [57]

3.7 Mechanical properties at varying strain rates

3.7.1 Guedes

Guedes et al. [58] performed compression tests on fresh bovine femoral bone specimens. Cubic cancellous specimens (10x10x10 mm^3) were compressed at four different quasi-static strain rates (0.15 s^{-1}, 0.015 s^{-1}, 0.0015 s^{-1}, 0.00015 s^{-1}). At least ten specimens were tested at each strain rate and the specimens were tested at the same time. The experimental stress-strain curve (Figure 3.10) shows that the bone undergoes structural collapse as opposed to failure and thereafter maintains a residual stiffness. The experimental results exhibit high scatter.

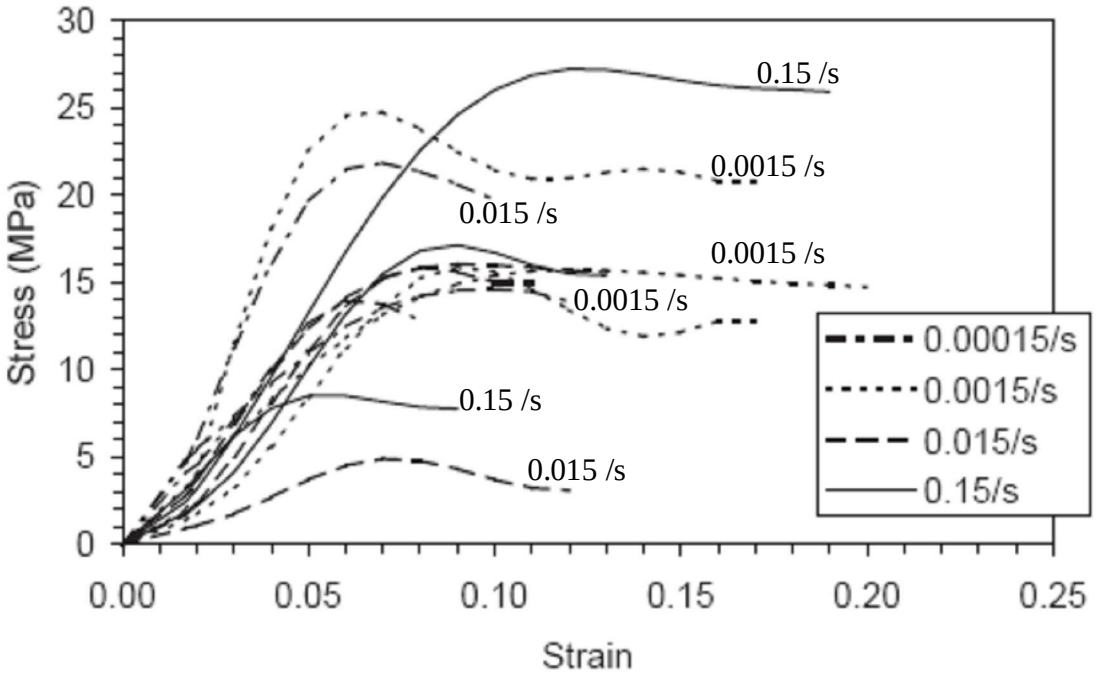

Figure 3.10: Stress-strain curves of bovine cancellous bone: Guedes [58].

3.7.2 Shim

Typical stress-strain curves derived from Shim's cancellous bone study (mentioned in section 3.6.6) are shown in Figures 3.11 and 3.12 for quasi-static and dynamic testing respectively. In both sets of tests, the failure stress is defined as the value 5% below the ultimate compressive stress.

Results of quasi-static testing at a strain rate of 10^{-3} s^{-1} show that the bone behaves in a linear elastic manner prior to failure, while the dynamic curves exhibit nonlinearity throughout. This non-linearity may be attributed to the viscoelastic nature of bone. In quasi-static tests, the strain rate is relatively constant, while the dynamic tests show a variation of strain rate throughout each test. Since the mechanical properties are dependent on strain rate, this may account for the non-linear behavior of the stress-strain curve prior to yield.

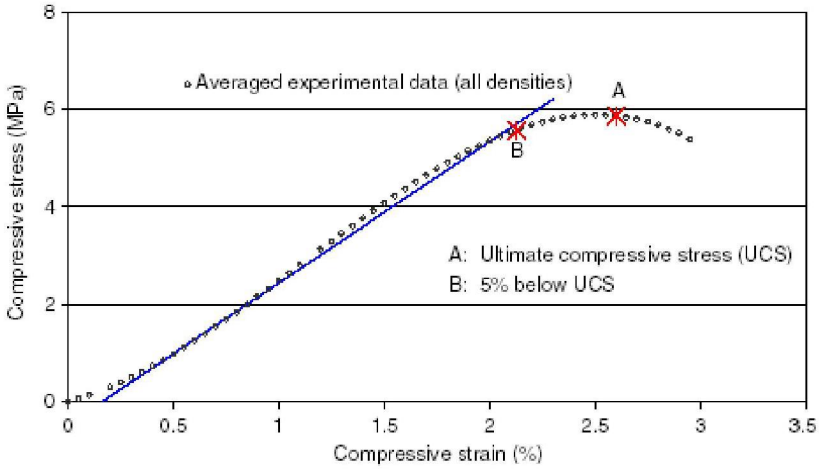

Figure 3.11: Quasi-static stress-strain curve: Shim [1].

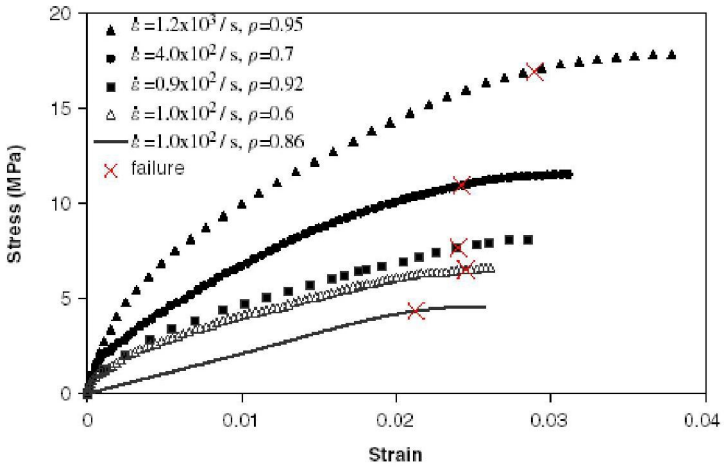

Figure 3.12: Dynamic stress-strain curves: Shim [1].

Table 3.2 compares the mechanical properties of cancellous bone determined in the above-mentioned investigations. Results from various other studies, namely Bayraktar [43], Schoenfeld [59], Oldgaard [60], Sierpowska [61], Tao [62] and Hakulinen [63] are included.

Table 3.2: Comparison of experimentally determined mechanical properties of cancellous bone in quasi-static compression.

Bone source	Bone type	Strain rate $\dot{\varepsilon}$	Apparent density ρ (g/ cm^3)	Young's Modulus E (MPa)	Yield strength σ (MPa)	Yield strain (%)	Reference
Human	Vertebra	0.005		322 ± 134	2.11 ± 0.97	0.85 ± 0.06	Morgan [38]
Human	Tibia	0.005		1058 ± 598	6.25 ± 3.45	0.80 ± 0.05	Morgan [38]
Human	Femur	0.005		564 ± 282	3.37 ± 1.91	0.78 ± 0.05	Morgan [38]
Bovine	Tibia	0.005		1795 ± 581	13.8 ± 4.93	0.97 ± 0.05	Morgan [38]
Human	Vertebra	0.005	0.18 ± 0.05	344 ± 148	2.02 ± 0.92	0.77 ± 0.06	Morgan [39]
Human	Tibia	0.005	0.23 ± 0.06	1091 ± 634	5.83 ± 3.42	0.73 ± 0.06	Morgan [39]
Human	Trochanter	0.005	0.22 ± 0.05	622 ± 302	3.21 ± 1.83	0.70 ± 0.05	Morgan [39]
Human	Femoral neck	0.005	0.58 ± 0.11	3230 ± 936	17.45 ± 6.15	0.85 ± 0.10	Morgan [39]
Human	Vertebra	0.005	0.17 ± 0.04	291 ± 113	1.92 ± 0.84	0.84 ± 0.06	Kopperdahl [41]
Human	Femoral neck	0.005	0.62 ± 0.09	18000 ± 2800	135.3 ± 34.3	1.04 ± 0.15	Bayraktar [43]
Bovine	Femoral neck	0.15	1.06 ± 0.09	310 ± 161	15.74 ± 9.57*	8.62 ± 2.16*	Guedes [58]
Bovine	Femoral neck	0.015	1.00 ± 0.13	190 ± 145	9.36 ± 6.5*	9.07 ± 3.39*	Guedes [58]
Bovine	Femoral neck	0.0015	1.05 ± 0.11	364 ± 201	15.73 ± 5.35*	8.23 ± 2.06*	Guedes [58]
Bovine	Femoral neck	0.00015	1.02 ± 0.11	306 ± 158	12.36 ± 5.65*	7.1 ± 2.1*	Guedes [58]
Human	Femoral head	0.0044		345	0.15-13.7		Schoenfeld [59]
Human	Tibia	5.9 x 10^{-5}		689-871	3.45		Oldgaard [60]
Human	Femur	0.0045	0.237 ± 0.066	624.4 ± 213.9	10.2 ± 4.0	2.1 ± 0.5	Sierpowska [61]
Human	Tibia	0.0045	0.213 ± 0.07	575.3 ± 178.7	9.0 ± 3.7	1.9 ± 0.3	Sierpowska [61]
Bovine	Femur	3.5 x 10^{-4}	0.418 ± 0.158	1200 ± 800	12.4 ± 7.3		Sierpowska [36]
Porcine	Vertebra	0.01		229 ± 138	13 ± 7	0.16 ± 0.12	Tao [62]
Human	Femur, tibia	4.5 x 10^{-3}		600 ± 194	10.2 ± 4.0*		Hakulinen [63]
Human	Proximal tibia	0.002	0.46 ± 0.12	635 ± 386	8.82 ± 3.5*	2.22 ± 0.67*	Ding [19]

* Refers to ultimate, not yield, property.

3.8 Viscoelastic behaviour

A viscoelastic material is one in which the behaviour is characterised by both elasticity and viscosity i.e. it has the properties of a linear elastic solid combined with a viscous fluid.

In the study by Shim [1], discussed in sections 3.6.6 and 3.7.2, a viscoelastic material model was developed to describe the mechanical behaviour of cancellous bone. This model incorporates two terms, one derived from linear elasticity and the other a function of nonlinear viscoelasticity, such that:

$$\sigma = \sigma^e + \sigma^v$$

The linear elastic term (σ^e) highlights the bone strength dependence on density and is derived from quasi-static testing, as discussed in section 3.6.6:

$$\sigma^e = E_0 \rho^b \varepsilon \tag{3.17}$$

The viscoelastic term (σ^v) is modeled as a Maxwell element in parallel with a nonlinear Newtonian dashpot, which yields the following equation (the derivation of which is shown in Appendix A):

$$\sigma^v = \int_0^t c_1 \dot{\varepsilon}(\tau) \exp\left(-\frac{t-\tau}{\theta}\right) d\tau + \eta \dot{\varepsilon}^{1/2} \tag{3.18}$$

where c_1 is the stiffness modulus, θ the relaxation time of the Maxwell model and η the viscosity. These material parameters are solved for via least squares fitting, using the dynamic test data.

Therefore, the one dimensional viscoelastic model can be expressed as:

$$\sigma = E_0 \rho^b \varepsilon + \int_0^t c_1 \dot{\varepsilon}(\tau) \exp\left(-\frac{t-\tau}{\theta}\right) d\tau + \eta \dot{\varepsilon}^{1/2} \tag{3.19}$$

or:

$$\sigma = 242\rho^{1.95}\varepsilon + \int_0^{\tau} 354\,\dot{\varepsilon}(\tau)\exp\left(-\frac{t-\tau}{5.5\text{x}10^{-5}}\right)d\tau + 0.122\dot{\varepsilon}^{1/2}$$

The strength of the model is illustrated in Figure 3.13, where the fitted curves are plotted against the experimental data. The predicted failure points are calculated from equation 3.16:

$$\sigma_y^d = 5.09\rho^{2.35} + 0.545\dot{\varepsilon}^{0.45} \qquad (3.16)$$

Shim concludes that his model is able to adequately describe the mechanical behaviour of cancellous bone at high strain rates.

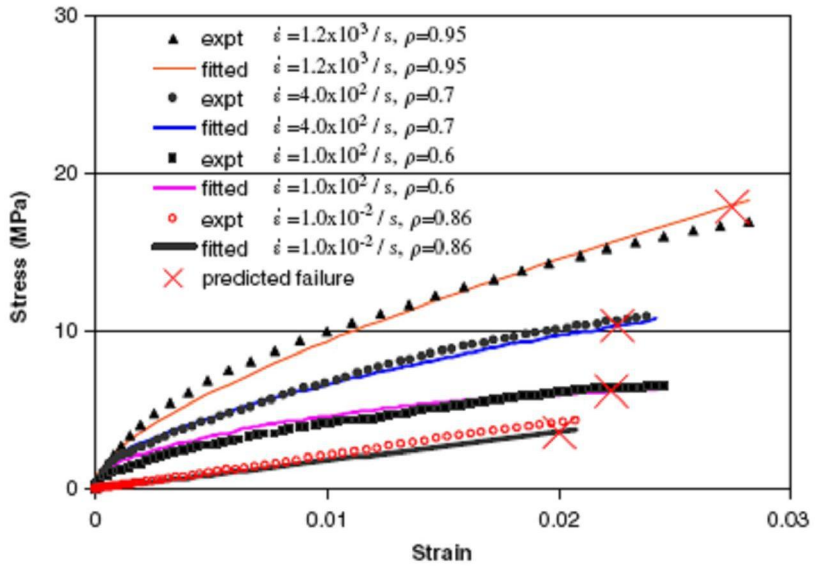

Figure 3.13: Comparison between experimental data and fitted curves [1].

3.9 Summary

Bone is an anisotropic composite material whose mechanical properties are dependent on its environment. The response of bone during mechanical testing is influenced by bone age, type, composition and stress history, specimen preparation and geometry as well as the testing conditions [7]. Therefore results exhibit high scatter.

Many of the studies reviewed show the strength and modulus of bone to be dependent on density and, to a lesser extent, strain rate. The majority of these studies show the dependence to have an exponential relationship in the form of:

$$y = a\rho_a^b \dot{\varepsilon}^c \tag{3.1}$$

where "a" varies from 5 to 90 for strength and 2 to 3800 for modulus of trabecular bone. The range of "b" values for strength and modulus are 1.3 to 2.35 and 1.95 to 3 respectively. In studies that show a strain rate dependence of mechanical properties, "c" values for both strength and modulus are 0.06 to 0.07.

Generally, failure strain is shown to have no dependence on density. However, Kopperdahl [41] hypothesised that if the relationship is weak it may not be detected due to high scatter in the results. Therefore density dependent strain results may be overlooked in investigations with a small sample size.

Shim [1] developed a viscoelastic material model to characterise cancellous bone behaviour. It incorporates two terms, the first derived from linear elasticity (using quasi-static data) and second a function of nonlinear viscoelasticity (using dynamic data) such that:

$$\sigma = 242\rho^{1.95}\varepsilon + \int_0^t 354\,\dot{\varepsilon}(\tau)\exp\left(-\frac{t-\tau}{5.6\times10^{-3}}\right)d\tau + 0.122\dot{\varepsilon}^{1/2} \tag{3.19}$$

The failure stress is predicted by:

$$\sigma_y^d = 5.09\rho^{2.35} + 0.545\dot{\varepsilon}^{0.45} \tag{3.16}$$

This model shows good correlation between the fitted and the experimental data and can therefore be used to describe the mechanical behaviour of cancellous bone.

4 SPLIT HOPKINSON PRESSURE BAR

4.1 Introduction

The split Hopkinson pressure bar (SHPB) test is the most widely used method of materials characterisation at high strain rates. It is typically used for compression testing up to strain rates of 10^4 s^{-1}. However, modifications to the apparatus have resulted in its use for testing in other loading modes.

4.2 SHPB history

The design of the split Hopkinson pressure bar is largely based on the work of three main contributors, namely Hopkinson, Davies and Kolsky [64].

In 1914, Hopkinson developed a pressure measuring device known as the Hopkinson pressure bar. Its function was to characterise materials using dynamic testing in the form of bullet impact and explosion detonation.

In 1948, Davies added electrical condenser units to the Hopkinson bar apparatus to record wave propagation in the pressure bar. In addition to improving the accuracy of the original apparatus, Davies also published a critical review of the Hopkinson bar.

In 1949, Kolsky modified the Hopkinson pressure bar by adding an extension bar so that the specimen was sandwiched between the pressure and extension bars. This set-up is now known as the split Hopkinson pressure bar. Kolsky used this technique to investigate the stress-strain response of various materials to dynamic compression.

Over the years, research into the SHPB has continued and experimental methods have been improved upon. The SHPB has also been modified in a number of ways in order to test loading modes other than compression, i.e. tension, torsion, bending and shear.

4.3 SHPB apparatus

The apparatus, shown in Figure 4.1, consists of the following main components:

- A compressed air gas gun to propel the striker bar
- A striker bar
- Two long symmetrical pressure bars (input and output), between which the specimen is sandwiched. The bars are made from the same material with a uniform cross-sectional area.
- Strain gauges, one mounted on each pressure bar, to record the strain histories of the bars.
- Data aquisition system to record test results in the form of stress waves.

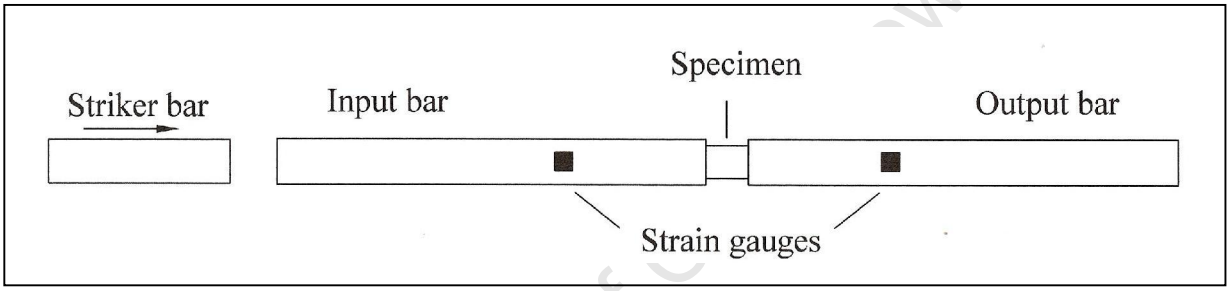

Figure 4.1: Schematic drawing of the Hopkinson bar set-up.

4.4 Test procedure

The striker bar is fired into the end of the input bar. This impact generates an elastic strain wave, known as the incident wave, which travels along the bar assembly. When it reaches the specimen, part of the wave, known as the transmitted wave, will continue through the output bar. The remaining part of the wave will be reflected back along on the input bar. The amplitudes of the transmitted and reflected waves are dependent on the plastic deformation of the specimen.

4.5 SHPB governing equations

The equations governing the split Hopkinson bar experiments are based on the assumption that the pressure bars are homogeneous and isotropic, with a uniform cross-sectional area, and undergo only

elastic deformation. One-dimensional wave propagation theory is used to determine the stress-strain behaviour of the specimen.

The one-dimensional wave equation applicable to waves traveling in bars is [64]:

$$\frac{\partial^2 u}{\partial x^2} - \frac{1}{c^2}\frac{\partial^2 u}{\partial t^2} \tag{4.1}$$

of which the solution is:

$$u = f(x - ct) + g(x + ct) = u_i + u_r \tag{4.2}$$

for the input bar, where the subscripts "i" and "r" refer to the incident and reflective waves respectfully (shown in Figure 4.2). The transmitted wave is denoted by the subscript "t".

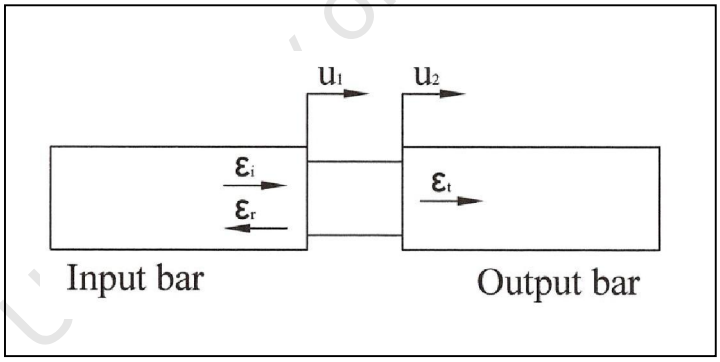

Figure 4.2: Direction of waves in the pressure bars

By definition, the strain is:

$$\varepsilon = \frac{\partial u}{\partial x} \tag{4.3}$$

Therefore the strain is determined by differentiating equation 4.2 with respect to x:

$$\varepsilon = \dot{f}+\dot{g} = \varepsilon_i + \varepsilon_r \tag{4.4}$$

Differentiating equation 4.2 with respect to time yields the velocities of the input and output bars:

$$\dot{u}_1 = c\left(-\dot{f} + \dot{g}\right) = c(-\varepsilon_i + \varepsilon_r) \tag{4.5}$$

$$\dot{u}_2 = c\varepsilon_t \tag{4.6}$$

where the subscripts "1" and "2" refer to the input and output bars respectively.

These velocities are applicable at the specimen-bar interface and the strain rate of the specimen is therefore determined from the following equation:

$$\dot{\varepsilon} = \frac{(\dot{u}_1 - \dot{u}_2)}{L_s} \tag{4.7}$$

where L_s is the instantaneous length of the specimen.

Substitution of equations 4.5 and 4.6 gives the following expression for strain rate:

$$\dot{\varepsilon} = \frac{c(-\varepsilon_i+\varepsilon_r+\varepsilon_t)}{L_s} \tag{4.8}$$

The forces in the input and output bars are:

$$F_1 = A_B E_B(\varepsilon_i + \varepsilon_r) \tag{4.9}$$

$$F_2 = A_B E_B \varepsilon_t \tag{4.10}$$

where A_B is the cross-sectional area and E_B is the Young's modulus of the pressure bars.

It is assumed that, after an initial period, the specimen is in dynamic equilibrium i.e. the forces at each bar/specimen interface are equal. The assumption of stress uniformity is only valid after an initial period during which the stress pulse must reverberate between the ends of the specimen approximately three times [24]. Soft materials, such as cancellous bone, have a low wave speed, which means that the transit time in the specimen is long and dynamic equilibrium cannot be reached quickly, relative to harder materials. Therefore, the utilisation of thin specimens should justify the assumption of dynamic equilibrium in soft materials.

Therefore:

$$\varepsilon_i + \varepsilon_r = \varepsilon_t \tag{4.11}$$

The strain rate in the specimen is determined by substituting equation 4.11 into 4.8:

$$\dot{\varepsilon} = \frac{2c\varepsilon_r}{L_s} \tag{4.12}$$

The true strain in the specimen is:

$$\varepsilon = \frac{2c\varepsilon_r}{L_s} \int \varepsilon_r dt \tag{4.13}$$

The true stress in the specimen is determined by dividing the force in the specimen (equation 4.10) by its instantaneous cross-sectional area:

$$\sigma = \frac{A_B E_B \varepsilon_t}{A_s} \tag{4.14}$$

By using equations 4.13 and 4.14, it is possible to determine the stress-strain curves and therefore characterise materials at high strain rates by using the Hopkinson bar.

4.6 Assumptions of a valid SHPB test

The following conditions need to be met to ensure the validity of the testing procedure:

- Stress wave propagation in the bar is 1D:
  This is achieved by ensuring that the bars are homogeneous and isotropic with a uniform cross-sectional area and a straight neutral axis; the stress in the bars remains below the elastic limit and is uniformly distributed over the entire cross-section; the bars are fee of dispersion effects.
- The specimen-bar interfaces remain plane during testing
- The specimen is in stress equilibrium after an initial ‘‘ringing-up’’ period
- The specimen is not compressible
- There are minimal friction and inertia effects:
  These effects can be decreased by using lubricant at the specimen-bar interfaces.

5 EXPERIMENTAL PROCEDURE

5.1 Test specimen preparation and preservation

The specimens used for testing were sourced from the vertebrae of bovine of slaughtering age. The vertebrae were chosen, as opposed to other cancellous bone sites, because the orientation with the highest stiffness and strength properties is generally aligned with the spine. In other sites, such as at the ends of long bones, the orientation of the trabeculae needs to be determined by other means in order to ensure uniformity in testing conditions.

The bovine spinal column consists of five sections, namely the cervical, thoracic, lumbar, sacral and coccygeal vertebrae (Figure 5.1).

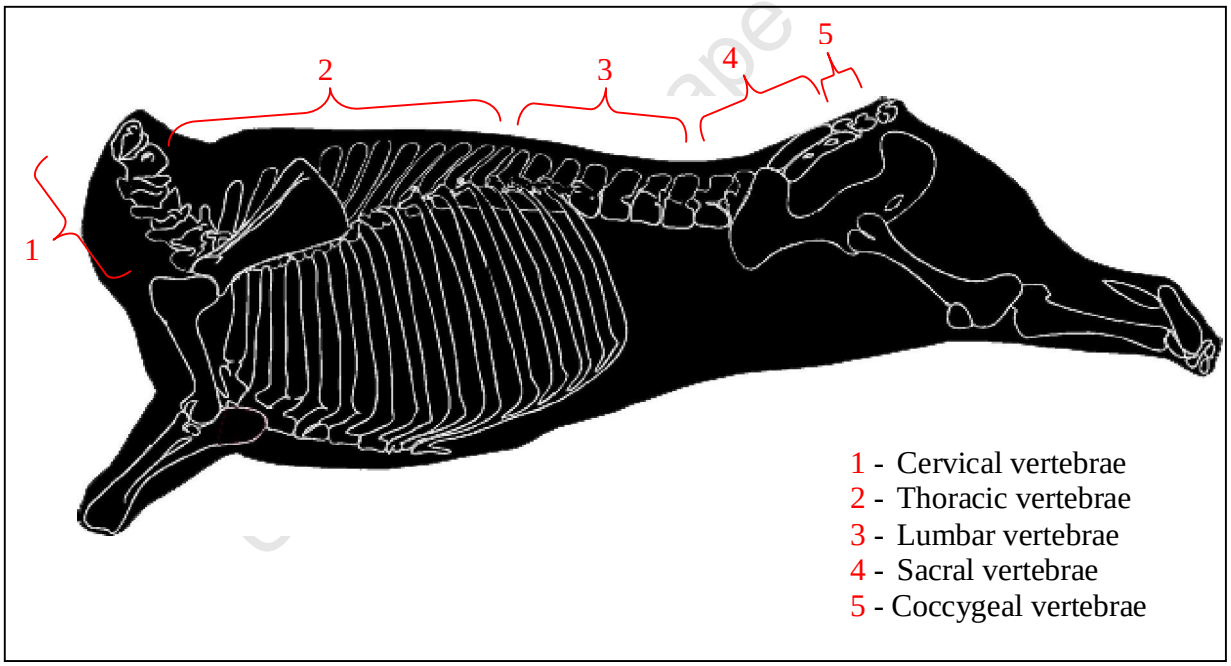

Figure 5.1: Bovine skeleton showing vertebrae [65]

Fresh whole thoracic vertebrae bones were obtained from the butcher and were machined to produce trabecular bone specimens such that the dimension correlating to the axis of applied stress during testing was aligned with the axis of the spine. For quasi-static tests, the nominal dimensions are 10 mm high and 5 mm in diameter (Figure 5.2). This is in accordance with the dimension recommended

in the literature for compression testing of cancellous bone, i.e. minimum height of 10 mm with an aspect ratio of 2:1 [16, 17]. The dynamic tests utilised specimens of 10 mm diameter and 5 mm length, giving an aspect (L/d) ratio of 0.5, as recommended by Hunter and Davis [26].

For both these geometries, the continuum assumption is valid, since the smaller dimension is an order of magnitude greater than the individual trabeculae thickness found in a vertebra, as measured by Singh [10]. Although the measurements were recorded for human bone, it is assumed that bovine bone does not differ greatly in terms of trabeculae thickness. The smallest dimension is also larger than 4 mm and therefore follows the criteria for continuum [20].

The bones were frozen at –20 °C for a period of no longer than 60 days from the time of slaughter. During this time, the bones did not undergo any treatments which would affect the mechanical properties. Prior to testing, the specimens were soaked in water for approximately 30 hours in order to rehydrate.

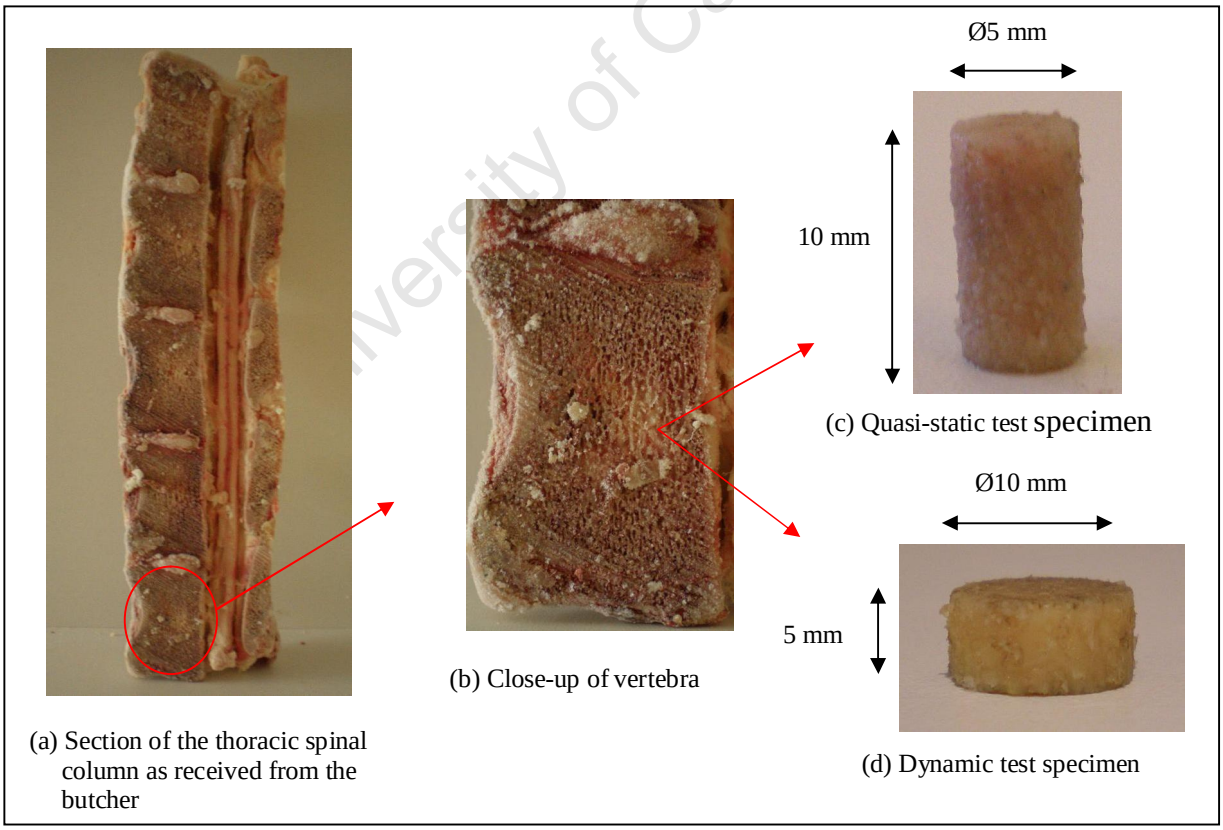

Figure 5.2: Bovine vertebral bone test specimens

5.2 Test specimen properties

The cancellous bone specimens were cut from six different animals and a total of twenty vertebrae. For each specimen, the initial volume was determined by measuring the lengths and diameters by means of a micrometer. The specimens were weighed prior to testing to include the mass of the blood and fat contained naturally in the bone. These masses were then used in conjunction with the recorded dimensions to determine the fresh bone densities of the test specimens, as shown in Table 5.1. In terms of comparison with the literature reviewed, it would be desirable to work with the apparent density. However, this is not possible since the formula requires the mass of the specimen after testing. During dynamic testing the specimens break into a number of small fragments, which makes this difficult.

Table 5.1: Calculated average fresh bone densities of test specimens at each strain rate

Strain rate (/s)	10^{-4}	10^{-3}	10^{-2}	10^{-1}	Dynamic
Density (g /cm^3):					
Mean ± standard deviation	1.38±0.073	1.39±0.091	1.41±0.095	1.40±0.1	1.33±0.1
Range	(1.26-1.49)	(1.20-1.50)	(1.23-1.59)	(1.24-1.65)	(1.10-1.49)

Specimens are labeled according to the bovine and vertebrae from which they are sourced, e.g. specimen number 1.2.3 implies that it is the first bovine, second vertebrae and third specimen.

5.3 Factors affecting properties of bone

There are three main factors that will determine the yield point of the bone specimens, namely:

- Bone density
- Bone microstructure
- Strain rate at which tests are conducted

According to the literature, density has a considerably larger effect on the mechanical properties than strain rate (typically, power law exponents are 2 and 0.06 for density and strain rate respectively) [13]. Without a full investigation into the microstructure of the five bones used in this study, it is not possible to determine the extent to which it affects results. However, for the purposes of this study, it assumed that the microstructure of each bone is similar.

5.4 Quasi-static testing

5.4.1 Test apparatus

The Zwick Universal Testing Machine with displacement control (Figure 5.3) was used in its compression mode to perform the quasi-static tests at user-defined crosshead speeds. Results of the tests determined by the 200 kN built-in load-cell are in the form of load-deflection curves, which can be used to extract the required data.

5.4.2 Test procedure

The specimen is placed upright on the lower plate and left unconstrained. The bottom plate is driven upwards until the top plate is almost in contact with the surface of the specimen. The bottom plate moves upwards at a prescribed velocity, which is determined by the required strain rate. The specimen undergoes uniaxial compression until such time that the test is stopped either automatically by meeting a set condition, or manually (Figure 5.4).

Tests were performed at four different strain rates, nominally 10^{-4}, 10^{-3}, 10^{-2} and 10^{-1} s^{-1}. Each strain rate group comprised specimens from three bovine bones. Seventeen destructive tests were performed at each strain rate. Fifteen of these tests were continued beyond the ultimate stress point to a strain of approximately 0.2 in order to observe the post-yield mechanical behaviour of bone. The other two tests were stopped manually as the ultimate stress point was reached. This was done in order to compare the microstructure of these specimens to those of the 0.2 strain specimens.

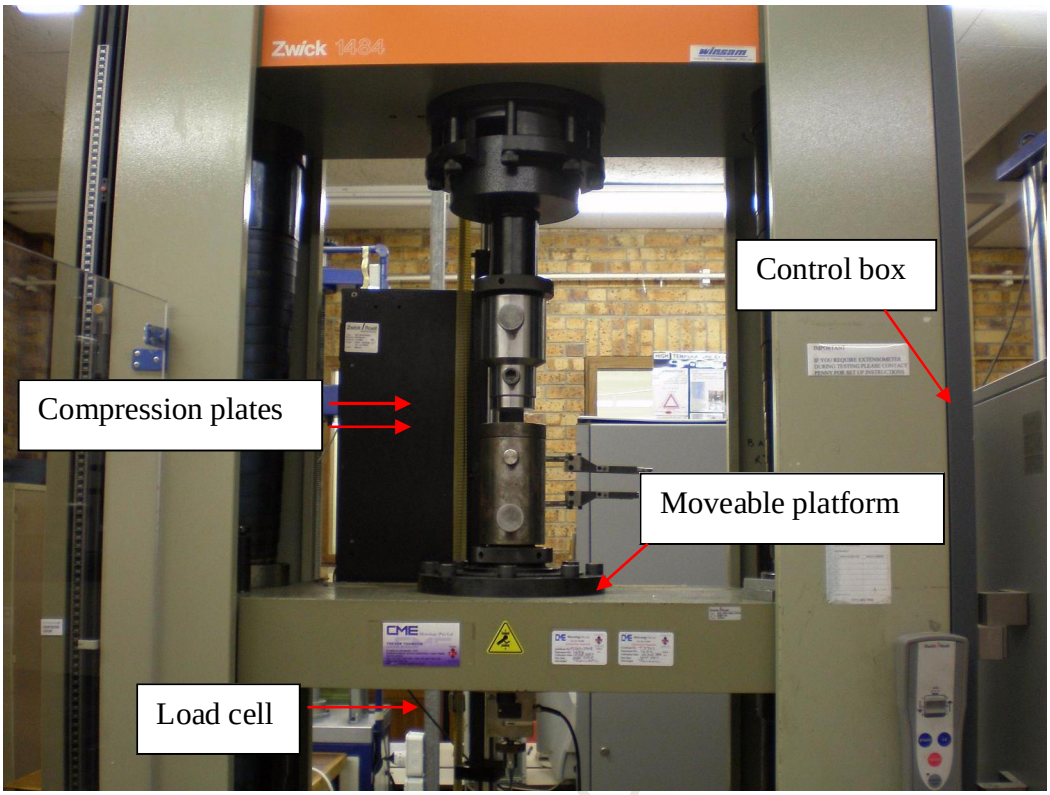

Figure 5.3: The Zwick Universal Testing Machine

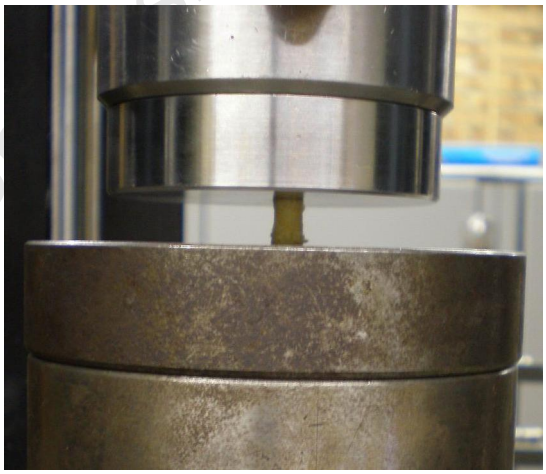

Figure 5.4: Specimen during testing

One specimen was compressed at a strain rate of 10^{-2} s^{-1} until total destruction, occurring in the region of 75% strain. This test was performed so that the entire stress-strain curve of cancellous bone in compression could be viewed.

5.5 Dynamic testing

The Split Hopkinson Pressure Bar is used to characterise materials at high strain rates. In this case, cancellous bone is tested at strain rates ranging from 828 to 1860 s^{-1}, where the strain rate is defined as the maximum strain rate before ultimate compressive stress is reached.

5.5.1 Test apparatus

The apparatus is described in detail in Chapter 4 and the system used in these tests is as shown in Figures 5.5 and 5.6.

Cancellous bone has a low mechanical impedance compared to the steel bars traditionally used for Hopkinson bar testing and will therefore produce a poor signal if these bars are used. For this reason, magnesium strikers and pressure bars are used. The properties of magnesium (E = 42.2 GPa, ρ = 1758 kg/m^3 and c = 4900 m/s, derived in Appendix B) are such that a good transmission signal will be recorded during testing. The input and output bars are identical, each being 1.998 m long with a diameter of 19.95 mm. The striker is 500 mm in length and 19.95 mm in diameter.

Strain gauges are mounted on the input and output bars at a distance of 0.988 m from the specimen/bar interface.

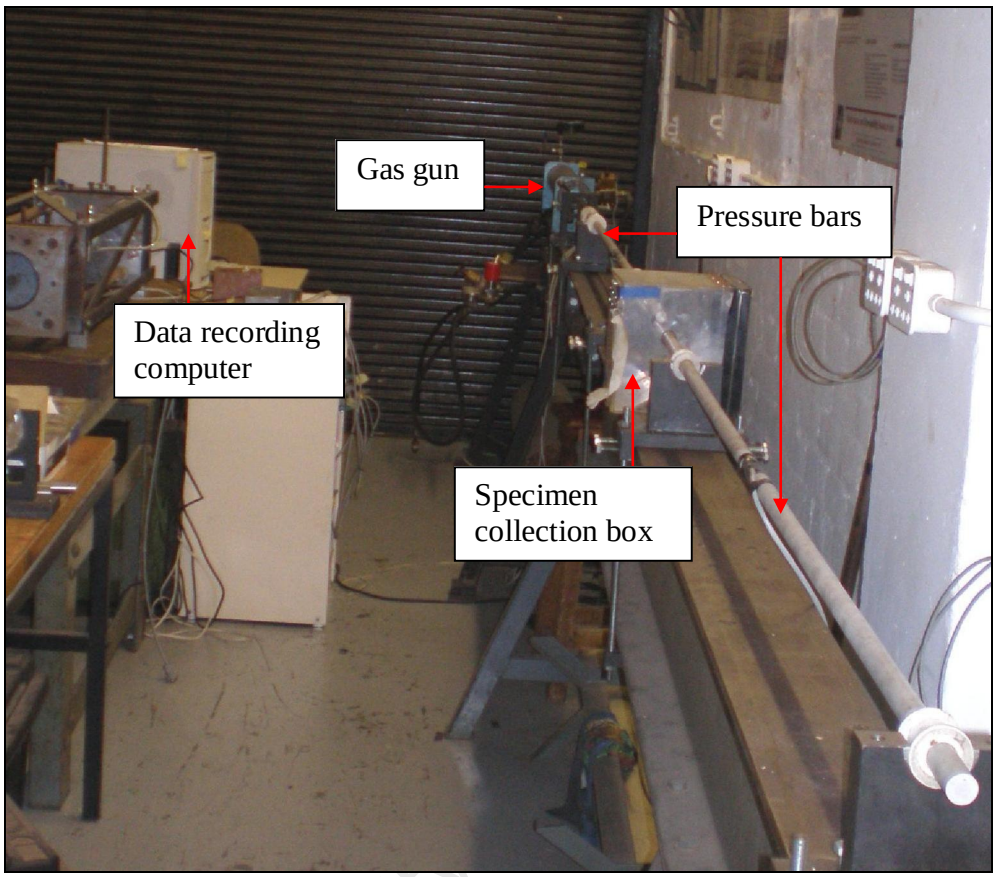

Figure 5.5: The Split Hopkinson Pressure Bar

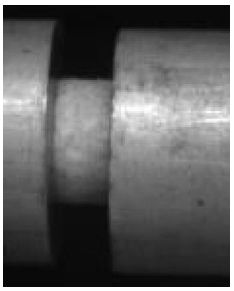

Figure 5.6: Specimen during testing

6 QUASI-STATIC RESULTS AND ANALYSIS

6.1 Stress-strain behaviour

6.1.1 Typical stress-strain behaviour

A typical stress-stress curve derived from testing is shown to the point of ultimate stress in Figure 6.1 and to total destruction in Figure 6.2. It comprises five main sections, namely:

- I – Initial non-linear region as a result of the specimen faces not being parallel and due to the end artifact (Figure 6.1).
- II – Linear elastic region to the yield point (Figure 6.1).
- III – Non-linear increase in stress until a peak compressive stress is reached (Figure 6.1).
- IV– Slight decrease in stress to a roughly constant stress region during which successive trabeculae fail and pores collapse (Figure 6.2).
- V– Densification as broken trabeculae make contact and stiffness increases sharply. This generally occurs after the specimen has been compressed to approximately half its original height (Figure 6.2).

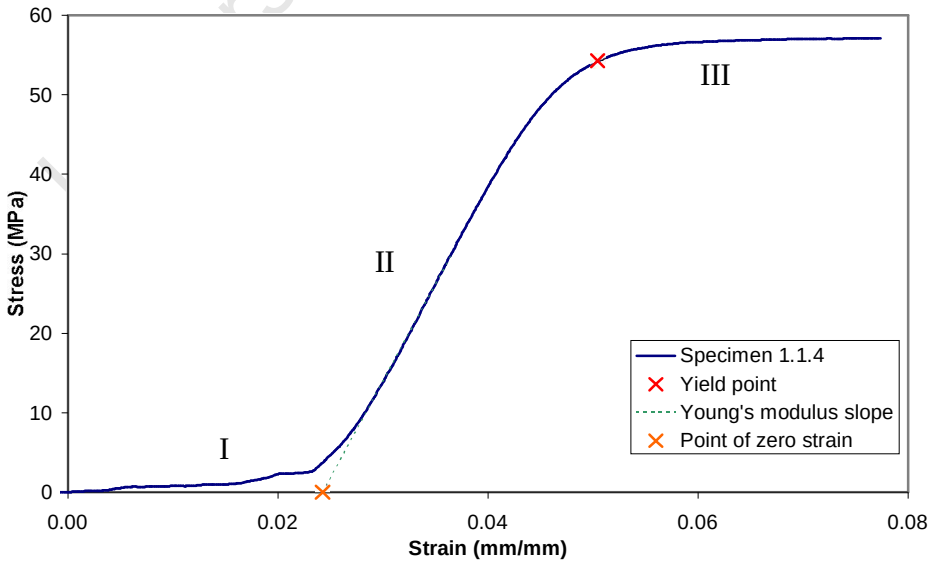

Figure 6.1: Typical stress-strain curve to ultimate compressive stress

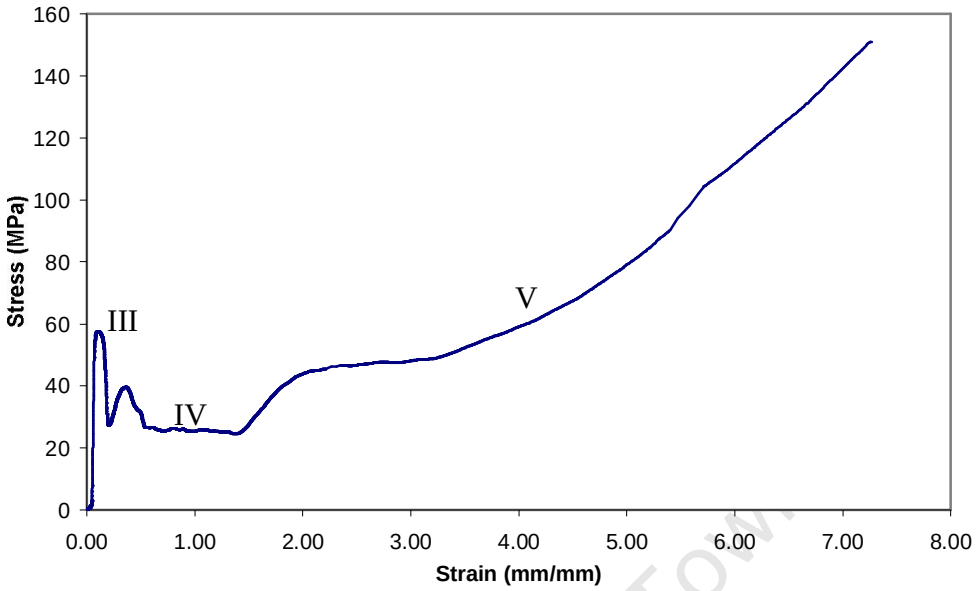

Figure 6.2: Typical stress-strain curve to total destruction

In this study, the yield stress is taken to be the stress value at 5% below the peak compressive strength, as defined by Shim [9]. The Young's modulus is defined as the slope of the stress-strain curve in the most linear section prior to yield. In order to adjust for the end artifact, stress-strain curves are shifted along the strain axis according to the point of zero strain. This is defined by the intersection of the modulus slope and the strain axis (Figure 6.1).

Three possible methods for determining the instantaneous stress were considered. These were the constant area assumption, the constant volume assumption and the use of Poisson's ratio (Figure 6.3). The assumption of constant volume may be invalid due to the porous nature of cancellous bone and the Poisson's ratio is not known exactly. Therefore the constant area approach is utilised. This also yields the most conservative results, as shown in Figure 6.3.

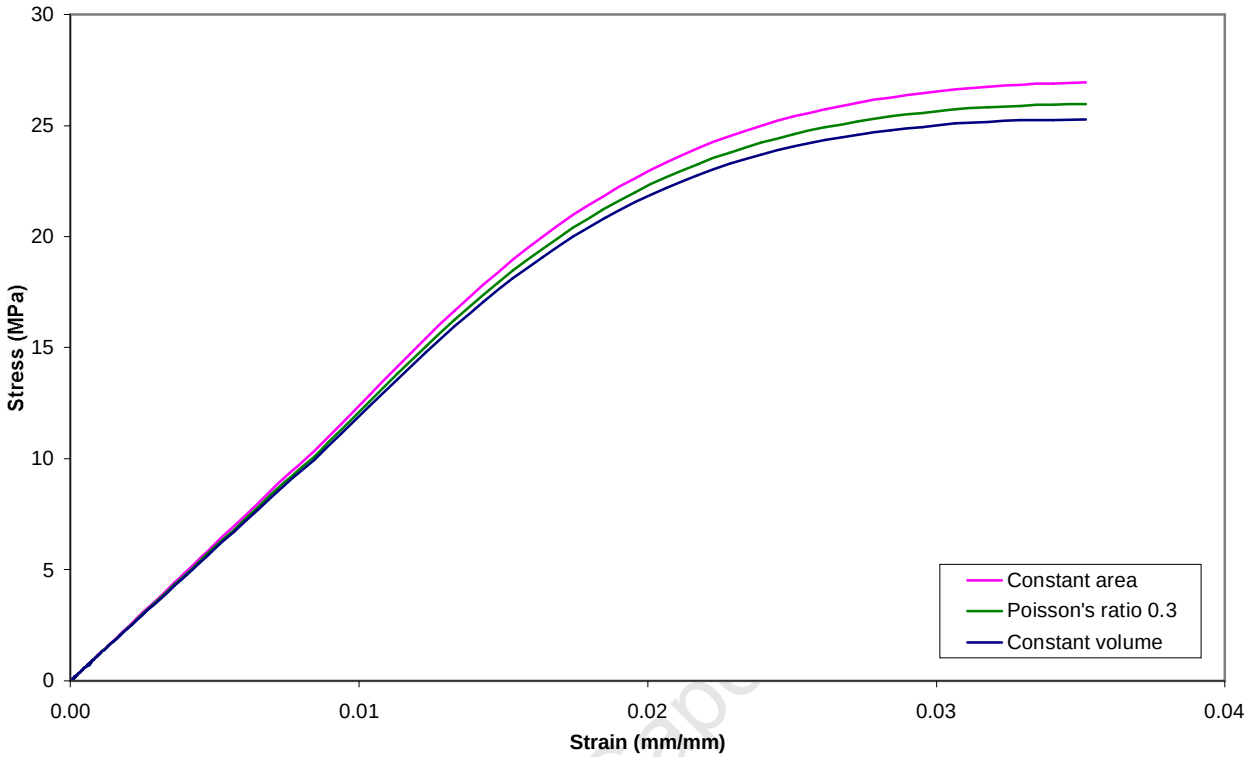

Figure 6.3: Possible methods for determining stress.

6.1.2 Stress-strain results

A comparison of the averages of the stress-strain curves at each strain rate is illustrated in Figure 6.4, with the graphs shown up until the point of ultimate compressive stress, with the yield point (and standard error) indicated. The curves can be compared since the average density of each strain rate group is similar and therefore the dependence of mechanical properties on density can be ignored. The average mechanical properties at each strain rate are listed in Table 6.1 in terms of the mean and standard deviation values, as well as the range of values. The individual failure properties of the specimens, as well as the stress-strain curves can be seen in Appendix C.

The compressive strength of bone increases with an increase in strain rate. Neither Young's modulus, nor failure strain show a distinct pattern with strain rate. However, each strain rate group was made up of specimens from three bovine bones, in varying ratios. The differing microstructures affect the mechanical properties. The effect of strain rate on the properties of bone is discussed further in section 6.2.2.

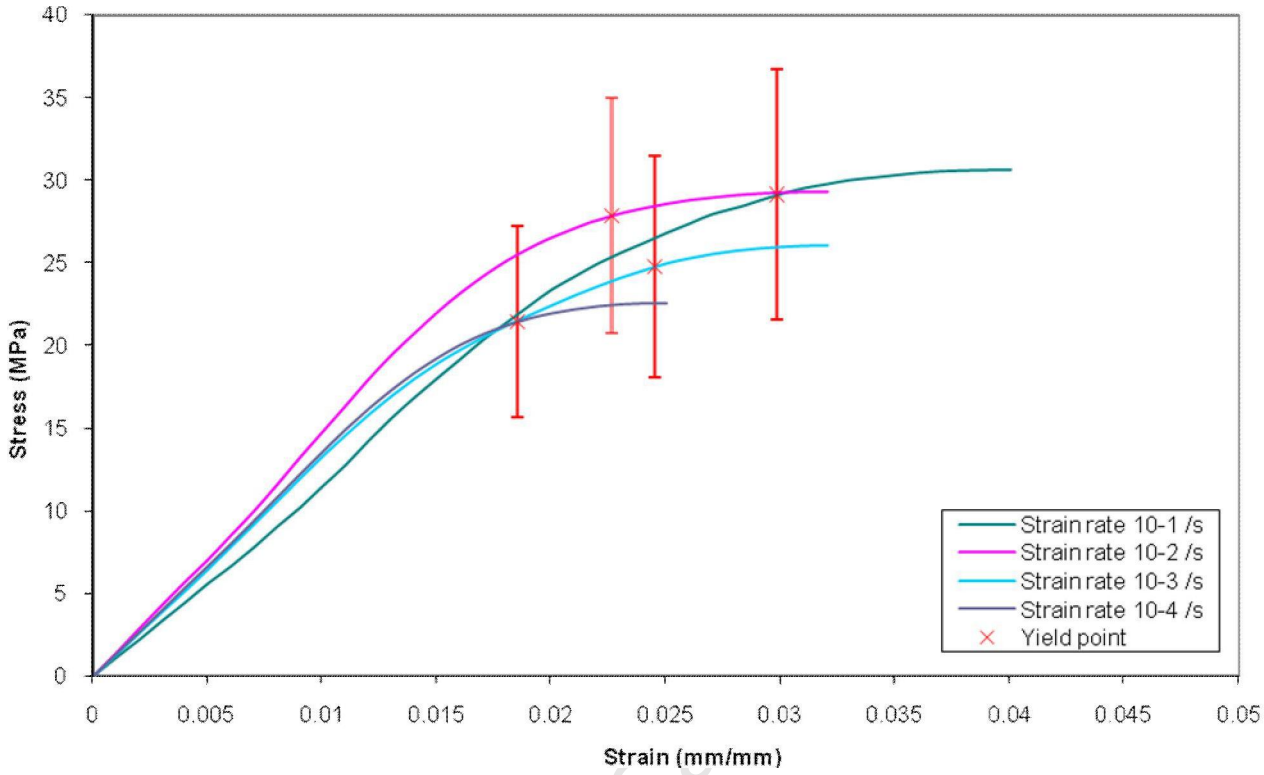

Figure 6.4: Average stress-strain curve at different strain rates.

Table 6.1: Average mechanical properties of specimens at different strain rates.

$\dot{\varepsilon}$ (s^{-1})	10^{-1}	10^{-2}	10^{-3}	10^{-4}
ρ (g/cm^3)	1.40±0.1 (1.24-1.65)	1.41±0.095 (1.23-1.59)	1.39±0.091 (1.20-1.50)	1.38±0.073 (1.26-1.49)
E (MPa)	1193±449 (354-2058)	1461±331 (788-1963)	1310±636 (374-2330)	1380±586 (441-2639)
σ_u (MPa)	31.2±9.84 (15.7-54.7)	29.6±5.22 (22.4-43.8)	26.9±10.2 (15.4-46.8)	23.3±8.20 (10.4-38.8)
ε_u (mm/mm)	0.0418±0.00942 (0.0305-0.0689)	0.0325±0.00604 (0.0244-0.0459)	0.0324±0.00934 (0.0489-0.0595)	0.0239±0.00460 (0.0142-0.0346)
σ_y (MPa)	29.7±9.34 (14.9-52.0)	28.2±4.96 (21.3-41.6)	25.6±9.73 (14.7-44.5)	22.1±7.79 (9.89-36.9)
ε_y (mm/mm)	0.0292±0.00508 (0.0230-0.0416)	0.0221±0.0037 (0.0173-0.0297)	0.0254±0.00977 (0.0146-0.0565)	0.0204±0.00889 (0.0114-0.0506)

In order to visualise the dual effects of strain rate and density, the individual stress-strain curves for each strain rate group are shown as a function of density in the in Figure 6.5. In addition, the data is presented in three-dimensional graphs, showing separately, the yield stress, yield strain and modulus values as a function of density at each strain rate (Figure 6.6).

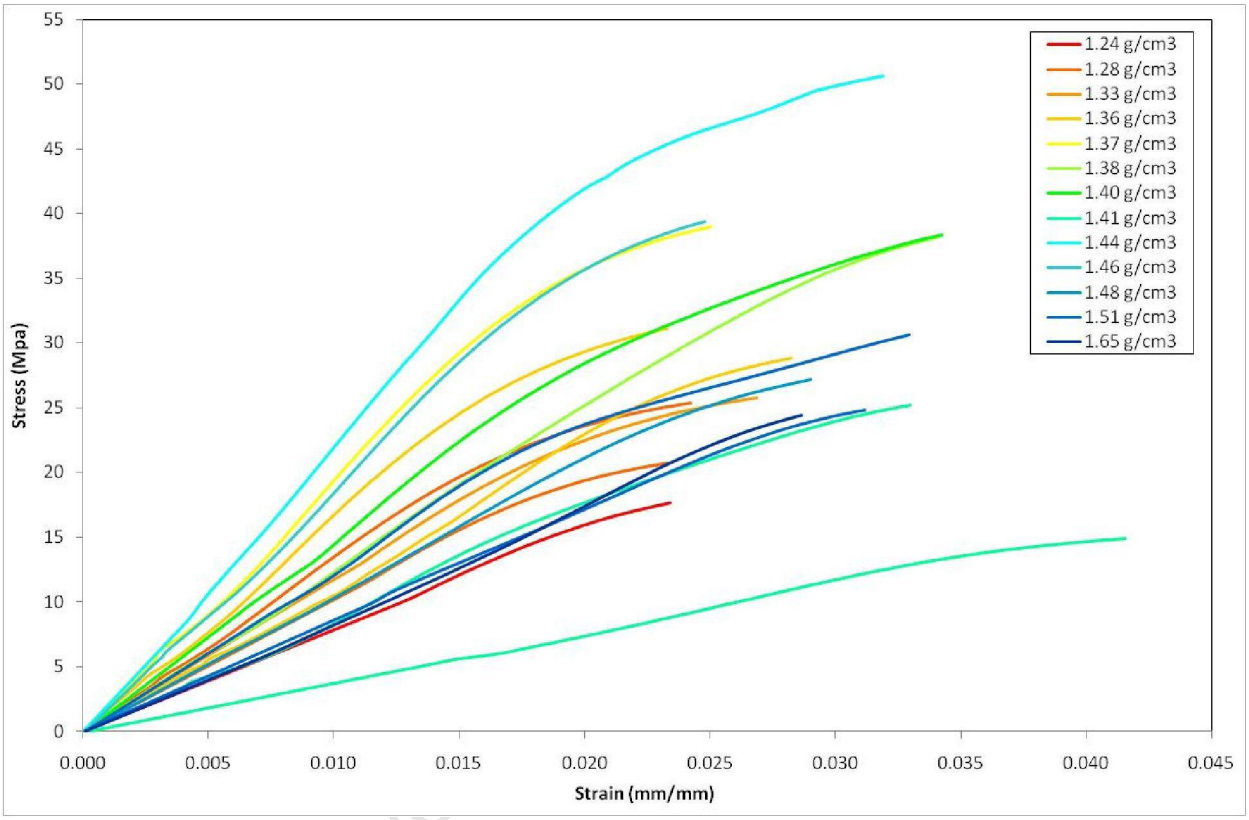

(a) Tests conducted at a strain rate of 10^{-1} s^{-1}

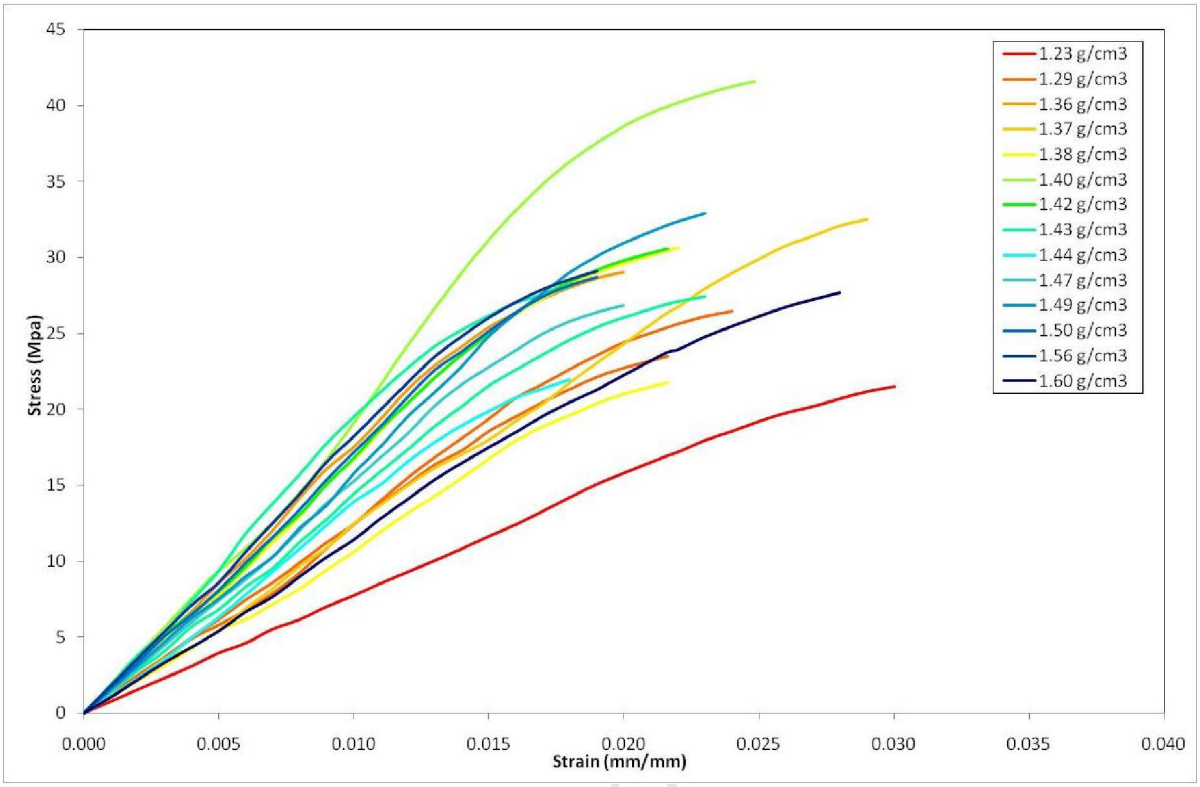

(b) Tests conducted at a strain rate of 10^{-2} s^{-1}

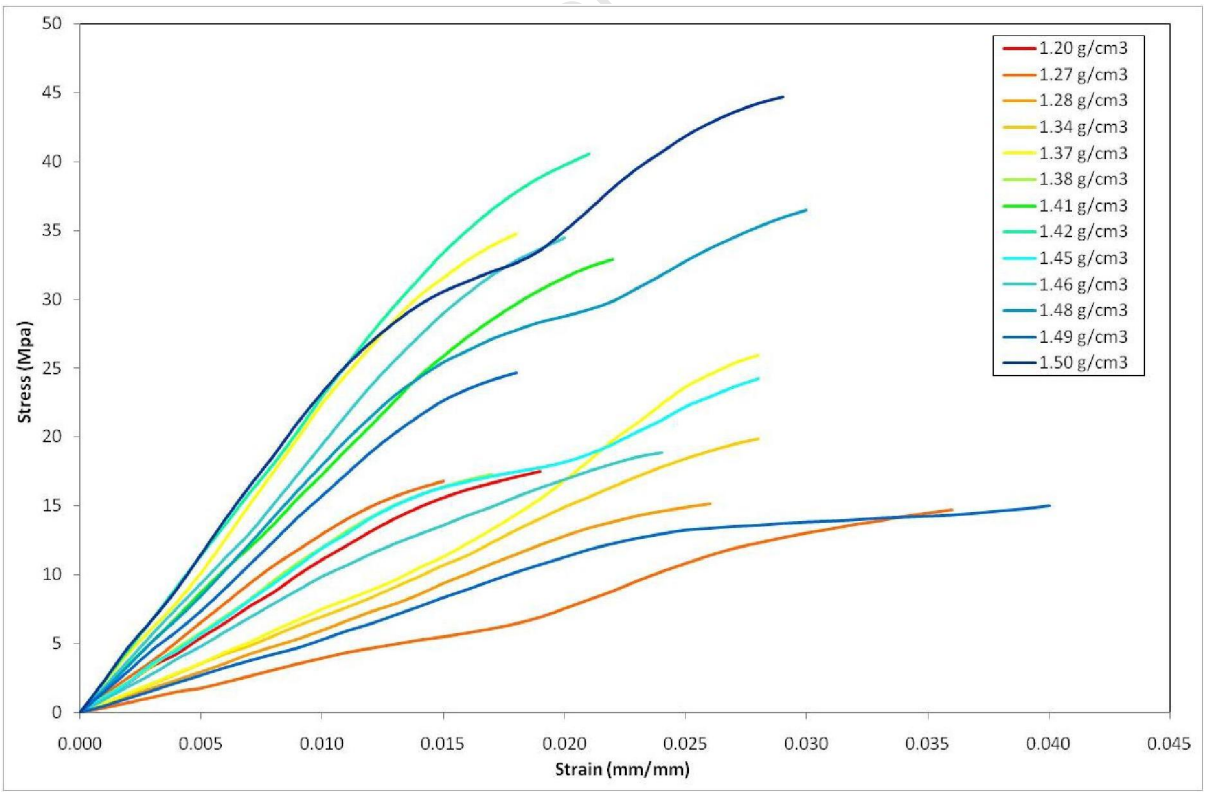

(c) Tests conducted at a strain rate of 10^{-3} s^{-1}

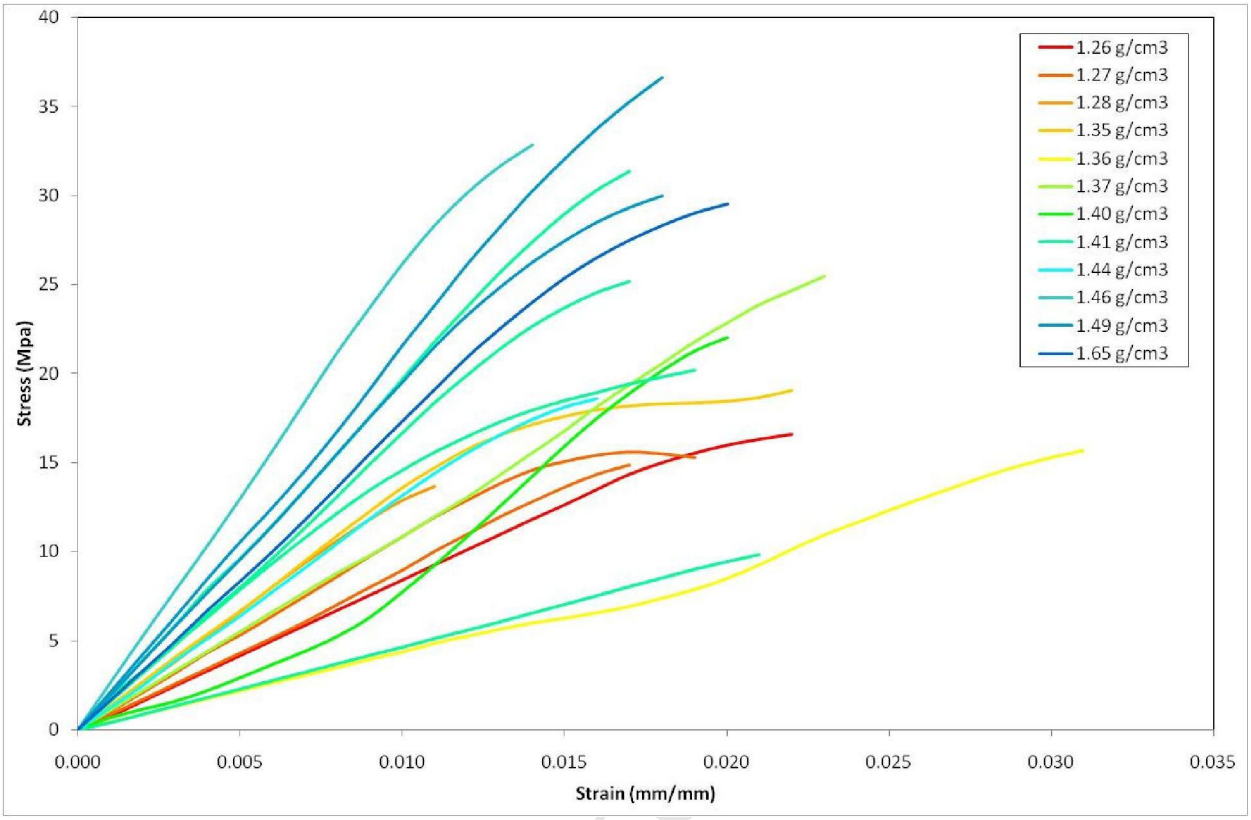

(d) Tests conducted at a strain rate of 10^{-4} s^{-1}

Figure 6.5: Average stress-strain curve at different strain rates as a function of density.

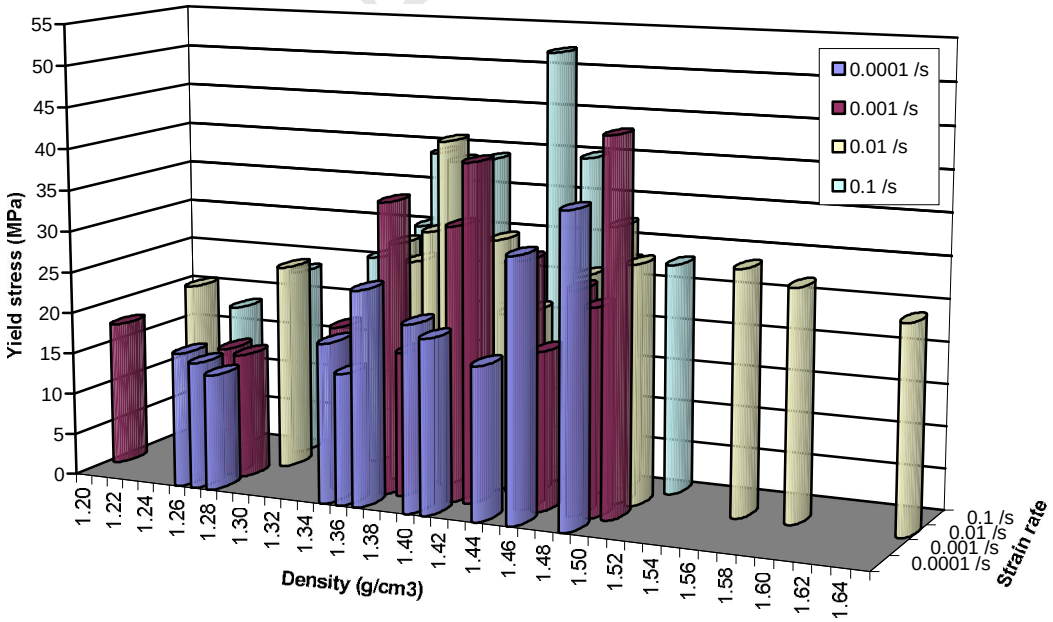

(a) Yield stress

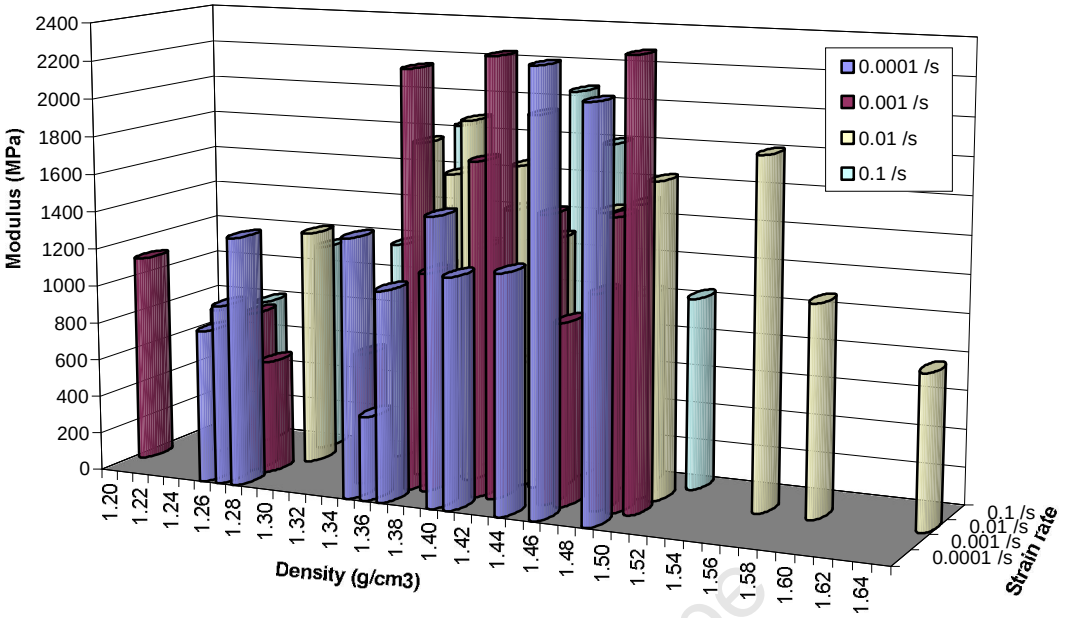

(b) Young's modulus

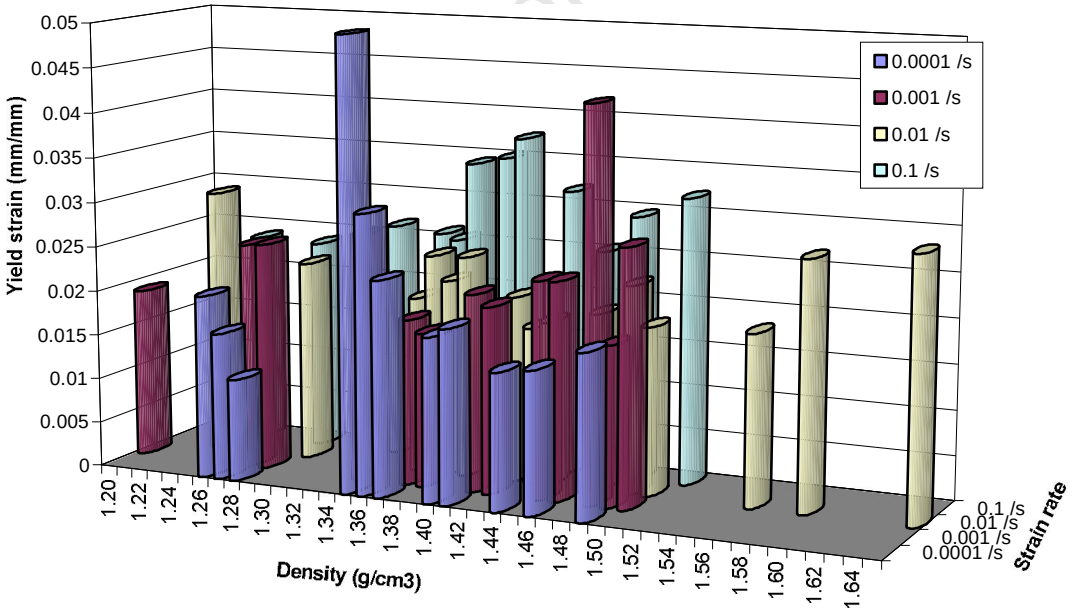

(c) Yield strain

Figure 6.6: Mechanical properties as a function of density at different strain rates.

6.1.3 Comparison of results to literature

Most previous studies have been conducted on human bone from various anatomical sites, which have low apparent densities in the region of 0.2 to 0.6 g/cm^3, which translates into fresh bone densities of below approximately 1.2 g/cm^3 [1]. Only three of the studies reviewed focused on quasi-static testing of bovine bone, which is known to be stronger than human bone [13, 41, 58]. Furthermore, mechanical properties such as strength and stiffness are expected to be dependent on bone density. Therefore the work by Guedes [58], which involves testing bovine cancellous bone specimens with an approximate apparent density of 1 g/cm^3 (1.4 g/cm^3 fresh bone density [1]), has the most comparable test material to this study. Tests were conducted at four different quasi-static strain rates, representing a similar procedure to that undergone in this study. Guedes found the yield strength to vary between 9 and 16 MPa and since the average densities in this work are approximately 1.4 g/cm^3 results are expected to be similar. However, this study shows a strength range of 22 to 30 MPa, which is higher than that of Guedes and most of the values presented in Table 3.2. The stiffness values presented here (1176 to 1433 MPa) are far greater than those found by Guedes (190 to 365 MPa). However, Table 3.2 shows Guedes' values to be lower than those derived in other studies for lower density bone. Therefore, compared to a number of previous studies in which the bone density is substantially lower, these modulus values seem to be in line with the literature. Yield strain is expected to have at most a weak dependence on density [38, 39], and values in the reviewed literature vary from 0.8 to 5%. Therefore, results from this work (2 to 2.9%) fall into the range, but are lower than those found by Guedes.

6.2 Trends in mechanical properties

Previous studies that have established relationships between the properties of bone and density or strain rate, have found these properties to vary either linearly or exponentially with the independent variable. Therefore both these relationships are explored and compared in this work. Trendlines are calculated using a least squares fit. Results are presented in the form of confidence intervals, the region in which it can be said with a certain percentage of confidence that the "y" value for a given "x" will lie. The confidence intervals used in this report are 68.3% and 95.4%, which correspond to

one and two standard deviations respectively. The equations used to derive these intervals are shown in Appendix D.

6.2.1 Trends with density

According to the literature, the dependence of the mechanical properties of bone on density is far greater than on strain rate [13]. Therefore the results from each group of tests at different strain rates can be combined.

6.2.1.1 Yield stress as a function of density

The relationship between yield stress and density is best described by a power law function, as shown in Table 6.2. Results show positive correlations between yield stress and density, with the density exponent ranging from 0.81 to 4.54 for the different strain rate groups. The combined results from all quasi-static tests, shown in Figure 6.7(b), give an exponent of 2.36, which is in agreement with the range of 1.29 to 2.35 found in the literature (see Table 3.1). However, the data has high scatter, as indicated by the poor correlation coefficients.

A visual comparison of these results to those of Shim [1] and Carter and Hayes [13] is provided in Figure 6.8. The dependence of stress on density is shown to be extremely well-matched to Shim's results. It is also clear that the bovine bone is stronger than human bone.

In addition, the experimental data is analysed according to groups containing specimens from the same bone, since it is believed that bone microstructure will affect mechanical behaviour. Again, specimens over the entire range of strain rates are included, since the sample size was not large enough to examine specimens from each bone at each strain rate. The dependence of the strength of each bone on density is shown in Table 6.2 and illustrated in Figure 6.9. It can be seen that bone 3 is the strongest and the strengths of bone 1 and 3 exhibit similar dependencies on density.

Table 6.2: Equation variables for strength dependence on density.

Data source	$\sigma_y = a\rho^b$			$\sigma_y = a\rho + b$		
	a	b	r^2	a	b	r^2
All specimens	11.4	2.36	0.206	39.7	-29.1	0.175
Strain rate 10^{-1} specimens	20.1	1.02	0.527	16.9	5.95	0.0331
Strain rate 10^{-2} specimens	21.0	0.810	0.103	13.5	9.12	0.0668
Strain rate 10^{-3} specimens	8.11	3.30	0.331	59.9	-57.8	0.315
Strain rate 10^{-4} specimens	4.83	4.54	0.444	76.9	-84.0	0.514
Bone 1: All specimens	7.04	3.97	0.341	64.5	-62.5	0.278
Bone 2: All specimens	9.60	2.15	0.347	31.8	-24.2	0.398
Bone 3: All specimens	8.89	3.89	0.744	83.1	-82.5	0.651

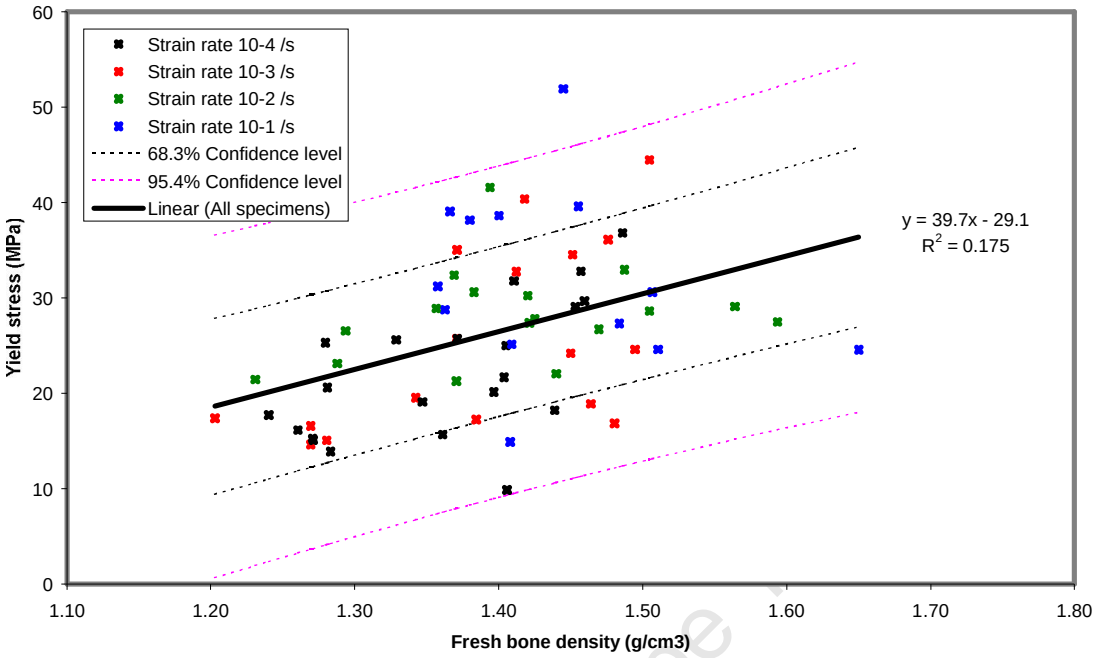

(a) Linear

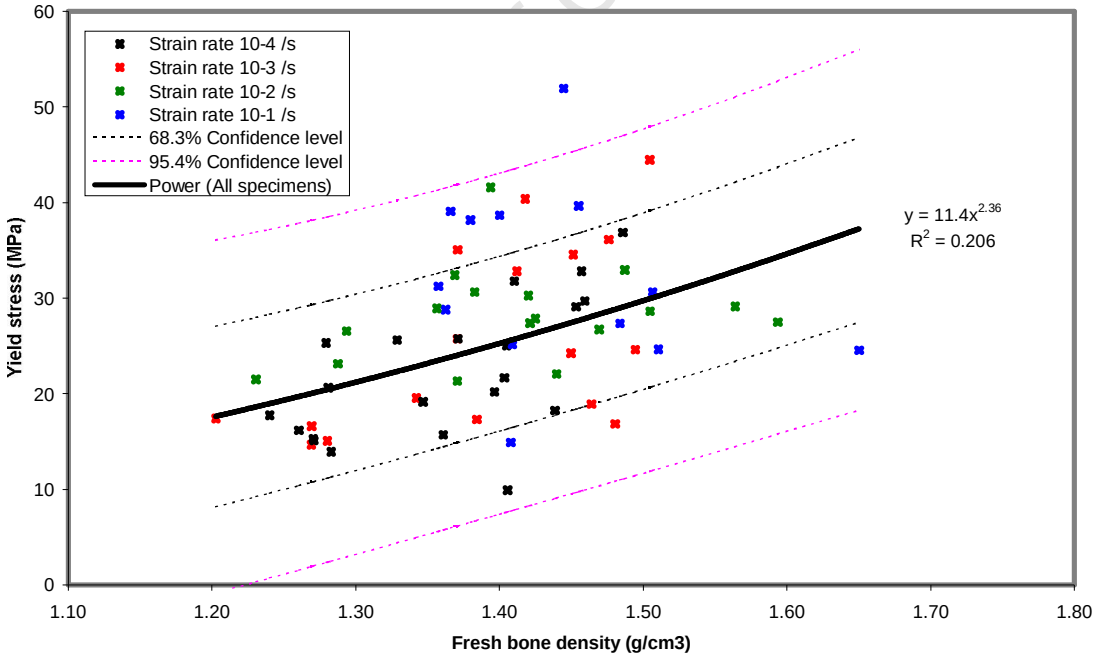

(b) Power law

Figure 6.7: The relationship between yield stress and density for all specimens.

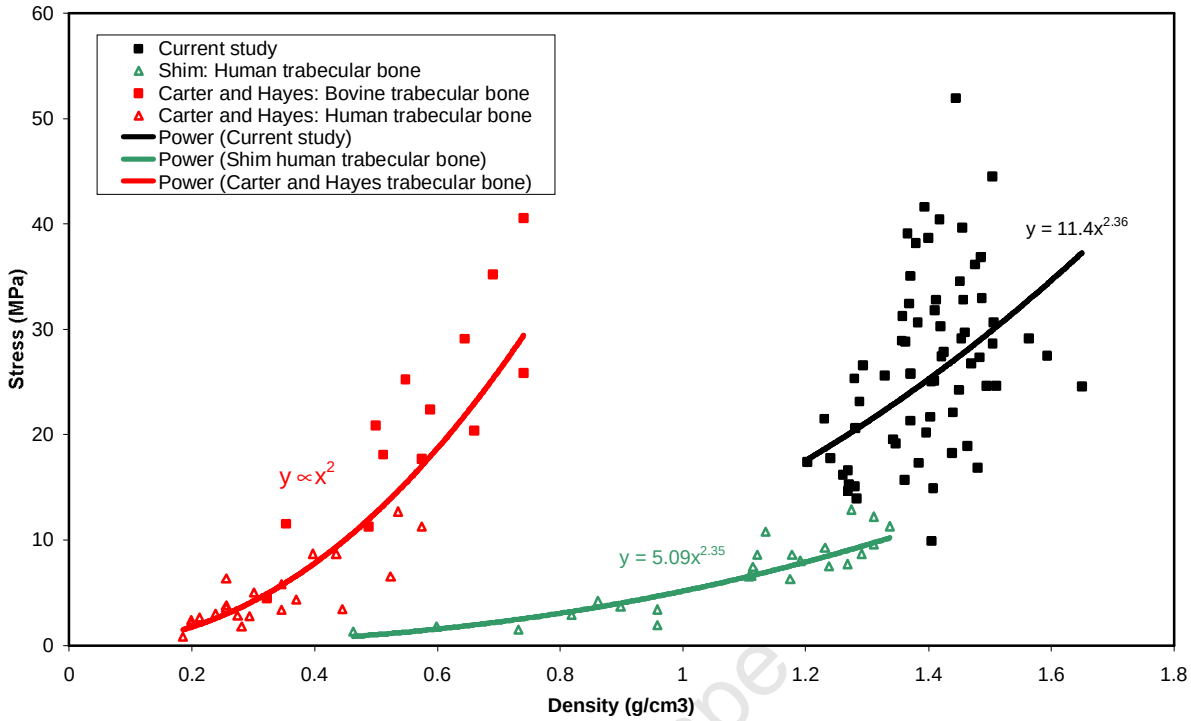

Figure 6.8: Comparison of stress results to those of previous studies [1,13].

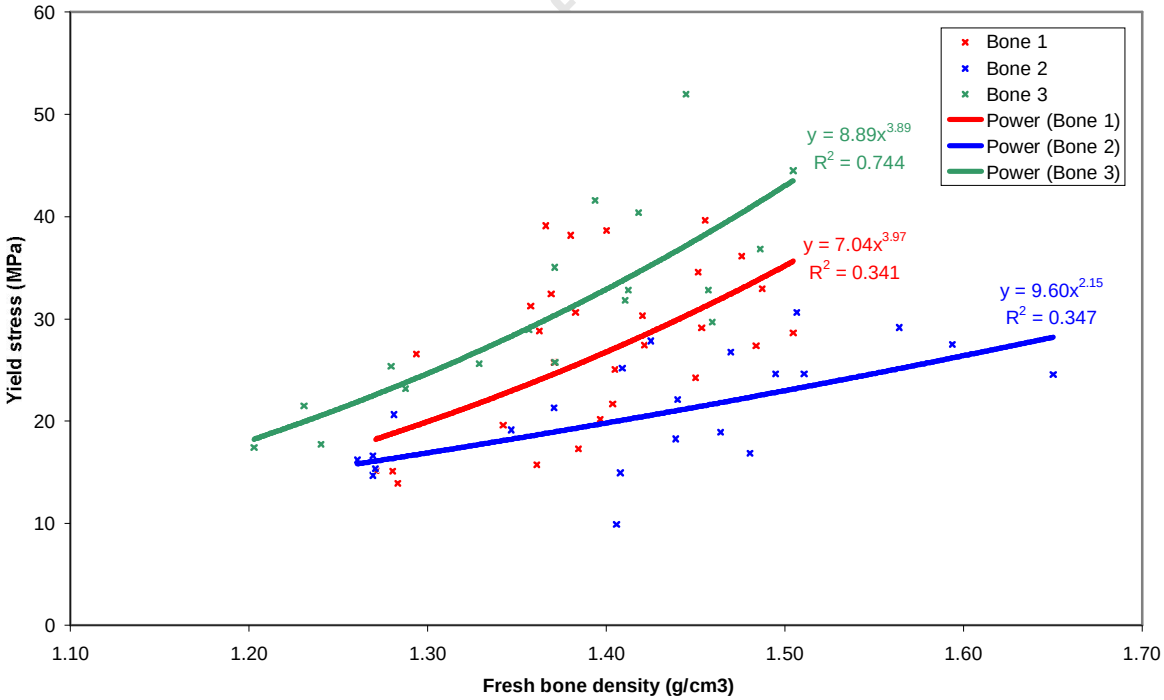

Figure 6.9: The relationship between yield stress and density for each bone.

6.2.1.2 Young's modulus as a function of density

Analysis of the results for the both the strain rate and bone groups show there to be no strong correlations between Young's modulus and density (see Table 6.3). Excluding the negative trend predicted by strain rate group 10^{-1}, results favour a linear trend, with high scatter, shown for all specimens in Figure 6.10(a). However, the correlation coefficients for the linear and power trends are similar and most of the studies reviewed presented results in the power law format. Therefore, the power fit curves are used as a means of comparison, shown in Figure 6.10(b). The strain rate and bone groups found power law exponent values ranging from 1.25 to 4.84 (Table 6.3). The trend of the entire group of specimens yields an exponent of 2.06. This is comparable to that found in previous studies of 1.88 to 3 (Table 3.1).

A comparison between this study and previous studies (Figure 6.11) shows bovine to be stiffer than human bone. The power law exponent is well matched to that of Shim [1].

Figure 6.12 shows the trends for each bone, presented in the power law form. Again, it is evident that bones 1 and 3 behave in a similar manner, with bone 3 having the highest stiffness.

Table 6.3: Equation variables for Young's modulus dependence on density.

Data source	$E = a\rho^b$			$E = a\rho + b$		
	a	b	r^2	a	b	r^2
All specimens	618	2.06	0.0883	1814	-1198	0.1003
Strain rate 10^{-1} specimens	1262	-0.387	0.004	-275	1579	0.004
Strain rate 10^{-2} specimens	824	1.59	0.192	1322	-406	0.144
Strain rate 10^{-3} specimens	374	3.43	0.173	2930	-2765	0.1765
Strain rate 10^{-4} specimens	274	4.71	0.225	5042	-5583	0.309
Bone 1: All specimens	336	3.97	0.249	3224	-3171	0.271
Bone 2: All specimens	624	1.25	0.415	788	-59.5	0.04
Bone 3: All specimens	352	4.84	0.754	5361	5650	0.745

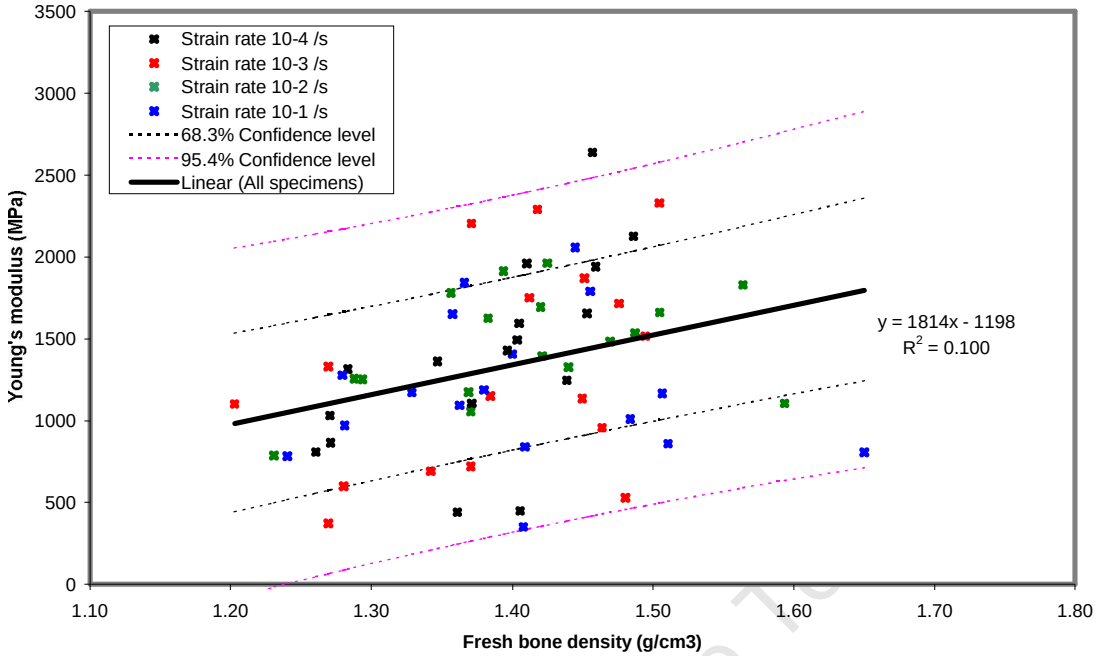

(a) Linear

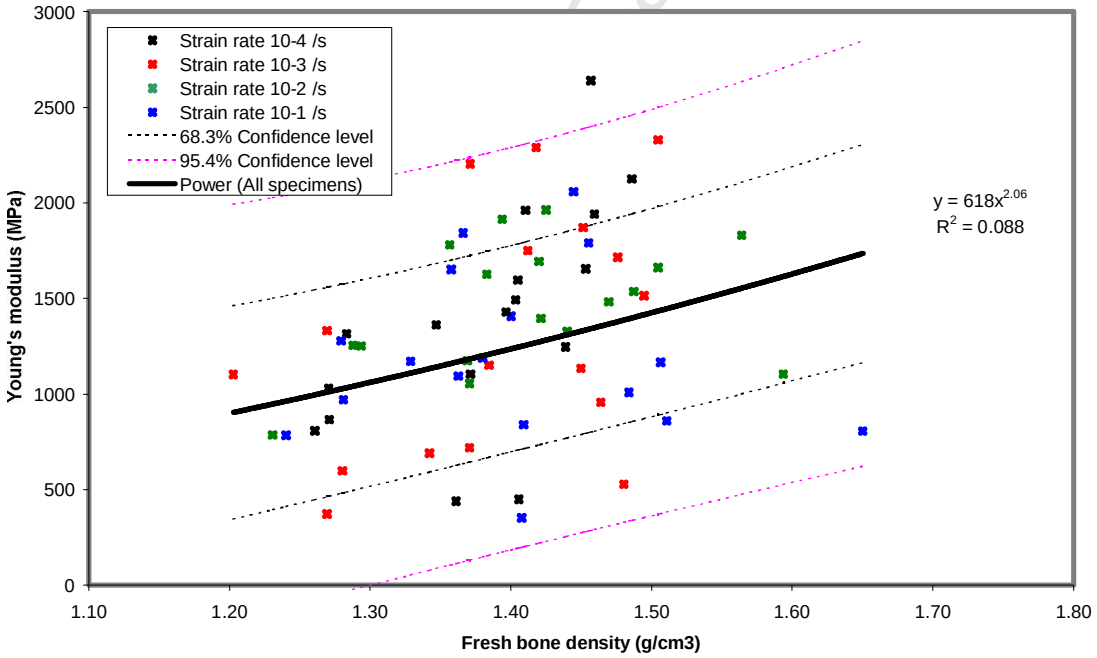

(b) Power law

Figure 6.10: The relationship between Young's modulus and density for all specimens.

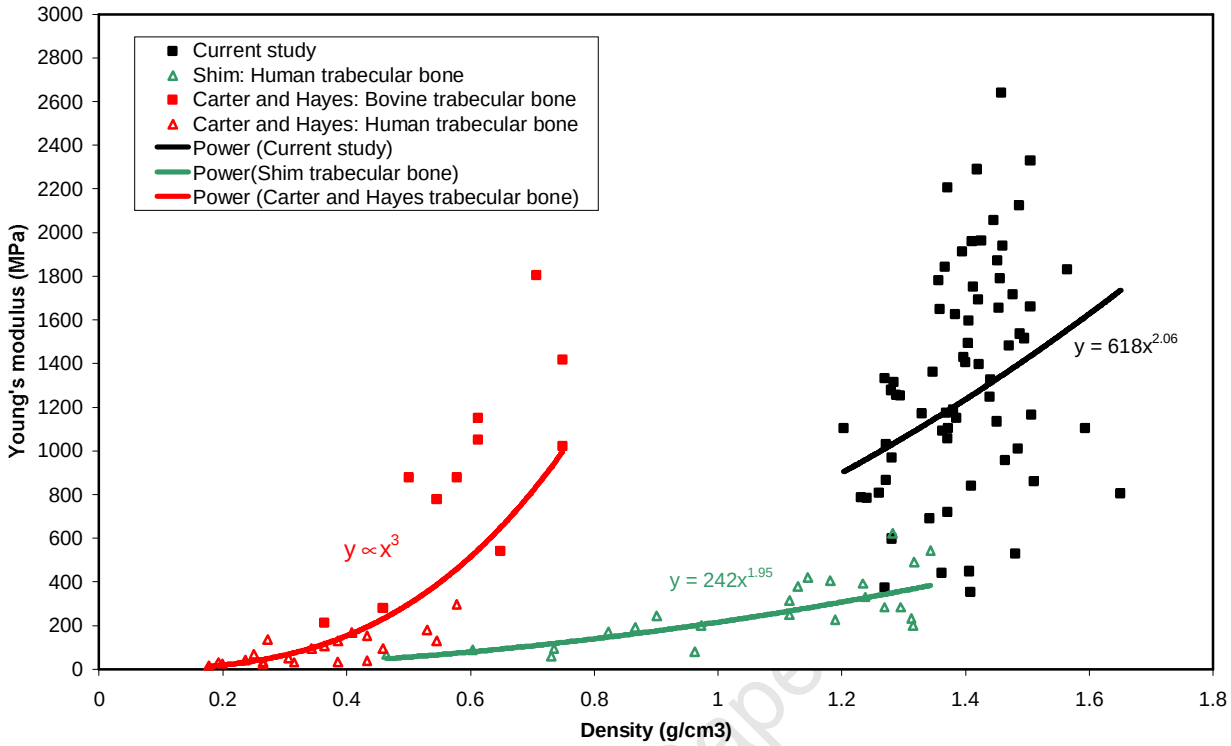

Figure 6.11: Comparison of modulus results to those of previous studies [1, 13].

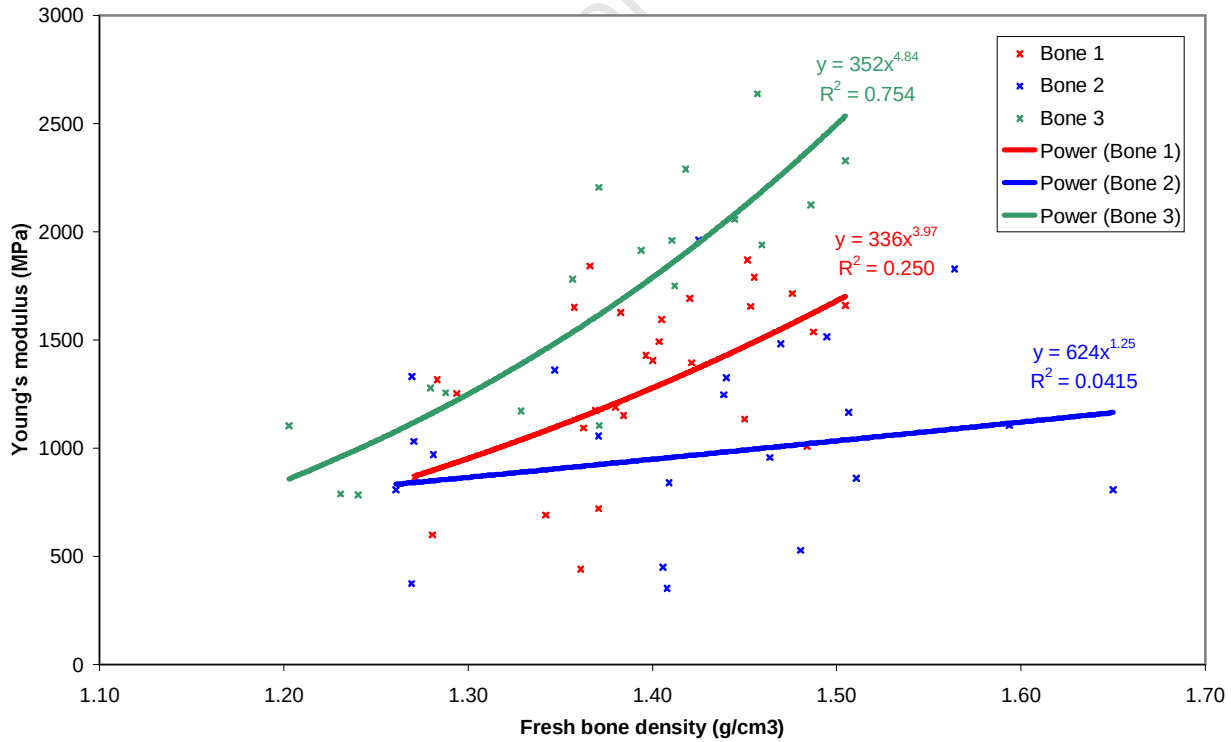

Figure 6.12: The relationship between Young's modulus and density for each bone.

6.2.1.3 Yield strain as a function of density

A number of the groups analysed reported negative trends in yield strain with density, while the remainder found the trend to be positive. The power law relationship is dominant. However, the correlation is extremely weak. This is shown in Table 6.4 and in Figure 6.13. Figure 6.14 shows bones 1 and 2 to have similar relationships of strain to density.

In general, studies presented in the literature focused on the density dependent properties of strength and modulus, ignoring strain. The exceptions are Ouyang [14] and Keaveny [40], who found no relationship between yield strain and density; and Kopperdahl [41], who reported a linear relationship between the two parameters.

Table 6.4: Equation variables for yield strain dependence on density

Data source	$\varepsilon_y = a\rho^b$			$\varepsilon_y = a\rho + b$		
	a	b	r^2	a	b	r^2
All specimens	0.0193	0.548	0.0142	0.0095	0.011	0.0115
Strain rate 10^{-1} specimens	0.0198	1.12	0.220	0.0203	0.0007	0.161
Strain rate 10^{-2} specimens	0.0280	-0.728	0.0937	-0.0111	0.0378	0.0818
Strain rate 10^{-3} specimens	0.0205	0.484	0.0099	0.0162	0.0029	0.0023
Strain rate 10^{-4} specimens	0.0209	-0.266	0.0018	-0.0125	0.0377	0.0105
Bone 1: All specimens	0.0172	0.899	0.0185	0.0101	0.0098	0.0131
Bone 2: All specimens	0.0185	0.810	0.0261	0.0107	0.0112	0.0107
Bone 3: All specimens	0.0265	-0.644	0.0409	0.0083	0.0336	0.0254

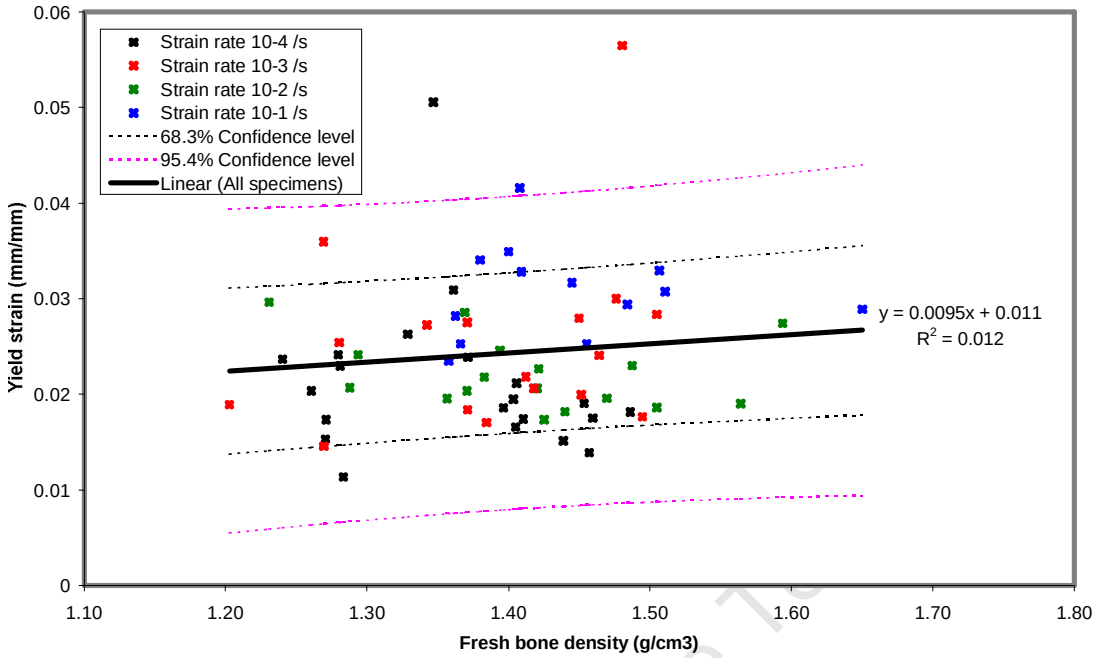

(a) Linear

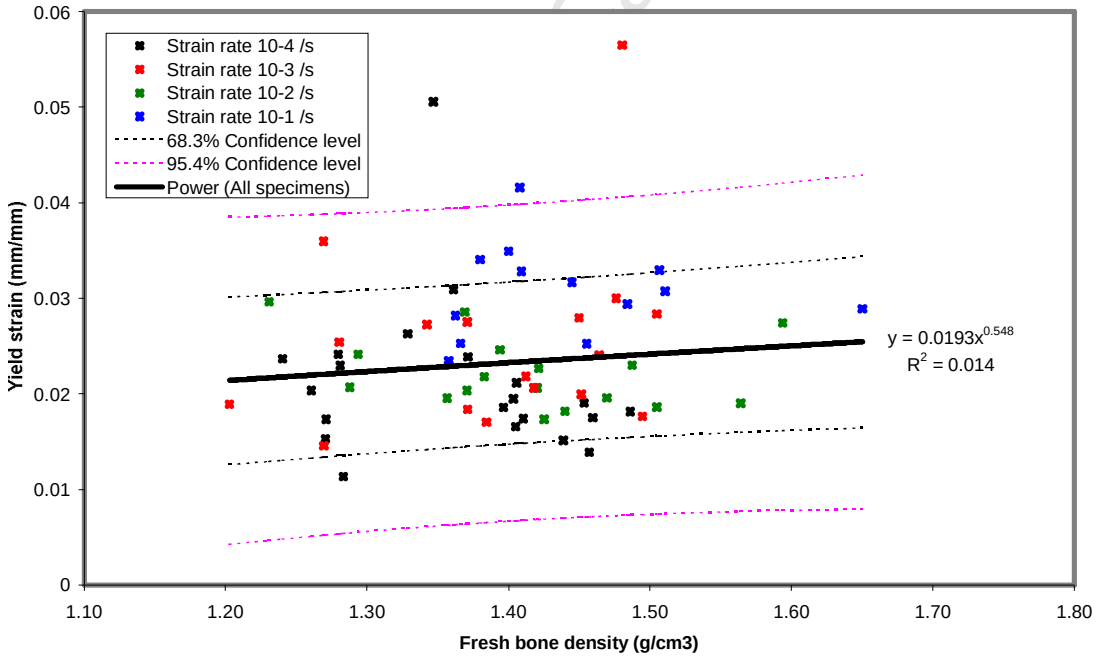

(b) Power law

Figure 6.13: The relationship between yield strain and density for all specimens

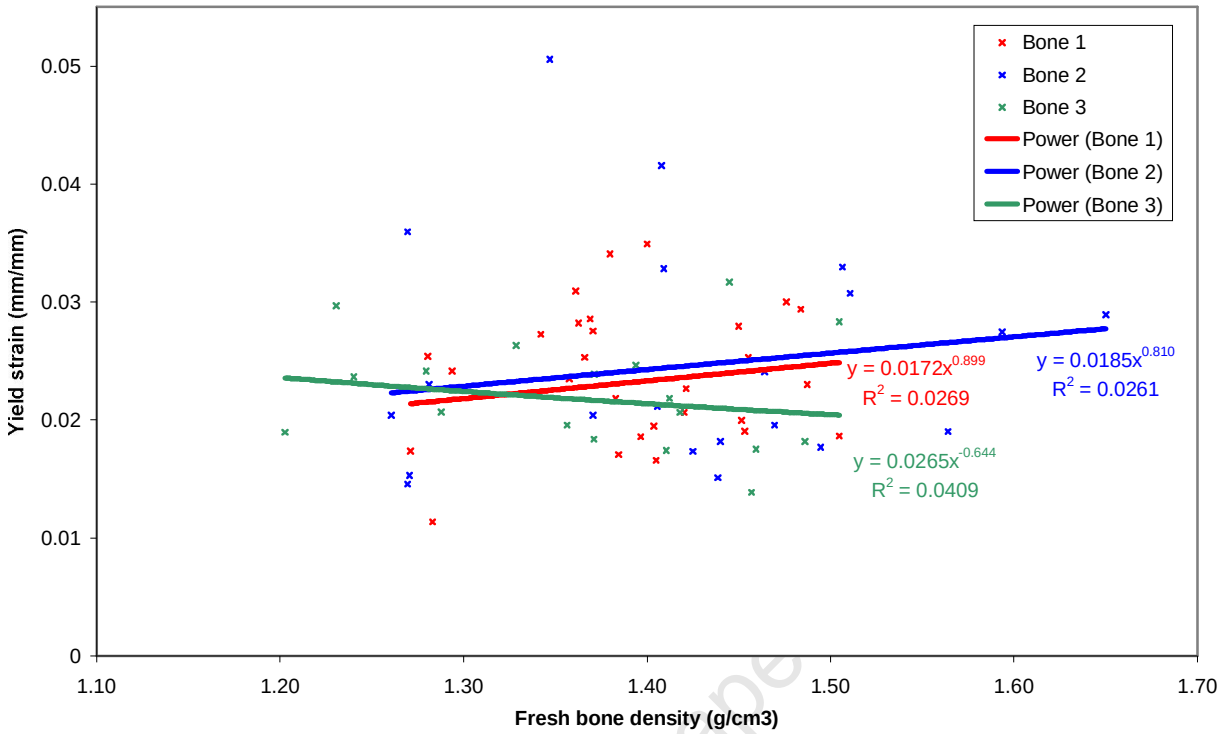

Figure 6.14: The relationship between yield strain and density for each bone.

6.2.2 Trends with strain rate

In order to examine the strain rate dependence of bone, the effect of density needs to be eliminated from the results. This is achieved by normalising the data to represent a specimen of the average density of 1.40 g/cm^3. The trendline equations illustrated in Figures 6.7(b), 6.10(a) and 6.13(b) are used to determine the trend for the average properties. Equations from Figures 6.9, 6.12 and 6.14 are used for the strain rate trends in each bone. The normalisation process is detailed in Appendix E.

The effect of strain rate on mechanical properties is best illustrated by showing the trend in the average property (± standard error) at each strain rate.

6.2.2.1 Yield stress as a function of strain rate

It is found that the yield stress is best related to strain rate by a power law function. The trend in average results (Figure 6.15(b)) shows the exponent to be 0.04. On analysis of the trends of

each bone, shown in Figure 6.16, it is found that bones 2 and 3 have similar dependencies on strain rate, with exponents of 0.0371 and 0.0306 respectively. The error bars show the standard error in all cases to be large, as a result of the high scatter in the results.

The studies by McElhaney [45], Carter and Hayes [13] and Ouyang [14] are the only ones found in which the trend of strength with strain rate is examined. McElhaney and Carter and Hayes both found a power law relationship, with Carter and Hayes reporting an exponent of 0.06. Ouyang found strength to be independent of strain rate. Results of the current study for bones 1 and 3 are therefore shown to be in fairly good agreement with that of Carter and Hayes. A visual comparison is shown in Figure 6.17.

Table 6.5: Equation variables for strength dependence on strain rate

Data source	$\sigma_y = a\dot{\varepsilon}^b$			$\sigma_y = a\dot{\varepsilon} + b$		
	a	b	r^2	a	b	r^2
All specimens (ave.)	32.86	0.0401	0.975	48.61	24.87	0.574
Bone 1	40.89	0.0712	0.993	107.8	24.62	0.778
Bone 2	24.68	0.0371	0.723	24.01	19.39	0.200
Bone 3	39.78	0.0306	0.677	30.66	32.64	0.179

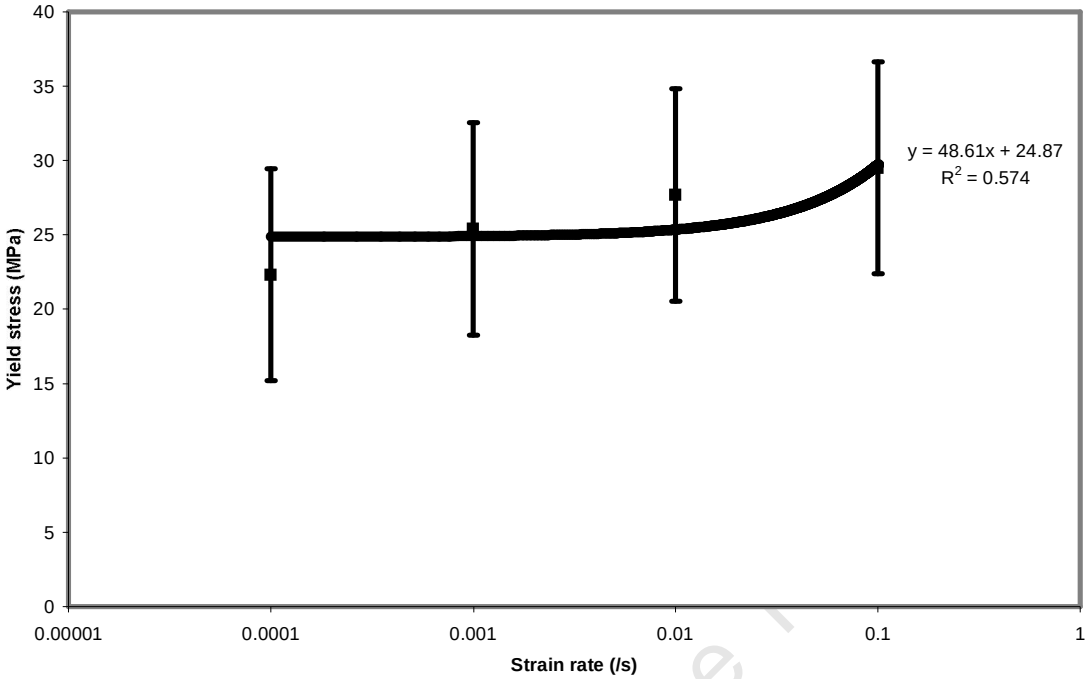

(a) Linear

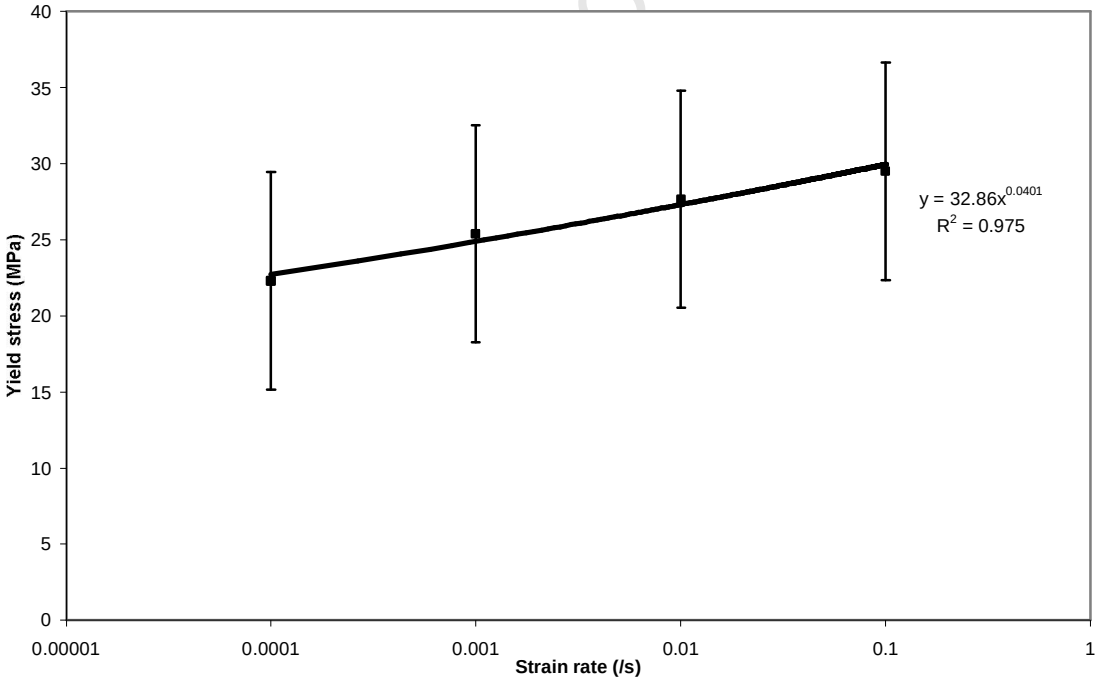

(b) Power law

Figure 6.15: The relationship between yield stress and strain rate for all specimens.

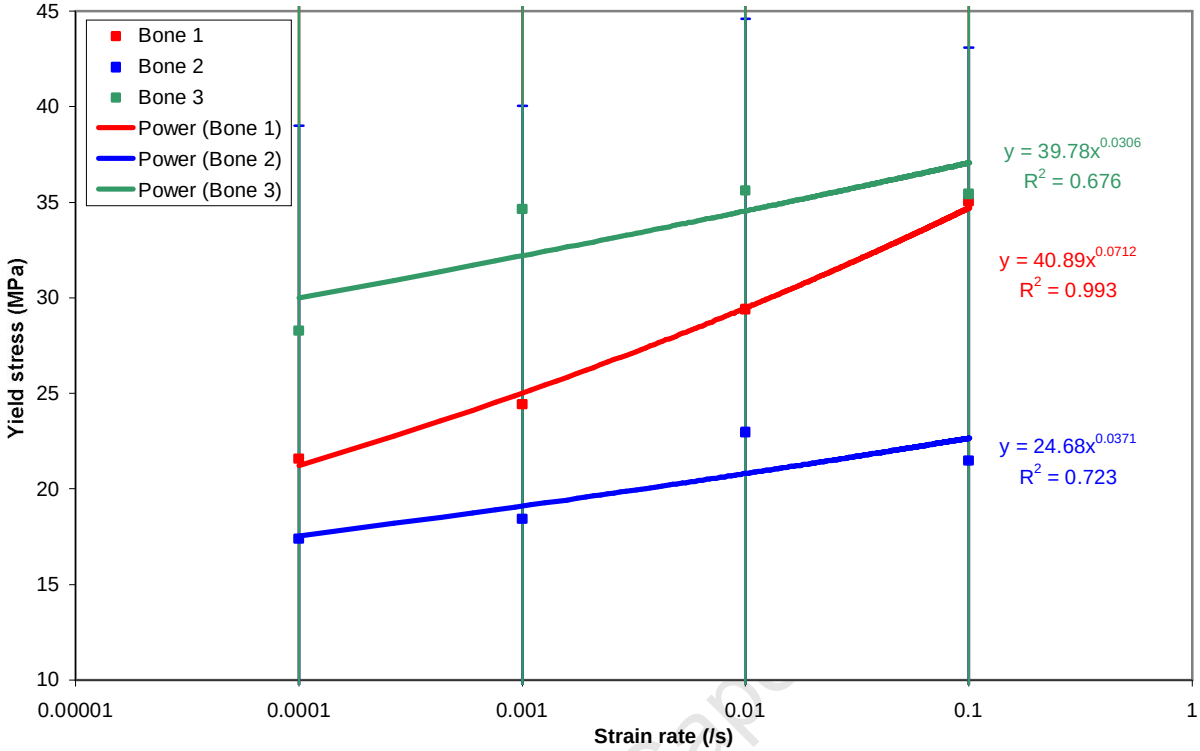

Figure 6.16: The relationship between yield stress and strain rate for each bone.

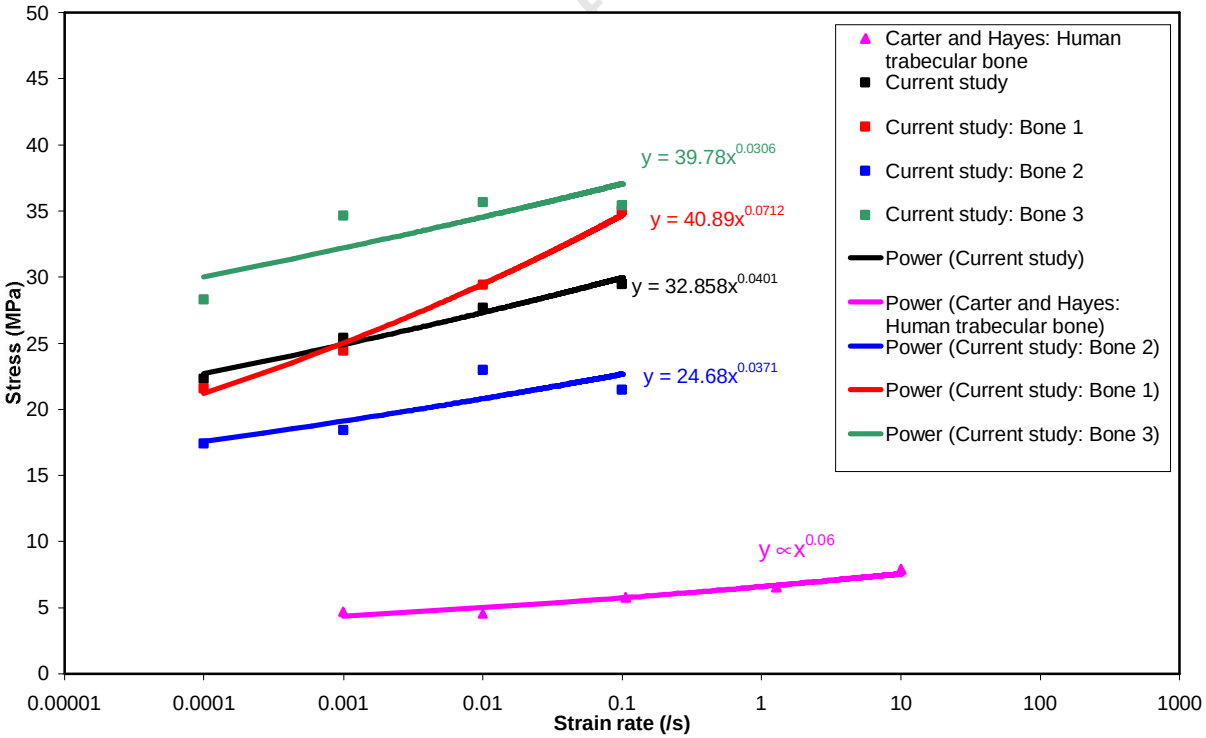

Figure 6.17: Comparison of results with Carter and Hayes [13].

6.2.2.2 Young's modulus as a function of strain rate

In general, a linear relationship between modulus and density is found to be most applicable (Table 6.5). The power and linear trends for all specimens are presented in Figure 6.18.

Results from the three bones are dissimilar, with bones 2 and 3 showing a linear decrease in modulus with increasing strain rate, while bone 1 exhibits a positive trend. This is shown in Figure 6.19. The trends of each bone are plotted for comparison with the results from the study by Carter and Hayes [13] in Figure 6.20.

As shown in Table 3.1 and Figure 6.20, the investigations reviewed reported positive power law relationships [13,14]. However, results of the current study generally exhibit a negative linear trend and are therefore not comparable to the literature.

Table 6.5: Equation variables for Young's modulus dependence on strain rate

Data source	$E = a\dot{\varepsilon}^b$			$E = a\dot{\varepsilon} + b$		
	a	b	r^2	a	b	r^2
All specimens (ave.)	1217	-0.0149	0.329	-1723	1377	0.674
Bone 1	1485	0.0195	0.194	1679	1289	0.241
Bone 2	915.5	-0.018	0.0556	-2962	1118	0.347
Bone 3	1939	-0.0066	0.0436	-2003	1868	0.313

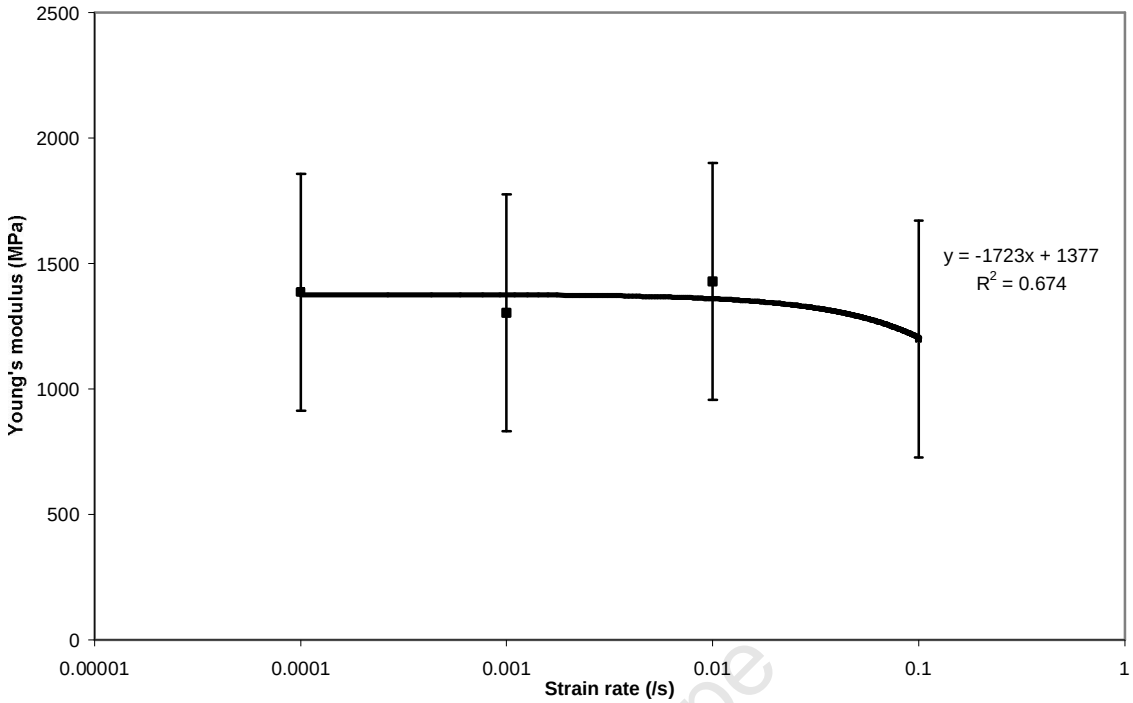

(a) Linear

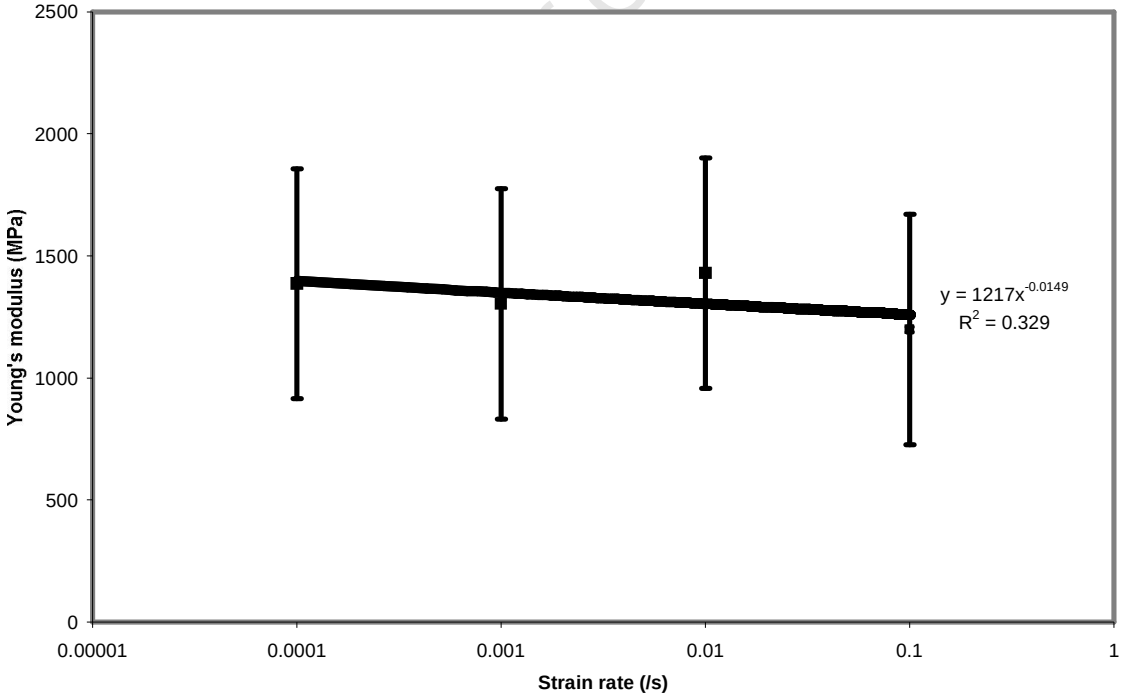

(b) Power law

Figure 6.18: The relationship between Young's modulus and strain rate for all specimens.

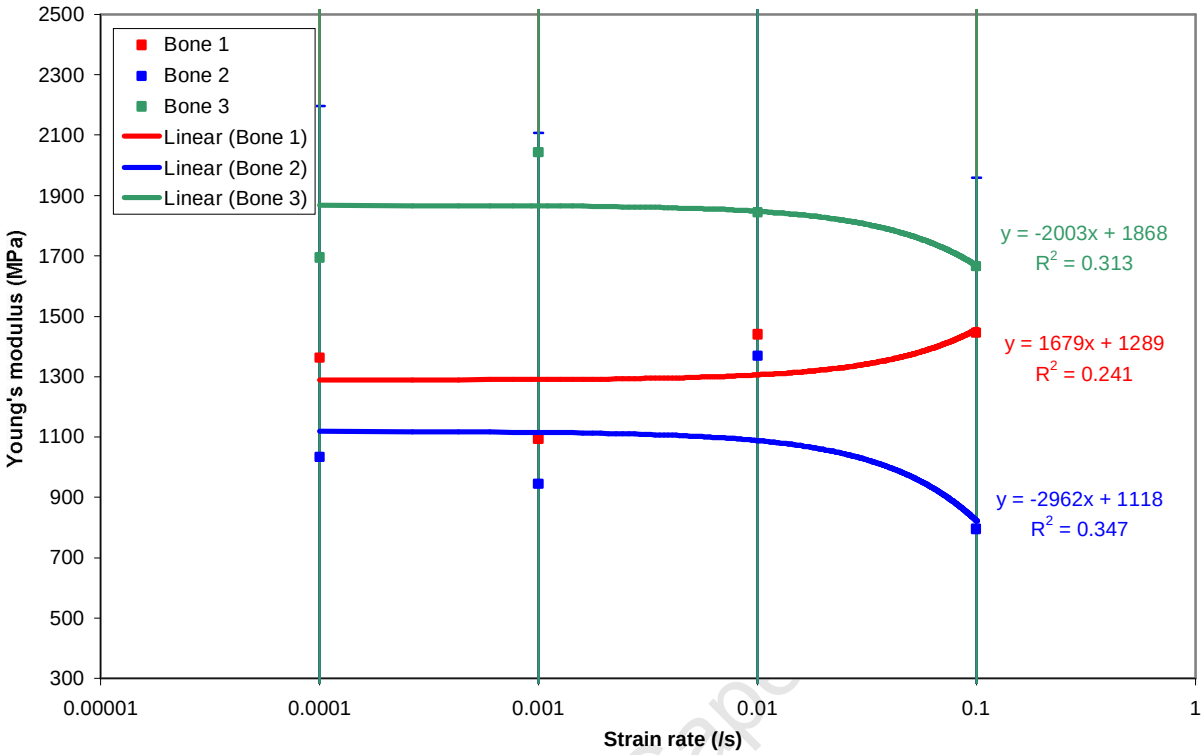

Figure 6.19: The relationship between Young's modulus and strain rate for each bone.

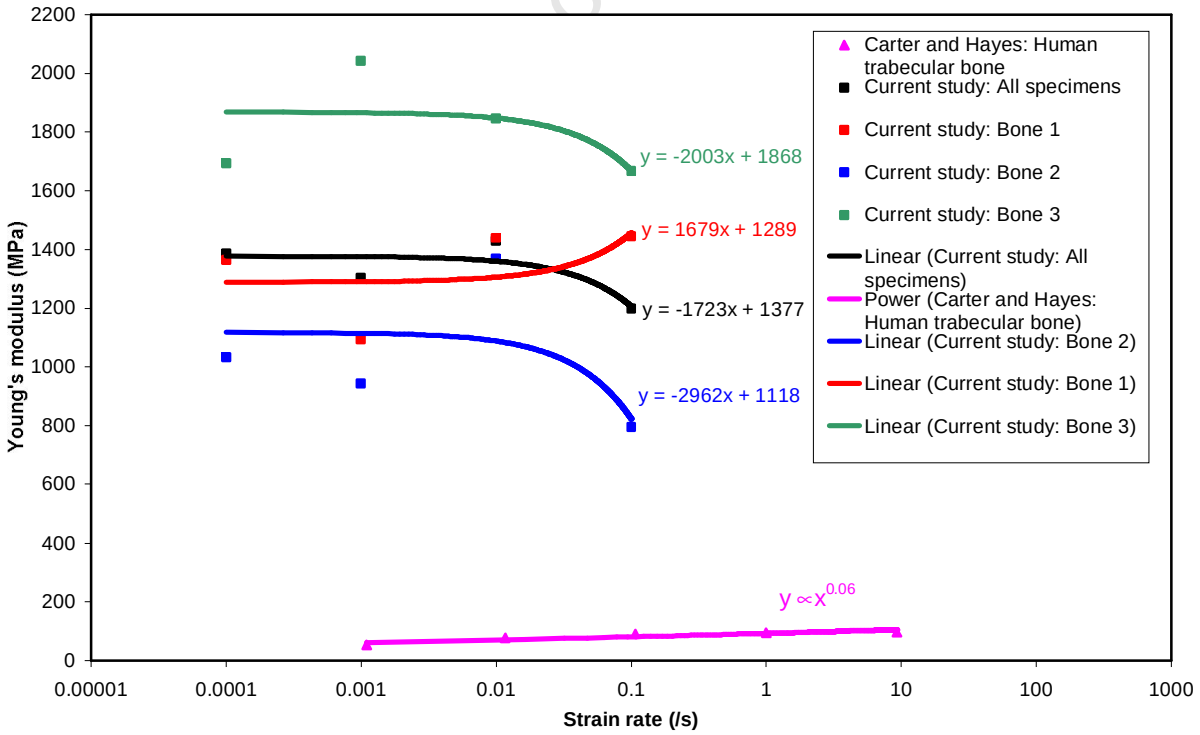

Figure 6.20: Comparison of results with Carter and Hayes [13].

6.2.2.3 Yield strain as a function of strain rate

Results are presented in both the power law and linear form in Figure 6.21. A linear relationship was found to exist on examination of the trend of the average results, shown in Figure 6.21(a) for all specimens. It can be seen in Table 6.5 and Figure 6.22 that the linear fits for each bone are similar.

No literature showing a positive relationship between failure strain and strain rate could be found. In fact, only two of the reviewed studies investigated the strain rate dependence of failure strains. McElhaney [45], studying cortical bone, found ultimate strain to decrease with increasing strain rate and Ouyang [14] found no significant correlation between ultimate strain and strain rate.

Table 6.5: Equation variables for yield strain dependence on strain rate

Data source	$\varepsilon_y = a\dot{\varepsilon}^b$			$\varepsilon_y = a\dot{\varepsilon} + b$		
	a	b	r^2	a	b	r^2
All specimens (ave.)	0.0304	0.0407	0.586	0.0671	0.0224	0.698
Bone 1	0.031	0.0463	0.7	0.0648	0.0222	0.645
Bone 2	0.0268	0.0062	0.008	0.053	0.0248	0.249
Bone 3	0.0284	0.045	0.966	0.0513	0.0206	0.700

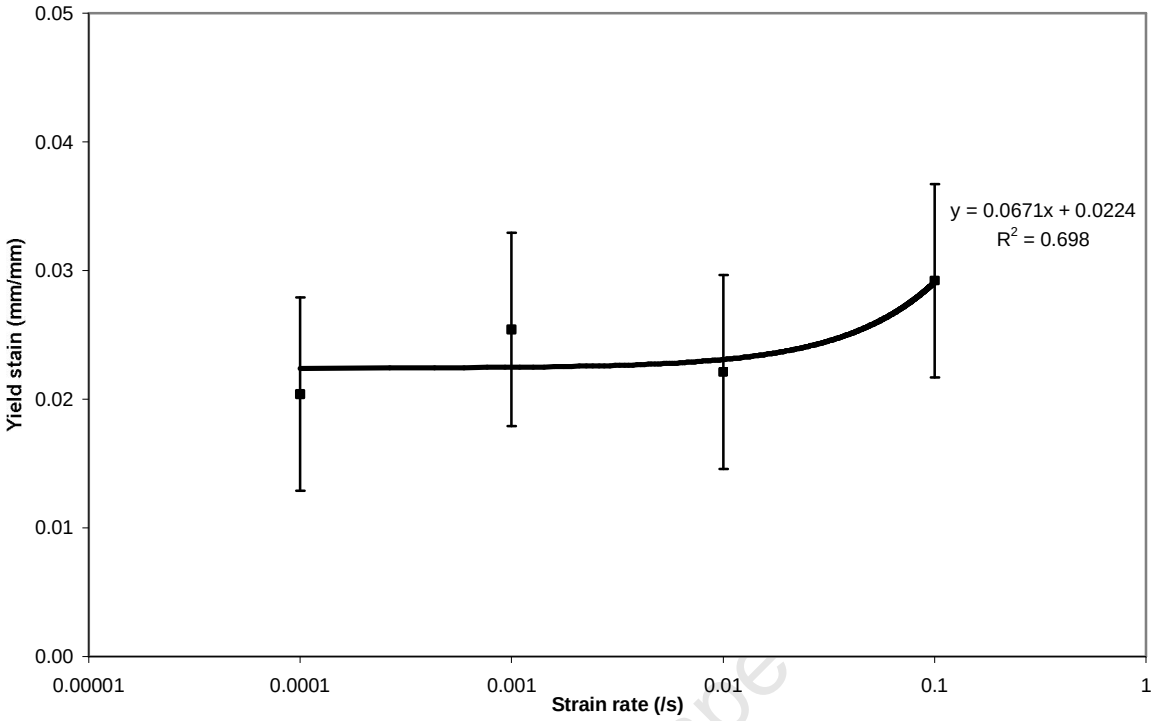

(a) Linear

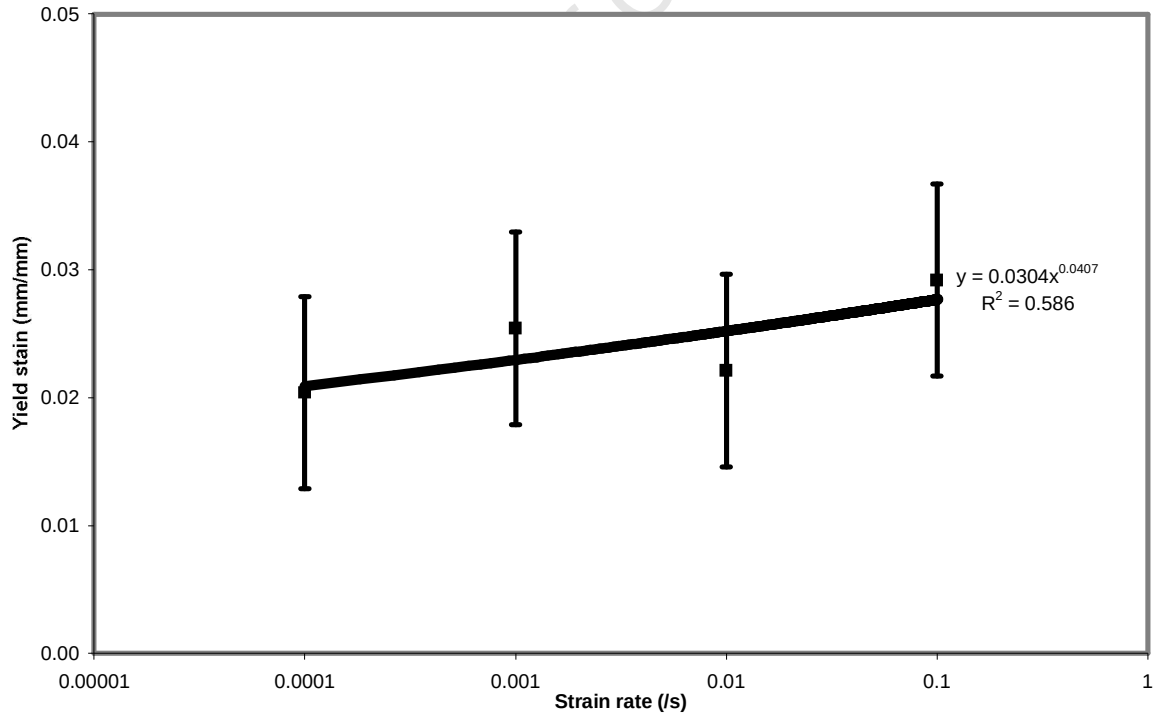

(b) Power law

Figure 6.21: The relationship between yield strain and strain rate for all specimens.

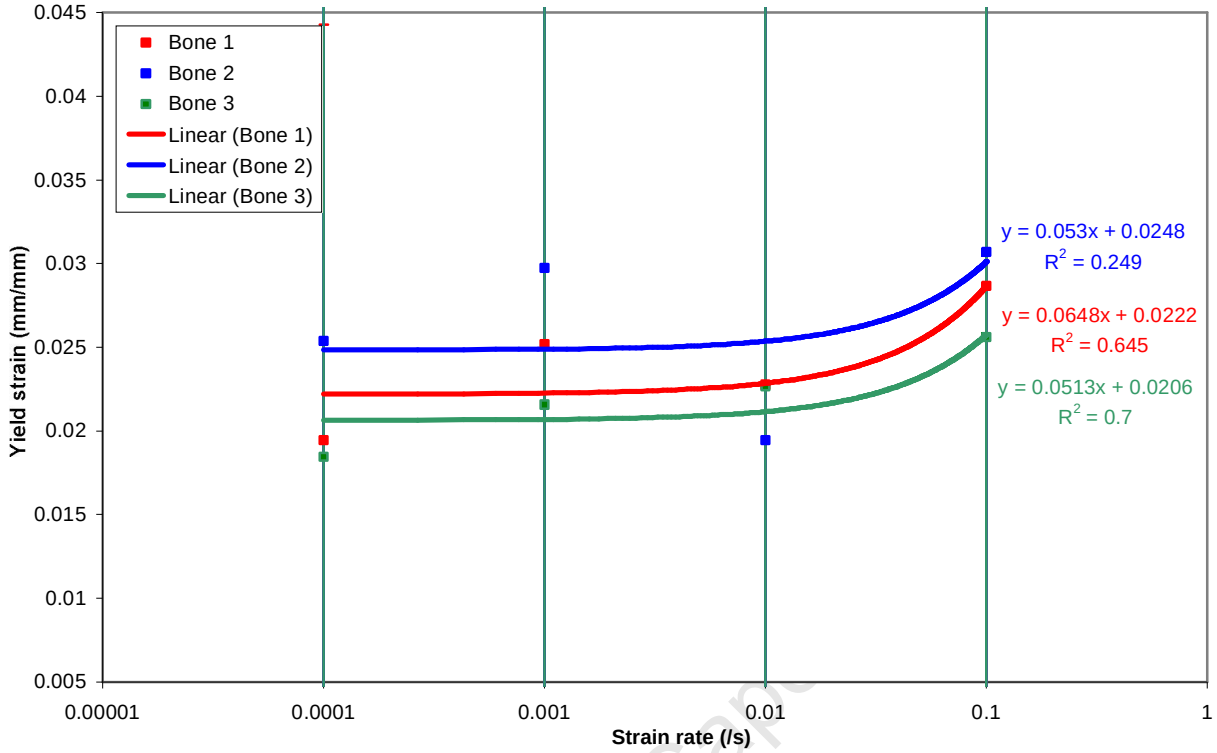

Figure 6.22: The relationship between yield strain and strain rate for each bone.

6.3 Tests with pre-conditioning cycles

In an attempt to minimise the scatter in results, it was decided to use pre-conditioning cycles before testing to destruction. Pre-conditioning cycles are non-destructive compression tests performed in order to reduce the initial nonlinear region of the stress-strain curve. Four specimens of similar densities were chosen and three cycles were performed on each specimen at a strain rate of 10^{-3} s^{-1} (Figure 6.23). Stress-strain curves (adjusted to exclude the end artifact) show that the pre-conditioning cycles did not substantially improve the scatter (Figure 6.24).

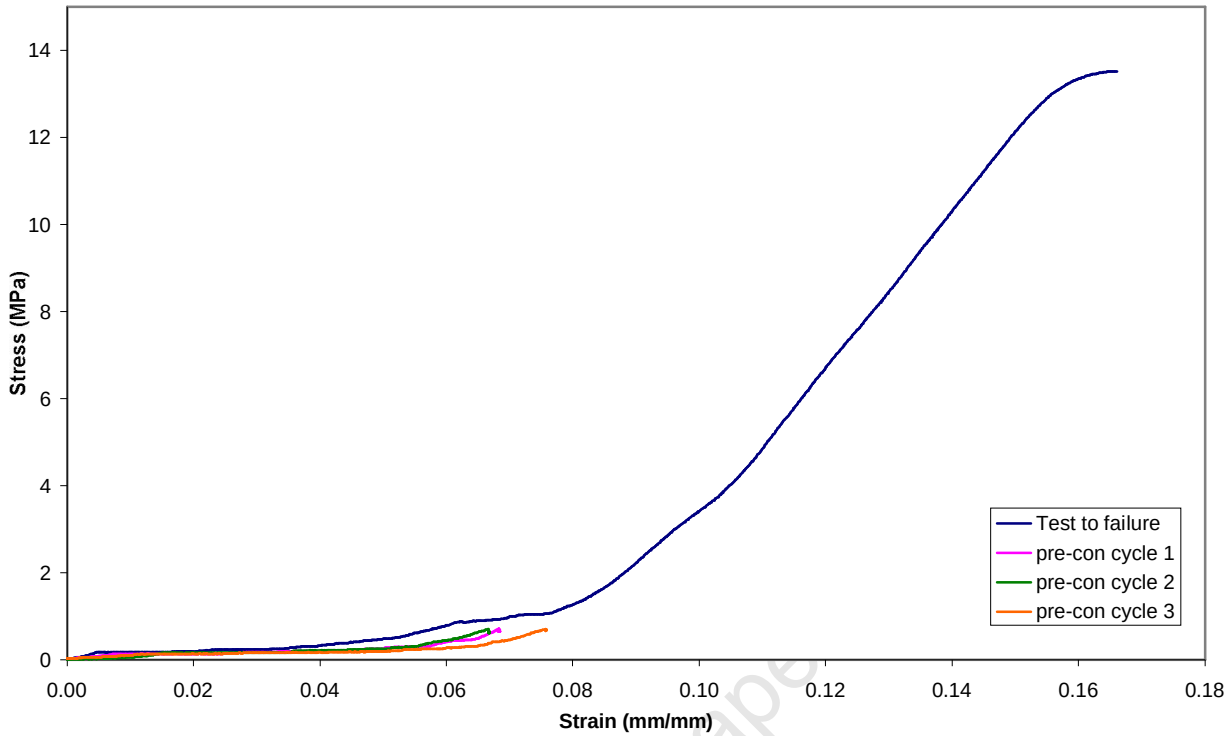

Figure 6.23: Pre-conditioning cycles for specimen 4.4.4

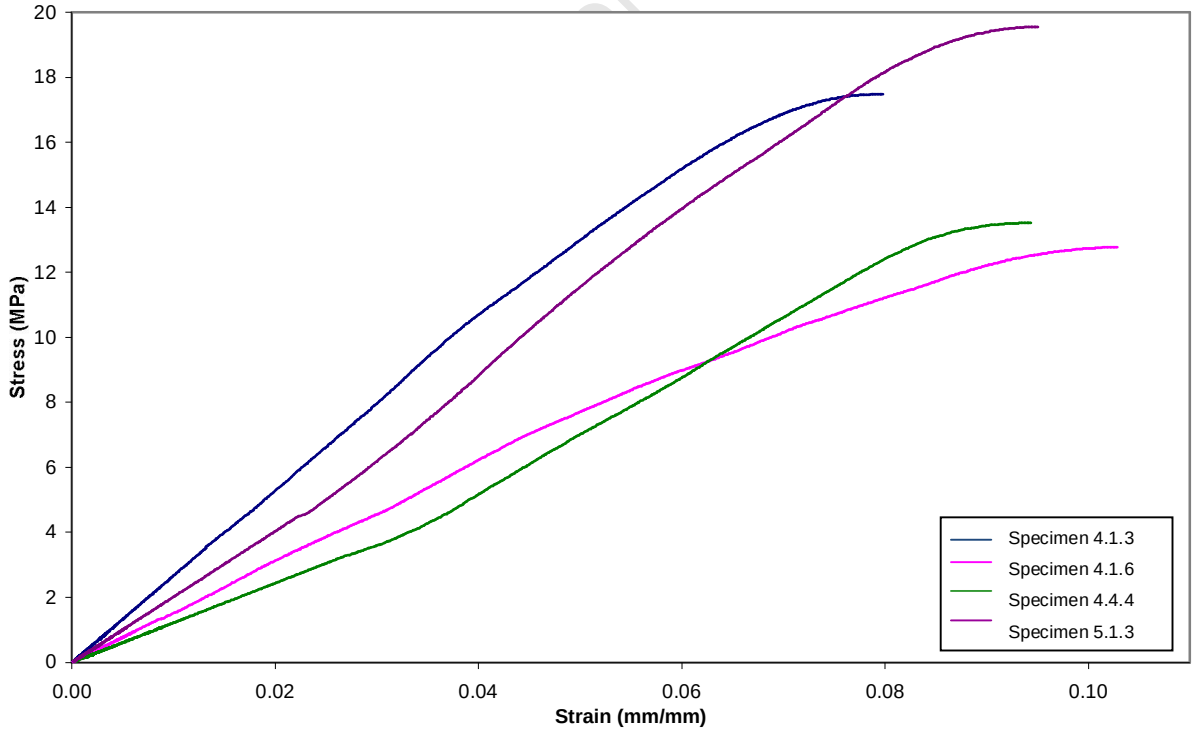

Figure 6.24: Stress-strain curve for specimens with pre-conditioning cycles

7 DYNAMIC RESULTS AND ANALYSIS

7.1 Split Hopkinson pressure data

Data from the split Hopkinson pressure bar recording equipment is in the form of voltage readings provided by the input and output bar strain gauges. To convert this data into stress, a calibration factor is used, the derivation of which is shown in Appendix B.

Typical raw data from the input and output pressure bars is shown in the form of a stress-time plot in Figure 7.1. Both the pressure bars are shown to be in compression after approximately 750 microseconds. This is believed to be as a result of the viscoelastic nature of bone, leading to the specimen "pushing back" on the bars after being initially compressed.

The stress wave measured on the input bar shows a compressive pulse (incident wave) followed by a tensile pulse (reflective wave). The stress wave measured on the output bar shows only the transmitted wave. Since these waves are recorded at the strain gauges, they are shifted in time in order to depict the stress state at the specimen-bar interface, shown in Figure 7.2.

The transmitted pulse reacts approximately 20 microseconds after the incident and reflected pulses. This lag in time indicates that the speed of sound in the magnesium bars and the cancellous bone is slightly mismatched.

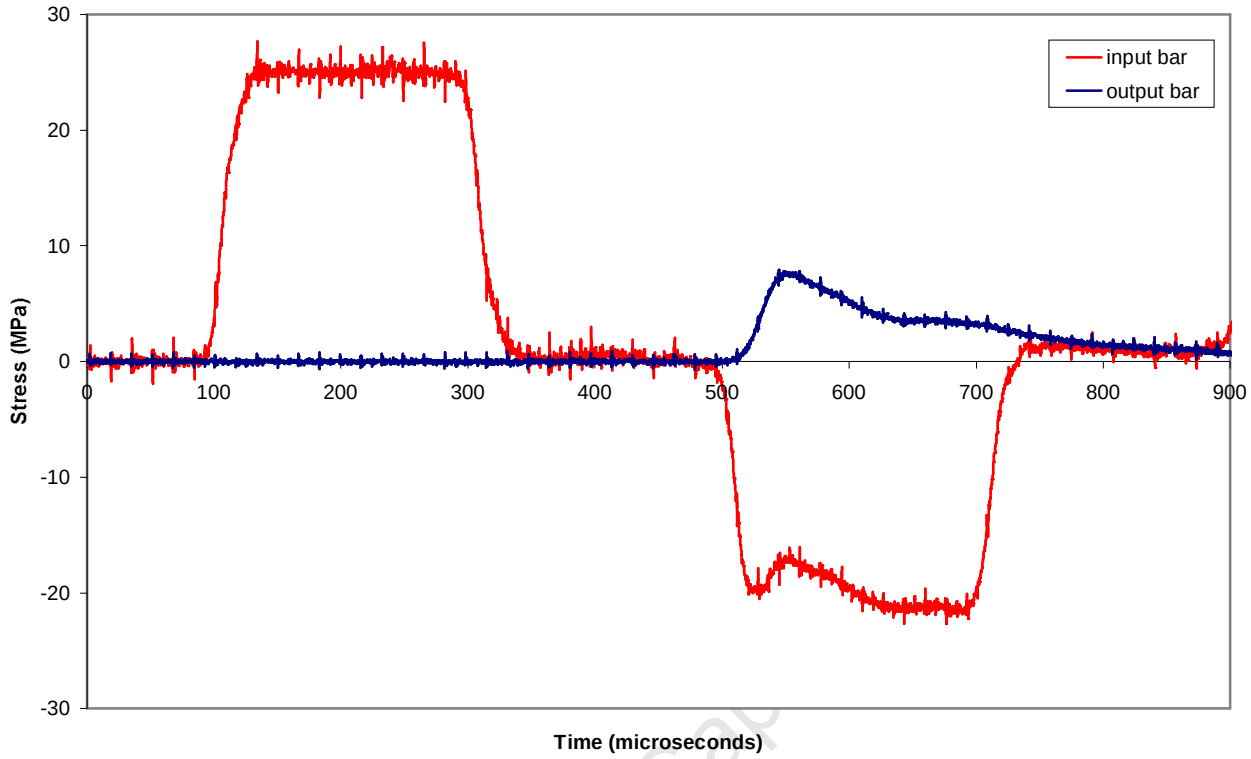

Figure 7.1: Stress-time plot for specimen 5.3.3.

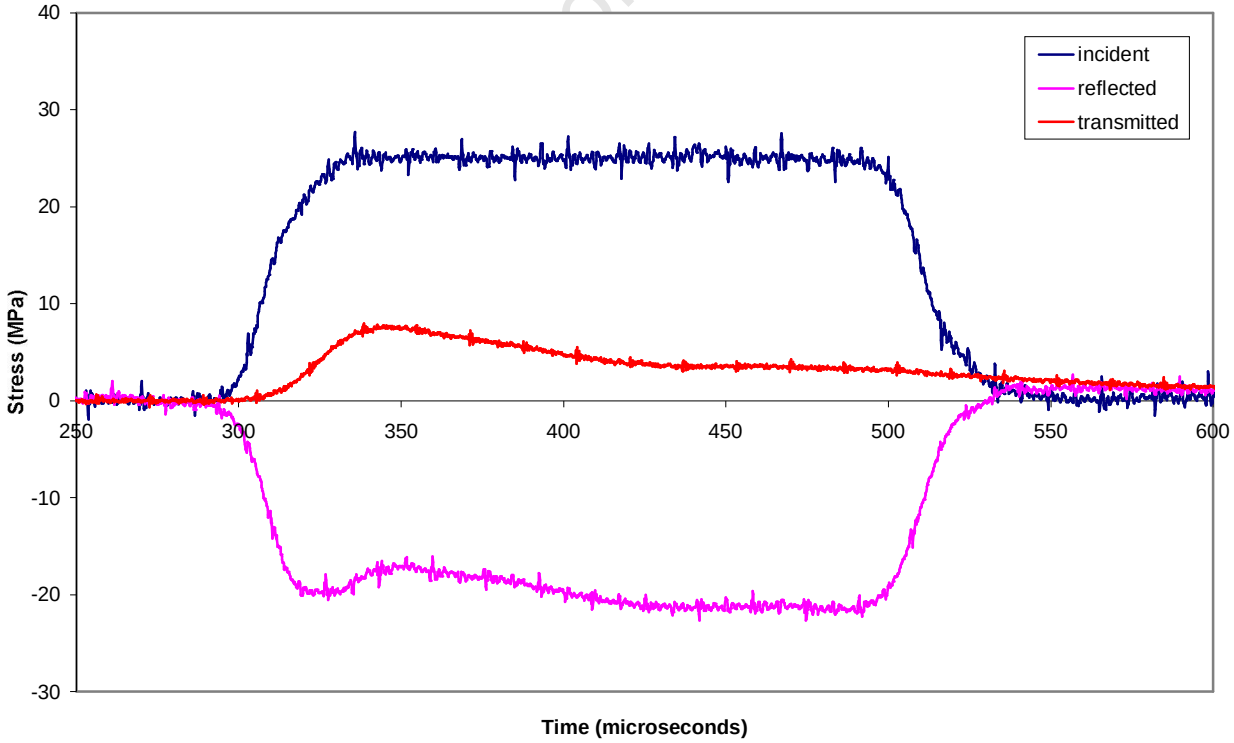

Figure 7.2: Shifted stress-time plot for specimen 5.3.3.

The stress in the bars is converted to specimen stress, strain and strain rate by the process described in Appendix B.

As shown in Figure 7.3, the strain rate varies during testing. For the purposes of analysis, the strain rate is defined as the maximum achieved prior to yield.

The raw data is smoothed out by plotting the average of every 50 data points, shown in Figure 7.3.

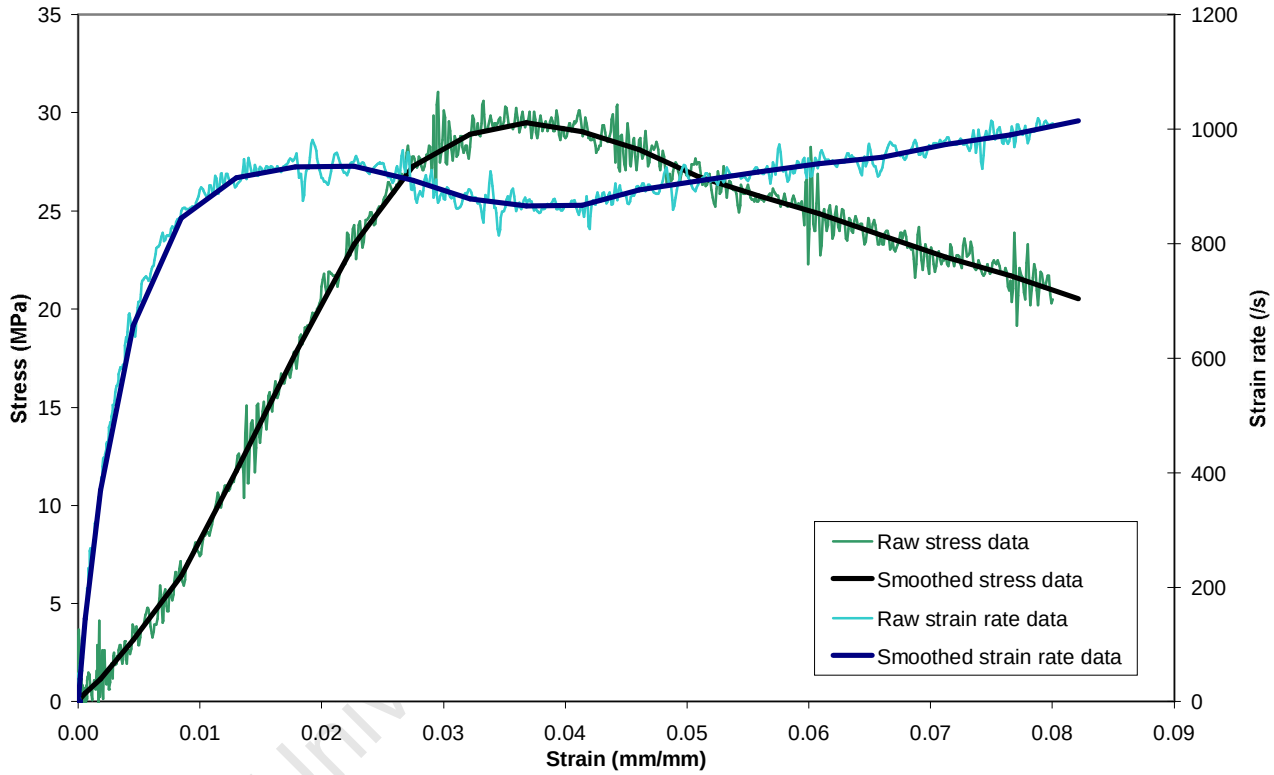

Figure 7.3: Comparison of raw to smoothed stress and strain rate data.

7.2 Stress-strain behaviour

In accordance with the quasi-static analysis, the yield stress is defined as 5% below the peak compressive strength; the Young's modulus is the slope of the stress-strain curve in the most linear section prior to yield, and the stress-strain curves are shifted along the strain axis according to the point of zero strain. Again, stress is determined using the constant area approach.

All the specimens used for dynamic testing were sourced from a single bone. In order to view the individual stress-strain curves, the specimens have been grouped according to the vertebrae from which they are taken (Figures 7.4 to 7.8). Graphs are shown up until the point of ultimate compressive stress, with the yield point indicated on the graphs representing individual vertebrae. Density, stress, strain and modulus values for the individual specimens are tabulated in Appendix F.

Figure 7.9 shows the three-dimensional graph of the stress-strain curves as a function of density.

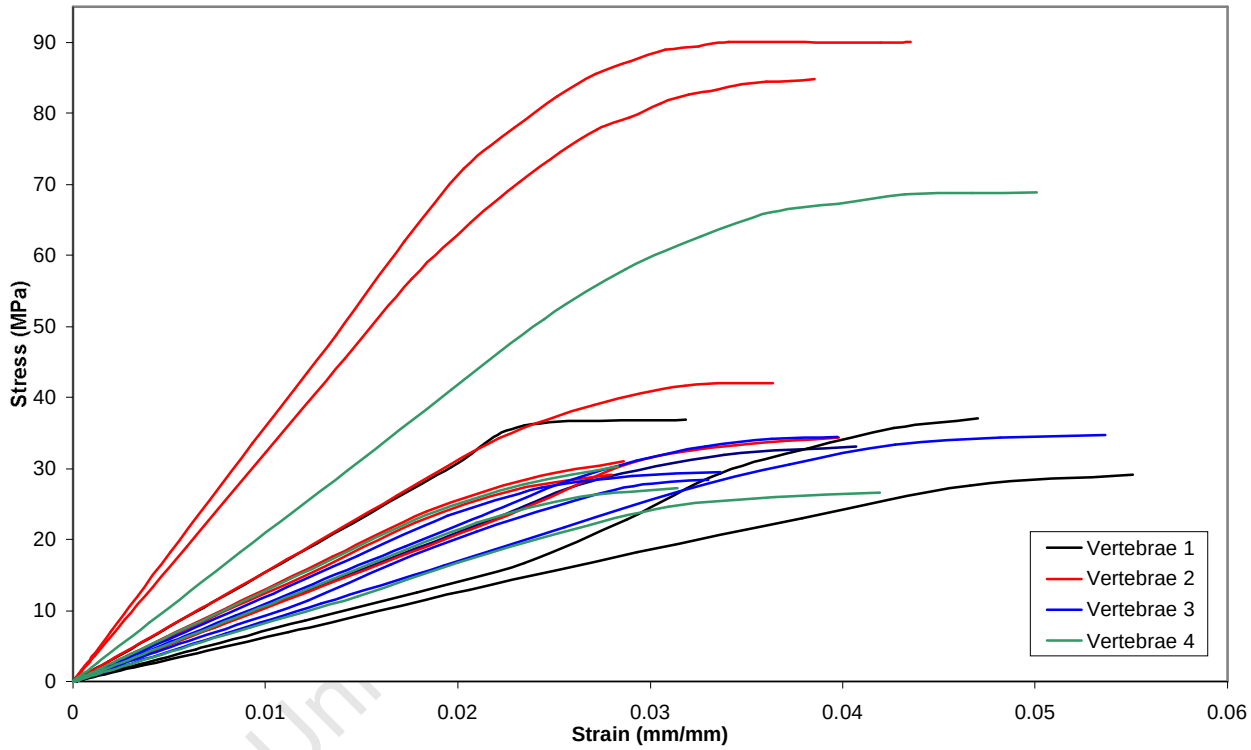

Figure 7.4: Stress-strain curves for all specimens.

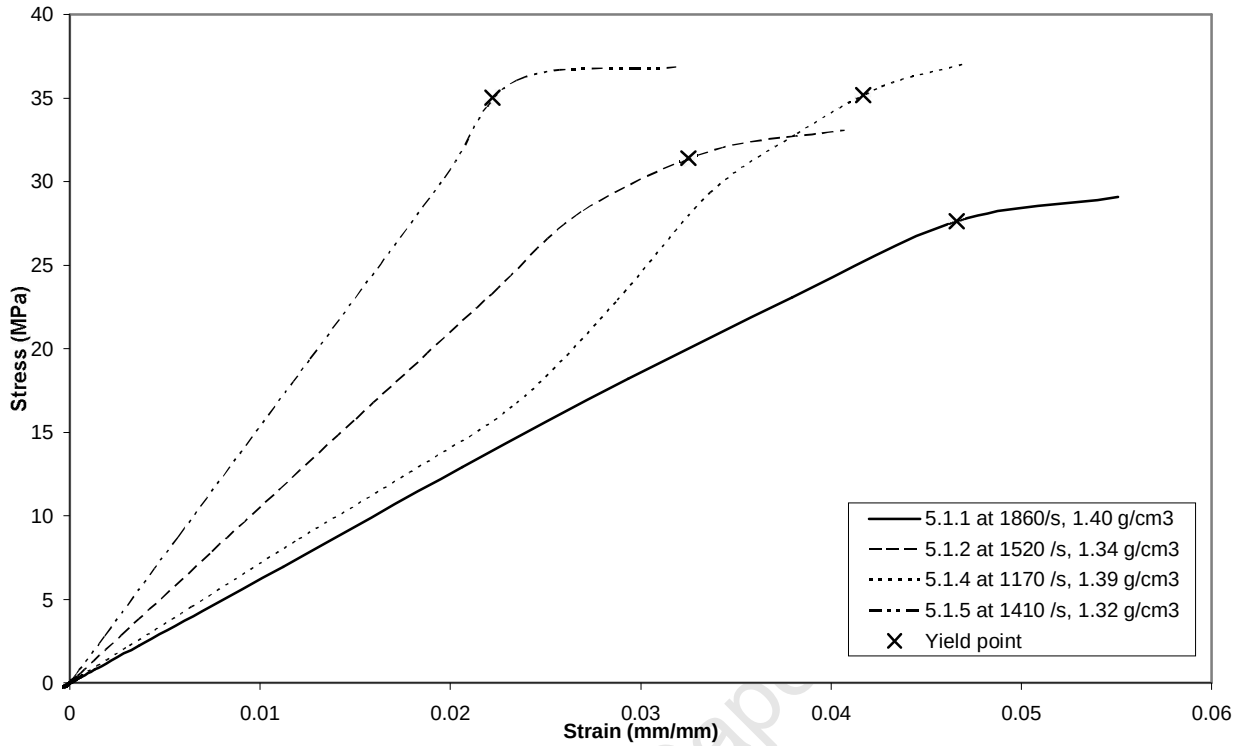

Figure 7.5: Stress-strain curves for specimens from vertebrae 1.

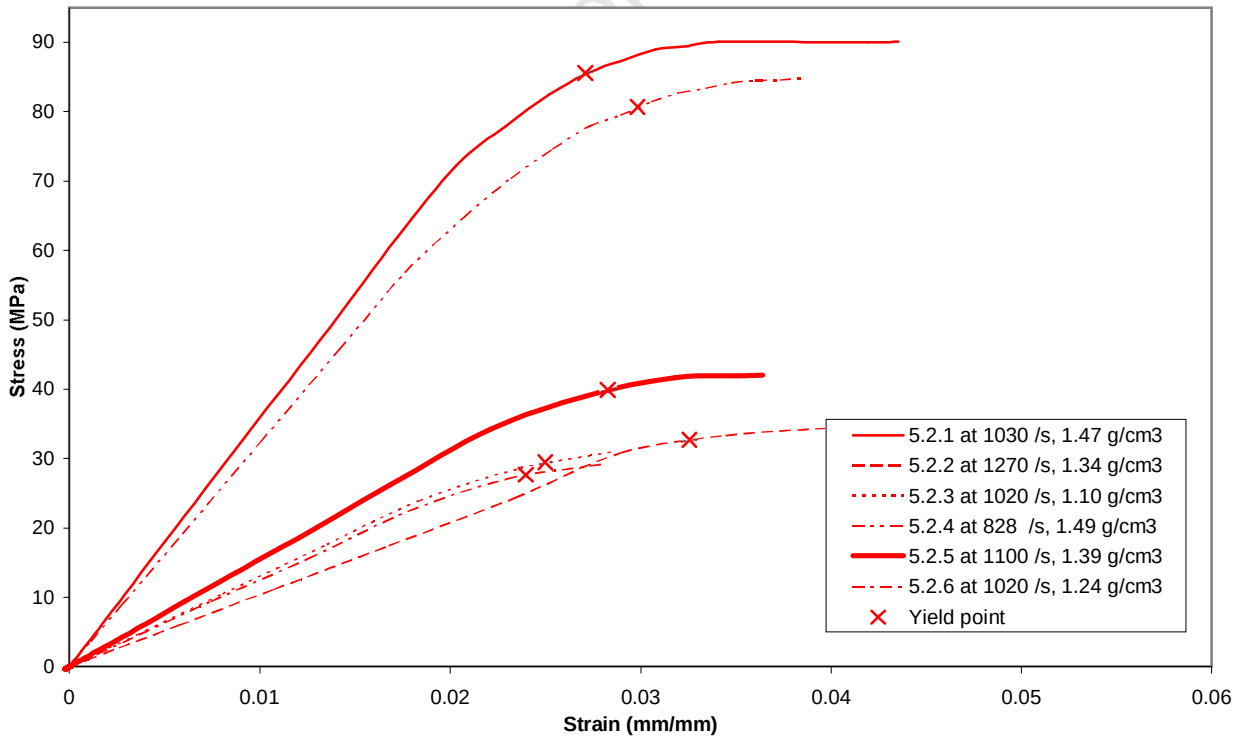

Figure 7.6: Stress-strain curves for specimens from vertebrae 2.

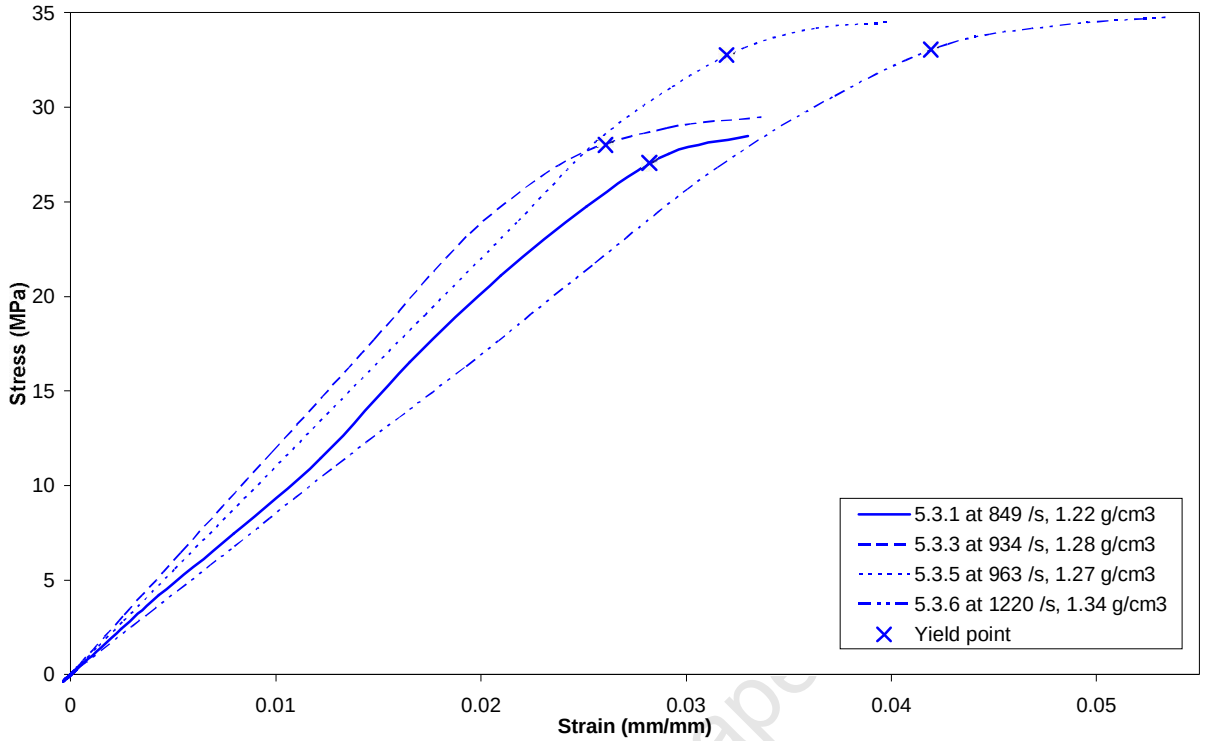

Figure 7.7: Stress-strain curves for specimens from vertebrae 3.

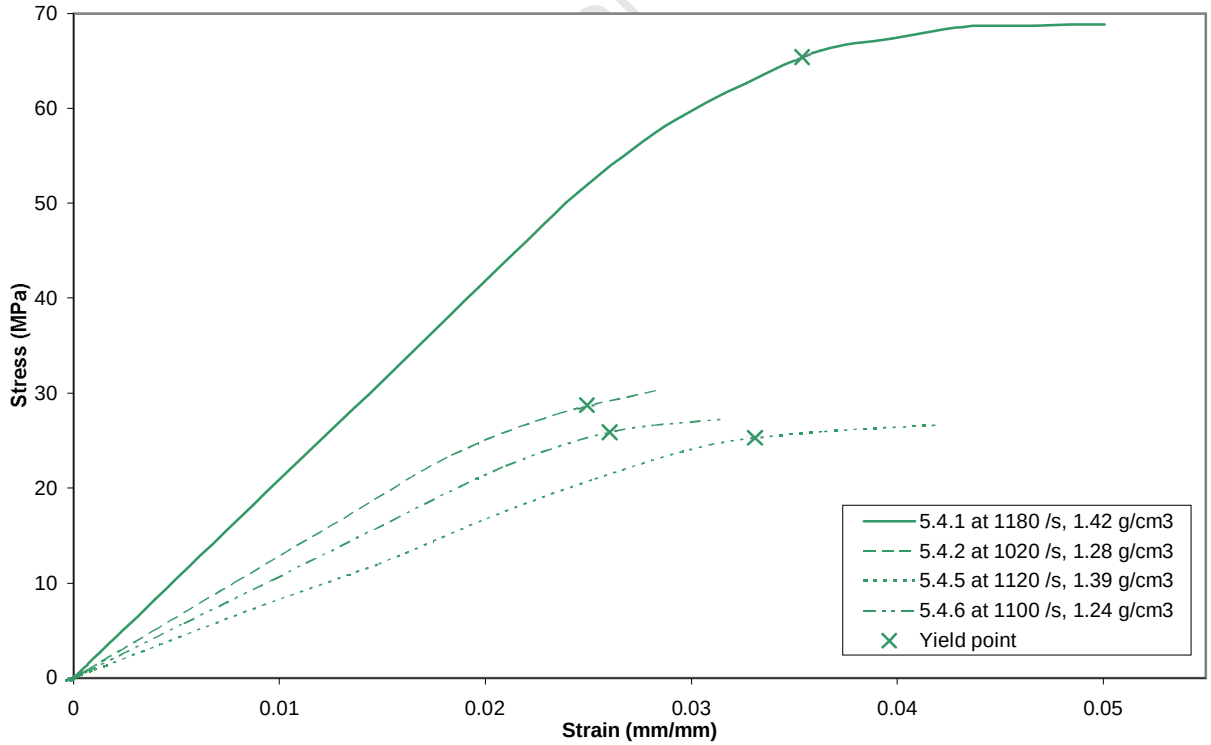

Figure 7.8: Stress-strain curves for specimens from vertebrae 4.

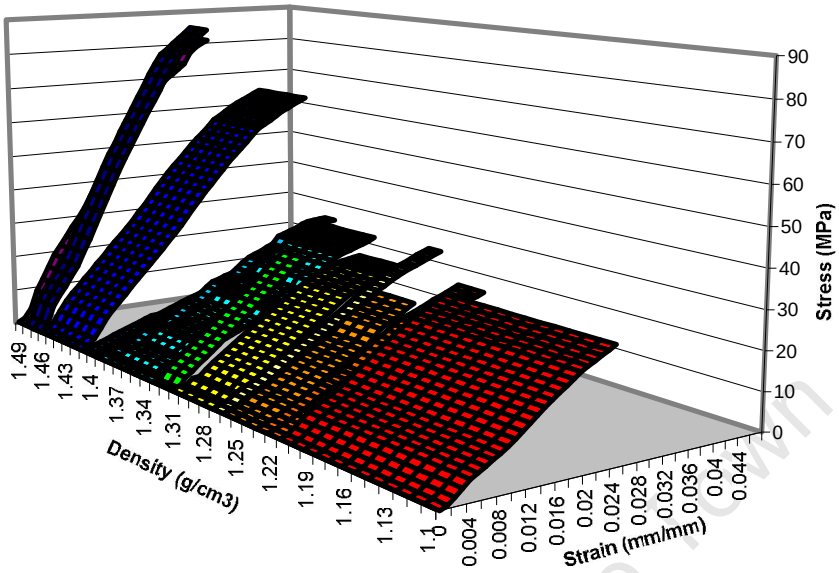

Figure 7.9: Stress-strain curves as a function of density

A number of specimens were filmed, using a high-speed camera, during impact. The compression of specimen 5.3.3 is shown in Figure 7.10. Note that the time shown does not correspond to the time of the dynamic test, since the camera is not linked to the Hopkinson bar setup. The last frame marks the end of the initial compressive pulse. Thereafter, the squashed specimen pushes back, causing compression of both pressure bars.

The dynamic compression process is characterised by the successive failure of individual trabeculae, with those on the periphery often becoming loose, as can be seen in frame 8. Typically, the bulk of the specimen remains in position for a number of cycles of reloading and then falls out.

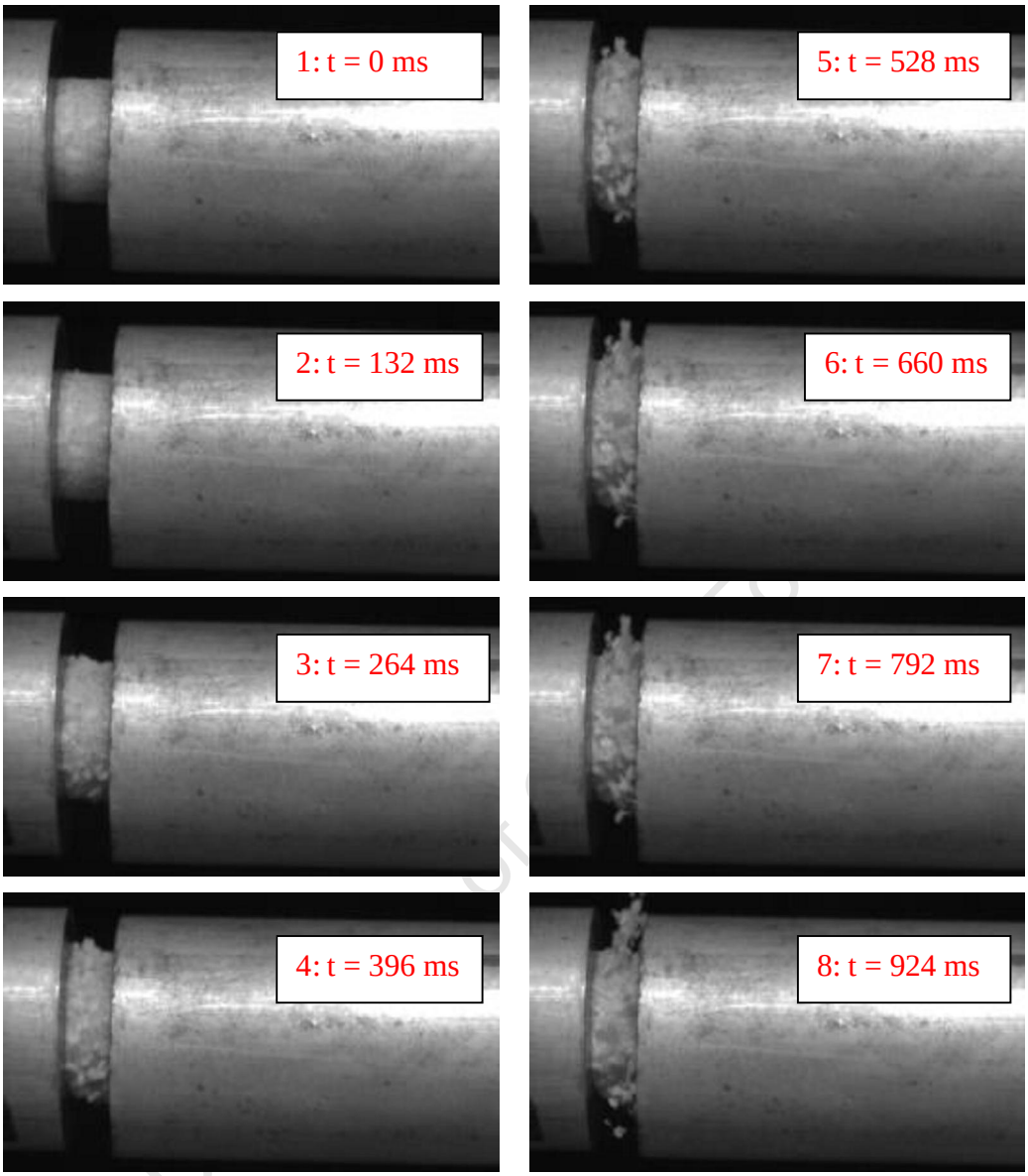

Figure 7.10: Compression of specimen 5.3.3.

7.2.1 Comparison of results to literature

Compared to quasi-static loading, dynamic loading on cancellous bone has not been explored extensively. Of the literature reviewed, dynamic stress-strain behaviour was limited to the investigation by Shim [1], shown in Figure 3.12. This figure shows a human vertebral specimen of 0.95 g/cm^3 fresh bone density tested at a strain rate of 1200 /s to yield at approximately 17 MPa and 0.03 strain. Results of the current study, with average density

1.33 g/cm^3, show the majority of specimens to yield between 25 to 35 MPa and 0.025 to 0.035 strain. Since the densities in the current study are higher and bovine bone is stronger than human, higher yield stresses are expected [6]. The yield strains are in the same range since strain is not heavily dependent on density and it does not differ greatly between species [40, 41, 6].

7.3 Trends in mechanical properties

As per the quasi-static analysis, linear and power fit relationships are explored and compared. Again, trends are shown with both 68.3 and 95.4% confidence intervals. The lower confidence level is not shown where it drops below zero since this is nonsensical.

7.3.1 Trends with density

The linear and power trends in yield stress, Young's modulus and yield strain with density are shown in Table 7.1 and are discussed in the following sections. The effect of strain rate is considered negligible since it covers a small range (approximately 800 to 1900 /s) and its effect on mechanical properties is not as pronounced as that of density.

Table 7.1: Equation variables for dependence on density

Data source	y	$y = a\rho^b$			$y = a\rho + b$		
		a	b	r^2	a	b	r^2
All specimens	σ_y	13.74	3.37	0.438	131	-135	0.461
All specimens	E	682	2.15	0.118	4239	-4231	0.257
All specimens	ε_y	0.021	1.30	0.215	0.031	-0.0101	0.192

7.3.1.1 Yield stress as a function of density

Table 7.1 shows that, although the correlation coefficients for linear and power law fits are similar, a linear relationship between stress and density is found to be the most appropriate (Figure 7.11(a)). This is in contradiction to most of the findings in the literature and in the

quasi-static analysis. Therefore results are also presented showing the power law trend (Figure 7.11(b).

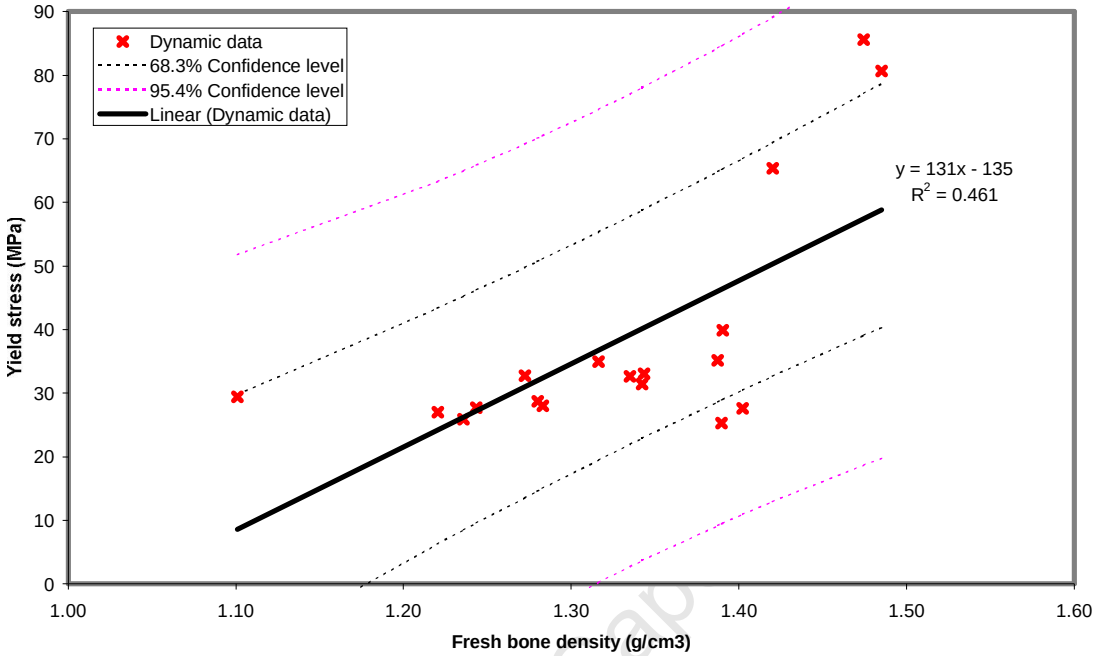

(a) Linear

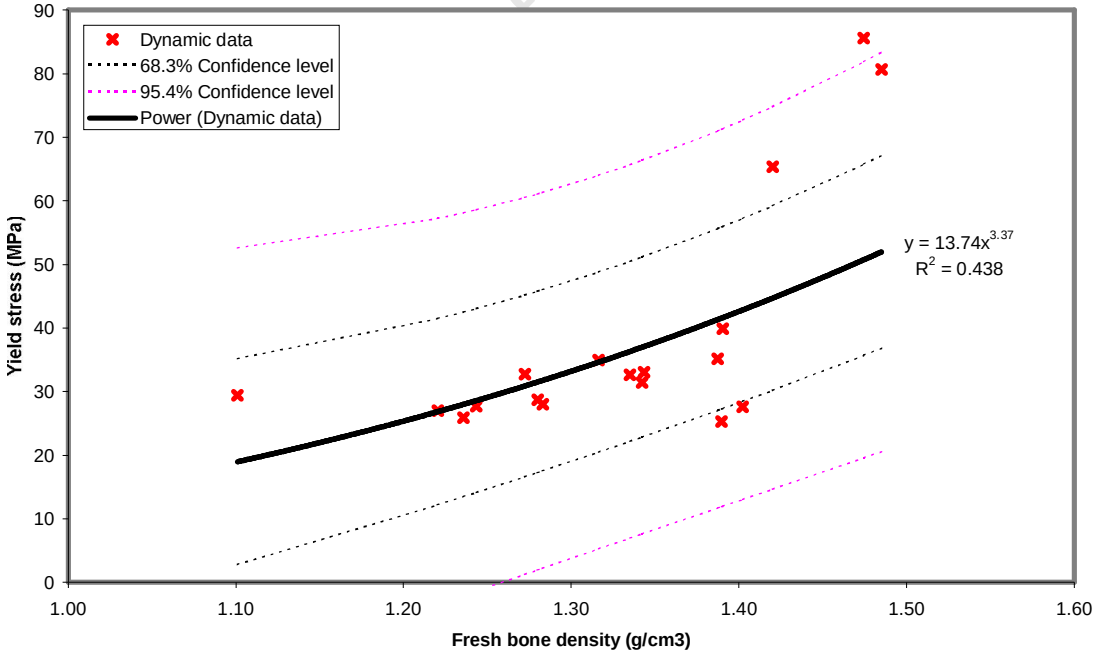

(b) Power law

Figure 7.11: The relationship between yield stress and density for all specimens.

7.3.1.2 Young's modulus as a function of density

The modulus-density trend is best described by a linear fit, shown in Figure 7.12(a). This is in agreement with the quasi-static analysis but in contradiction to the bulk of the literature (Table 3.1). Figure 7.12(b) shows the trend in the expected power law form.

7.3.1.3 Yield strain as a function of density

As expected from results in the quasi-static analysis, yield strain favours a power law trend with density, shown in Figure 7.13(b). However, this dynamic trend shows yield strain to increase more steeply (exponent of 1.30) than found in the quasi-static analysis (exponent of 0.55), discussed in section 6.2.1.3.

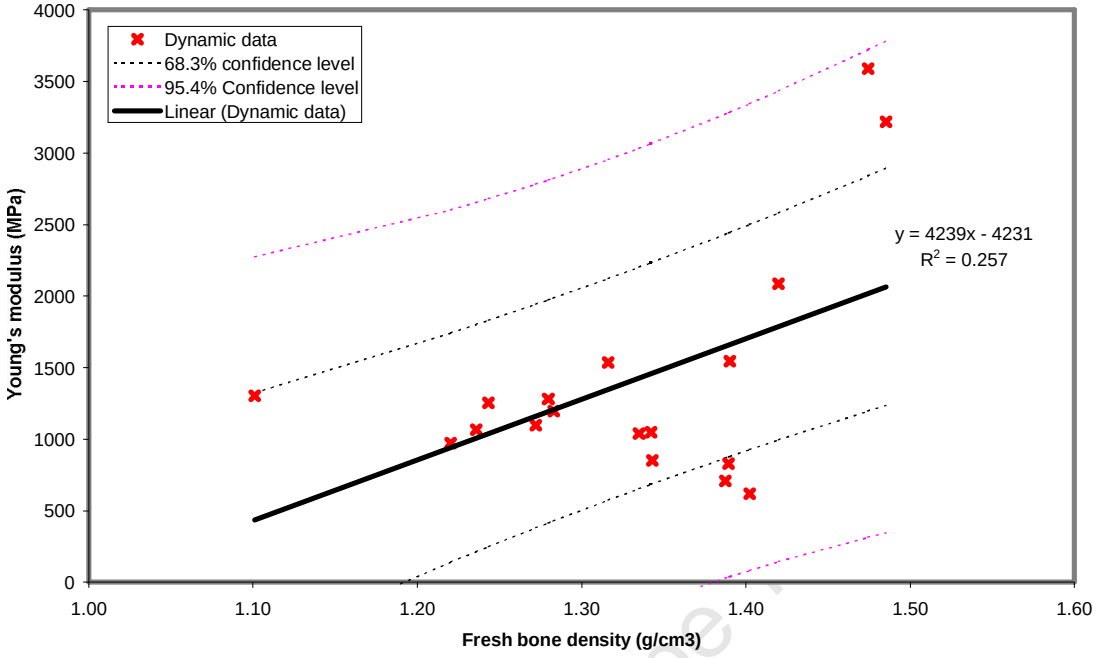

(a) Linear

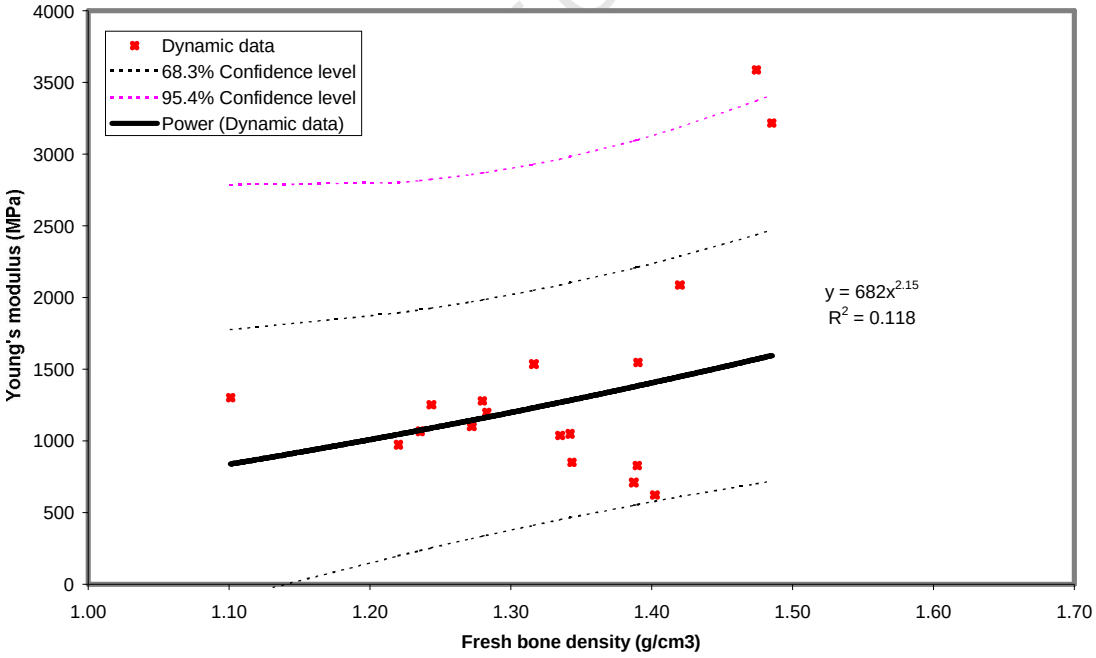

(b) Power law

Figure 7.12: The relationship between Young's modulus and density for all specimens.

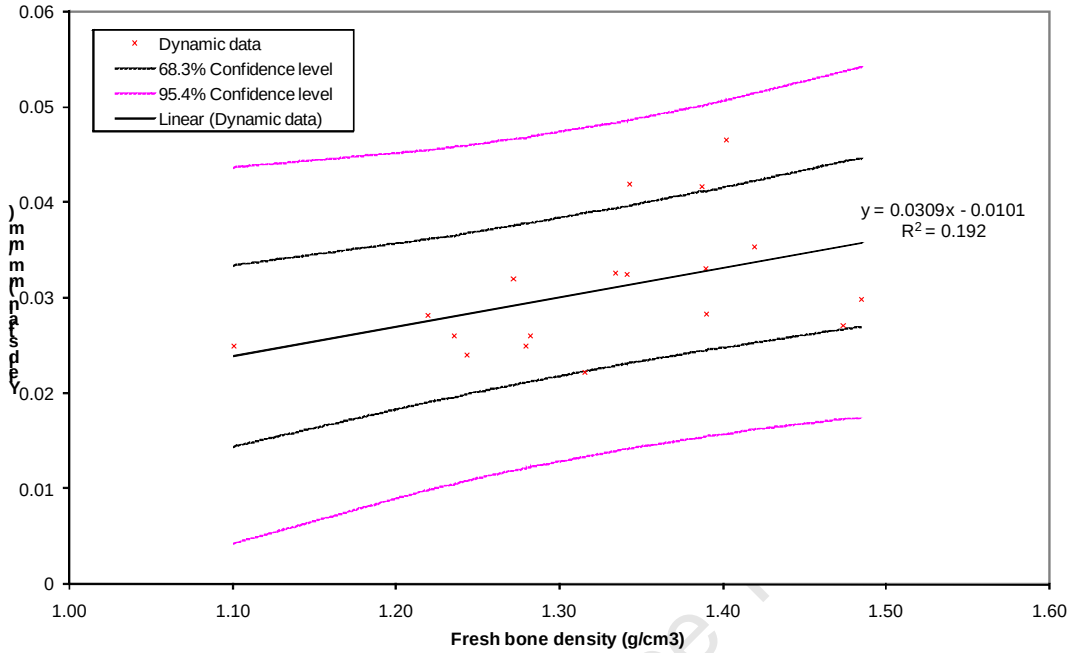

(a) Linear

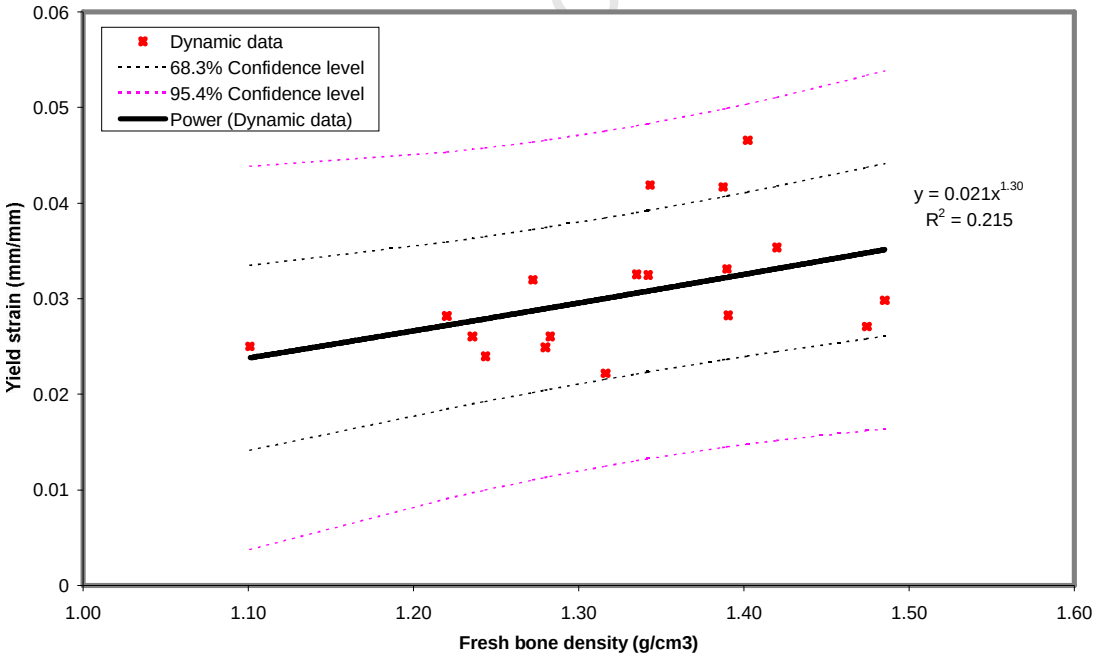

(b) Power law

Figure 7.13: The relationship between yield strain and density for all specimens

7.3.2 Trends with strain rate

The properties of each specimen have been normalised so as to represent the equivalent value at a mean density of 1.33 g/cm^3.

The linear and power trends in yield stress, Young's modulus and yield strain with density are shown in Table 7.2 and are discussed in the following sections.

Table 7.2: Equation variables for dependence on strain rate

Data source	y	$y = a\dot{\varepsilon}^b$			$y = a\dot{\varepsilon} + b$		
		a	b	r^2	a	b	r^2
All specimens	σ_y	4542	-0.690	0.242	-0.02	60	0.204
All specimens	E	2 x 10^6	-1.01	0.194	-1.18	2750	0.135
All specimens	ε_y	3 x 10^{-4}	0.647	0.194	2 x 10^{-5}	0.01	0.266

7.3.2.1 Yield stress as a function of strain rate

Results show yield stress to decrease with increasing strain rate, according to a power law trend, as shown in Figure 7.14(b). This is in disagreement with the literature and the trends found in the quasi-static analysis, which report positive trends only (section 6.2.2.1). However, the range of strain rates is narrow (approximately 800 to 1900 /s) and the correlation poor. Therefore trends may be difficult to determine.

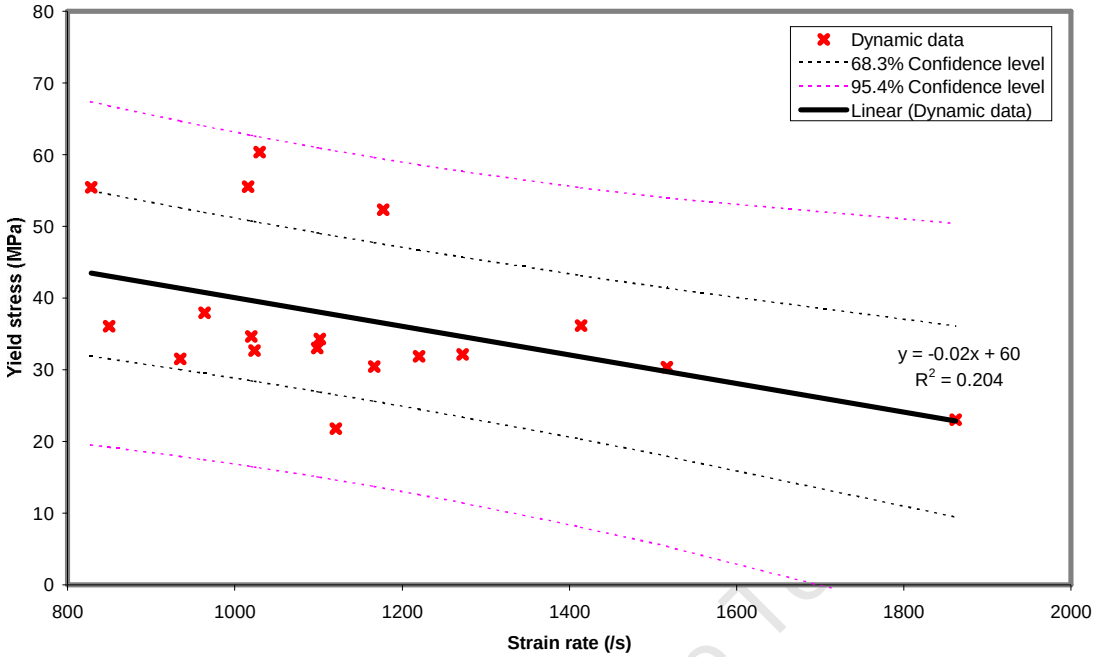

(a) Linear

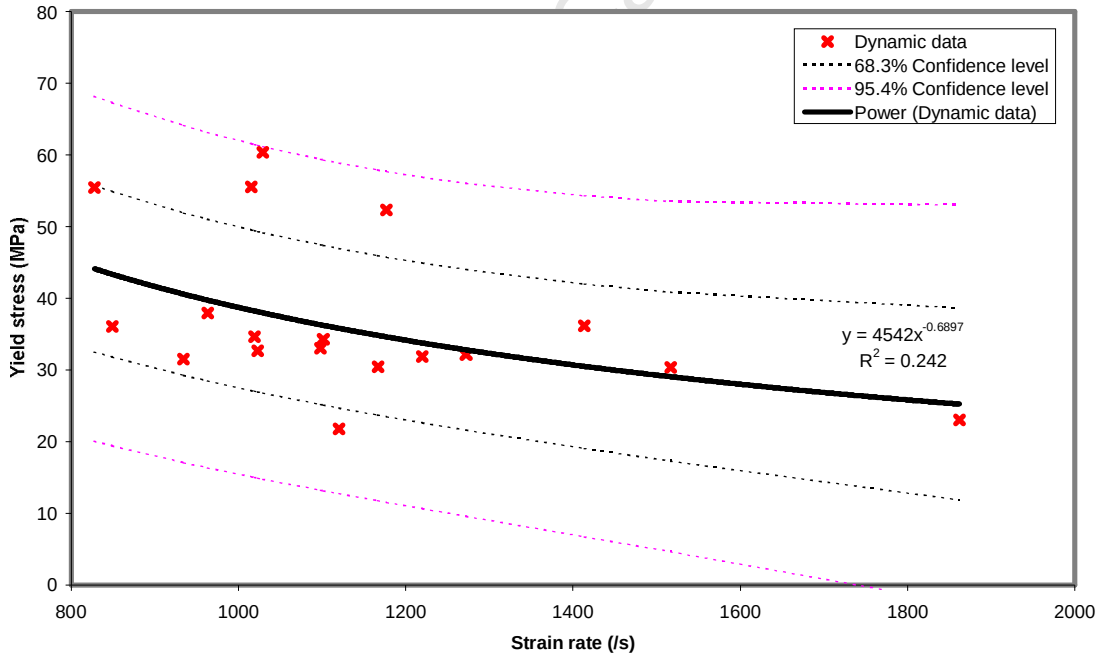

(b) Power law

Figure 7.14: The relationship between yield stress and strain rate for all specimens.

7.3.2.2 Young's modulus as a function of strain rate

The stiffness of the bone does not behave in the expected manner i.e. the relationship between modulus and strain rate is negative as opposed to positive (Figure 7.15). Again, this is likely due to the range of strain rates being too small.

7.3.2.3 Yield strain as a function of strain rate

Yield strain is the only dynamic property determined from this group of specimens that behaves in a predictable manner. It is characterised by a positive linear relationship to strain rate, as illustrated in Figure 7.16.

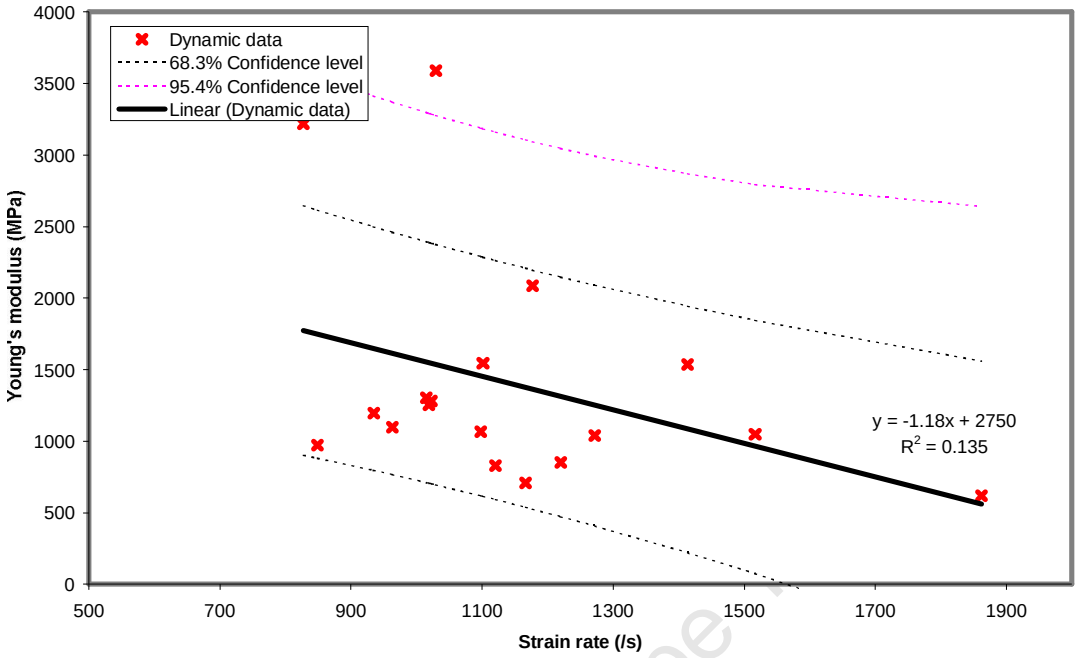

(a) Linear

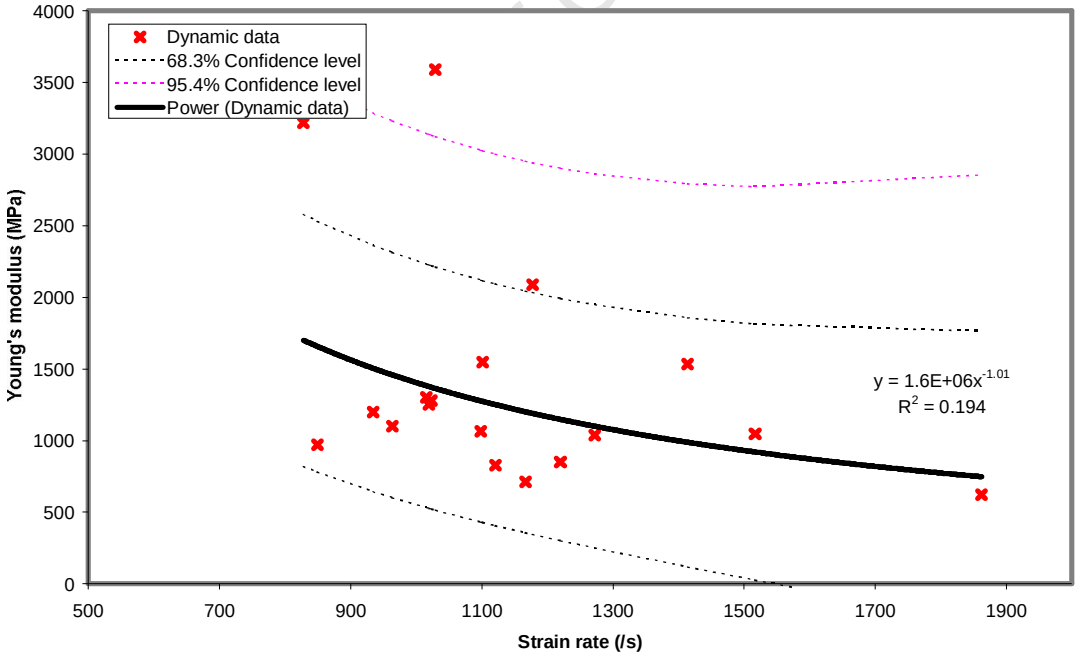

(b) Power law

Figure 7.15: The relationship between Young's modulus and strain rate for all specimens.

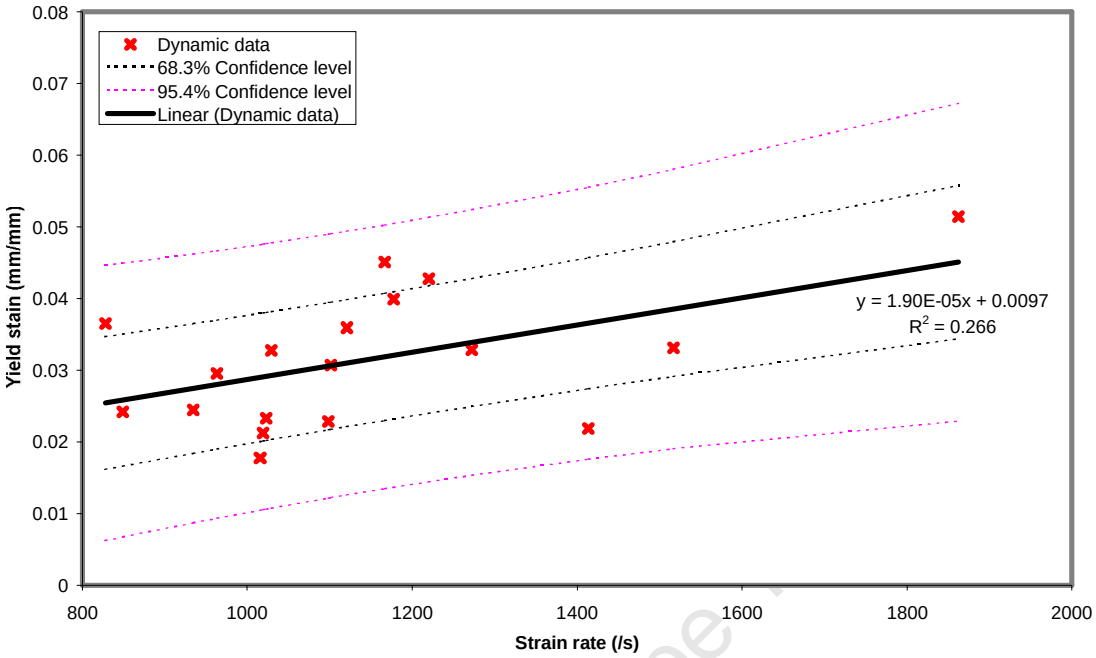

(a) Linear

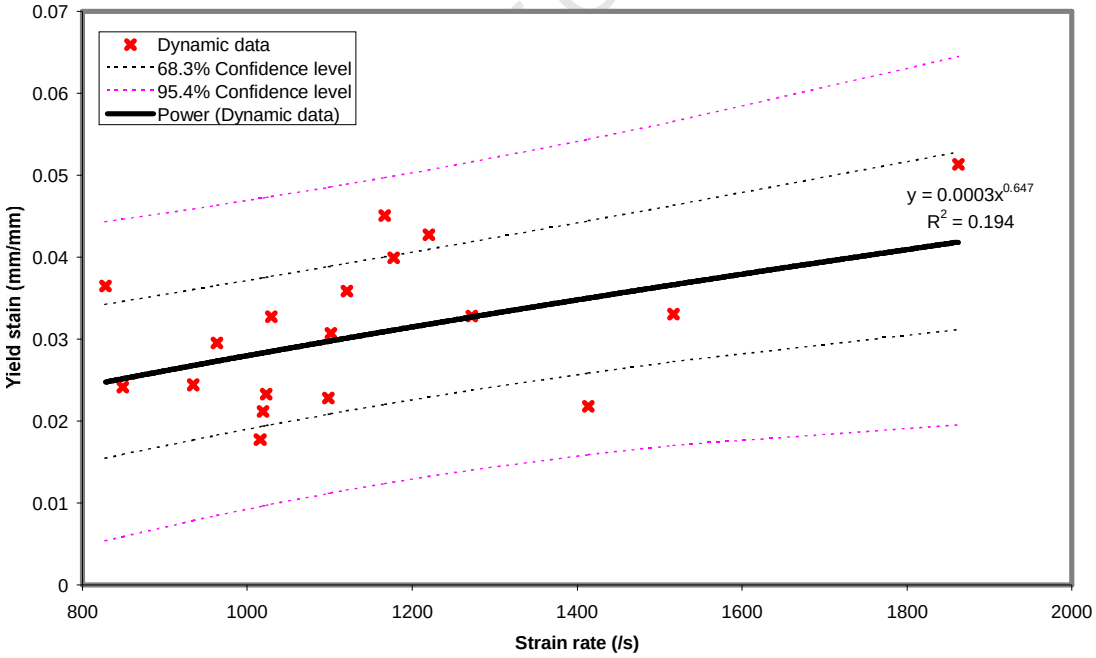

(b) Power law

Figure 7.16: The relationship between yield strain and strain rate for all specimens.

8 COMBINED RESULTS AND ANALYSIS

8.1 Stress-strain behaviour

A comparison of the quasi-static and dynamic stress-strain curves are shown in Figure 8.1. It is clear that there is no marked difference between the two sets of data. However, the average density of the quasi-static set is 1.40 g/cm^3, while the dynamic has a lower average of 1.33 g/cm^3. This may account for the lack of distinction between the data sets, since density has a far greater influence on mechanical properties than strain rate.

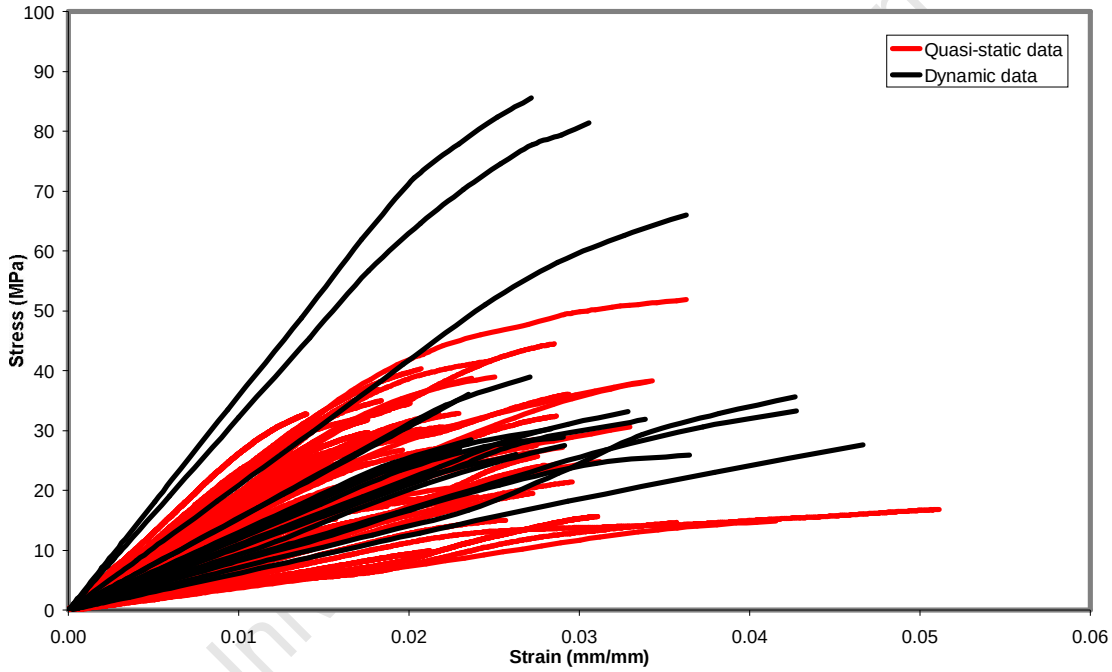

Figure 8.1: Comparison of quasi-static and dynamic stress-strain curves

8.2 Trends in mechanical properties

In the preceding sections, strain rate was considered to be negligible when investigating the effect of density on mechanical properties. This is because the range of strain rates was small in both the quasi-static and the dynamic data. However, combining the data leads to strain rates covering a range

from 10^{-4} to 1900 /s. Consider a mechanical property "y" dependent on the bone density and strain rate in the following manner:

$$y = a\rho^b \dot{\varepsilon}^c$$

Assuming a "c" value of 0.06, as reported in the literature [13]:

For $\dot{\varepsilon} = 10^{-4}$, $\dot{\varepsilon}^c = 0.575$

For $\dot{\varepsilon} = 1900$, $\dot{\varepsilon}^c = 1.573$

Therefore, strain rate may have a considerable effect, with results reading up to 2.7 times higher if it is not accounted for.

8.2.1 Trends with strain rate

Results are normalised to represent the average density of all the specimens, 1.38 g/cm^3. The equations used for this process are those derived in the quasi-static and dynamic analysis and are listed below in the relevant sections.

8.2.1.1 Yield stress as a function of strain rate

In order to normalise the data with respect to density, the following equations are used:

$\sigma_{qs} = 11.4\rho^{2.36}$ (Table 6.2)

$\sigma_d = 131\rho - 135$ (Table 7.1)

The relationship between stress and density is shown in Figure 8.2. The equation variables are listed and compared to results from quasi-static and dynamic data groups in Table 8.1.

Table 8.1: Equation variables for yield stress dependence on strain rate

Data source	$\sigma_y = a\dot{\varepsilon}^b$			$\sigma_y = a\dot{\varepsilon} + b$		
	a	b	r^2	a	b	r^2
Quasi-static data	32.86	0.0401	0.975	48.61	24.87	0.574
Dynamic data	4542	-0.690	0.242	-0.02	60	0.204
Combined data	32.07	0.0458	0.425	0.0174	26.34	0.249

As per results of both the quasi-static and dynamic data groups, the combined data shows stress to be best related to strain rate by a power law function similar to that found in the quasi-static analysis. The power law exponent of 0.046 is comparable to, albeit slightly lower than, that of 0.06 found by Carter and Hayes [13].

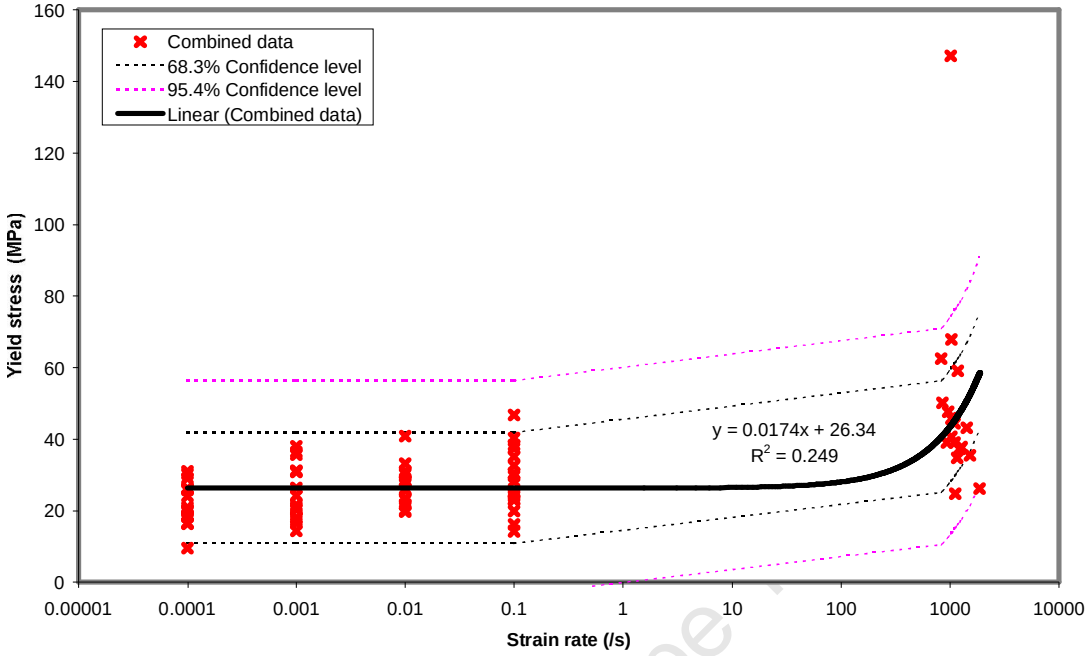

(a) Linear

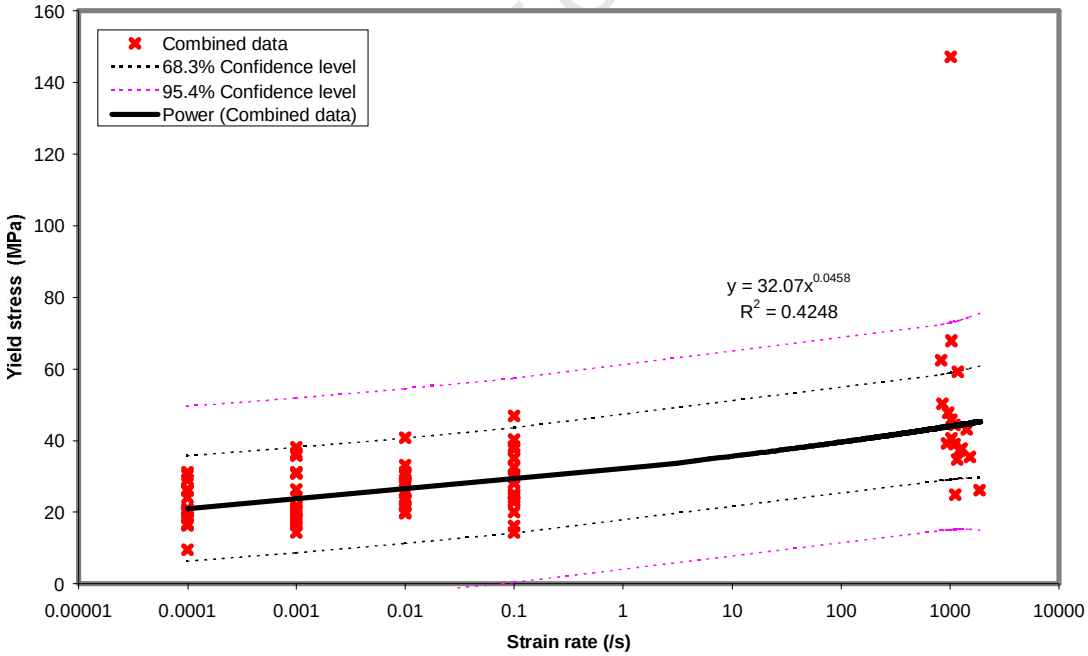

(b) Power law

Figure 8.2: The relationship between yield stress and strain rate for all specimens.

8.2.1.2 Young's modulus as a function of strain rate

The density normalisation equations used are:

$\sigma_{qs} = 1814\rho + 1198$ (Table 6.3)

$\sigma_{d} = 4239\rho - 4231$ (Table 7.1)

The strain rate dependence of the Young's modulus of all specimens is illustrated in Figure 8.3. This relationship is compared to those found under quasi-static and dynamic loading in Table 8.2.

Table 8.2: Equation variables for Young's modulus dependence on strain rate

Data source	$E = a\dot{\varepsilon}^b$			$E = a\dot{\varepsilon} + b$		
	a	b	r^2	a	b	r^2
Quasi-static data	1217	-0.0149	0.329	-1723	1377	0.674
Dynamic data	$2x10^6$	-1.01	0.194	-1.18	2750	0.135
Combined data	1332	0.0133	0.0247	0.249	1349	0.0349

Results favour a positive linear trend, as found in the quasi-static analysis. There is no data in the literature reviewed with which to compare this trend. However, comparisons of the power law equation show the exponent to be approximately five times lower than those found by Carter and Hayes [13] and Ouyang [14] (0.06 and 0.07 respectively).

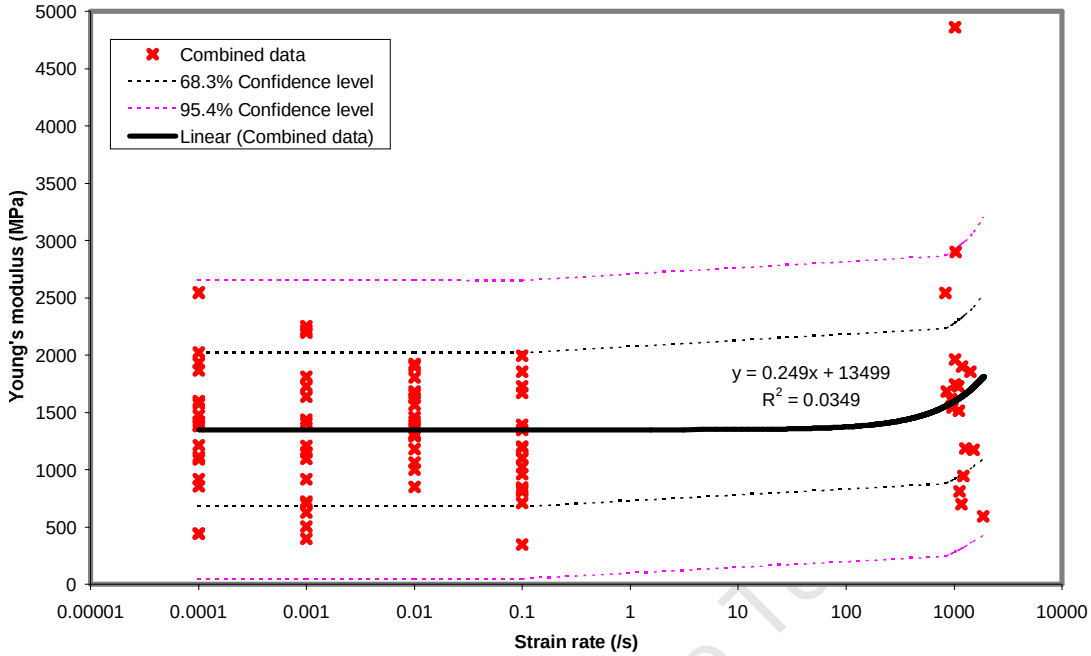

(a) Linear

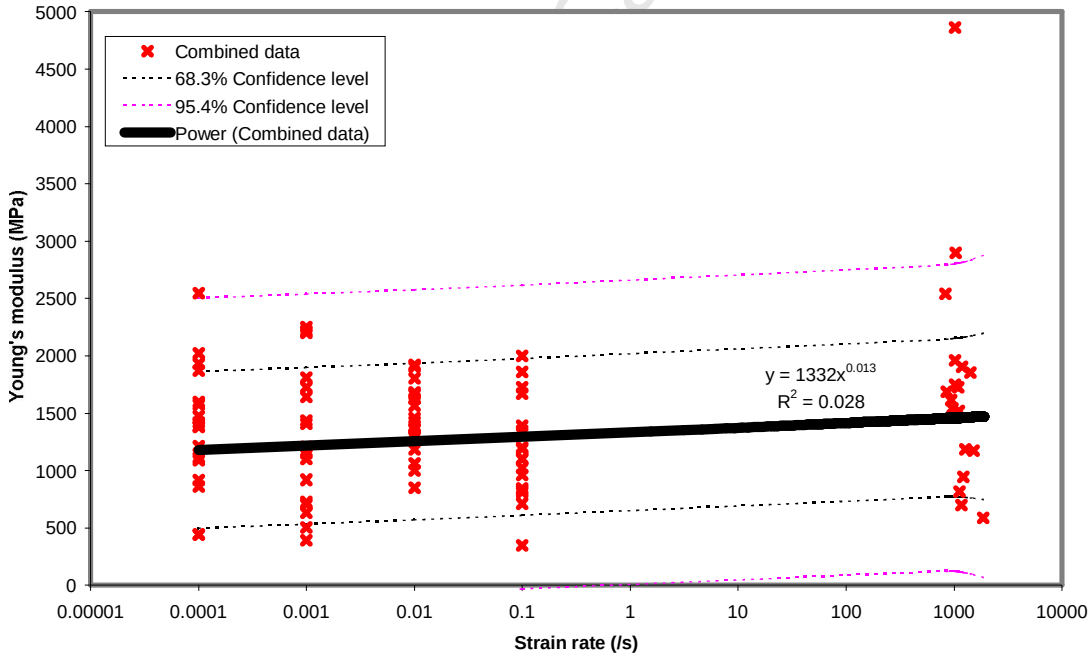

(b) Power law

Figure 8.3: The relationship between Young's modulus and strain rate for all specimens.

8.2.1.3 Yield strain as a function of strain rate

The density normalisation equations used are:

$\sigma_{qs} = 0.0193\rho^{0.548}$ (Table 6.4)

$\sigma_{d} = 0.021\rho^{1.30}$ (Table 7.1)

The equation variables relating yield strain to strain rate are given in Table 8.3. The relationship for the combined data is shown in Figure 8.4.

Although both the quasi-static and dynamic analysis found yield strain to be linearly related to strain rate, the combination of data shows a power law relationship to be the most suitable. As stated in section 6.2.2.3, none of the investigations reviewed in Chapter 3 found a positive relationship for the strain rate dependence of yield strain and therefore results found here cannot be validated by other studies.

Table 8.3: Equation variables for yield strain dependence on strain rate

Data source	$\varepsilon_y = a\dot{\varepsilon}^b$			$\varepsilon_y = a\dot{\varepsilon} + b$		
	a	b	r^2	a	b	r^2
Quasi-static data	0.0304	0.0407	0.586	0.0671	0.0224	0.698
Dynamic data	$3x10^{-4}$	0.647	0.194	$2x10^{-5}$	0.01	0.266
Combined data	0.0271	0.0292	0.302	$8x10^{-6}$	0.0241	0.198

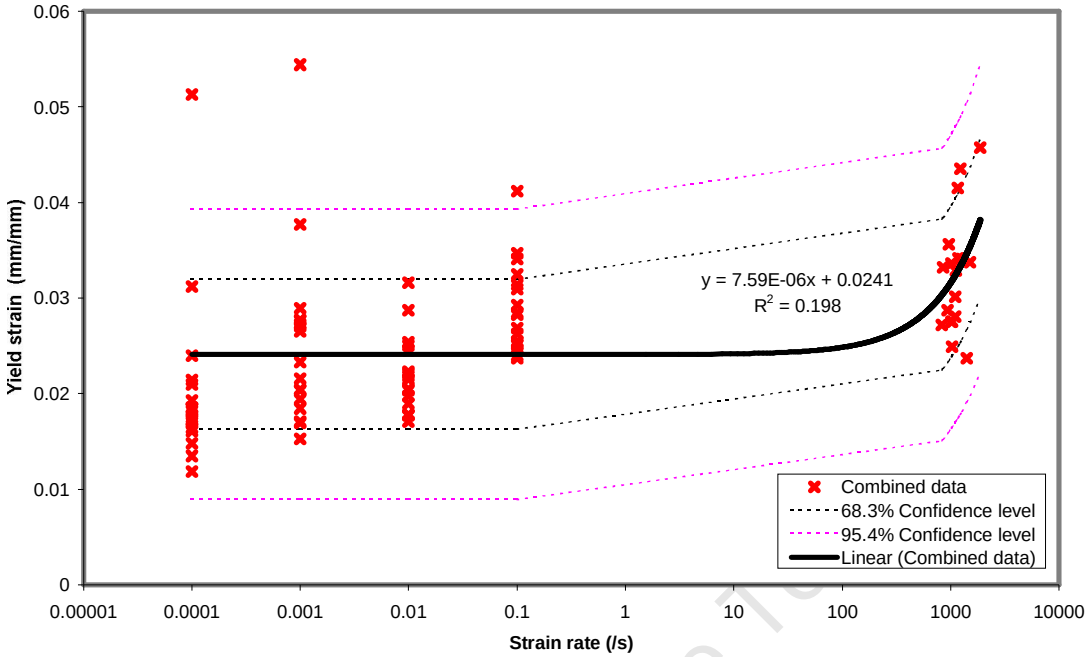

(a) Linear

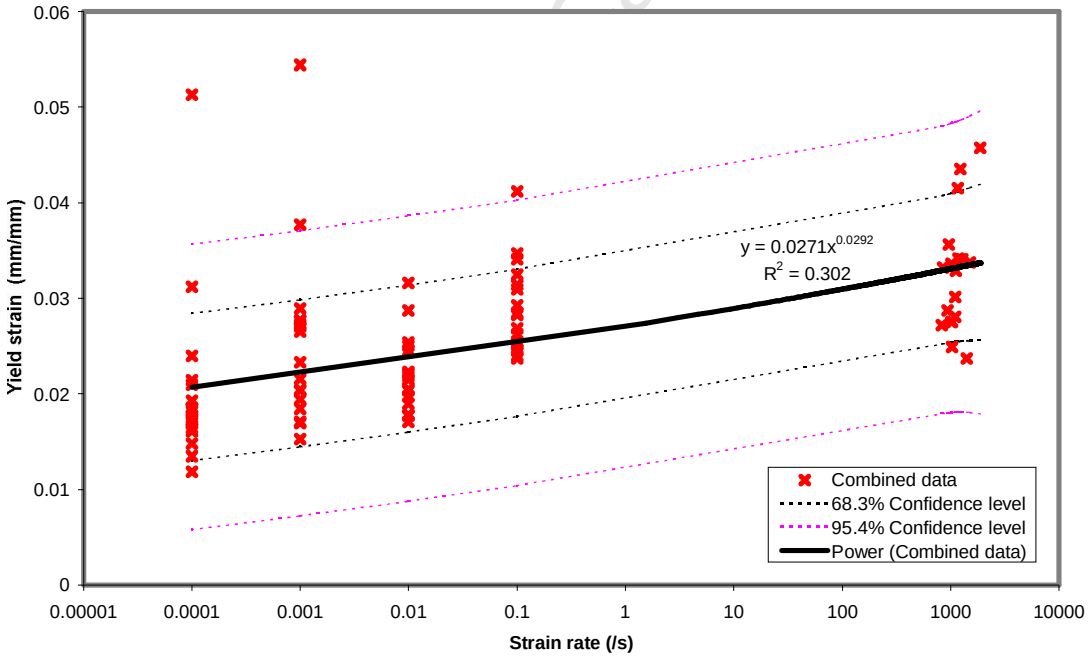

(b) Power law

Figure 8.4: The relationship between yield strain and strain rate for all specimens.

8.2.2 Trends with density

The relationships of yield stress, modulus and yield strain to strain rate derived in the preceding sections, are used to examine the density-dependence of these properties at a normalised strain rate of 1 /s.

8.2.2.1 Yield stress as a function of density

Table 8.4 shows that yield stress is dependent on density in power law fashion for all sets of data. The relationship for the combined data is illustrated in Figure 8.5.

Table 8.4: Equation variables for yield stress dependence on density

Data source	$\sigma = a\rho^b$			$\sigma = a\rho + b$		
	a	b	r^2	a	b	r^2
Quasi-static data	11.4	2.36	0.206	39.7	-29.1	0.175
Dynamic data	13.74	3.37	0.438	131	-135	0.257
Combined data	13.17	2.67	0.295	62.53	-53.64	0.265

The power law exponent of 2.67 compares favourably with the range of 1.29 to 2.35 reported in the literature (see Table 3.1).

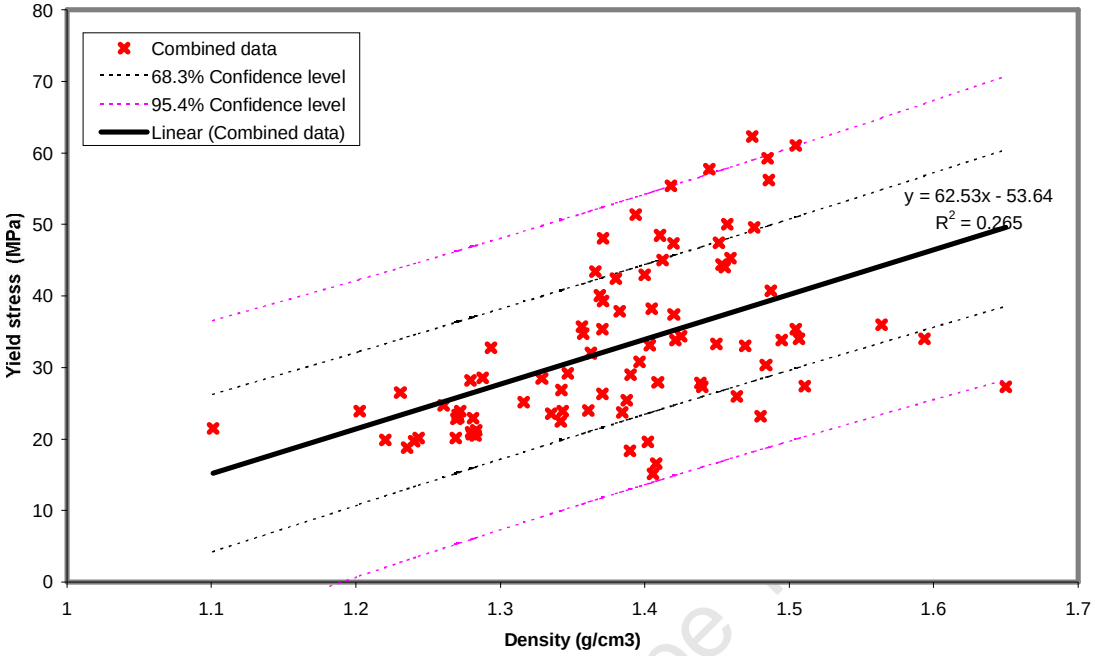

(a) Linear

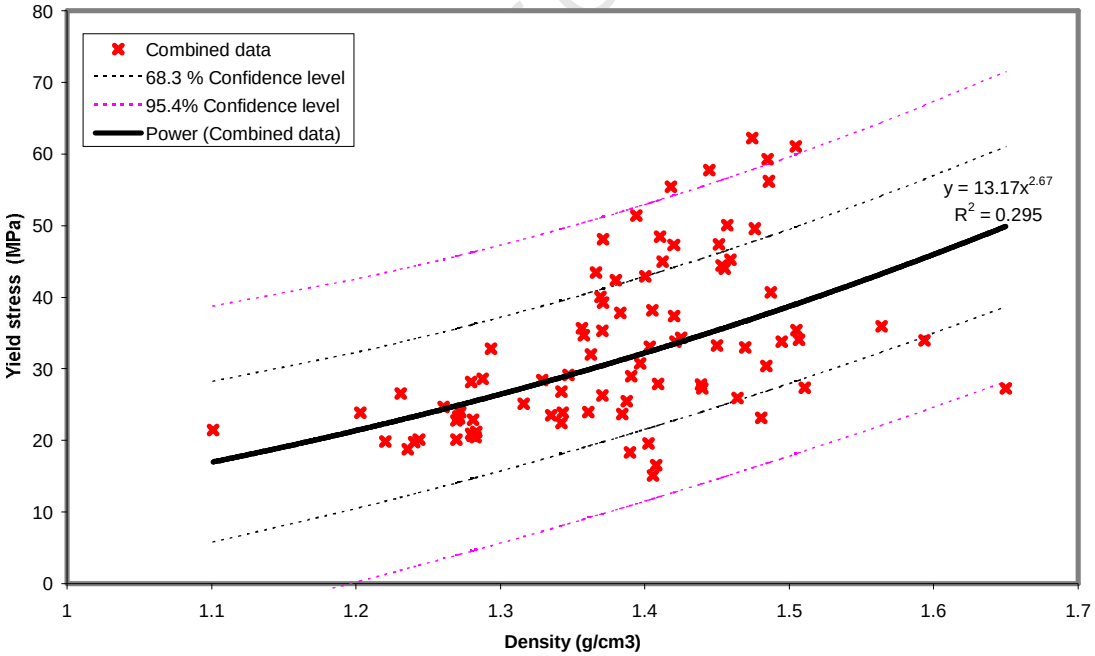

(b) Power law

Figure 8.5: The relationship between yield stress and density for all specimens.

8.2.2.2 Young's modulus as a function of density

The equation variables for modulus as a function of density are tabulated below and the relationship for the combined data is plotted in Figure 8.6.

Table 8.5: Equation variables for Young's modulus dependence on density

Data source	$E = a\rho^b$			$E = a\rho + b$		
	a	b	r^2	a	b	r^2
Quasi-static data	618	2.06	0.0883	1814	-1198	0.1003
Dynamic data	682	2.15	0.118	4239	-4231	0.257
Combined data	588	2.17	0.1088	2235	-1790	0.145

In both loading cases and when results are combined, modulus is best represented as a linear function of density. The gradient of 2235 shown here correlates well the value of 2100 reported by Kopperdahl [41]. However, the majority of the studies reviewed found power law relationships with exponents ranging from 1.88 to 3 [Table 3.1]. Using the power law function as a comparison to these studies, it can be seen that the value of 2.17 reported here is within the expected range.

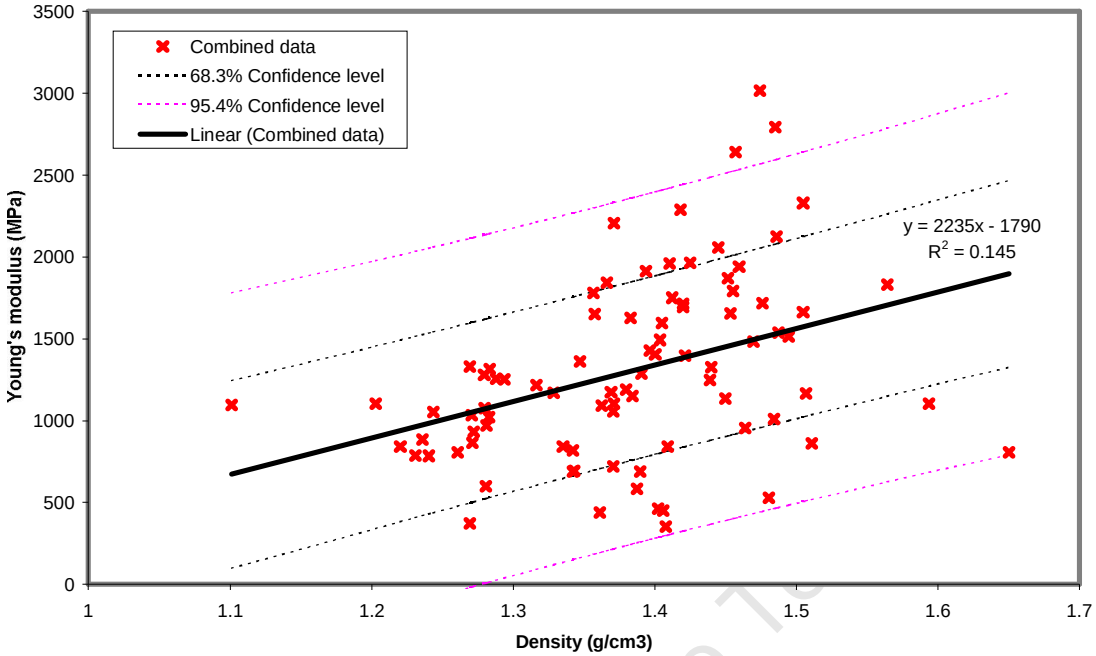

(a) Linear

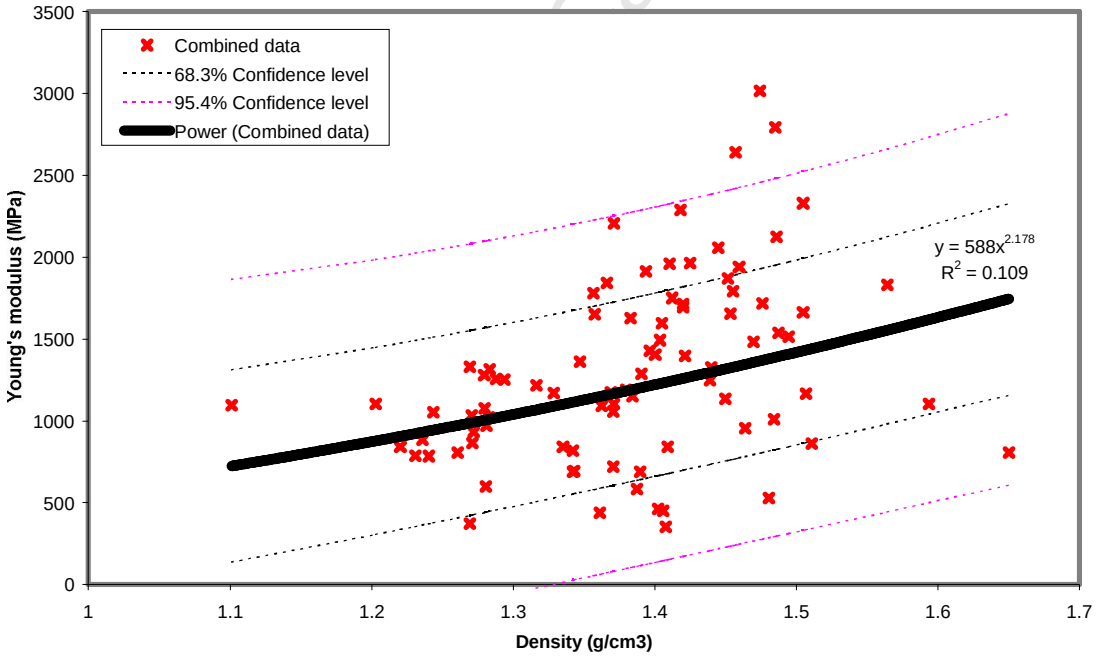

(b) Power law

Figure 8.6: The relationship between Young's modulus and density for all specimens.

8.2.2.3 Yield strain as a function of density

A comparison of the relationships for quasi-static, dynamic and combined data is shown in Table 8.6. The plot of yield strain vs. density for all the specimens is shown in Figure 8.7.

Table 8.6: Equation variables for yield strain dependence on density

Data source	$\varepsilon = a\rho^b$			$\varepsilon = a\rho + b$		
	a	b	r^2	a	b	r^2
Quasi-static data	0.0193	0.548	0.0142	0.0095	0.011	0.0115
Dynamic data	0.021	1.30	0.215	0.031	-0.0101	0.192
Combined data	0.021	0.771	0.0415	0.0151	0.0069	0.0274

A power law trend is found to be the most adequate in describing the yield strain relationship to density. The investigation by Kopperdahl [41], which shows a linear trend, is the only one in which a relationship between these two parameters was reported. Looking at the linear trend of the current work, the gradient of 0.015 is an order of magnitude lower than Kopperdahl's value of 0.66.

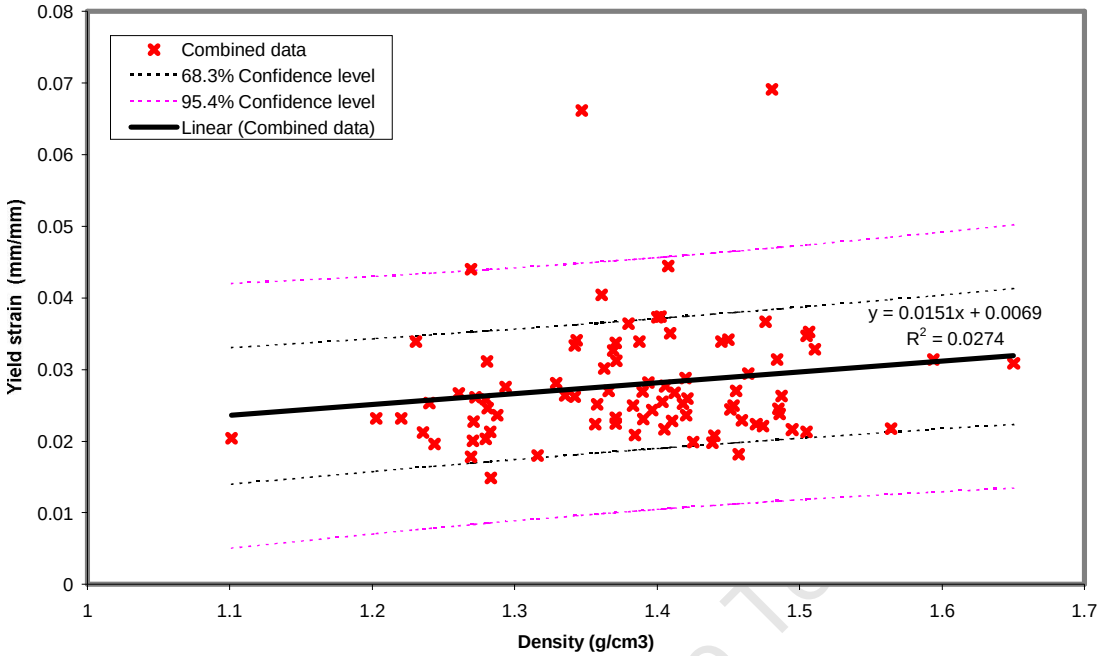

(a) Linear

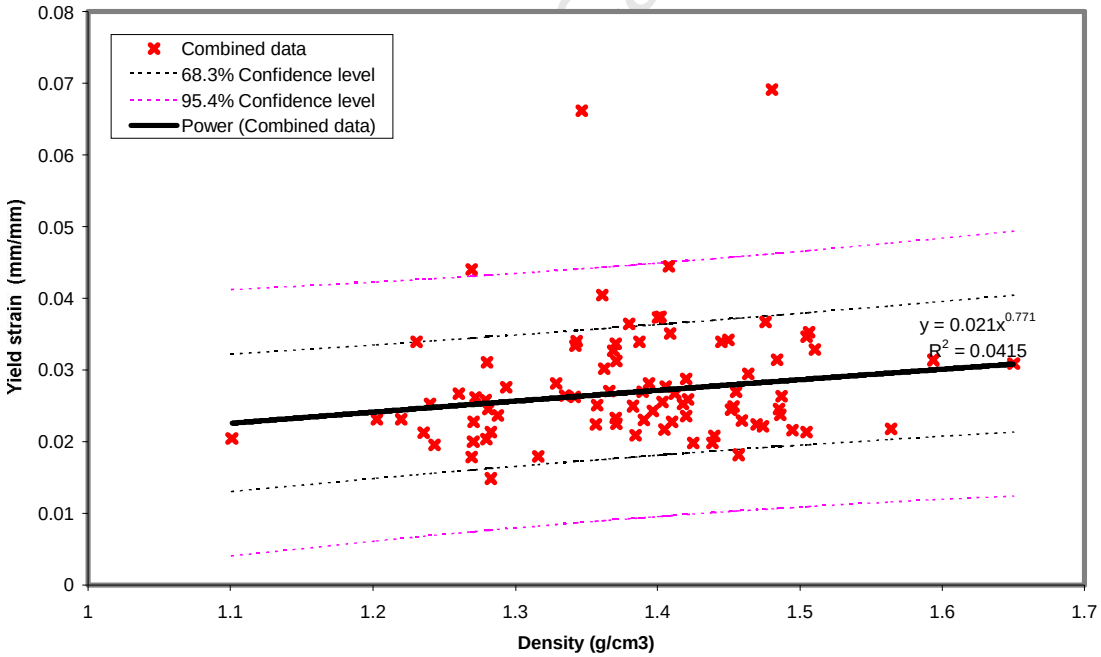

(b) Power law

Figure 8.7: The relationship between yield strain and density for all specimens.

8.3 Modelling of data using Shim's 1-d viscoelastic equation

As discussed in the literature review, Shim [1] developed a viscoelastic material model to describe the mechanical behaviour of cancellous bone, for which:

$\sigma = \sigma^e + \sigma^v$

where the first term is derived from linear elasticity and is expressed as:

$\sigma^e = E\varepsilon$

By substitution of the equation relating modulus to density found in the quasi-static analysis, this can be written as:

$\sigma^e = (1814\rho - 1198)\,\varepsilon$ (8.1)

The second term is derived from nonlinear viscoelasticity:

$$\sigma^v = \int_0^t c_1\,\dot{\varepsilon}(\tau)\,\exp\left(-\frac{t-\tau}{\theta}\right)d\tau + \eta\dot{\varepsilon}^{1/2}$$ (8.2)

8.3.1 Solving for the constants in Shim's equation

The constants c, η and θ, representing modulus, relaxation time and viscosity respectively, are solved for by substitution of the dynamic data into equation 3.19. The average values determined for these constants are shown as a comparison to the results of Shim [1] in Table 8.7.

Table 8.7: Comparison of equation constants to those of Shim [1].

Study	c_1 (MPa)	η (MPa $s^{1/2}$)	θ (s)
Current	-3.47×10^4	0.142	5.37×10^7
Shim [9]	354	0.122	5.5×10^{-5}

The values derived for the individual specimens are listed in Appendix G.

The one-dimensional viscoelastic equation for the data in this study is therefore:

$$\sigma = (1814\rho - 1198)\varepsilon + \int_0^t -3.47x10^4\,\dot{\varepsilon}(\tau)\exp\left(-\frac{t-\tau}{5.37x10^7}\right)d\tau + 0.142\dot{\varepsilon}^{1/2} \quad (8.3)$$

These constants differ greatly to those found by Shim. However, this is expected since results exhibit high scatter. In particular, the equation used to determine the stress due to linear elasticity (Equation 8.1) has an extremely low correlation coefficient (r^2 = 0.1, see Figure 6.10(a)). Therefore these calculated stress values may vary greatly from the actual values and errors will be introduced.

8.3.2 Prediction of failure points

In the quasi-static analysis it was determined that stress is dependent on density according to the following equation:

$$\sigma_y^{qs} = 11.4\rho^{2.36} \quad (8.4; \text{Table } 6.2)$$

It then follows that the difference in static and dynamic strength is:

$$\sigma_y^d - \sigma_y^{qs} = \sigma_y^d - 11.4\rho^{2.36}$$

which is plotted as a function of strain rate, shown in Figure 8.8. This relationship can therefore be expressed as:

$$\sigma_y^d - \sigma_y^{qs} = 4 \times 10^6 \dot{\varepsilon}^{-1.823} \quad (8.5)$$

or : $$\sigma_y^d = 11.4\rho^{2.36} + 4 \times 10^6 \dot{\varepsilon}^{-1.823} \quad (8.6)$$

Equation 8.6 is used to predict the stress values at the failure points of the fitted curves found using equation 3.19. The predicted yield stress values for each specimen are compared to the actual values in Appendix H.

Equation 8.6 differs from that found by Shim ($\sigma_y^d = 5.09\rho^{2.36} + 0.545\dot{\varepsilon}^{0.46}$) in that it displays a negative relationship i.e. the difference in strength decreases as strain rate increases. This is most likely due to the large scatter in results, meaning that equation 8.4 may not be applicable to many density values and therefore results may not be a true reflection of the actual values. In addition, the narrow range over which the tests were conducted may contribute towards poor correlation in trends with strain rate.

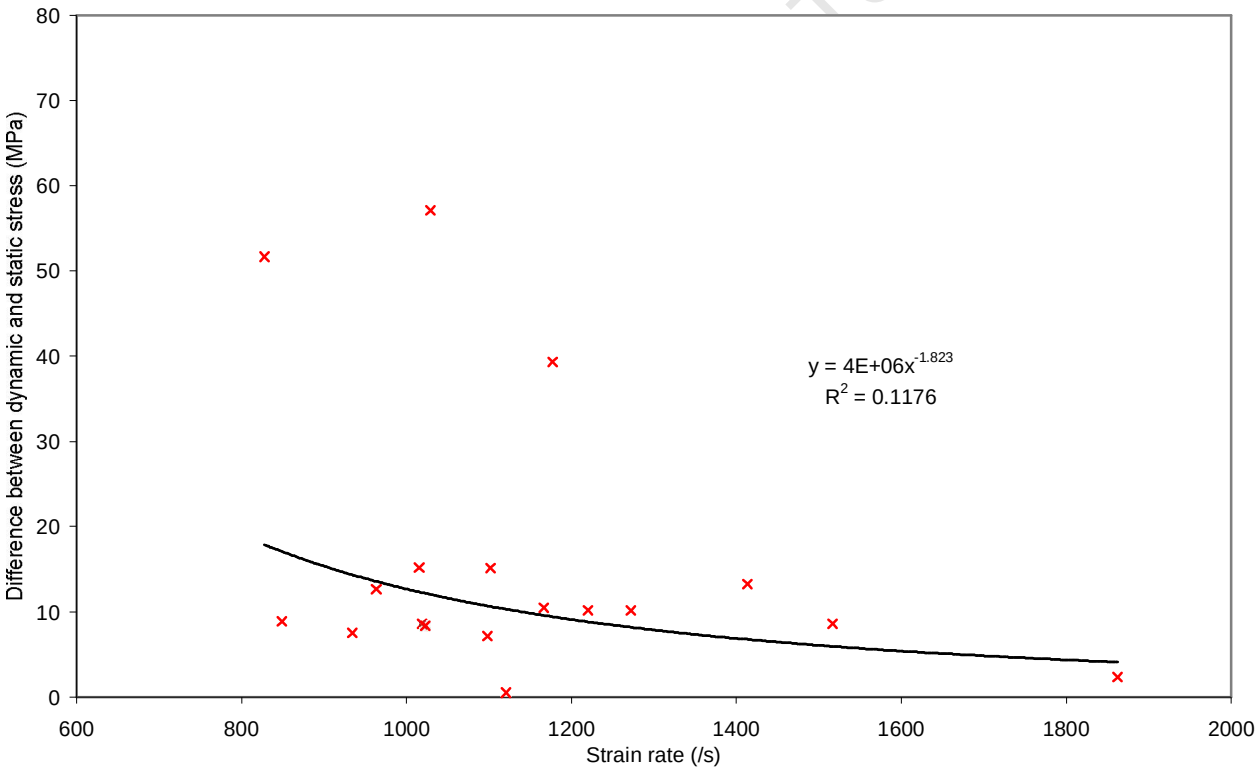

Figure 8.8: Difference in dynamic and static strength as a function of strain rate.

8.3.3 Comparison of fitted to experimental data

The fitted data is plotted using equation 8.3. The fitted vs. experimental curves are shown in Figures 8.9 to 8.11. The predicted yield stresses are indicated on the fitted curves. In cases where these values lie above the curves, they are not indicated.

It can be seen that there is not a particularly good agreement between the fitted and experimental results with the highest and lowest lying curves generally showing the greatest discrepancies. This is due to the fact that they have the highest or lowest modulus values and therefore fall on the outskirts of the modulus-density plots. The modulus-density plot derived in the quasi-static analysis (Figure 6.10(a)) is used to determine the stress based on linear elasticity (σ^e), as per equation 8.1. Therefore the curves with the highest and lowest moduli will have the greatest errors in σ^e values. Therefore the corresponding viscoelastic constants will deviate the most from the mean values. Since these mean values are used to predict the fitted curves, the highest and lowest lying curves will have the poorest correlation between fitted and experimental values. To illustrate this phenomenon, the specimens corresponding to the two highest lying curves, 5.2.1 and 5.2.4 are shown in the modulus density scatterplot, for the combined data from section 8.2.2.2, in Figure 8.12.

It is clear that, of the points the above trendline, these fall the furthest from it. The viscoelastic constants corresponding to these specimens are expected to have great deviations from the mean. This can be seen in Appendix G, as well as in Figures 8.9 and 8.10, which show the curves corresponding to these specimens have the highest mismatch between fitted and experimental data.

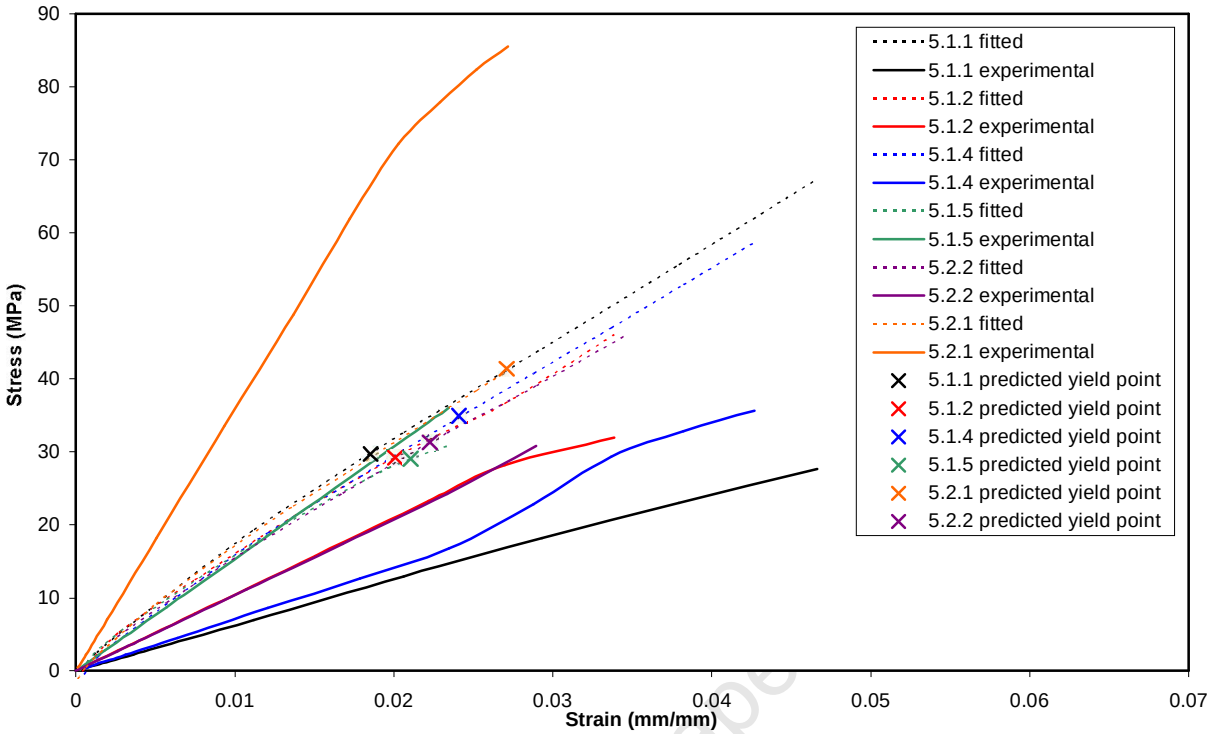

Figure 8.9: Comparison of fitted to experimental curves: Specimens 5.1.1 to 5.2.2

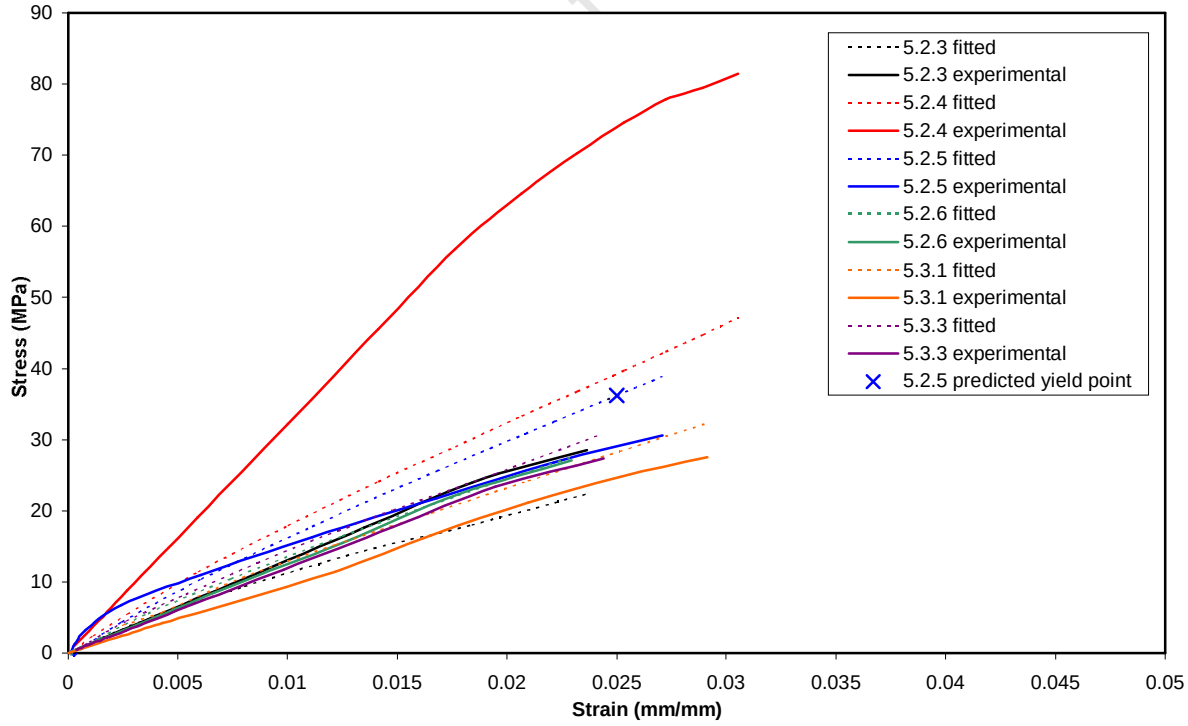

Figure 8.10: Comparison of fitted to experimental curves: Specimens 5.2.3 to 5.3.3

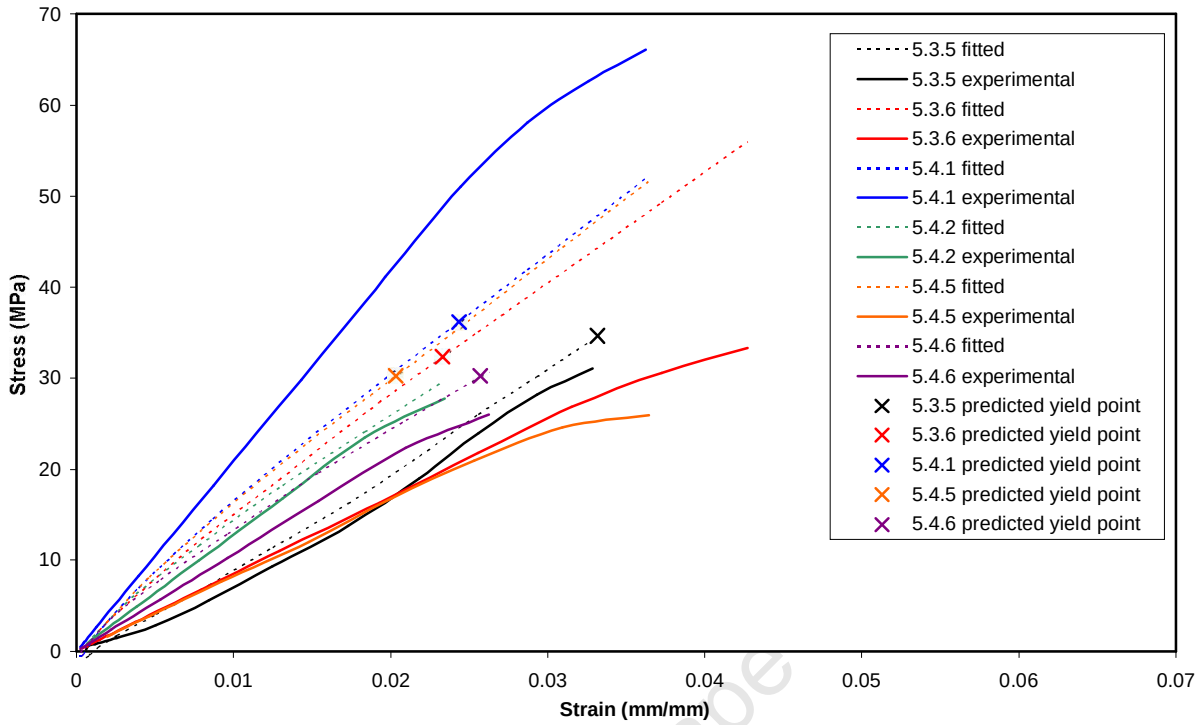

Figure 8.11: Comparison of fitted to experimental curves: Specimens 5.3.5 to 5.4.6

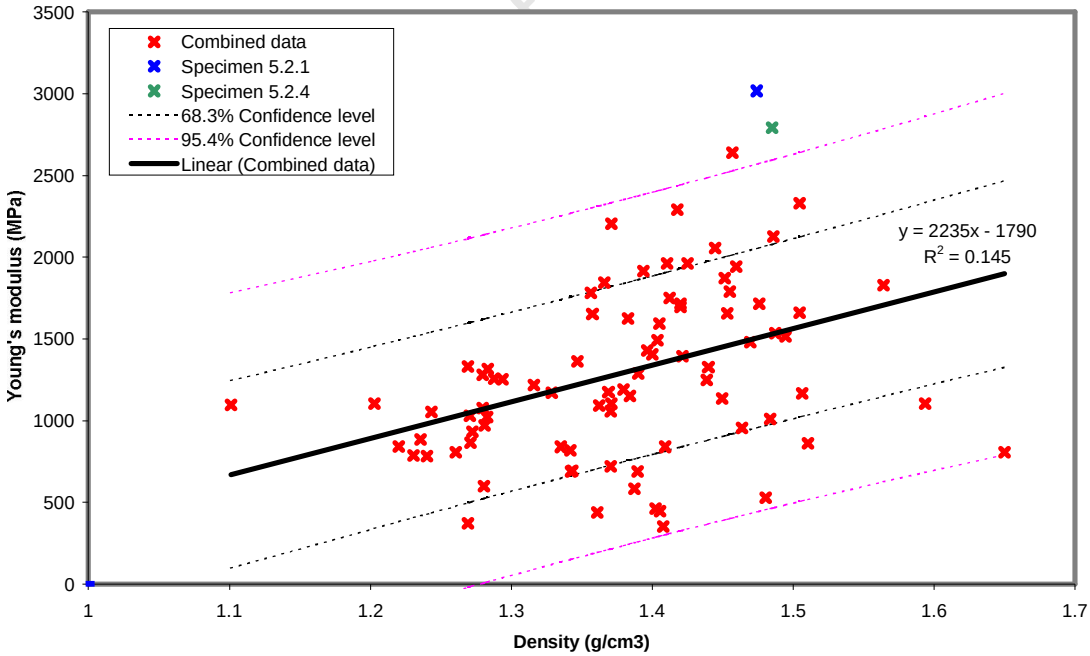

Figure 8.12: Position of specimens 5.2.1 and 5.2.4 in the modulus density scatterplot

9 MICROSTRUCTURAL INVESTIGATION

This section is an add-on to the main report. It is intended to be a visual introduction to the microstructure of cancellous bone. At this stage, no conclusions on the behavior of bone can be drawn from the micrographs.

In order to gain a better understanding of the material bone and its mechanical behaviour, it is necessary to view it on a microstructural level. Micrographs were prepared from a number of specimens, the majority of which were sourced from the same bovine vertebral section (bovine 3), but not necessarily the same vertebra. Only the unloaded specimen was taken from a different animal, bovine 6. The following specimens were used for this microstructural investigation:

- Specimen 6.1.3 – Unloaded.
- Specimen 3.3.3 – Quasi-static compression at 10^{-1} s^{-1} until 0.2 strain.
- Specimen 3.1.2 – Quasi-static compression at 10^{-2} s^{-1} until 0.2 strain.
- Specimen 3.2.3 – Quasi-static compression at 10^{-3} s^{-1} until 0.2 strain.
- Specimen 3.1.4 – Quasi-static compression at 10^{-4} s^{-1} until 0.2 strain.
- Specimen 3.3.4– Quasi-static compression at 10^{-1} s^{-1} until ultimate stress.
- Specimen 3.3.5 – Quasi-static compression at 10^{-2} s^{-1} until ultimate stress.
- Specimen 3.2.6 – Quasi-static compression at 10^{-3} s^{-1} until ultimate stress.
- Specimen 3.2.4 – Quasi-static compression at 10^{-4} s^{-1} until ultimate stress.

9.1 Preparation of slide [68]

The slide preparation procedure is illustrated in Figure 9.1. It begins by mounting the specimen in clear cold-curing epoxy resin in a plastic mould and allowing it to harden overnight. Once the resin block is removed, a water-cooled rotating diamond-encrusted blade is used to cut a longitudinal section through the embedded specimen at the desired location. The exposed face is ground down on successively finer waterproof abrasive disks (600, 1200 and 4000 grit) mounted on a rotating wheel. This is done to remove the scratches on the surface caused by cutting. After grinding, the specimen is polished on a rotating special velvet cloth. Frosted slides are prepared by rubbing abrasive paste on

the surface to which the specimen will be stuck. This is done in order to improve the optical resolution and the adhesion properties. The specimen is then stuck face down onto a slide using resin. After curing, the bulk of the resin block is cut away using a section-cutting machine that holds the slide in place by a vacuum. The rotating blade leaves the slide with a 1 mm thick layer of specimen attached to it. This is then ground and polished using the process described above, until it is possible to view the bone microstructure under the microscope.

Figure 9.1: Micrograph procedure

9.2 Micrographs

9.2.1 Complete cross-sections through specimens

The micrographs of all the prepared slides are presented in Figures 9.2 to 9.9. Specimen 3.3.4 was damaged in the preparation process and is therefore not shown. The lighter areas represent the bone matrix and the darker areas the marrow.

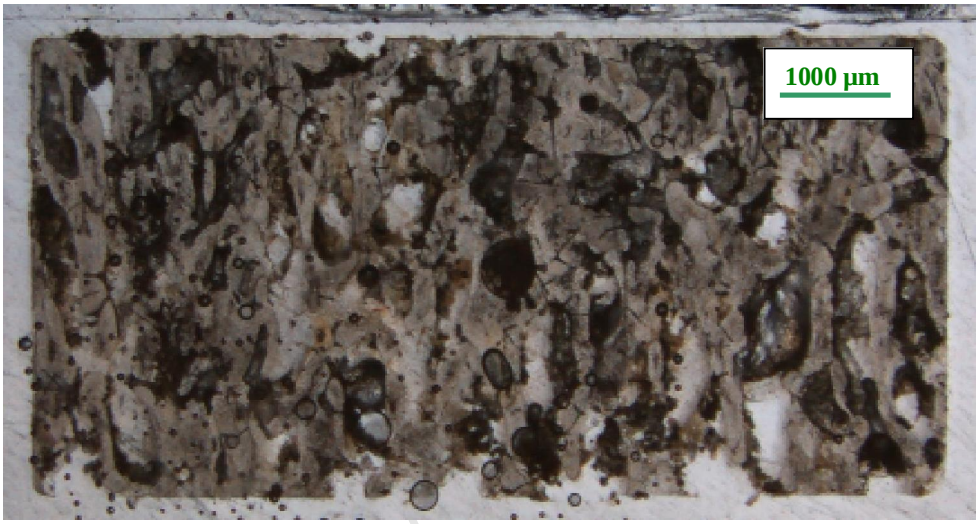

Figure 9.2: Specimen 6.1.3 – Unloaded.

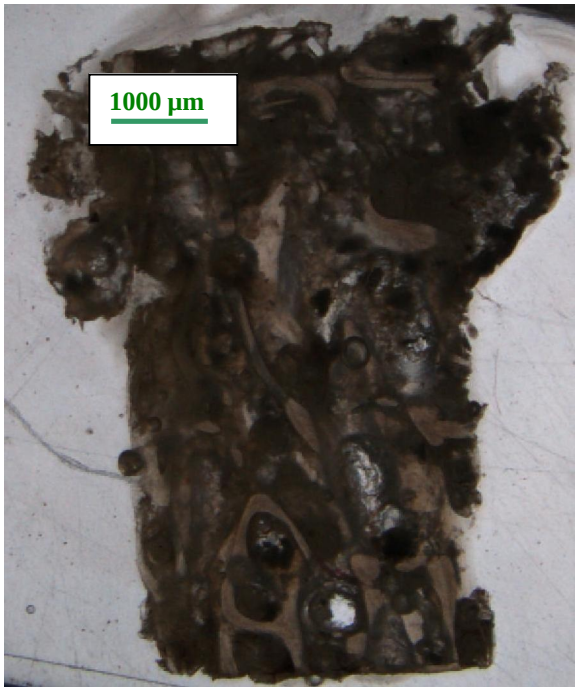

Figure 9.3: Specimen 3.3.3 – Quasi-static compression at 10^{-1} s^{-1} until 0.2 strain.

Figure 9.4: Specimen 3.1.2 – Quasi-static compression at 10^{-2} s^{-1} until 0.2 strain.

Figure 9.5: Specimen 3.2.3 – Quasi-static compression at 10^{-3} s^{-1} until 0.2 strain.

Figure 9.6: Specimen 3.1.4 – Quasi-static compression at 10^{-4} s^{-1} until 0.2 strain.

Figure 9.7: Specimen 3.3.5 – Quasi-static compression at 10^{-2} s^{-1} until ultimate stress.

Figure 9.8: Specimen 3.2.6 – Quasi-static compression at 10^{-3} s^{-1} until ultimate stress.

Figure 9.9: Specimen 3.2.4 – Quasi-static compression at 10^{-4} s^{-1} until ultimate stress.

It can be seen, particularly in specimens 3.1.4, 3.2.4, 3.2.6 and 3.3.5 (Figures 9.6 to 9.9), that the longitudinal axes of the individual trabeculae are approximately aligned with the direction of loading.

The cancellous bone presented in this study is composed of both rods and plates, present in varying degrees in different specimens. It therefore appears to fall into the Type II category, as defined by Singh [12] (see page 5).

9.2.2 Characteristics of bone

A number of interesting biological characteristics of bone can be seen on the micrographs. Figure 9.10 shows a primary osteon in a trabecular of specimen 3.1.4. This occurs when bone forms rapidly (as is the case with woven bone), with the result that a space is left around the blood vessel. At a later stage, these spaces are filled in as lamellar tissue is formed around the vessel. In the figure, concentric circles of lamellar bone are visible [68].

Small spaces, known as lacunae, are present in bone tissue. These spaces are filled with bone cells called osteocytes, the size and shape of which vary according to the rate of bone formation. Figure 9.11 shows that these osteocytes are arranged so as to follow the contours of the bone. Typically, the density of osteocytes is expected to be 30 000 mm^{-3} in bovine bone. The osteocytes communicate with eachother through interconnecting channels (canaliculi), which are approximately 0.2 to 0.3µm in diameter and therefore not visible on these micrographs [12, 68].

It is clear that the type of bone shown is woven bone (see Figure 2.4), which indicates that the bovines experienced rapid growth.

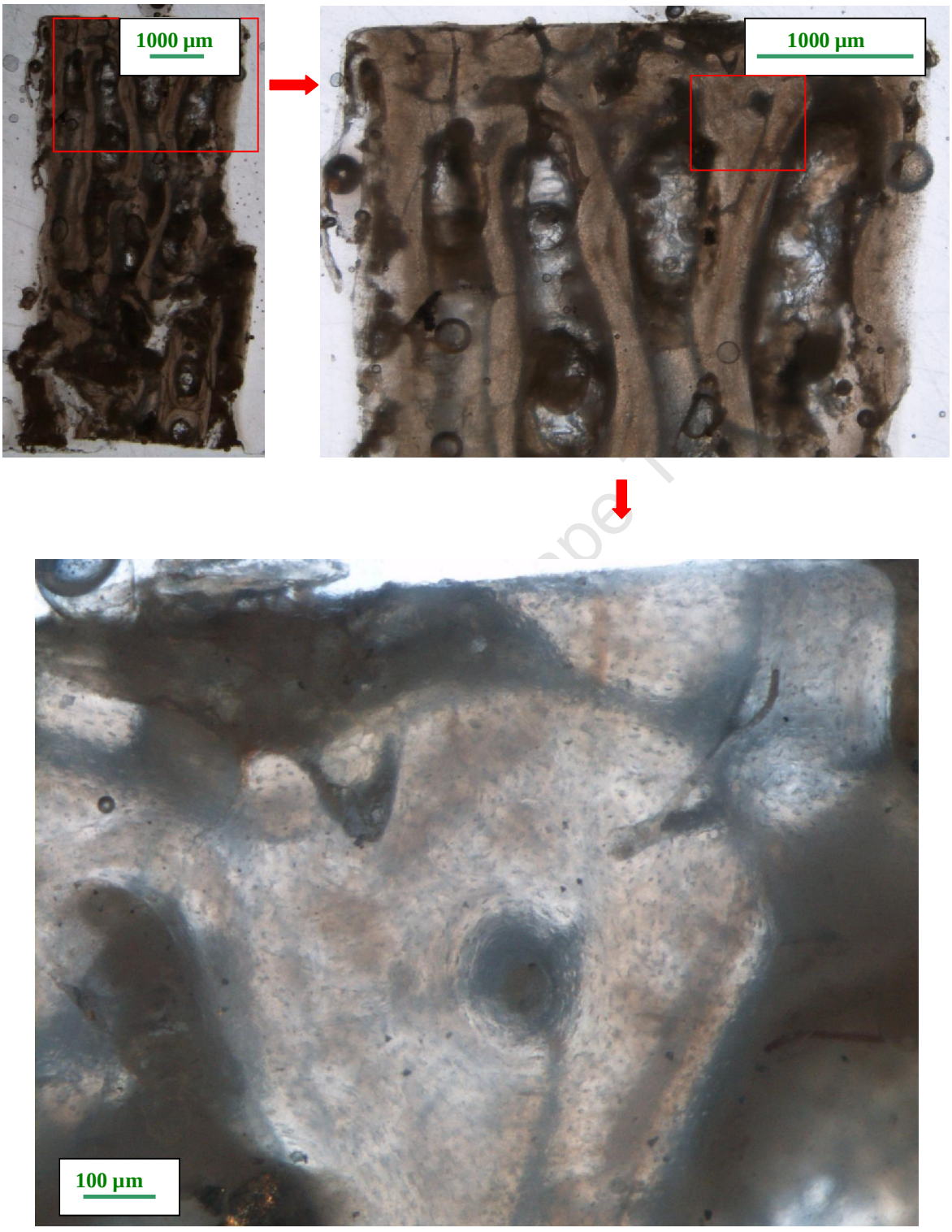

Figure 9.10: Primary osteon present in specimen 3.1.4

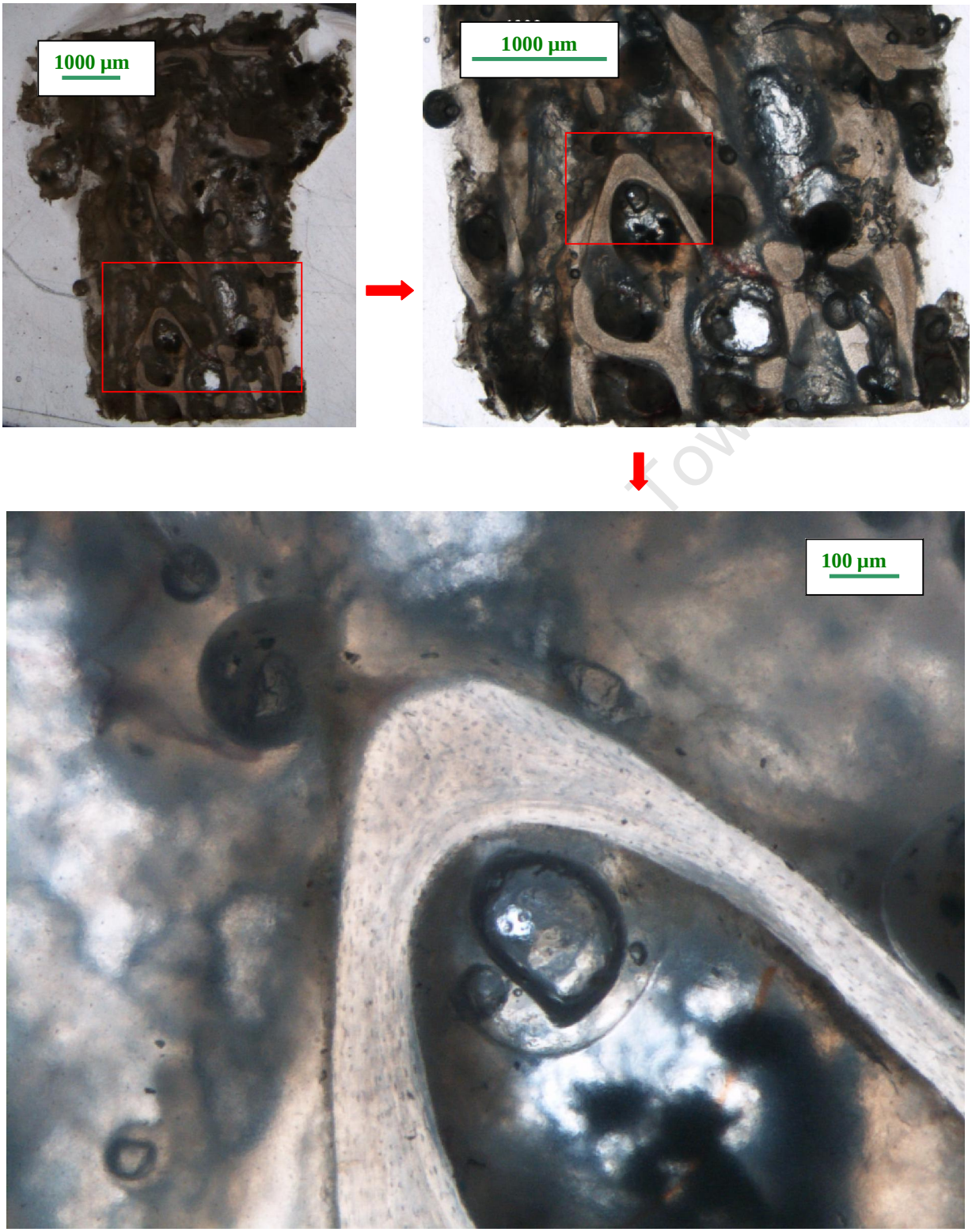

Figure 9.11: Osteocytes in specimen 3.3.3

9.2.3 Bone failure

A trabecular strut fracture of bone in specimen 3.1.4 is shown in Figure 9.12. It consists of a single crack surrounded by cross-hatched cracks, which indicate failure by compressive loading, as defined by Arthur-Moore and Gibson [69]. Mercer [70] suggests that kink bands are characteristic of bone failure in compression. These bands are evident in the figure where the material changes orientation across the main crack.

Specimen 3.2.4 shows two distinct cracks in separate trabeculae. Figure 9.13(a) shows two parallel cracks, the direction of which determines the material orientation. Figure 9.13(b) shows a complete trabecular fracture.

Figure 9.14 shows a region of crushed trabeculae, present in specimens 3.3.3, 3.1.2, 3.2.3 and 3.1.4 as a result of straining the specimens to 20%, far beyond the yield strains of 2% to 3%.

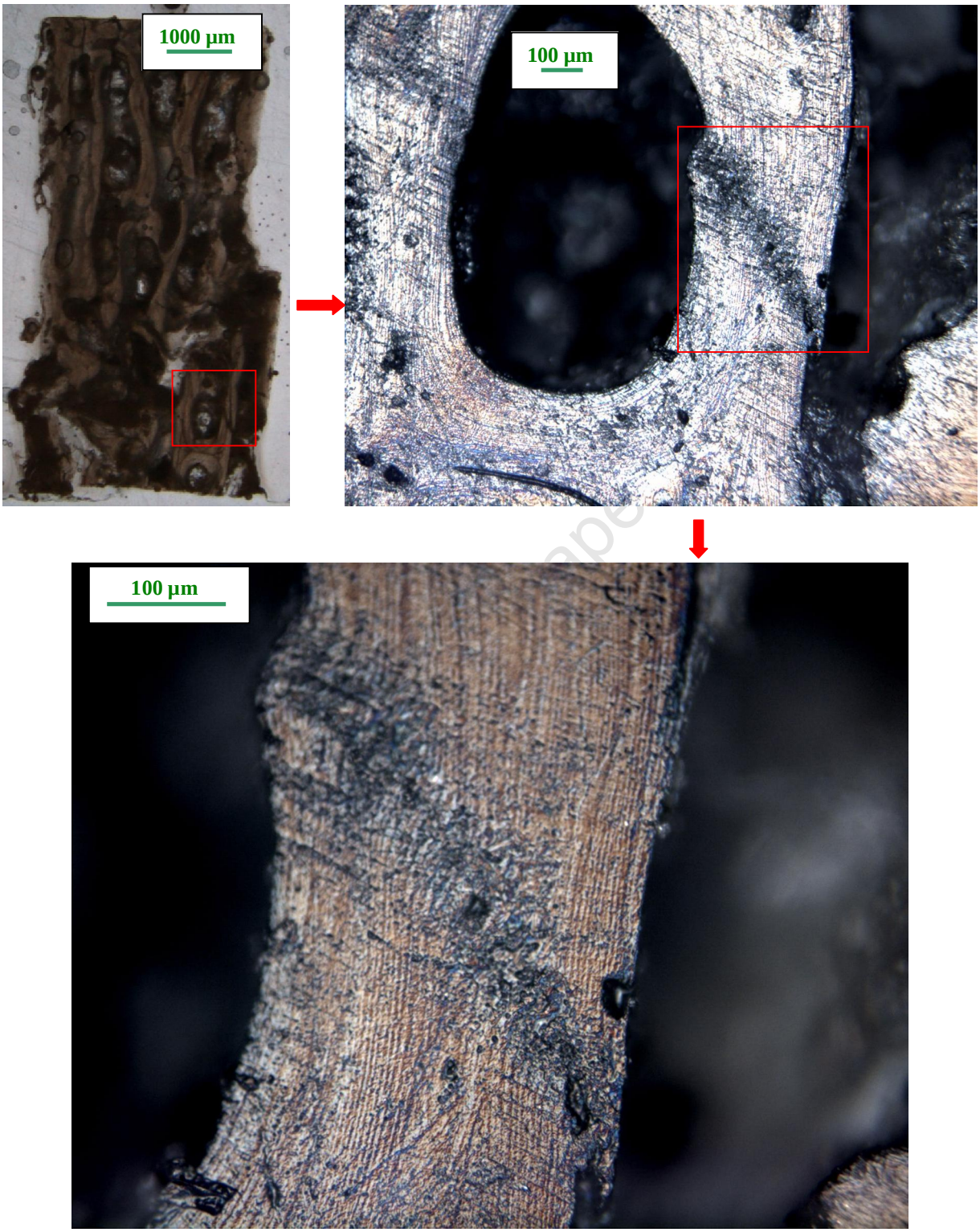

Figure 9.12: Crack in specimen 3.14

(b) Parallel cracks (a) Complete fracture

Figure 9.13: Cracks in specimen 3.2.4.

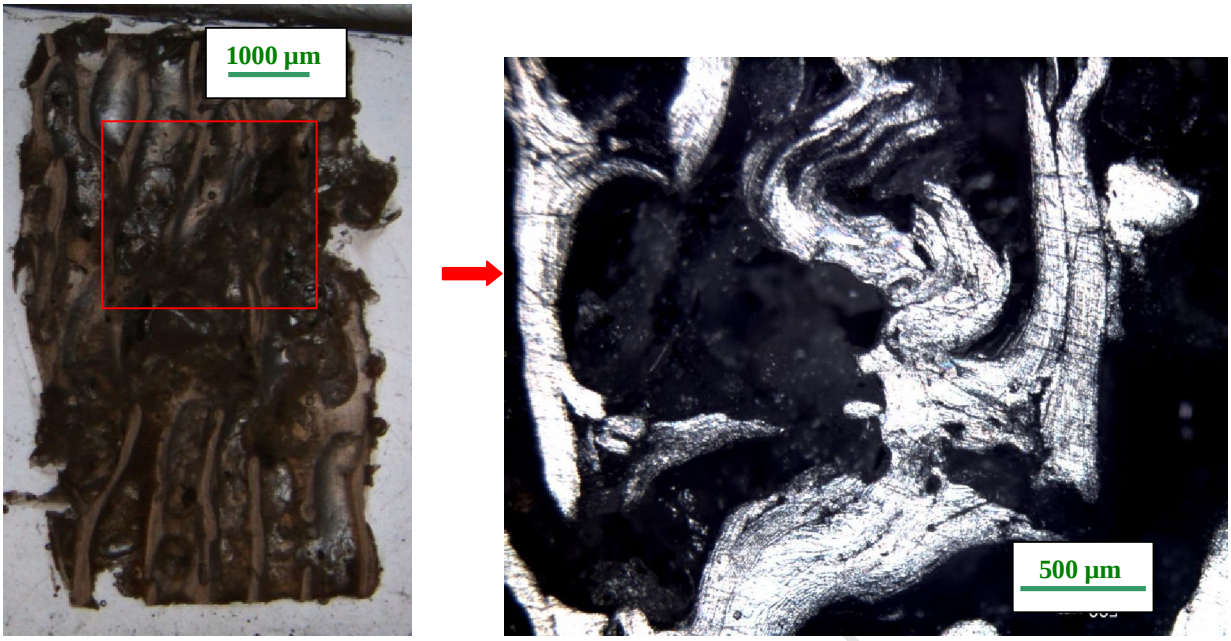

Figure 9.14: Crushed trabeculae in specimen 3.2.3.

10 CONCLUDING REMARKS

Due to the nature of the material used in this study, significant scatter is expected in all the experimental data. This is evident throughout this report. In addition, other factors contributing towards the scatter may be:

- The non-parallel surfaces of the specimens.
- The difficulty in accurately measuring the density
- Localised weaknesses in the specimens
- Specimens sourced from different bovines
- Inconsistent strain rate in dynamic testing

With the exception of Shim [1], all studies reviewed work in terms of apparent density. Shim noted that fresh bone density appears to have a nonlinear relationship to apparent density. Thus there may be a discrepancy when comparing the trends with density in this work to results presented in the literature. However, this is not expected to be significant since Shim's equation variables of stress and modulus dependence on density fall within the range presented by other authors (see Table 3.1).

Density values for all specimens ranged from 1.10 to 1.65 g/cm^3. This narrow range may account for the weak correlations between the mechanical properties and density. Given that bone exhibits high scatter, the sample size at each strain rate may not be large enough to see significant correlations.

The pre-conditioning cycles in the quasi-static analysis were performed in an effort to ensure adequate contact between the specimen and plates. However, this did not seem to reduce the scatter in results. This may be due to the fact that only three pre-conditioning cycles were employed and the cycles did not progress far into the elastic range.

The range of dynamic strain rates is small and therefore trends with strain rate reported in Chapter 7 may not be an accurate reflection of the true nature of cancellous bone under dynamic loading.

In both the quasi-static and dynamic analysis, yield stress favoured a power law relationship with both density and strain rate with exponents lying within the expected range given in the literature (Tables 8.1 and 8.4).

The dependence of modulus on density seemed to follow a linear trend in both sets of data, although the correlation coefficients for the linear and power law trendlines were similar (Table 8.5). This linear trend is in agreement with studies by Kopperdahl [41] and Li and Aspden [57], but the bulk of the studies reviewed reported power law trends (Table 3.1). The strain rate dependence (Table 8.2) followed a linear trend in the quasi-static data and a negative power law trend in the dynamic. However, the trend found from the dynamic data may be misleading due to the relatively small sample size and the narrow range of strain rates. Carter and Hayes [13] and Ouyang [14] were the only studies found in which modulus was related to strain rate, both of which reported power law relationship characterised by an exponent of 0.06/0.07.

The density and strain rate dependence of yield strain has not been extensively explored. In this work, it is found to have a power law relationship to density (Table 8.6), but the correlation is poor and results do not concur with Kopperdahl [41]. Results show yield strain to be linearly related to strain rate for both the quasi-static and dynamic data, while a power law relationship defines the trend of the combined data (Table 8.3). However, no literature showing a positive relationship between these two parameters could be found.

Results show that, as expected, density has a far greater effect on the mechanical properties of cancellous bone than strain rate.

The fitted data derived from the viscoelastic equation does not, for the most part, show good correlation with the experimental stress-strain curves. This is likely to be a compounded inaccuracy based on the high scatter in the quasi-static results used to determine the equation constants.

It can therefore be concluded that the mechanical properties of cancellous bone are highly dependent on density and marginally dependent on strain rate. Due to the high scatter in results, the exact relationships are difficult to determine. In general, the correlation coeffiecients were not good. This

may raise concerns over using these models as a predictive tool for the mechanical behavior of bone. However, the results of this work generally fall within the findings of the literature reviewed.

Although the high scatter is as a result of the nature of bone, refinement of the specimen preparation and testing methods may help to yield results which would more accurately predict the mechanical behavior of cancellous bone.

11 RECOMMENDATIONS

One of the problems associated with dynamic compression testing is the difficulty in achieving a constant strain rate during testing. This is especially important in the testing of bone since its mechanical properties are strain rate dependant. For future studies it is recommended that a method of achieving constant strain rate be employed. Methods such as pulse shaping and the use of conical strikers deserve some consideration.

If the sample size is not high, then individual specimens that may exhibit inconsistent behaviour can substantially affect results. This may be due to its microstructure or the faces of the specimen not being sufficiently smooth or parallel. Therefore it is recommended that a sufficiently large number of samples be tested.

The method used in this study to determine fresh bone density is not highly accurate. The majority of the studies presented in the literature review worked in terms of apparent density, which involves removal of the bone marrow after testing However, this method is only possible in quasi-static testing where the specimens remain intact. Thus the method used to determine the density needs to be refined.

The surfaces of the cylindrical specimens used in this work were not sufficiently parallel and thus not completely aligned with the loading plate/pressure bars. This results in stress concentrations being formed and causes inaccuracies in results. It is recommended that alternative method be used for producing specimens, such as a diamond-tipped coring tool, as used by Guedes [58].

The method of using preconditioning cycles was briefly explored and results did not show a marked improvement in the scatter. However, many studies dealing with compression testing on cancellous bone make use of these cycles [36, 38]. Therefore, this topic should be further investigated in terms of number and duration of cycles.

12 REFERENCES

[1] Shim VPW, Yang LM, Liu JF, Lee VS. *Characterisation of the dynamic compressive mechanical properties of cancellous bone from the human cervical spine*. International Journal of Impact Engineering 32 (2005) 525–540.

[2] Athanasiou KA, Zhu CF, Lancott DR, Agrawal CM, Wang X. *Fundamentals of Biomechanics in Tissue Engineering of Bone*. Tissue Engineering, 6 (4), (2000).

[3] Fernandez-Seara MA, Wehrli SL, Wehrli F. *Diffusion of exchangeable water in cortical bone studied by nuclear magnetic resonance*. Biophysical Journal, vol. 82, Jan 2002, pp 522-529.

[4] [3] referring to: Mueller KH, Trias A, Ray RD. *Bone density and composition: age-related and pathological changes in water and mineral content*. Journal of Bone and Joint Surgery: 48: 140-148 (1966).

[5] [3] referring to: Robinson RA, Elliot SR. *The water content of Bone*. Journal of Bone and Joint Surgery: 39A: 167-188 (1957).

[6] Liebschner MAK. *Biomechanical considerations of animal models used in the engineering of bone*. Biomaterials, 25 (2004), pp.1697-1714.

[7] Turner CH, Burr DB. *Basic biomechanical measurements of bone*. Bone, 14, 595 (1993).

[8] www.ama-cmeonline.com. October 2007.

[9] www.merckmedicus.com. November 2007.

[10] Singh, I. *The architecture of cancellous bone*. J. Anat. (1978) 127, 2, pp. 305-310.

[11] Jacobs CR. *The mechanobiology of cancellous bone structural adaption*. Journal of Rehabilitaion Research and Development, 37 (1), (2000).

[12] Currey JD. *Bones*. Princeton University Press, 2002. Ch.1.

[13] Carter DR, Hayes WC. *The compressive behaviour of bone as a two-phase porous structure*. The Journal of Bone and Joint Surgery, 59, pp.7954-962.

[14] Ouyang J, Yang GT, Wu WZ, Zhul QA, Zhongl SZ. *Biomechanical characteristics of human trabecular bone*. Clinical Biomechanics vol. 12, no. 718, pp. 522-524, 1997.

[15] [58] referring to: Brown TD, Ferguson AB. *Mechanical property distributions in the cancellous bone of the human proximal femur*. Acta Orthopaedica Scandinavica 51, 429-437 (1980).

[16] [58] referring to: Goldstein SA, Wilson DL, Sonstegard DA, Matthes LS. *The mechanical properties of human tibial trabecular bone as a function of metaphyseal location*. Journal of biomechanics 16, 965-969 (1983).

[17] Carter DR, Hayes WC. *Bone compressive strength: The influence of density and strain rate*. Science, 194 (4270), (1976), pp.1174-1176.

[18] McCaldon RW, McGeough JA, Court-Brown CM. *Age-related changes in the compressive strength of cancellous bone. The relative importance of changes in density and trabecular architecture*. The Journal of Bone and Joint surgey, vol. 79, 421-7 (1997).

[19] Ding M, Dalstra M, Danielsen CC, Kabel J, Hvid I, Linde F. *Age Variations In The Properties Of Human Tibial Trabecular Bone*. J Bone Joint Surg. 1997;79-B:995-1002.

[20] Zysset P. *A constitutive law for trabecular bone*. EPFL PhD thesis 1252, Lausanne (1994).

[21] Zhu M, Keller TS, Spengler DM. *Effects of specimen load-bearing and free surface layers on the compressive mechanical properties of cellular materials*. Journal of Biomechanics, vol. 1, issue 1, Jan 1994, pp 57-66.

[22] Keaveny TM, Borchers RE, Gibson LJ, Hayes WC. *Trabecular bone modulus and strength can depend on specimen goemetry*. Journal of Biomechanics 1993 Aug, 26 (8): 991-1000.

[23] Linde F, Hvid I, Madsen F. *The effect of specimen geometry on the mechanical behaviour of trabecular bone specimens*. Journal of Biomechanics, Volume 25, Issue 4, April 1992, Pages 359-368.

[24] Gama, Lopatnikov, Gillespie Jr. *Hopkinson bar experimental technique*. Appl Mech Rev vol 57, no 4, July 2004.

[25] [64] referring to: Gray III GT. *Classic split-Hopkinson pressure bar testing*, ASM Handbook Vol 8, Mechanical Testing and Evaluation, ASM Int, Materials Park OH, 462–476 (2000).

[26] [64] referring to: Davies EDH and Hunter SC. *The dynamic compression testing of solids by the method of split Hopkinson pressure bar (SHPB)*. J. Mech. Phys. Solids 11, 155–179 (1963).

[27] [7] referring to: Ashman RB. *Ultrasonic determination of the elastic properties of cortical bone: Techniques and limitations*. New Orleans, LA, Tulane University, 1982. Thesis.

[28] [7] referring to: Sedlin ED. *A rheologic model for cortical bone. A study of the physical properties of human femoral samples*. Acta Orthopaedica Scandinavica Supplement 83: 51-577 (1965).

[29] [7] referring to: Evans FG, Lebow M. *Regional differences in some of the physical properties of the human femur*. Journal of Applied Physiology. 3:563-572, 1951.

[30] Adharapurapu RR, Jiang F, Vechio KS. *Dynamic Fracture of Bovine Bone*. Materials Science and Engineering C26 (2006) 1325-1322.

[31] Passi N, Gefen A. *Trabecular Bone contributes to strength of the proximal femur under mediolateral impact in the avian*. Journal of Biomechanical Engineering, vol. 127 (Feb 2005).

[32] Currey JD. *The effects of drying and rewetting on some mechanical properties of cortical bone*. Journal of Biomech 21(5) (1988) 439-441.

[33] [7] referring to: Carter DR, Hayes WC. *Fatigue life of compact bone – Effects of stress, temperature and density*. Journal of Biomech, 9:27-34, 1976.

[34] Odgaard A, Linde F. *The underestimation of Young's modulus in compressive testing of cancellous bone specimens*. J Biomech. 1991;24(8):691-8.

[35] Un K, Bevilla G, Keaveny TM. *The effects of side-artifacts on the elastic modulus of trabecular bone*. Journal of Biomechanics 39 (2006) 1955–1963.

[36] Sierpowska J, Toyras J, Hakulinen MA, Saarakkala S, Jurvelin JS, Lappalainen R. *Electrical and dielectric properties of bovine trabecular bone relationships with mechanical properties and mineral density*. Phys. Med. Biol. 48 (2003) 775–786.

[37] Mercer C, He MY, Wang R, Evans AG. *Mechanisms governing the inelastic deformation of cortical bone and application to trabecular bone*. Acta Biomaterialia 2 (2006) 59–68.

[38] Morgan EF, Yeh OC, Chan WC, Keaveny TM. *Nonlinear Behaviour of Trabecular Bone at Small Strains*. Journal of Biomechanical Engineering 123 (2001).

[39] Morgan EF, Keaveny TM. *Dependence of yield strain of human trabecular bone on anatomic site*. Journal of Biomechanics 34 (2001) 569–577.

[40] Keaveny TM, Wachtel EF, Ford CM, Hayes WC. *Differences between the tensile and compressive strengths of bovine tibial trabecular bone depend on modulus*. Journal of Biomechanics. Volume 27, Issue 9, September 1994, Pages 1137-1146.

[41] Kopperdahl DL, Keaveny TM. *Yield strain behavior of trabecular bone*. Journal of Biomechanics 31 (1998) 601-608.

[42] Chang WCW, Christensen TM , Pinilla TP, Keaveny TM. *Uniaxial yield strains for bovine trabecular bone are isotropic and asymmetric*. Journal of Orthopaedic Research. Volume 17, Issue 4, Pages 582 – 585.

[43] Bayraktar HB, Morgan EF, Niebur GL, Morris GE, Wong EK, Keaveny TM. *Comparison of the elastic and yield properties of human femoral trabecular and cortical bone tissue*. Journal of Biomechanics 37 (2004) 27–35.

[44] Reilly DT, Burstein AH, Frankel VH. *Elastic modulus for bone*. Journal of Biomechanics (1974), 7 (3), 271-272.

[45] McElhaney JH, *Dynamic response of bone and muscle tissue*, Journal of Applied Physiology 21 (1966) 1231.

[46] Crowninshield RD, Pope MH. *The response of compact bone in tension at various strain rates*. Annals of Biomedical Engineering 2, 217-225 (1974).

[47] [46] referring to: Burstein AH. *The biomechanics of torsional fractures: The effect of loading on ultimate properties*. Am. Soc. Med. Engineers Annual Meeting 70-WA BFH-9 1970.

[48] Wright TM, Hayes WC. *Tensile Testing of Bone over a Wide Range of Strain Rates: Effects of Strain Rate, Microstructure and Density*. Med. Biol. Eng. , 14: 671-680, 1976.

[49] Galante J, Rostoker W, Ray RD. *Physical Properties of Trabecular Bone*. Calcif. Tissue Res., 5: 236-246, 1970.

[50] Linde F, Hvid I. 1989. *The effect of constraint on the mechanical behaviour of trabecular bone specimens*. J. Biomech.22:485–90.

[51] Lotz JC, Gerhart TN, Hayes WC. 1990. *Mechanical properties of trabecular bone from the proximal femur: a quantitative CT study*. J. Comput. Assist. Tomogr.14:107–14

[52] Hansson TH, Keller TS, Panjabi MM. *A study of the compressive properties of lumbar vertebral trabeculae: effects of tissue characteristics.* Spine 12:56–62 (1987).

[53] Mosekilde L, Mosekilde L, Danielsen CC. *Biomechanical competence of vertebral trabecular bone in relation to ash density and age in normal individuals*. Bone 8:79–85 (1987).

[54] Helgason B, Perilli E, Schileo E, Taddei F, lfsson SB, Viceconti M. *Mathematical relationships between bone density and mechanical properties: A literature review.* J. Clin. Biomech. (2007)

[55] [54] referring to: Linde F, Hvid I, Madsen F. *The effect of specimen geometry on the mechanical behaviour of trabecular bone specimens*. J. Biomech. 25, 359–368 (1992).

[56] [54] referring to: Dalstra M, Huiskes R, Odgaard A, van Erning L. *Mechanical and textural properties of pelvic trabecular bone*. J. Biomech. 26, 523–535 (1993).

[57] [54] referring to: Li B, Aspden RM. *Composition and mechanical properties of cancellous bone from the femoral head of patients with osteoporosis or osteoarthritis*. J. Bone Miner. Res. 12, 641–651 (1997).

[58] Guedes RM, Simoes JA, Marais JL. *Viscoelastic behaviour and failure of bovine cancellous bone under constant strain rate*. Journal of Biomechanics 39 (2006) 49-60.

[59] [2] referring to: Schoenfeld CM, Lautenschlager EP, Meyer PRJ. *Mechanical properties of human cancellous bone in the femoral head*. Med. Biol. Eng. 12**,** 313–317, 1974.

[60] [2] referring to: Odgaard A, Linde F. *The underestimation of Young's modulus in compressive testing of cancellous bone specimens*. J. Biomech. 24, 691–698, 1991.

[61] Sierpowska J, Hakulinen MA, Toyras J, Day JS, Weinans H, Jurvelin JS, Lappalainen R. *Prediction of mechanical properties of human trabecular bone by electrical measurements*. Physiol. Meas. 26 (2005) S119–S131.

[62] Teo CM, Teo EYL, Shim VPW, Teoh SH. *Determination of Bone Trabeculae Modulus—An Ultrasonic Scanning and MicroCT (μCT) Imaging Combination Approach*. Experimental Mechanics. Volume 46, Number 4 / August, 2006.

[63] Hakulinen MA, Day JS, Toyras J, Timonen M, Kroger H, Weinans H, Kiviranta I, Jurvelin JS. *Prediction of density and mechanical properties of human trabecular one in vitro by using ultrasound transmission and backscattering measurements at 0.2–6.7 MHz frequency range*. Phys. Med. Biol. 50 (2005) 1629–1642.

[64] Gama BA, Lopatnikov SL, Gillespie Jr JW. *Hopkinson bar experimental technique: A critical review.* Appl Mech Rev vol 57, no 4, July 2004.

[65] www.bovine.unl.edu. July 2007.

[66] Bonorchis, D. *Stress wave propagation in uniform bars*. Unpublished summary of work taken from: Spotts MF. *Mechanical Design Analysis*. New Jersey. Prentice-Hall Inc. 1964.

[67] Berenson ML, Levine DM. *Basic Business Statistics: Concepts and applications.* Prentice Hall, Inc. 1996.

[68] Chinsamy-Turan A. *The microstructure of dinosaur bone: Deciphering biology with fine-scale techniques*. Baltimore and London: The Johns Hopkins University Press, 2005.

[69] Arthur Moore TL, Gibson LJ. *Microdamage Accumulation in Bovine Trabecular Bone in Uniaxial Compression.* Journal of Biomechanical Engineering, Vol. 124, February 2002.

[70] Mercer C, He MY, Wang R, Evans AG. *Mechanisms governing the inelastic deformation of cortical bone and application to trabecular bone.* Acta Biomaterialia 2 (2006) 59-68.

APPENDIX A: DERIVATION OF SHIM'S EQUATION

Shim's constitutive viscoelastic model for bone is represented diagramatically in Figure A1 and is characterised by a combination of springs and dashpots [1].

The spring represents a linear elastic solid and models the instantaneous deformation of the material:

$$\sigma_s = E\varepsilon_s$$

By differentiating the strain, this can be written as:

$$\dot{\varepsilon}_s = \frac{\dot{\sigma}_s}{E} \tag{A1}$$

The Newtonian dashpot represents the viscous part of the model and produces a velocity in response to an applied stress such that:

$$\sigma_d = \eta\dot{\varepsilon}_d$$

or:

$$\dot{\varepsilon}_d = \frac{\sigma_d}{\eta} \tag{A2}$$

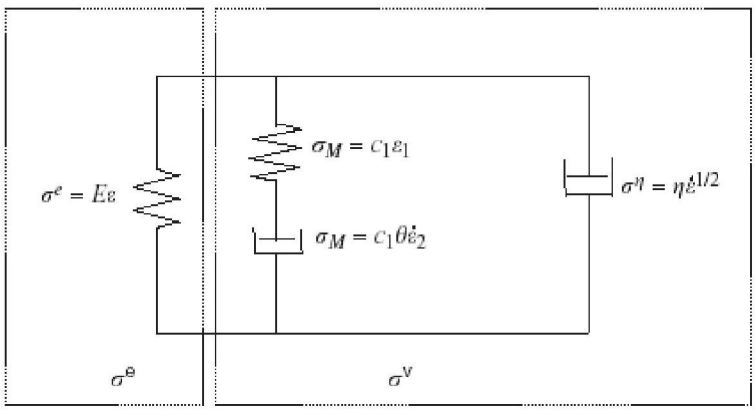

Figure A1: Diagrammatic representation of Shim's model [1].

The model is described by the following equation:

$$\sigma = \sigma^e + \sigma^v$$

The viscoelastic term (σ^v) is modeled as a Maxwell element in parallel with a nonlinear Newtonian dashpot (Figure A2). The Maxwell model consists of a spring and a dashpot connected in series.

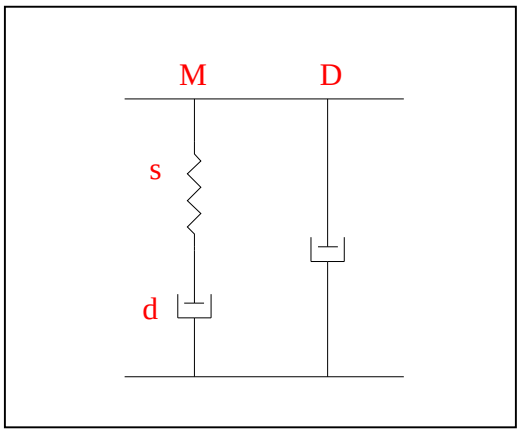

Figure A2: Maxwell element in parallel with a dashpot

In series connection (Maxwell element), the stress on each component is equal, while the total strain of the model is the sum of the strain on the components:

$$\sigma_M = \sigma_s = \sigma_D$$
$$\varepsilon_M = \varepsilon_s + \varepsilon_D$$

Therefore in the Maxwell model,

$$\dot{\varepsilon}_M = \dot{\varepsilon}_s + \dot{\varepsilon}_d \qquad \text{(A3)}$$

Substitition of equations A1 and A2 yields:

$$\dot{\sigma}_M = \dot{\varepsilon}_s E - \frac{\sigma_M E}{\eta} \qquad \text{(A4)}$$

The relaxation response of the model is derived by applying a constant strain to the system, beginning at time t = τ. Therefore $\dot{\varepsilon} = 0$ and equation A4 is reduced to:

$$\dot{\sigma}_M = \frac{\sigma_M}{\eta} E \tag{A5}$$

Thus:

$$\int_{\sigma_0}^{\sigma_M} \frac{d\sigma}{\sigma_M} = -\frac{E}{\eta} \int_{\tau}^{t} dt$$

By designating θ = η/E as the relaxation time, the expression for stress becomes:

$$\sigma_M(t) = E\varepsilon_0 \exp\left(-\frac{t-\tau}{\theta}\right) \tag{A6}$$

In parallel connection, the total stress is the sum of the elements:

$$\sigma^v = \sigma_M + \sigma_D$$

Thus

$$\sigma(t) = E\varepsilon_0 \exp\left(-\frac{t-\tau}{\theta}\right) + \eta\dot{\varepsilon}_D$$

Shim manipulated the last term of the equation to read $\eta\dot{\varepsilon}_D^{1/2}$ in order to make it applicable to a larger range of strain rates:

$$\sigma(t) = E\varepsilon_0 \exp\left(-\frac{t-\tau}{\theta}\right) + \eta\dot{\varepsilon}_D^{1/2} \tag{A7}$$

The viscoelastic term of Shim's model is solved for by using Duhamel's integral:

$$\sigma^v = \int_0^t E\,\dot{\varepsilon}(t) \exp\left(-\frac{t-\tau}{\theta}\right) d\tau + \eta\dot{\varepsilon}^{1/2} \tag{A8}$$

APPENDIX B: SPLIT HOPKINSON PRESSURE BAR

B1 Material properties of the pressure bars

The density of the magnesium pressure bars was determined by weighing and measuring a striker bar of the same material. The recorded signal from the calibration test, shown in Figure B1, was used to derive the wave speed. The distance between the strain gauges on the input and output bars is divided by the time difference between the start of the compressive pulses in the input bar and output bars. From this and using one-dimensional wave theory, the Young's modulus is calculated as:

$$E = c^2\rho \qquad \text{(B1)}$$

The bar properties are listed in Table B1.

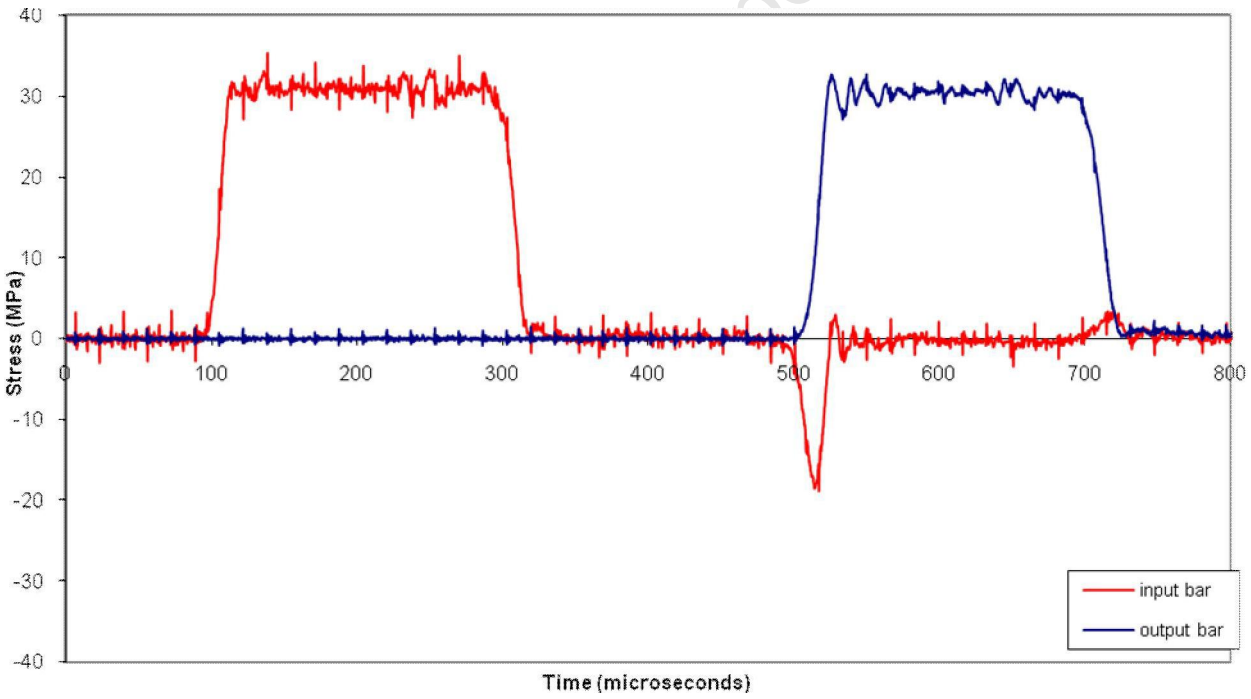

Figure B1: Stress-time plot during pressure bar calibration

Table B1: Properties of the magnesium pressure bars

Striker bar length	500 mm
Striker bar diameter	19.95 mm
Striker bar mass	274.7 g
Pressure bar length	1.998 m
Pressure bar diameter	19.95 mm
Density	1758 kg/m^3
Time between input and output bar pulses	400µs
Distance between input and output bar strain gauges	1.976 m
Wave speed	4940 m/s
Young's modulus	42.9 GPa

B2 Calibration factor

The recorded signals from the strain gauges, V_{read}, are converted to stress values using a theoretical calibration factor, K, which is calculated as follows for the system used in these tests [60]:

The stress measured in the bar is defined as:

$$\sigma = KV_{read} \tag{B2}$$

for which: $$K = \frac{4E}{G_{amp}K_{gf}NV_{in}}$$

where

- G_{amp} = 1000 is the gain on the amplifiers
- K_{gf} = 2.13 is the gauge factor
- N = 2 is the number of arms on the Wheatstone bridge
- V_{in} = 4 is the bridge voltage of the strain gauge circuit

Thus, for a specific Hopkinson bar system, the calibration factor is dependent only on the Young's modulus and the bridge voltage used. For the current system it can be expressed as:

$$K = \frac{E}{1065 V_{in}} \tag{B3}$$

B3 Specimen data

The velocities of the input and output pressure bars are calculated using the stresses in the bars at the interfaces, as follows:

$$v_{input} = \frac{\sigma_i - \sigma_r}{\rho c} \tag{B3}$$

$$v_{output} = \frac{\sigma_t}{\rho c} \tag{B4}$$

where the subscripts i, r and t refer to the input, reflected and transmitted pulses respectively, and c is the speed of sound in the bar.

These velocities are then used to calculate the change in length of the specimen, the strain and the strain rate:

$$\Delta L = (v_{input} - v_{output})\Delta t \tag{B5}$$

$$\varepsilon = \frac{\Delta L}{L_0} \tag{B6}$$

$$\dot{\varepsilon} = \frac{v_{input} - v_{output}}{L_{inst}} \tag{B7}$$

where L_o is the original and L_{inst} the instantaneous length of the specimen.

The specimen is in equilibrium and therefore the forces at the interfaces are equal. The stress in the specimen can therefore be calculated using the transmitted stress in the following equation:

$$\sigma_s = \frac{\sigma_t A_b}{A_s} \tag{B8}$$

where σ_s is the stress in the specimen and A_s is the instantaneous cross-sectional area of the specimen. A_b is the cross-sectional area of the output bar. Note that the constant area assumption is used in this study for cancellous bone due to its porous nature. Therefore the instantaneous area is equivalent to the original area.

APPENDIX C: QUASI-STATIC TEST RESULTS

Table C1: Results of quasi-static tests at a strain rate of 10^{-1} s^{-1}

Specimen no.	ρ (g/cm^3)	E (MPa)	σ_u (MPa)	ε_u (mm/mm)	σ_y (MPa)	ε_y (mm/mm)
1.1.4	1.48	1009	28.79	0.0413	27.35	0.0294
1.2.4	1.46	1791	41.73	0.0393	39.64	0.0253
1.3.4	1.40	1407	40.69	0.0491	38.66	0.0349
1.3.6	1.36	1094	30.31	0.0433	28.79	0.0282
1.4.4	1.37	1843	41.16	0.0454	39.10	0.0253
1.4.6	1.36	1651	32.88	0.0332	31.23	0.0235
1.5.4	1.38	1189	40.19	0.0456	38.18	0.0340
2.1.4	1.28	971	21.70	0.0311	20.62	0.0230
2.2.4	1.51	1167	32.25	0.0398	30.63	0.0330
2.2.6	1.51	861	25.93	0.0402	24.64	0.0307
2.3.4	1.41	353	15.70	0.0545	14.92	0.0416
2.3.6	1.65	806	25.86	0.0354	24.57	0.0289
2.4.4	1.41	840	26.47	0.0409	25.15	0.033
3.1.1	1.28	1279	26.66	0.0353	25.32	0.0241
3.2.1	1.33	1172	26.96	0.0370	25.61	0.0263
3.3.3	1.24	785	18.67	0.0305	17.74	0.0237
3.3.4	1.44	2058	54.69	0.0689	51.95	0.0317
Average	1.40	1193	31.21	0.0418	29.65	0.0292

Table C2: Results of quasi-static tests at a strain rate of 10^{-2} s^{-1}

Specimen no.	ρ (g/cm^3)	E (MPa)	σ_u (MPa)	ε_u (mm/mm)	σ_y (MPa)	ε_y (mm/mm)
1.1.3	1.49	1537	34.67	0.0362	32.95	0.0230
1.1.6	1.50	1661	30.15	0.0258	28.64	0.0186
1.2.3	1.42	1396	28.84	0.0320	27.40	0.0227
1.3.3	1.38	1627	32.25	0.0333	30.63	0.0218
1.3.5	1.42	1694	31.86	0.0339	30.27	0.0206
1.4.3	1.37	1174	34.13	0.0422	32.43	0.0286
1.5.3	1.29	1252	27.95	0.0376	26.55	0.0241
2.1.3	1.37	1056	22.44	0.0267	21.31	0.0204
2.2.3	1.47	1483	28.14	0.0281	26.73	0.0196
2.2.5	1.43	1963	29.30	0.0257	27.84	0.0173
2.3.3	1.59	1105	28.95	0.0358	27.50	0.0274
2.3.5	1.56	1830	30.67	0.0297	29.13	0.0190
2.4.3	1.44	1327	23.25	0.0244	22.09	0.0182
3.1.2	1.39	1914	43.80	0.0458	41.61	0.0246
3.2.2	1.23	788	22.62	0.0371	21.49	0.0297
3.3.5	1.36	1781	30.44	0.0293	28.92	0.0196
3.4.2	1.29	1256	24.37	0.0293	23.15	0.0207
Average	1.41	1461	29.64	0.0325	28.16	0.0221

Table C3: Results of quasi-static tests at a strain rate of 10^{-3} s^{-1}

Specimen no.	ρ (g/cm^3)	E (MPa)	σ_u (MPa)	ε_u (mm/mm)	σ_y (MPa)	ε_y (mm/mm)
1.1.2	1.28	599	15.87	0.0344	15.077	0.0254
1.1.5	1.38	1151	18.20	0.0246	17.29	0.0171
1.2.1	1.48	1716	38.03	0.0377	36.12	0.0300
1.2.6	1.45	1135	25.50	0.0338	24.23	0.0280
1.3.1	1.34	691	20.59	0.0335	19.56	0.0273
1.4.1	1.45	1871	36.38	0.0272	34.56	0.0200
1.5.1	1.37	720	27.11	0.0335	25.75	0.0276
2.1.1	1.27	374	15.43	0.0425	14.65	0.0360
2.1.6	1.27	1332	17.48	0.0189	16.60	0.0146
2.2.1	1.46	957	19.91	0.0309	18.91	0.0241
2.3.1	1.48	529	17.75	0.0595	16.86	0.0565
2.4.1	1.49	1516	25.91	0.0249	24.62	0.0177
3.1.3	1.50	2330	46.84	0.0408	44.50	0.0283
3.1.5	1.20	1103	18.34	0.0253	17.42	0.0189
3.2.3	1.37	2205	36.90	0.0255	35.05	0.0184
3.2.6	1.41	1751	34.52	0.0278	32.80	0.0218
3.3.2	1.42	2291	42.52	0.0309	40.39	0.0206
Average	1.39	1310	26.90	0.0324	25.55	0.0254

Table C4: Results of quasi-static tests at a strain rate of 10^{-4} s^{-1}

Specimen no.	ρ (g/cm^3)	E (MPa)	σ_u (MPa)	ε_u (mm/mm)	σ_y (MPa)	ε_y (mm/mm)
1.1.1	1.45	1656	30.65	0.0253	29.12	0.0191
1.2.2	1.40	1493	22.83	0.0228	21.69	0.0195
1.2.5	1.27	866	15.90	0.0211	15.11	0.0174
1.3.2	1.40	1596	26.36	0.0221	25.05	0.0166
1.4.2	1.40	1429	21.24	0.0264	20.18	0.0186
1.4.5	1.36	441	16.54	0.0346	15.71	0.0309
1.5.2	1.28	1316	14.65	0.0142	13.92	0.0114
2.1.2	1.27	1031	16.10	0.0272	15.29	0.0153
2.1.5	1.35	1362	20.14	0.0267	19.13	0.0506
2.2.2	1.26	808	17.03	0.0260	16.17	0.0204
2.3.2	1.44	1248	19.20	0.0201	18.24	0.0151
2.4.2	1.41	449	10.41	0.0243	9.89	0.0212
3.1.4	1.46	2639	34.55	0.0182	32.82	0.0139
3.1.6	1.46	1941	31.26	0.0235	29.70	0.0175
3.2.4	1.37	1105	27.11	0.0294	25.76	0.0239
3.3.6	1.41	1961	33.46	0.0225	31.79	0.0174
3.4.1	1.49	2125	38.79	0.0216	36.85	0.0182
Average	1.38	1380	23.31	0.0239	22.14	0.0204

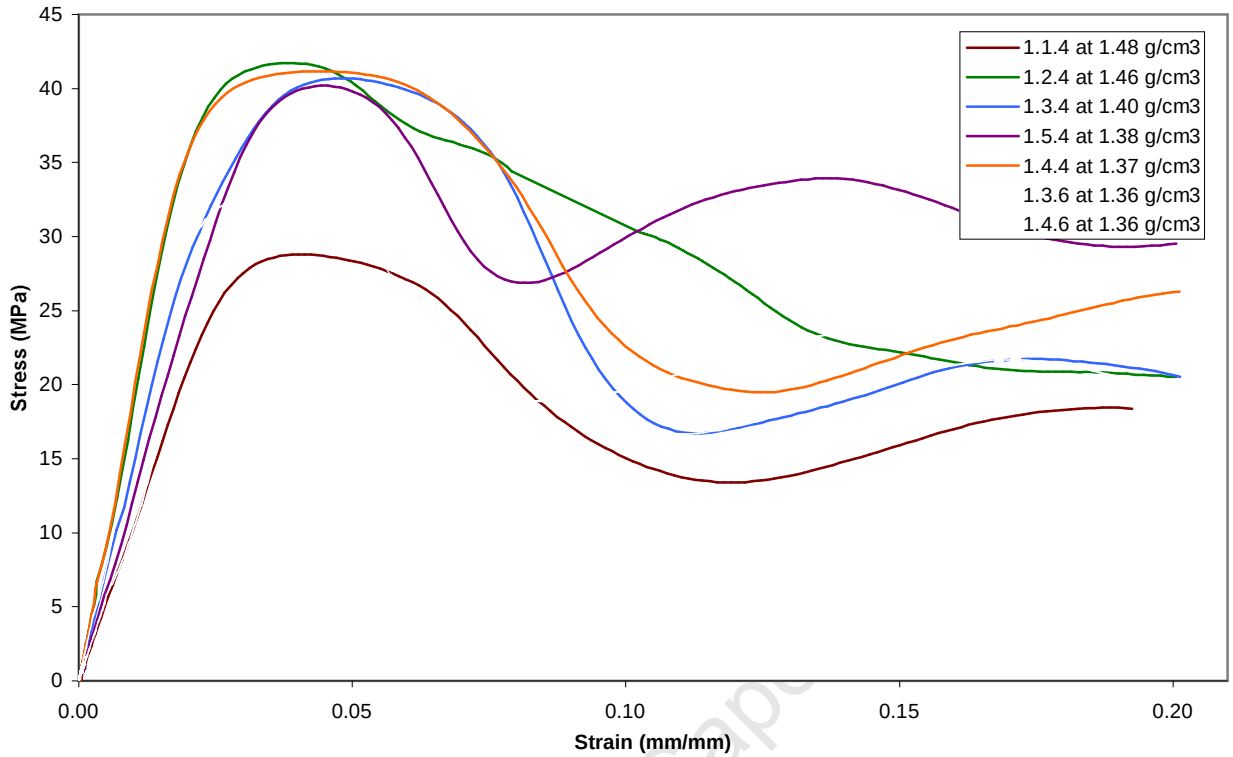

Figure C1: Stress-strain curves of Bovine 1 specimens at a strain rate of 10^{-1} s^{-1}

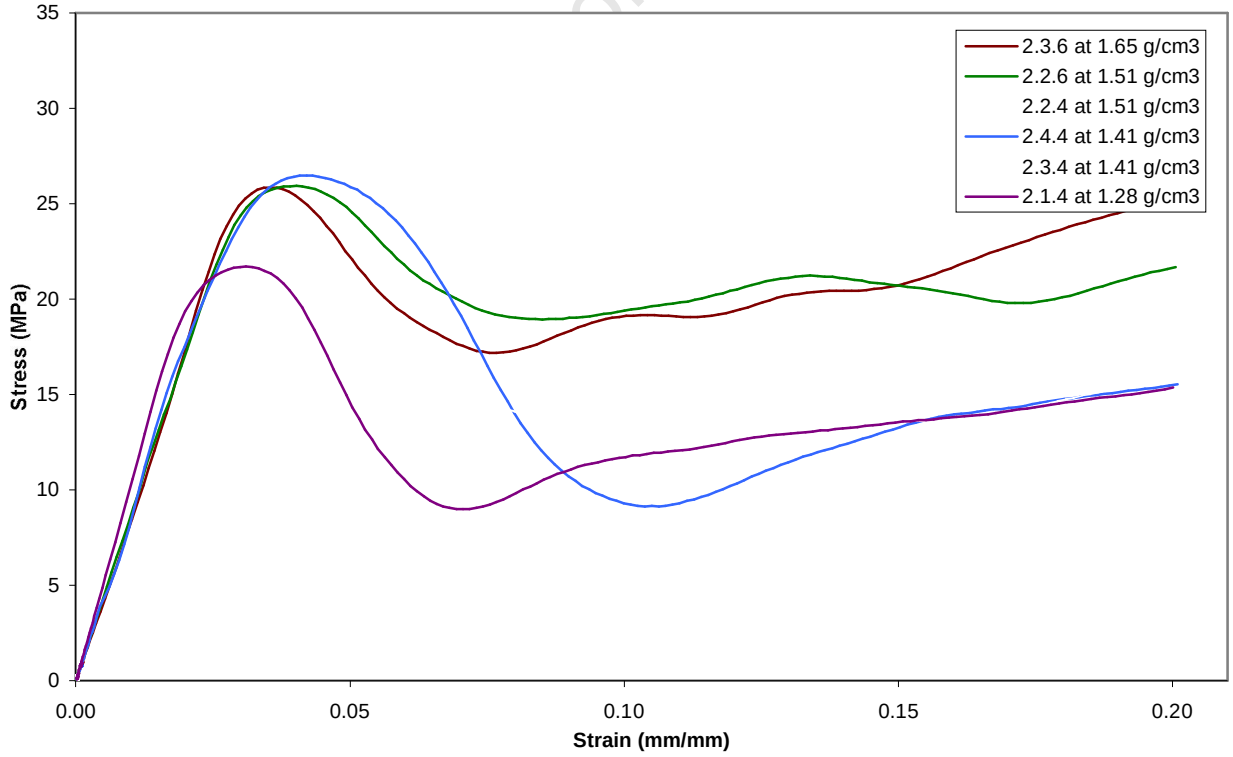

Figure C2: Stress-strain curves of Bovine 2 specimens at a strain rate of 10^{-1} s^{-1}

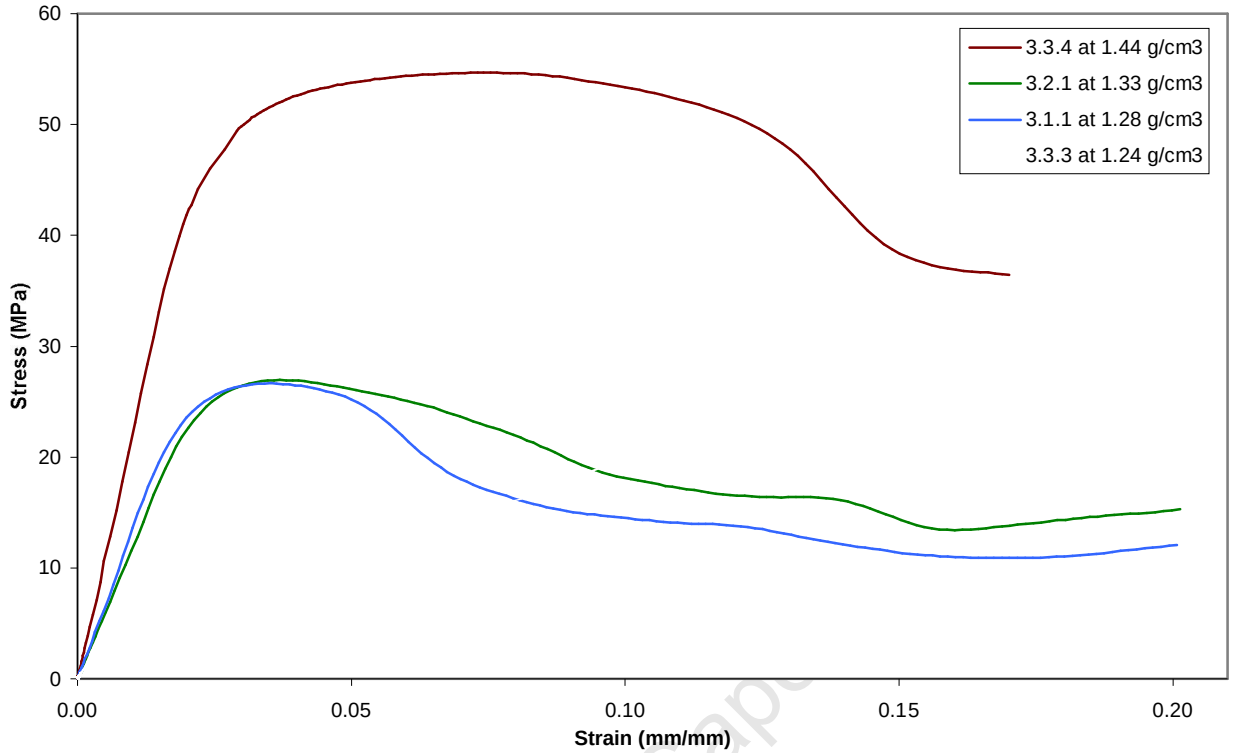

Figure C3: Stress-strain curves of Bovine 3 specimens at a strain rate of 10^{-1} s^{-1}

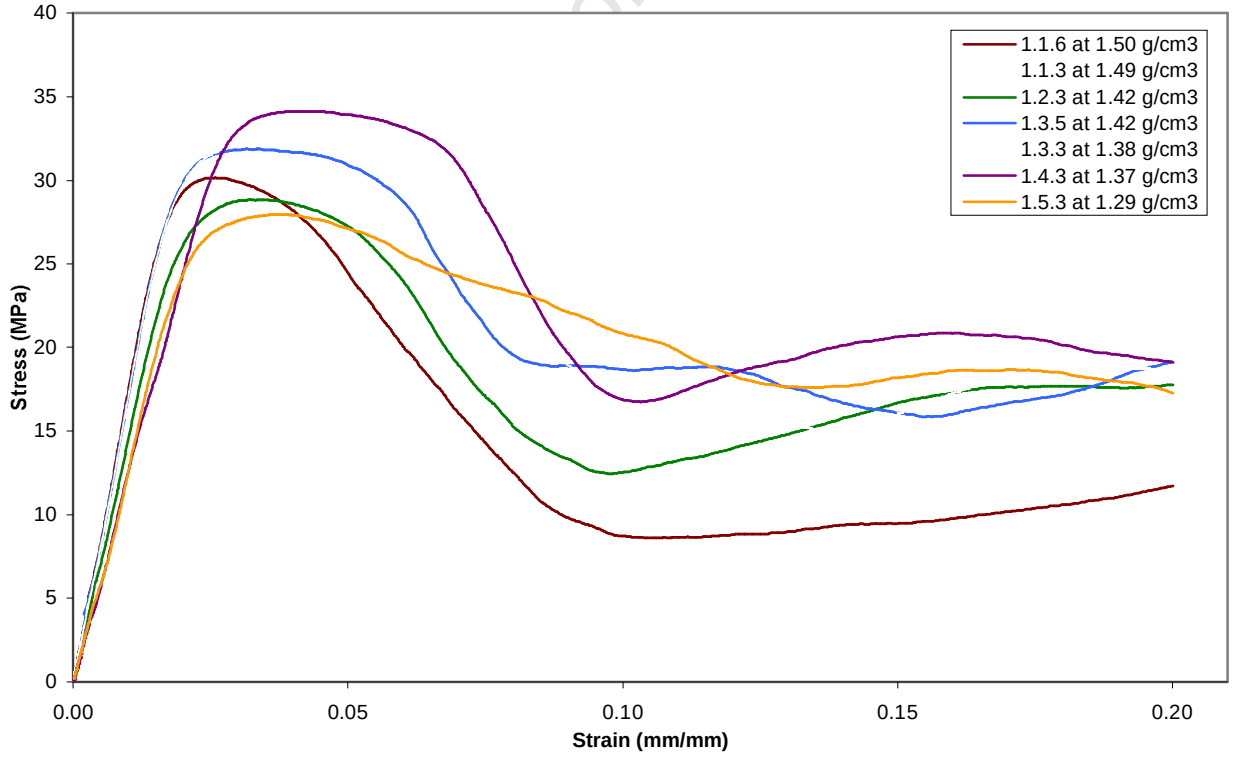

Figure C4: Stress-strain curves of Bovine 1 specimens at a strain rate of 10^{-2} s^{-1}

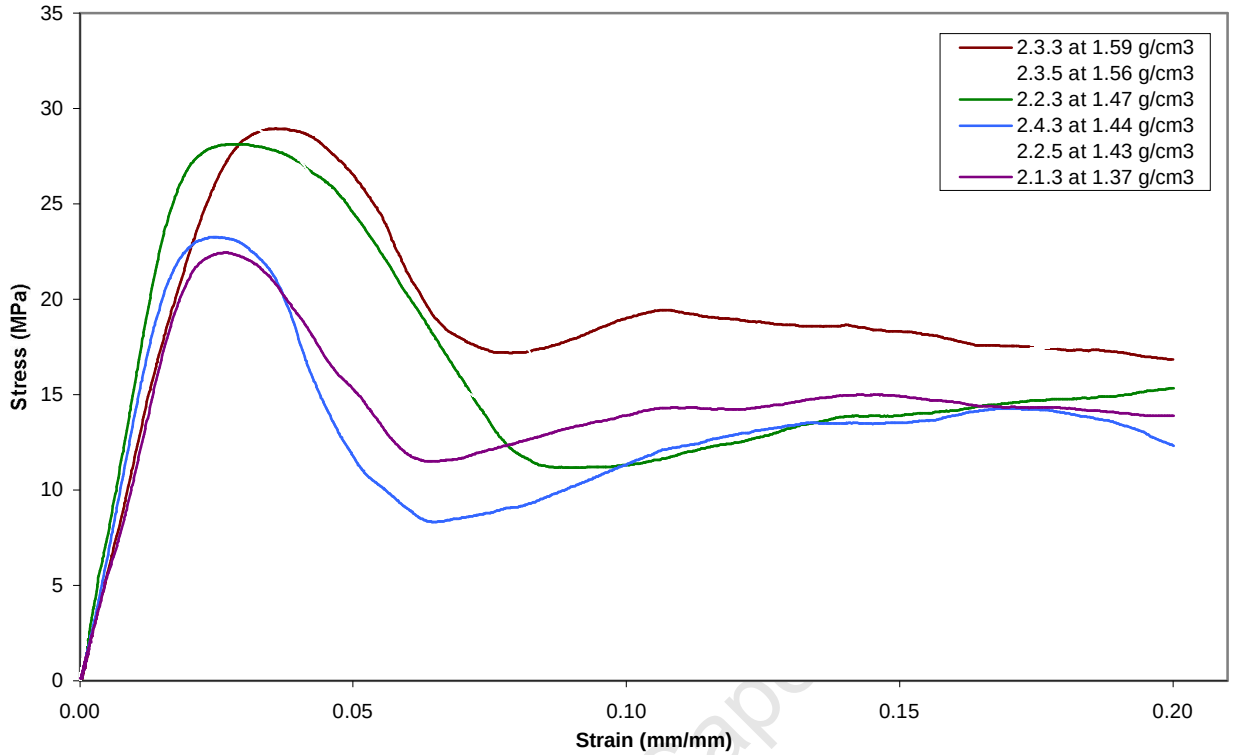

Figure C5: Stress-strain curves of Bovine 2 specimens at a strain rate of 10^{-2} s^{-1}

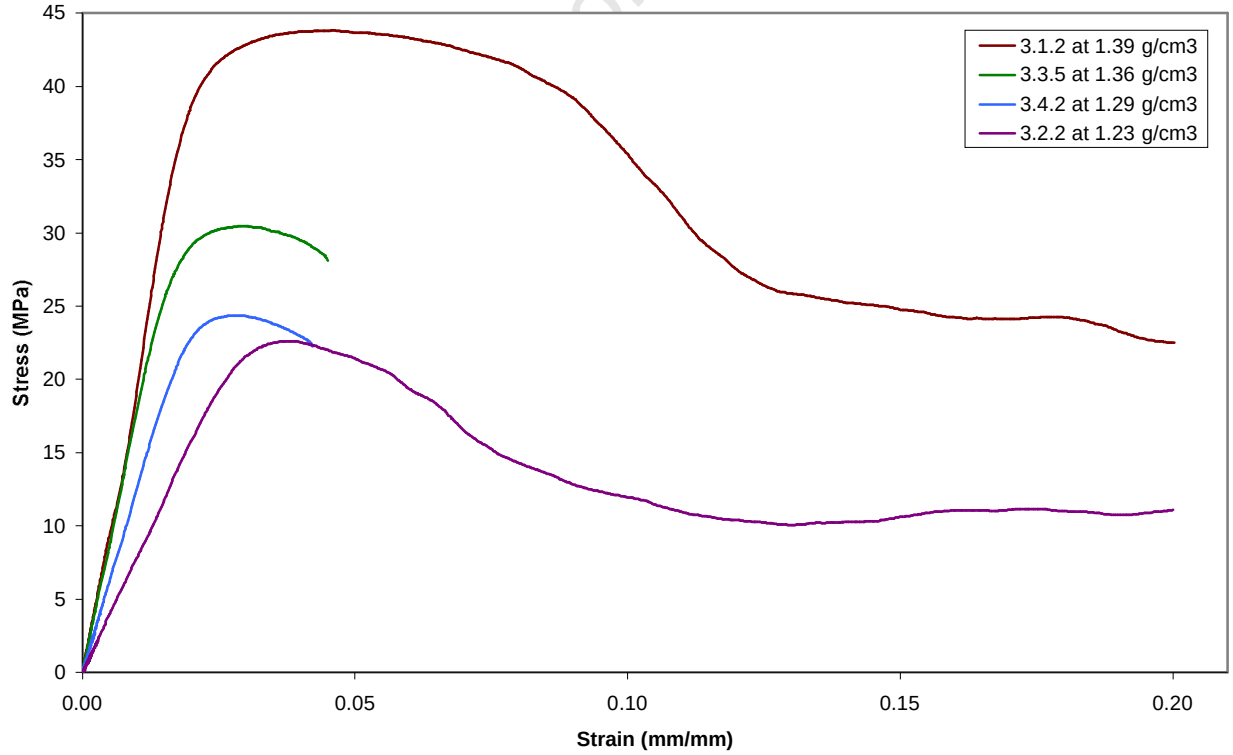

Figure C6: Stress-strain curves of Bovine 3 specimens at a strain rate of 10^{-2} s^{-1}

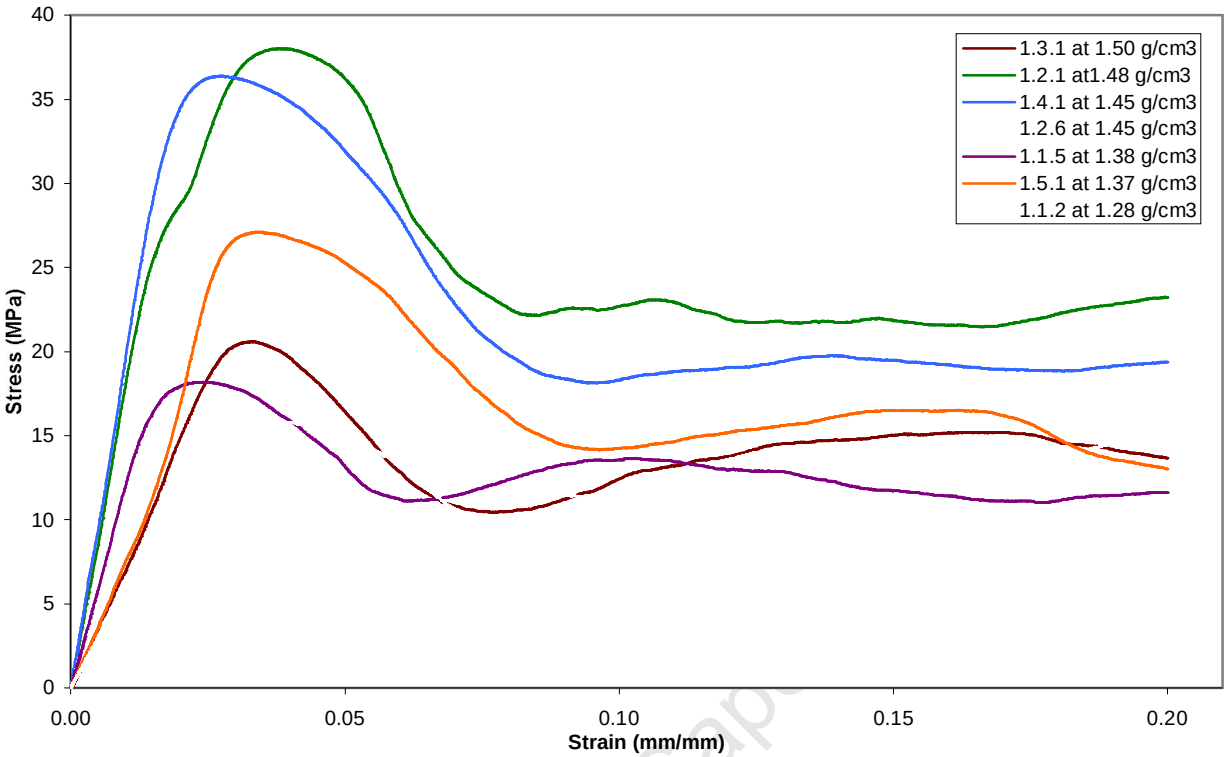

Figure C7: Stress-strain curves of Bovine 1 specimens at a strain rate of 10^{-3} s^{-1}

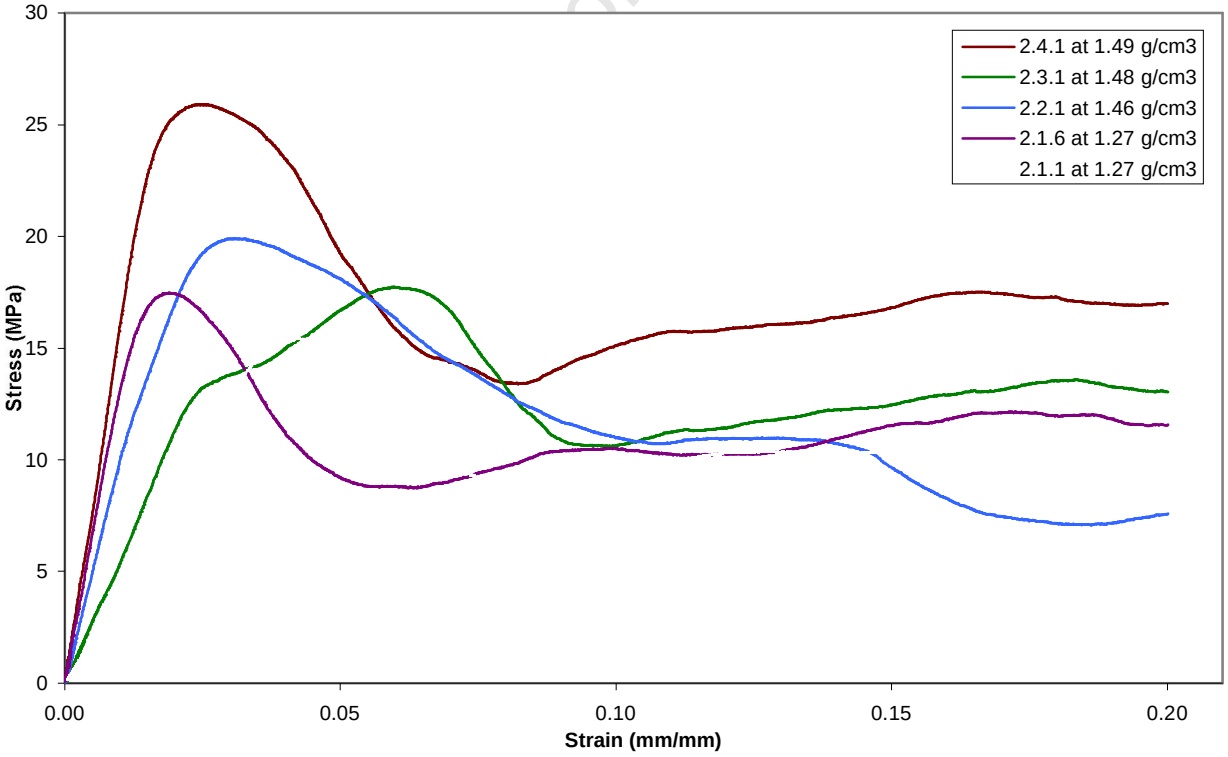

Figure C8: Stress-strain curves of Bovine 2 specimens at a strain rate of 10^{-3} s^{-1}

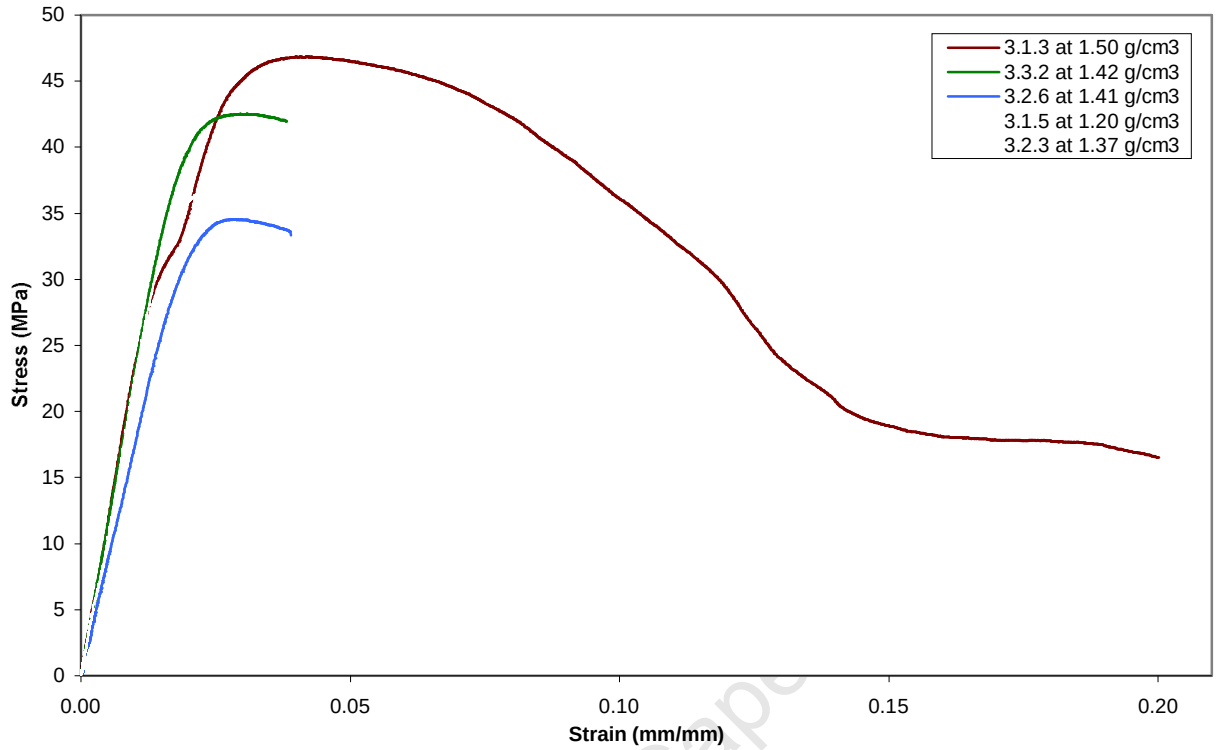

Figure C9: Stress-strain curves of Bovine 3 specimens at a strain rate of 10^{-3} s^{-1}

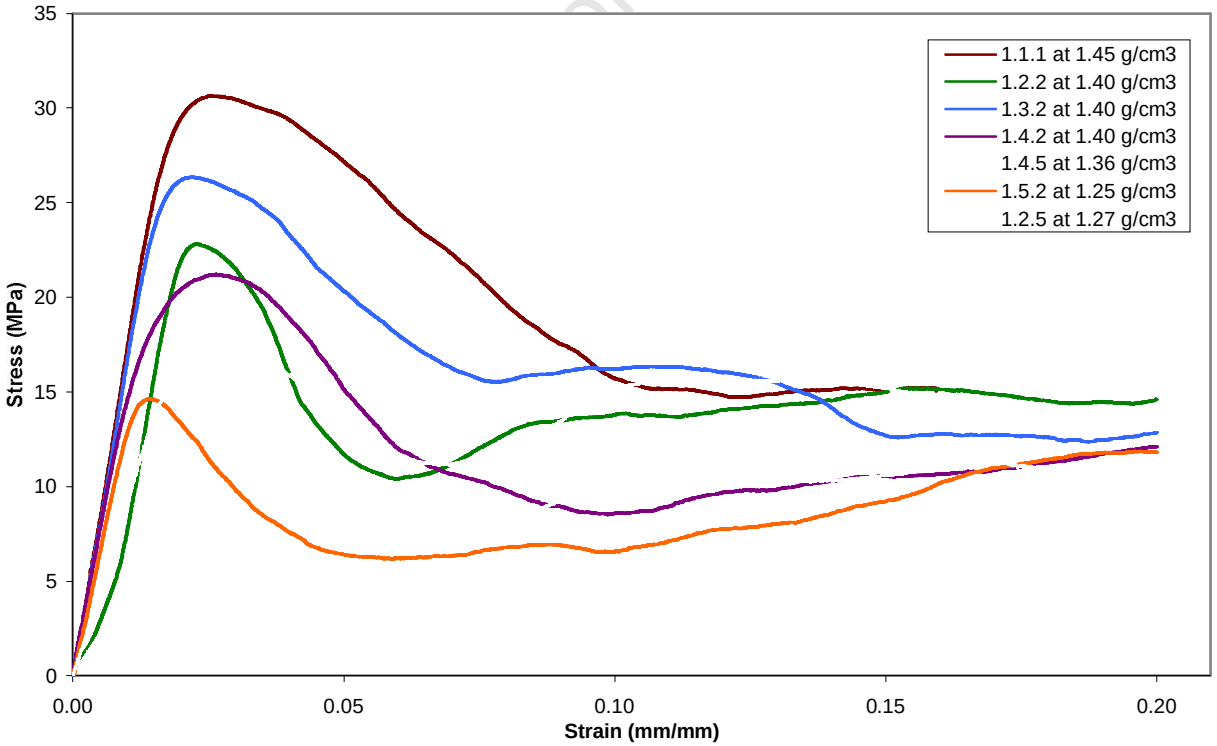

Figure C10: Stress-strain curves of Bovine 1 specimens at a strain rate of 10^{-4} s^{-1}

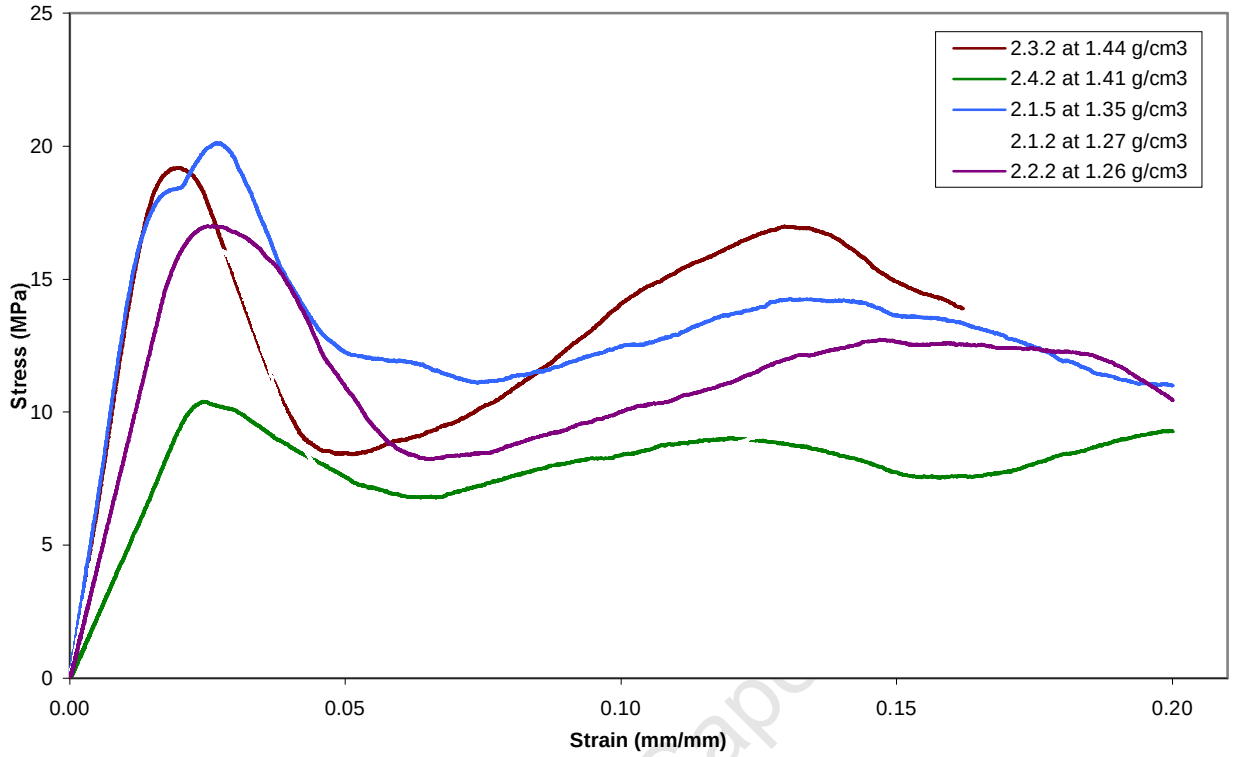

Figure C11: Stress-strain curves of Bovine 2 specimens at a strain rate of 10^{-4} s^{-1}

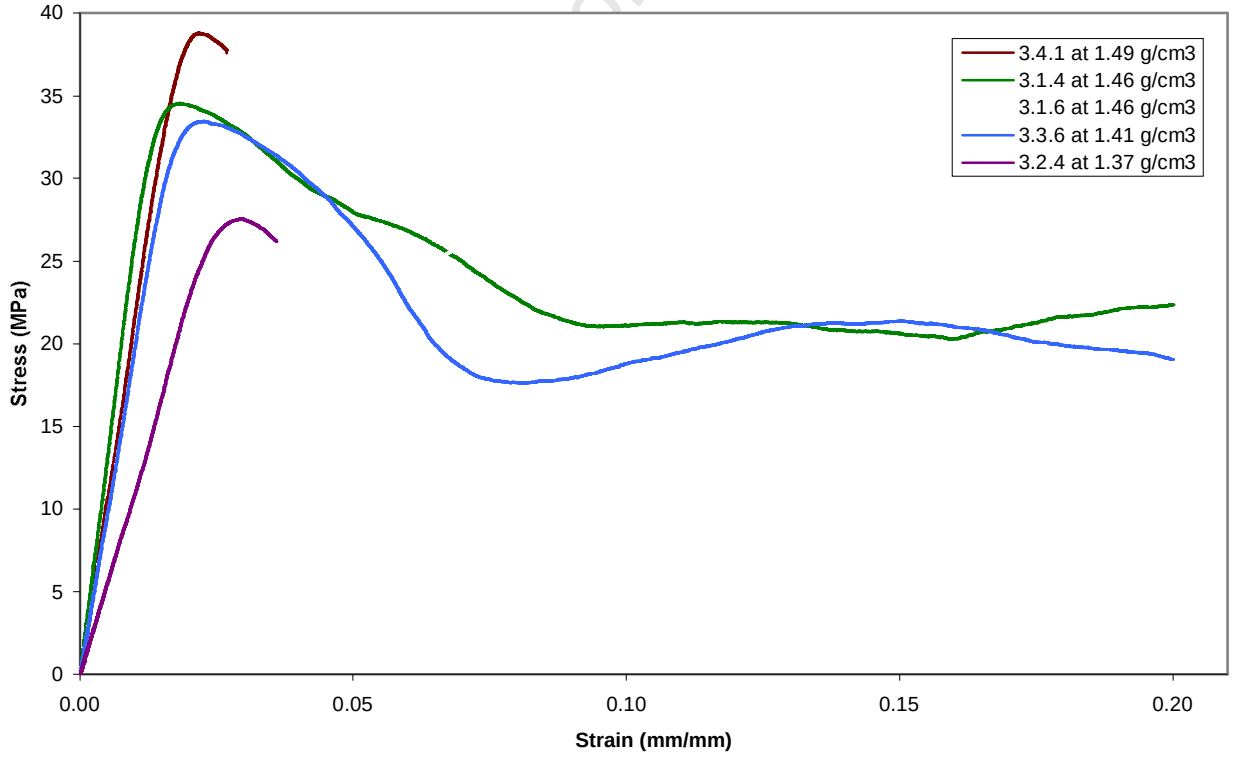

Figure C12: Stress-strain curves of Bovine 3 specimens at a strain rate of 10^{-4} s^{-1}

APPENDIX D: CALCULATION OF CONFIDENCE INTERVALS

The confidence interval (C.I.) is calculated as follows:

$$C.I. = \hat{Y}_i \pm t_{n-2} S_{yx} \sqrt{1 + h_i}$$

Where: $$h_i = \frac{1}{n} + \frac{(x_i - \bar{x})^2}{\sum_{i=1}^{n} x_i^2 - n\bar{x}^2}$$

$\hat{Y}_i$ = predicted value of y

s_{yx} = standard error of the estimate

n = sample size

x_i = given value of x

$\bar{x}$ = mean value of x

t_{n-2} = "t" value from t-distribution tables corresponding to (n-2) degrees of freedom [67]

APPENDIX E: DENSITY NORMALISATION

The densities of each specimen are normalized to an average value. The corresponding dependent values (stress, strain, Young's modulus) are found by the process illustrated in Figure E1 and described below for yield stress as a power law function of density.

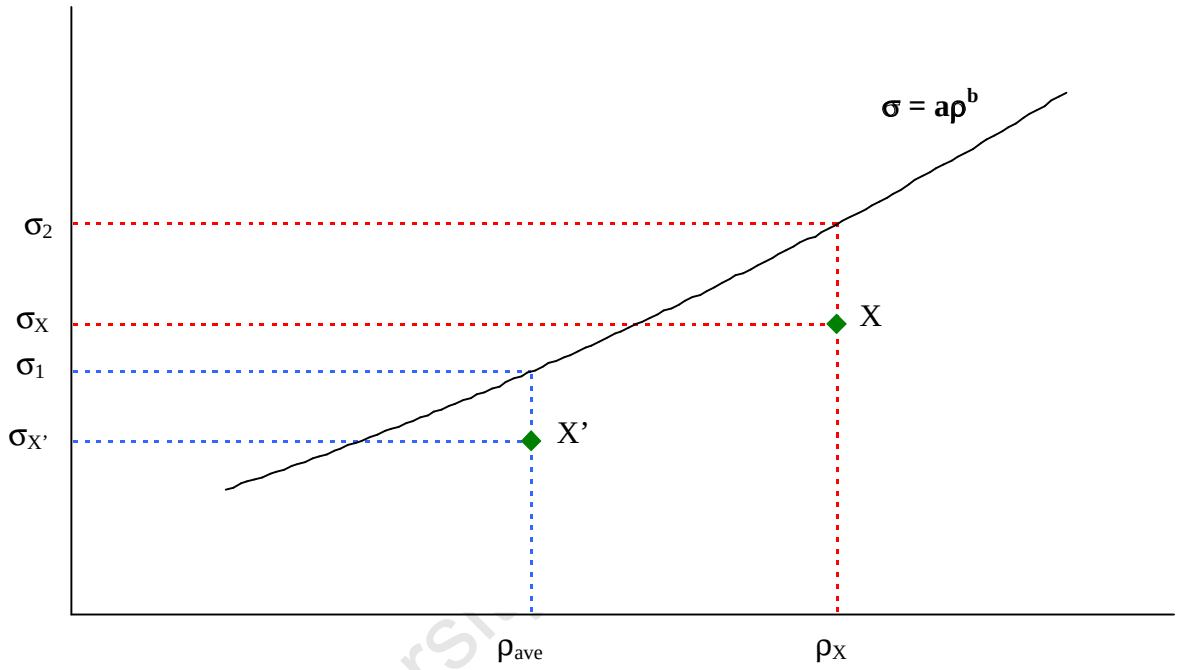

Figure E1: Density normalization graph

The symbols used are:

- ρ_{ave}: Average density of all specimens
- σ_1: Stress on curve corresponding to average density
- ρ_X: Density of specimen X
- σ_X: Yield stress of specimen X
- σ_2: Stress on curve corresponding to density of specimen X
- $\sigma_{X'}$: Normalised stress of specimen X with average density

The points lying on the curve have the following equations:

$$\sigma_1 = a\rho_{ave}^{b} \quad \text{(E1)}$$

$$\sigma_2 = a\rho^{b}x \quad \text{(E2)}$$

The stress ratio of the actual to predicted values for equivalent specimens is equal at any density value:

$$\frac{\sigma_X}{\sigma_2} = \frac{\sigma_{X'}}{\sigma_1} \quad \text{(E3)}$$

Therefore the normalized stress is:

$$\sigma_{X'} = \frac{\sigma_X \sigma_1}{\sigma_2}$$

which can be expressed as:

$$\sigma_{X'} = \sigma_X \left(\frac{\rho_{ave}}{\rho_X}\right)^{b} \quad \text{(E4)}$$

Similarly for linear relationship, the normalised stress is:

$$\sigma_{X'} = \sigma_X \frac{a\rho_{ave}+b}{a\rho_X+b} \quad \text{(E5)}$$

APPENDIX F: DYNAMIC TEST RESULTS

Specimen no.	ρ (g/cm^3)	E (MPa)	σ_u (MPa)	ε_u (mm/mm)	σ_y (MPa)	ε_y (mm/mm)
5.1.1	1.40	621	29.08	0.0692	27.63	0.0466
5.1.2	1.34	1049	33.05	0.0422	31.40	0.0325
5.1.4	1.39	710	37.01	0.0627	35.16	0.0417
5.1.5	1.32	1535	36.86	0.0398	35.02	0.0222
5.2.1	1.47	3589	90.07	0.0435	85.57	0.0271
5.2.2	1.34	1038	34.37	0.0400	32.65	0.0326
5.2.3	1.10	1302	31.03	0.0298	29.48	0.0250
5.2.4	1.49	3218	84.86	0.0412	80.62	0.0298
5.2.5	1.39	1548	42.02	0.0393	39.91	0.0283
5.2.6	1.24	1252	29.14	0.0295	27.68	0.0240
5.3.1	1.22	973	28.47	0.0366	27.05	0.0282
5.3.3	1.28	1197	29.48	0.0368	28.01	0.0261
5.3.5	1.27	1099	34.49	0.0638	32.77	0.0320
5.3.6	1.34	849.8	34.78	0.0631	33.04	0.0419
5.4.1	1.42	2087	68.85	0.0593	65.41	0.0354
5.4.2	1.28	1279	30.27	0.0348	28.75	0.0249
5.4.5	1.39	829.33	26.61	0.0475	25.28	0.0331
5.4.6	1.24	1066	27.24	0.0425	25.88	0.0260
Average	1.33	1402	40.43	0.0456	38.41	0.0310

APPENDIX G: VISCOELASTIC EQUATION CONSTANTS

Specimen	c_1 (MPa)	η (MPa s1/2)	θ (s)
5.1.1	-3.47×10^{4}	-0.284	5.37×10^{7}
5.1.2	-3.47×10^{4}	-0.0261	5.37×10^{7}
5.1.4	-3.47×10^{4}	-0.222	5.37×10^{7}
5.1.5	-3.47×10^{4}	3.44×10^{-6}	5.37×10^{7}
5.2.1	-3.47×10^{4}	1.20	5.37×10^{7}
5.2.2	-3.47×10^{4}	-0.290	5.37×10^{7}
5.2.3	-3.47×10^{4}	0.221	5.37×10^{7}
5.2.4	-3.47×10^{4}	1.19	5.37×10^{7}
5.2.5	-3.47×10^{4}	0.167	5.37×10^{7}
5.2.6	-3.47×10^{4}	0.138	5.37×10^{7}
5.3.1	-3.47×10^{4}	0.0304	5.37×10^{7}
5.3.3	-3.47×10^{4}	0.0832	5.37×10^{7}
5.3.5	-3.47×10^{4}	0.107	5.37×10^{7}
5.3.6	-3.47×10^{4}	-0.139	5.37×10^{7}
5.4.1	-3.47×10^{4}	0.437	5.37×10^{7}
5.4.2	-3.47×10^{4}	0.106	5.37×10^{7}
5.5.5	-3.47×10^{4}	-0.246	5.37×10^{7}
5.4.6	-3.47×10^{4}	0.0834	5.37×10^{7}
Average	-3.47×10^{4}	0.142	5.37×10^{7}

APPENDIX H: PREDICTED VS. ACTUAL YIELD STRESS

Specimen	Yield stress (MPa)	
	Predicted	Actual
5.1.1	29.69	27.63
5.1.2	29.18	31.40
5.1.4	34.95	35.16
5.1.5	29.03	35.02
5.2.1	41.38	85.57
5.2.2	31.31	32.65
5.2.3	27.51	29.48
5.3.4	48.16	80.62
5.2.5	36.20	39.91
5.2.6	32.19	27.68
5.3.1	36.54	27.05
5.3.3	35.89	28.01
5.3.5	34.67	32.77
5.3.6	32.33	33.04
5.4.1	36.17	65.41
5.4.2	33.43	28.75
5.4.5	35.82	25.28
5.4.6	30.24	25.88